Synthesis, Reactivity and Application of $\lambda^3\sigma^2$-Phosphinines

Inaugural-Dissertation

to obtain the academic degree
Doctor rerum naturalium (Dr. rer. nat.)

submitted to the Department of Biology, Chemistry, Pharmacy of
Freie Universität Berlin

by

M. Sc. Jinxiong Lin
from Fujian province, People's Republic of China

2022

The described work was carried out from October 2019 until March 2022 under the supervision of Prof. Dr. Christian Müller at Freie Universität Berlin.

1. Reviewer: Prof. Dr. Christian Müller
2. Reviewer: Prof. Dr. Sebastian Hasenstab-Riedel

Disputation: 06.12.2022

Declaration

I herewith confirm that I have prepared this dissertation without the help of any inappropriate resources. All citations are marked reasonable and shown in reference. The present dissertation summarizes the research results which have never been reported in any previous doctorate procedure.

Jinxiong Lin

Berlin, November 2022

Acknowledgement

I would like to thank Prof. Dr. Christian Müller. He gave me the chance to join his group as a Ph.D candidate. He always gave me reasonable suggestions and appropriate guidance when I faced troubles with my research projects.

Prof. Dr. Muriel Hissler has contributed greatly to the characterization of luminescent λ^5-phosphinines and gave many valuable suggestions.

I am very grateful to Dr. Nathan Coles, especially for the article revisions and crystal measurements. He also taught me a lot of useful knowledge. I feel fortunate to have met him and become a good friend.

Dr. Friedrich Wossidlo worked with me in the same lab. He gave me many tips, suggestions and guidance.

Dr. Jelena Wiecko is a patient and gentle lady. Talking to her always helped me to get rid of my depression. This has helped me a lot to persevere through my Ph.D career.

I am also grateful to Dr. Daniel Frost, who is one of my best friends. We often communicated and discussed relevant projects. He also devotes for my projects in DFT calculations.

Dr. Jan Felix Witte, Luca Steiner and Lea Dettling provided a huge help for the DFT calculations.

Andrey Petrov provided a great help in performing the cyclic voltammetry measurements of my compounds and useful suggestions for my projects.

Lara Šibila and Luise Sander have been a great help in the experiments and laboratory maintenance. Special thanks to Lara Šibila, who makes me feel at ease when I communicated with her.

I am thankful to all the people who helped me a lot during my study period in one way or another.

Manuela Weber for her help with the crystallographic characterization of several compounds.

Dorian Reich and Markus Peschke for the daily maintenance of laboratories and instruments.

Dr. Steven Giese, Dr. Alex Plajer, Alexander Krappe, Tim Görlich, Richard Kopp, Moritz Ernst, Samantha Frank, Sabrina Kleynemeyer, Oskar Mummenhoff, Michael Marquardt, Katrin Klimov, Lucie Jutta Groth, Niklas Limberg, Otto Staudhammer, for

all the kind help, discussion, suggestions, cakes, drinks and all those fun days.
My student Henrietta Adeseva helped me with the synthesis of phosphinines.
I am also very grateful to all the Ph.D students in the group for their help in revising my dissertation.
Especial thanks to the Prof. Dr. Chao Zou and Prof. Dr. Shigang Wan for this dissertation reviews and corrections.
I am particularly grateful to my family. I have not accompanied them for four years because of the *Covid-19*. In order to give me a peace of mind for my studies, many troubles at home were never told to me, such as my brother who had terminal leukemia and my father and mother who had several operations over the years. After I recently found out about these things, the gratitude and guilt I feel towards them makes me wish I could go back to them immediately.

List of publications

Jinxiong Lin, Nathan T. Coles, Manuela Weber, Christian Müller, **Phosphinine selenide: Nonconvalent Interactions with Organoiodines and Elemental Iodine, and Reactivity towards Potassium Cyanide**, *ChemPlusChem*, *DOI*: *10.1002/cplu.202200284*.

Jinxiong Lin,† Friedrich Wossidlo,† Nathan T. Coles, Manuela Weber, Simon Steinhauer, Tobias Böttcher, Christian Müller, **Borane Adducts of Aromatic Phosphorus Heterocycles: Synthesis, Crystallographic Characterization and Reactivity of a Phosphinine-B(C_6F_5)$_3$ Lewis Pair**, *Chem. Eur. J.* **2022**, *28*, e202104135.

Friedrich Wossidlo, Daniel S. Frost, Jinxiong Lin, Nathan. T. Coles, Katrin Klimov, Manuela Weber, Tobias Böttcher, Christian Müller, **Making Aromatic Phosphorus Heterocycles More Basic and Nucleophilic: Synthesis, Characterization and Reactivity of the First Phosphinine Selenide**, *Chem. Eur. J.* **2021**, *27*, 12788-12795.

†: These authors have contributed equally.

Unpublished result:

Jinxiong Lin, Nathan T. Coles, Lea Dettling, Luca Steiner, J. Felix Witte, Beate Paulus, Christian Müller, **How to Shrink the Ring: Phospholenes from Phosphabenzenes via Selective Ring Contraction**, *submitted*.

Jinxiong Lin, Daniel S. Frost, Nathan T. Coles, Manuela Weber, Christian Müller, **Copper(I) and Gold(I) Complexes of 3-Aminofunctionalized Phosphabenzenes: Synthesis and Structural Characterization**, *to be submitted.*

Table of abbreviations

Bu: Butyl
Cp: Cyclopentadienyl
CV: Cyclic Voltammetry
d: Doublet
DCM: Dichloromethane
DFT: Density Functional Theory
Et_2O: Diethyl ether
EtOH: Ethanol
Eq.: Equivalents
EN: Electronegativity
h: Hour
J: Coupling constant
HOMO: Highest Occupied Molecular Orbital
HMBC: Heteronuclear Multiple Bond Correlation
HMQC: Heteronuclear Multiple Quantum Coherence
IUPAC: International Union of Pure and Applied Chemistry
LUMO: Lowest Unoccupied Molecular Orbital
MeCN: Acetonitrile
m: Multiple
Me: Methyl
min: Minutes
MO: Molecular Orbital
NBO: Natural Bond Orbital
NMR: Nuclear Magnetic Resonance
nm: Nanometer
NICS: Nucleus Independent Chemical Shift
o: *ortho*
OLED: Organic Light Emitting Diode
Ph: Phenyl
p: *para*
r. t.: Room Temperature
sec: Seconds
T: Torsion Angle
^{t}Bu: Tert-butyl
THF: Tetrahydrofuran
TMS: Trimethylsilyl
UV: Ultraviolet
UV/Vis: Ultraviolet-Visible Spectroscopy
vs.: Versus

Table of Contents

Chapter 1

Introduction. General Properties of Phosphinines

1.1 Phosphinines

Compared to the classical phosphorus(III) compounds, the investigation on low-coordinated phosphorus(III) compounds is still scarce. In these compounds, the number of binding partners (σ) is smaller than the valency (λ) of the phosphorus atom, due to the formation of PC multiple bonds.[1,2] In 1966, Märkl has achieved the first preparation of a $\lambda^3\sigma^2$-phosphinine. This was a milestone because the reactive P=C double bond in the phosphinine was thermodynamically stabilized by the incorporation into one aromatic system. A few years later, the parent phosphinine C_5H_5P **2** was reported by Ashe III (Figure 1).[3,4] Phosphinines belong to a class of aromatic phosphorus heterocycles and represent the heavier analogues of pyridines. Phosphinine is similar to benzene, in which a CH unit is substituted by an isolobal phosphorus(III) atom. An alternative name of phosphinine is "phosphabenzene", but nowadays it is usually called $\lambda^3\sigma^2$-phosphinine in accordance with the IUPAC nomenclature. For a long time, phosphinines were considered as ''chemical curiosities'' since they violate the classical double bond rule, according to which elements of the third and higher periods cannot form stable double bonds.[5]

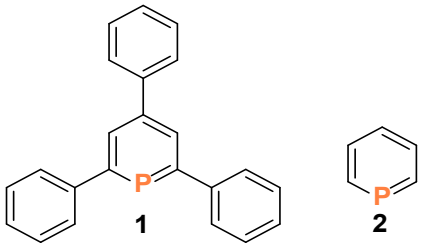

Figure 1: 2,4,6-triphenyl-$\lambda^3\sigma^2$-phosphinine and parent phosphinine.

1.2 Synthesis of phosphinines

Märkl *et al*. synthesized 2,4,6-triphenylphosphinine **1** by the reaction of 2,4,6-triphenylpyrylium tetrafluoroborate **3** and tri(hydroxymethyl)phosphane **4** in boiling pyridine (Scheme 1).[4] The initiation of this reaction involves the nucleophilic attack of $P(CH_2OH)_3$ to the C_α atom of the pyrylium salt.

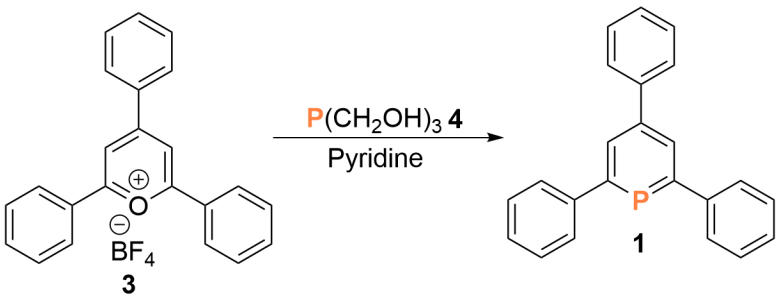

Scheme 1: Synthesis of **1** by Märkl in 1966.

This synthetic route allows a range of substituents and functional groups to be introduced into the 2-, 4-, and 6-positions of the phosphinine ring, and proved to be a versatilely and modular synthetic approach.[6,7,8,9,10]

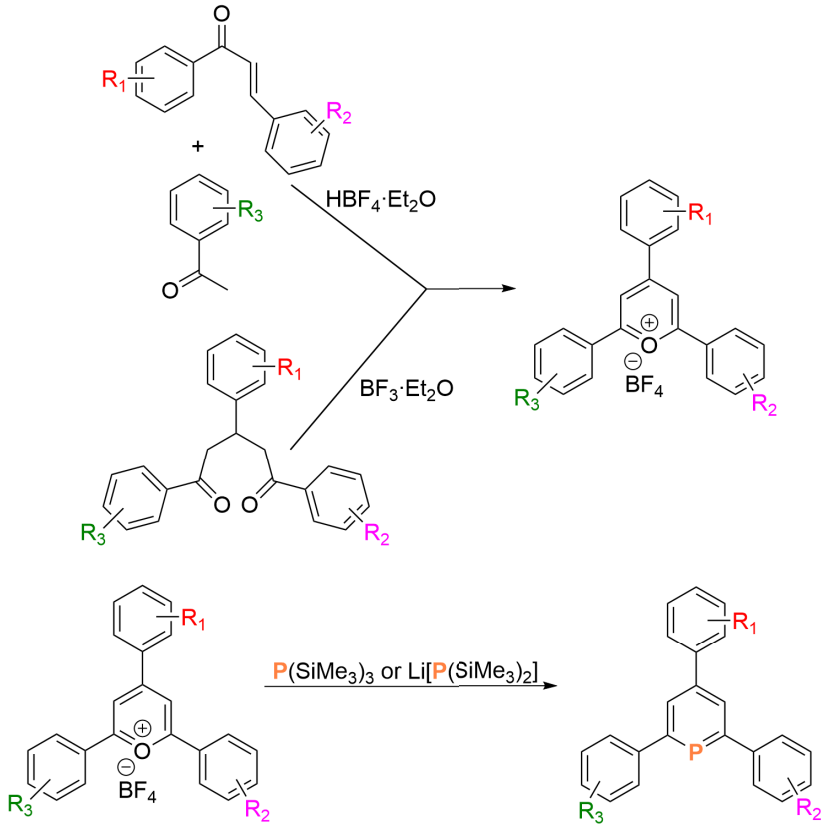

Scheme 2: Synthesis of pyrylium salts and phosphinines.

The starting materials for the synthesis of pyrylium salts are commercially available benzaldehyde and acetophenone derivatives. The triaryl-substituted pyrylium salts can be synthesized *via* the chalcone route: the first step is a classical aldol condensation between benzaldehydes and acetophenones resulting in the formation of the chalcones, which are subsequently reacted with acetophenones and tetrafluoroboric acid in diethyl ether for the formation of pyrylium salts. Alternatively, pyrylium salts can be prepared

via the 1,5-diketone route, in which 1.5-diketones undergo cyclization in the presence of boron trifluoride diethyl etherate.[11] Subsequently, phosphinines can be obtained directly in the reaction of pyrylium salts with $P(SiMe_3)_3$ or $Li[P(SiMe_3)_2]$ (Scheme 2).[12,13] This pyrylium salt route is still the main synthetic method for the preparation of 2,4,6-trisubstituted phosphinines today.

The parent phosphinine C_5H_5P **2** was synthesized and reported by Ashe III in 1971.[5] The reaction of phosphorus tribromide, 1,4-dihydro-1,1-dibutylstannabenzene **5** and the base 1,5-diazabicyclo[4.3.0]non-5-ene forms the parent phosphinine (Scheme 3). This route also allows the synthesis of heavier analogues of phosphinine, arsabenzene, stibabenzene and bismabenzene.[36]

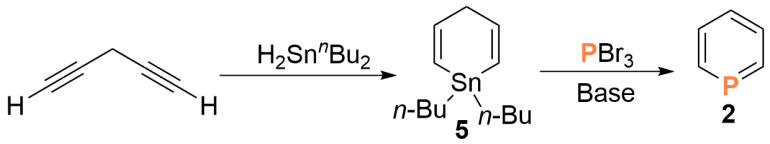

Scheme 3: Synthesis of the parent phosphinine.

Another approach to phosphinines was developed by Mathey and co-workers in 1979. The 1,2-dihydro-λ^5-phosphinine **7** was obtained by reaction of 1-benzyl-3,4-dimethylphosphole **6** and P_4S_{10}, which was further reduced by Ni(0) to form the 2-phenyl-3,4-dimethylphosphinine **8** (Scheme 4).[14]

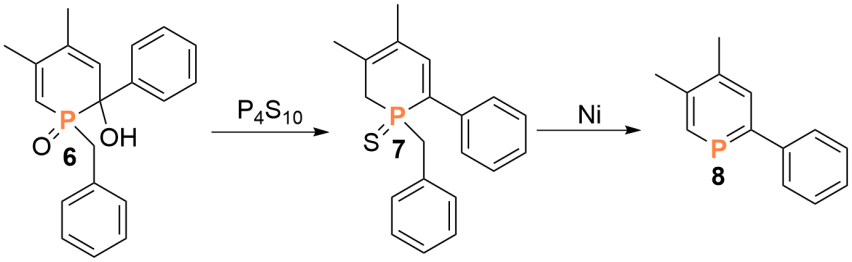

Scheme 4: Synthesis of phosphinine **8**.

Seven years later, Regitz and co-workers reported that the phosphaalkyne **9** can act as dienophile in [4+2] cycloaddition reactions with cyclopentadienones or pyrones affording alkyl-substituted phosphinines. The low stability of phosphaalkynes led to a limited applications of this method in the synthesis of a phosphinine library (Scheme 5).[15]

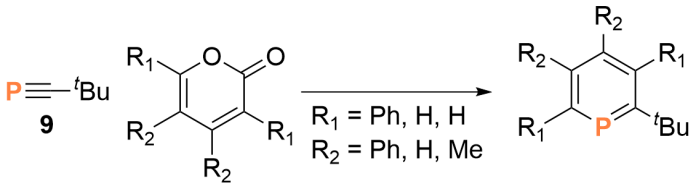

Scheme 5: Synthesis of alkyl-substituted phosphinines.

The diazaphosphinine route was developed by Mathey *et al*. in 1996. It was found that 1,3,2-diazaphosphinine **10** could be converted into phosphinines by multiple [4+2] cycloaddition-cycloreversion reactions with alkynes (Scheme 6).[16] Bis(cyclopentadienyl)titanium(IV) dichloride reacts with methylmagnesium chloride to form Cp_2TiMe_2 which subsequently reacts with pivalonitrile and PCl_3 to give 1,3,2-diazaphosphinine **10**.[17-21] 1,3,2-diazaphosphinine can react with one equivalent of an alkyne to form 1,2-azaphosphinines by extrusion of one nitrile molecule. Subsequent addition of the second equivalent of alkyne gives rise to phosphinines. This method has distinct advantages, such as simplicity, considerable product yields and versatility, affording a vast number of phosphinines with various functional groups. Therefore, this method was mainly used in this work.

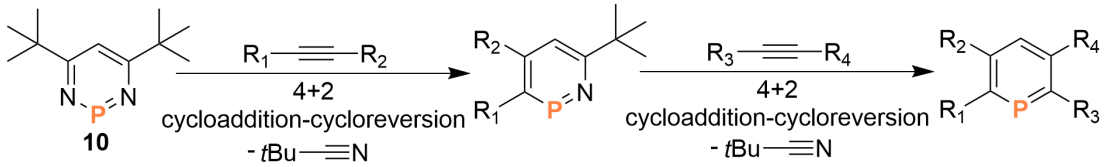

Scheme 6: Synthesis of phosphinines *via* the diazaphosphinine route.

Nishibayashi reported that FeI_2 can catalyze the [2+2+2] cycloaddition reaction between diynes **11** and phosphaalkynes in *m*-xylene affording a variety of 2,4,5-trisubstituted phosphinines (Scheme 7).[22]

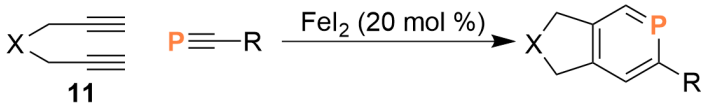

Scheme 7: Synthesis of phosphinines *via* catalytic [2+2+2] cycloaddition reactions.

In summary, a series of synthetic routes enable the introduction of specific functional groups into different positions of the aromatic heterocycle to modulate the steric and electronic properties of λ^3-phosphinines. This allows to use those phosphorus heterocycles as functionalized molecules in various research fields, such as

homogeneous catalysis, materials science and coordination chemistry (see chapters 1.5 and 1.6). The λ^3-phosphinines discussed in this work were mainly synthesized by the pyrylium salt route or by the 1,3-diaza-2-phosphinine route.

1.3 Electronic properties of phosphinines

In coordination chemistry, phosphinines usually act as weak σ-donor but rather strong π-acceptor ligands. They show significantly different reactivity and coordination abilities compared to classical trivalent phosphorus compounds and pyridines due to the inherent features of their electronic and steric properties.[23-26] Pyridine is as aromatic as benzene by both bond separation and superhomodesmic calculations, while the aromaticity of phosphinines has been calculated at SCF/3-21G* energy level as only 88-90 % of that of benzene. This phenomenon can be partly explained by the increase of heteroatom size accompanied by a small steady decrease in the delocalization of the 6π-electrons.[27,28]

electronegativity:	C: 2.55	N: 3.04	P: 2.19
angle °:	C-C-C: 120	C-N-C: 117	C-P-C: 100
bond length Å:	C-C: 1.39	C-N: 1.34	C-P: 1.75

Scheme 8: Comparison of electronegativities, angles and bond lengths in benzene, pyridine and the parent phosphinine.

The different electronegativities of nitrogen (Pauling scale: 3.04) and phosphorus (Pauling scale: 2.19) lead to an opposite polarization of the C-E bonds in the respective heterocycles (E = N, P). While the N-atom in pyridine holds a partial negative charge, phosphinine possesses a positively charged phosphorus atom (Scheme 8).[29] The lone pair of the nitrogen atom in pyridine is almost perfectly sp^2-hybridised with an s-character of 29.1 %. At the same time, the reluctance of the phosphorus atom to undergo 3s-3p hybridization results in a strong 3s-orbital character (63.8 %) of the lone pair.[30] For these two reasons, the basicity and nucleophilicity of the phosphorus atom in phosphinine is rather low [*pKa* ($C_5H_6P^+$) = 16.1 ± 1.0; *pKa* ($C_5H_6N^+$) = 5.23)].[31,32]

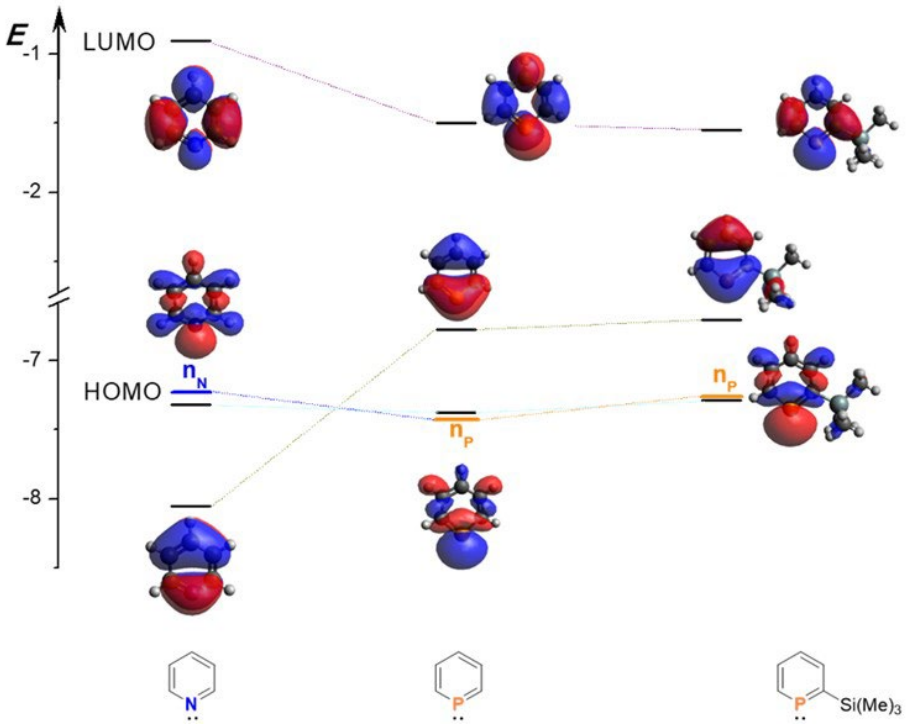

Figure 2: Kohn-Sham orbitals of pyridine, the parent phosphinine and 2-$SiMe_3$-phosphinine; the energy level of the lone pair in yellow; Calculated at B3LYP-D3/def2-TZVP energy level.

The frontier molecular orbitals of the unsubstituted phosphinine **2**, pyridine and 2-$SiMe_3$-phosphinine are depicted in Figure 2.[33-35] The phosphorus lone pair in the parent phosphinine C_5H_5P is represented by the HOMO-2, which lies lower in energy than the lone pair of nitrogen in pyridine (represented by the HOMO), and, additionally, is more diffuse and less directional than that of pyridine. The presence of the electron-donating $SiMe_3$ substituent at the α-position of the phosphinine ring increases the energy of the lone pair (HOMO-1), with respect to the parent phosphinine (HOMO-2), and, therefore, enhances the basicity and nucleophilicity of the aromatic heterocycle. The LUMO of the parent phosphinine is a π* antibonding orbital with a large coefficient at the phosphorus atom. In contrast, the LUMO of pyridine is significantly higher in energy and possesses a low coefficient on the nitrogen atom. Interestingly, the *ortho*-$SiMe_3$ substituent in the phosphinine does not significantly impact the energy level of the LUMO (Figure 2).

Classical nucleophilic and electrophilic aromatic substitution reactions are usually excluded for phosphinines. For example, the reaction of RLi with pyridine results in

the anion **12**, while the reaction of RLi and phosphinine results in the 1-*R*-phosphacyclohexadienyl-anion **13** (Scheme 9).[36,37]

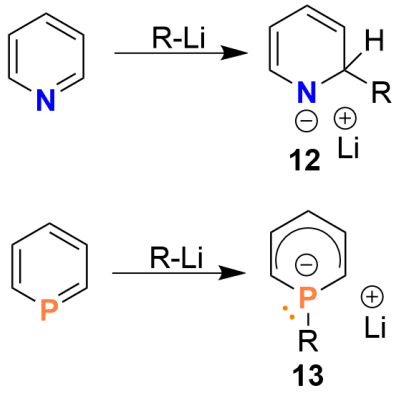

Scheme 9: Reactions of pyridine and parent phosphinine with alkyllithium reagent.

As mentioned above, it was observed that the basicity and nucleophilicity of the phosphorus atom in 2-$SiMe_3$-phosphinine is enhanced by the introduction of an *σ*-electron donor to the heterocycle.[34] It can be anticipated that the introduction of multiple strong *σ*-electron donating groups to the phosphorus heterocycle will lead to a significantly different reactivity of the corresponding phosphinines compared to the parent phosphinine. This is one of the focuses of the research in this work.

1.4 Structural properties of phosphinines

The structural analysis of phosphinines revealed that they form a distorted hexagon with a C-P-C angle of around 101°.[38] The P-C bond lengths in phosphinines are 1.71-1.78 Å, which is in-between a single and a double P-C bond distance ($\sum r_{cov}$(P-C) = 1.86 Å, $\sum r_{cov}$(P=C) = 1.69 Å).[39,40] The C-C bond lengths in phosphinines are also in accordance with a delocalized 6π-electron system within the heterocycle. The cone angle concept for a measure of steric bulk of a ligand was proposed by Tolman. It remains in widespread use, because it is relatively straightforward to determine and provides an established context of knowledge for the development of new ligands.[41-44] However, because the ring of a phosphinine is planar, the steric demand of such compounds cannot be evaluated well by Tolman's cone angle concept. Therefore, the occupancy angles α and β were introduced to evaluate the steric bulk in the perpendicular planes. They show that the steric demand of phosphinines in *y* plane is relatively small, while that in *x* plane is very large in *ortho*-substituted phosphinines (Figure 3).[45-47]

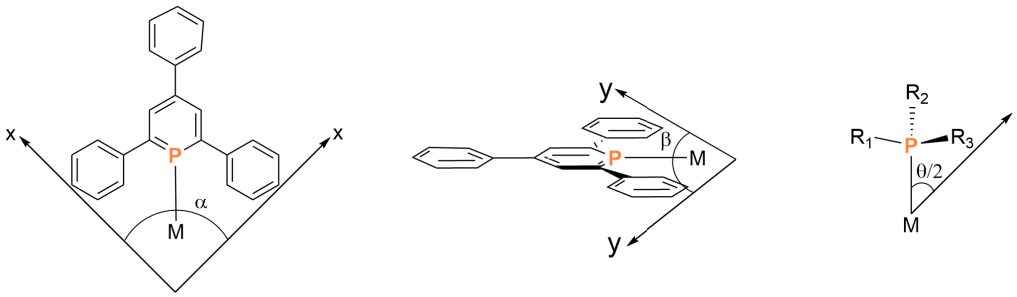

Figure 3: Left: 2,4,6-triphenylphosphinine as an example to show the occupancy angles α and β; right: Tolman's angle θ/2 for a classical phosphine.

The most recent method developed by Cavallo and co-workers for the evaluation of the steric hindrance of ligands is the ‘‘percent buried volume’’ (%V_{bur}) that is defined as the percent of the total volume of a sphere occupied by the ligand. The sphere has a defined radius of 3.50 Å and has the metal center (away from the donor atoms of 2.00 or 2.28 Å) at the core. %V_{bur} is calculated using crystallographic data (Figure 4). This method allows a better comparison of sterically different ligands, including both planar and three-dimensional ligands.[113] A large amount of values for various classical trivalent phosphorus compounds and N-heterocyclic carbenes have been published.[114,115] The group of Müller reported the %V_{bur} values for phosphinines, 1-phosphabarrelenes and 5-phosphasemibullvalenes, for the first time.[116]

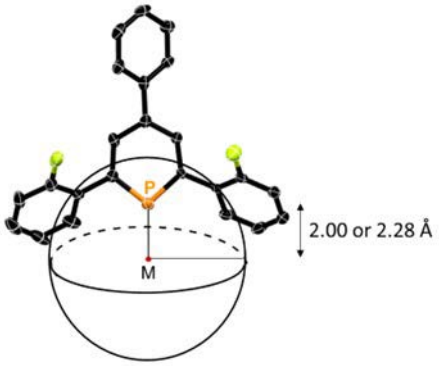

Figure 4: Percent buried volume %V_{bur}.

1.5 Coordination chemistry of phosphinines

The electronic and steric properties discussed above indicate that phosphinines can bind

to transition metals in various coordination modes *via* two different coordination sites: the lone pair of the phosphorus atom, the aromatic π system, and a combination of the two different coordination sites.[48-53] The energetically low-lying lone pair at the phosphorus atom is suitable for a *σ*-coordination with a metal center, while the π-orbital of the aromatic cycle results in η^6-coordination.[54-59] The coordination modes of the phosphinine ligand depend on the oxidation state of the metal, the type of metal precursor and the steric features of the phosphinine.[60-66] Common coordination modes of phosphinines are shown in Figure 5.

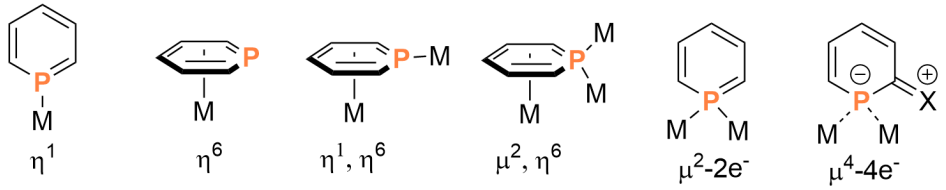

Figure 5: Coordination modes of phosphinine.

The reaction of the parent phosphinine **2** with $CuBr{\cdot}SMe_2$ results in the formation of the coordination polymer **14** which has repeating $[(C_5H_5P)_2CuBr]$ units of two phosphinine and one bromide ligands (Scheme 10).[34]

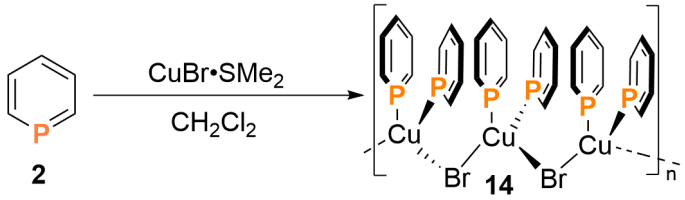

Scheme 10: Reaction of **2** with $CuBr{\cdot}S(Me)_2$ and formation of the coordination polymer **14**.

Interestingly, the presence of a π-donor-substituent in *ortho*-position of the phosphinine ring results in a significantly different coordination pattern of the heterocycle. A series of known 2-donor-functionalized phosphinines have been reported. When used as ligands, they exhibit different coordination modes when linked to late transition metals compared to the parent phosphinine.

Grützmacher and co-workers found that the anionic phosphinin-2-olate acts as a 4e donor and bridges a cationic $[Au(PPh_3)]^+$ and a neutral [AuCl] fragment (Scheme 11).[67]

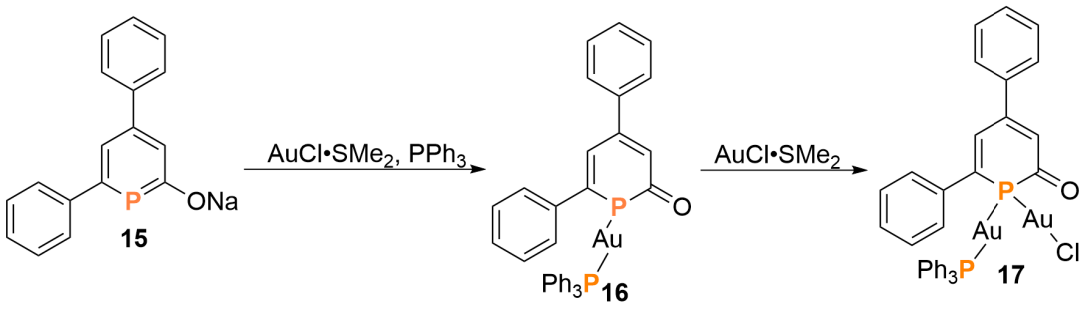

Scheme 11: Reaction of phosphinin-2-olate with AuCl·S(Me)$_2$ and formation of the gold complex **17**.

The group of Müller reported that 2-amino-substituted phosphinine **18** shows a strong interaction between the π-donating NMe_2 group and the aromatic system resulting in a high π-density at the phosphorus atom. It forms the μ_2-P-4e Cu complexes **19** when reacted with CuBr·SMe_2 (Scheme 12).[68]

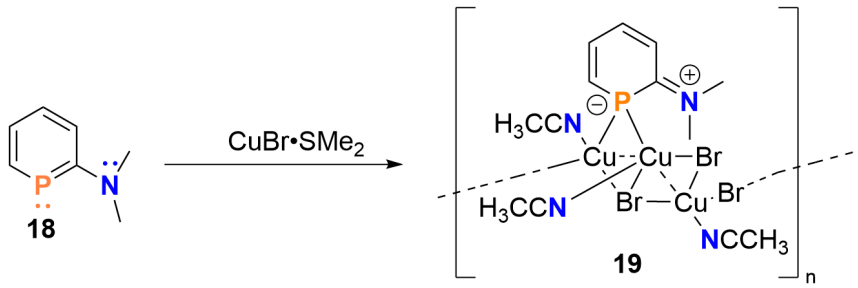

Scheme 12: Reaction of **18** with CuBr·S(Me)$_2$ and formation of the copper complex **19**.

The diversity of possible substitution patterns in the phosphinine ring as well as multiple possible coordination modes make the coordination chemistry of these heterocycles very attractive for further studies. The investigation of the coordination chemistry of donor-functionalized phosphinines is one of the directions of this work.

1.6 Reactivity and applications of phosphinines

The high s-character at the lone pair at the phosphorus atom and the energetic stabilization of the corresponding frontier molecular orbital make the reactivity of phosphinines obviously different from that of classical P(III) compounds. It was shown that phosphinines can be protonated only by non-oxidizing superacids containing weakly coordinating anions. Reed and co-workers successfully protonated 2,4,6-tris-^{t}Bu-λ^3-phosphinine **20** with H[$CHB_{11}Me_5Cl_6$] (Figure 6).[69]

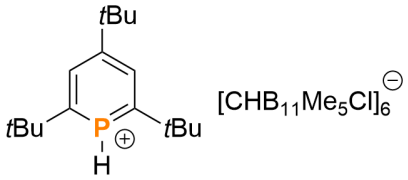

20

Figure 6: The protonated 2,4,6-tri-*tert*-butyl-phosphinine **20**.

Deberitz and co-workers observed a decrease of the vapor pressure when B_2H_6 was added to **1** at low temperatures, indicating the reversible formation of the phosphinine-borane adduct **21**. However, the product could not be isolated and fully characterized (Scheme 13).[70] No additional reports on adduct formations of phosphinines with other main group compounds have been published. In contrast, the lone pair on the nitrogen atom of pyridine is more nucleophilic and basic, which enables the formation of stable pyridine-borane adducts.[31,32,117] Based on these results, it can be anticipated that the **1**-borane adduct has a relatively weak P-B bond strength and is not sufficiently stable, all of which are due to the weaker nucleophilicity and basicity of **1**. The group of Müller found that the introduction of strong σ-donating groups at the *ortho*-position of the aromatic heterocycle increases the energy of the phosphorus lone-pair.[34] This observation opens the possibility of forming more stable phosphinine-borane adducts.

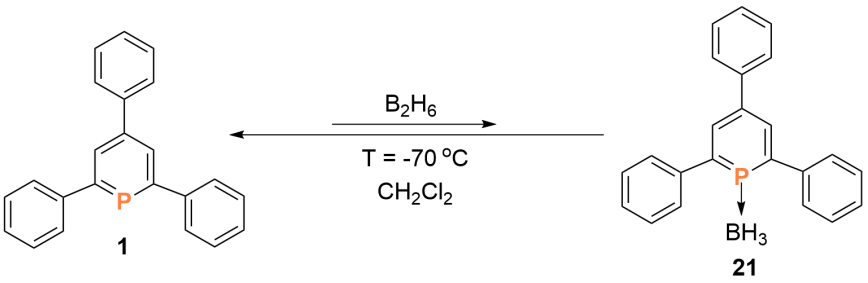

Scheme 13: Reaction of phosphinine **1** with B_2H_6.

Moreover, phosphinines cannot be alkylated directly with classical alkylating reagents. However, the corresponding phosphininium salts are accessible *via* a multistep synthesis. The synthesis of phosphininium salts relies on the oxidation of 1-methyl-phosphahexadienyl anions, which are produced by treating methyllithium with 2,6-

bis(SiMe$_3$)-3,5-diphenylphosphinine or 2,6-bis(SiMe$_3$)-3,5-dimethylphosphinine.[71] Recently, the groups of Müller and Riedel achieved for the first time the methylation of a phosphinine using the strongly electrophilic methylation reagent $[(Me)_2Cl]^+[Al(OTeF_5)_4]^-$, resulting in novel 1-methyl-phosphininium salts (Scheme 14).[72]

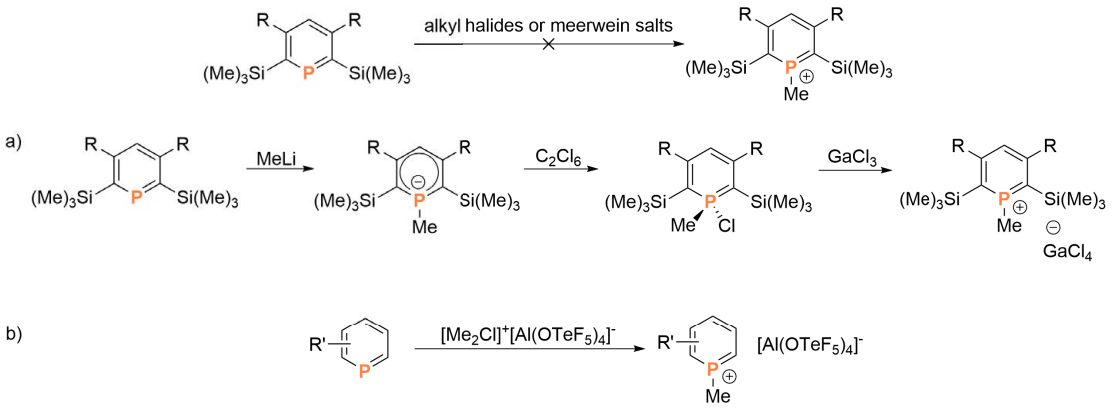

Scheme 14: Synthesis of phosphininium salts *via* a): a multistep synthesis; b): *via* a the strongly electrophilic methylchloronium reagent.

Compared to classical phosphorus(III) compounds, the oxidation of phosphinines with chalcogens is rather challenging. Mathey and co-workers reported the synthesis and isolation of phosphinine sulfide **23** by the reaction of 2-phenyl-4,5-dimethyl-phosphinine **22** with S_8 under harsh reaction conditions (Scheme 15).[73-75] Phosphinine oxides have never been directly detected and exist only as highly reactive species.[76] At the same time, phosphinine selenides were still unknown.

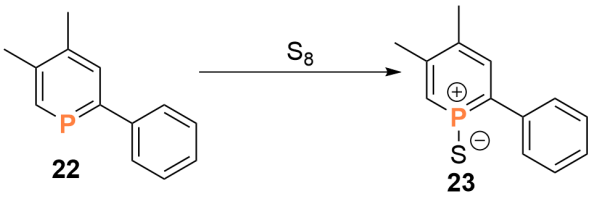

Scheme 15: Synthesis of phosphinine sulfide.

It has been shown that phosphinines can react at the phosphorus atom with strong nucleophiles, such as organolithium reagents, to yield (1*R*)-phosphahexadienyl anions (Scheme 16). They were called λ^4-phosphinines to distinguish them from λ^3- and λ^5-phosphinines. However, they should be regarded as λ^3-phosphinines with a pseudo-ylide structure.[77] (1*R*)-phosphahexadienyl anions can subsequently react with

electrophiles, giving λ^5-phosphinines. Due to the rather reactive nature of the (1*R*)-phosphahexadienyl anions, reactions with electrophiles result in the formation of by-products which are difficult to separate from the products by regular purification methods, for example, column chromatography and recrystallization. More details will be given in Chapter 5.

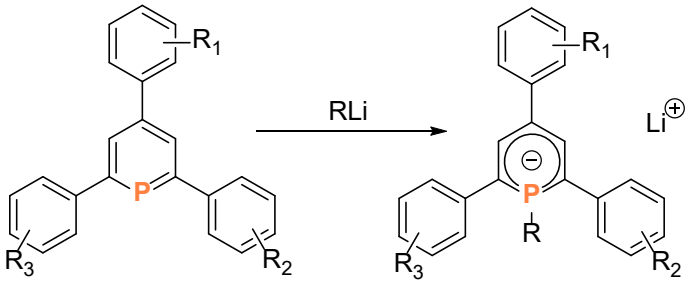

Scheme 16: Synthesis of λ^4-phosphinines.

Moreover, λ^3-phosphinines can be oxidized by $Hg(OAc)_2$ in the presence of alcohols or amines to give the highly fluorescent λ^5-phosphinines (Scheme 17).[9,76] The group of Müller synthesized a series of 2,4,6-triaryl-λ^5-phosphinines *via* this efficient oxidation process of λ^3-phosphinines to introduce additional different R_2N- or RO- substituents at the phosphorus atom.[77]

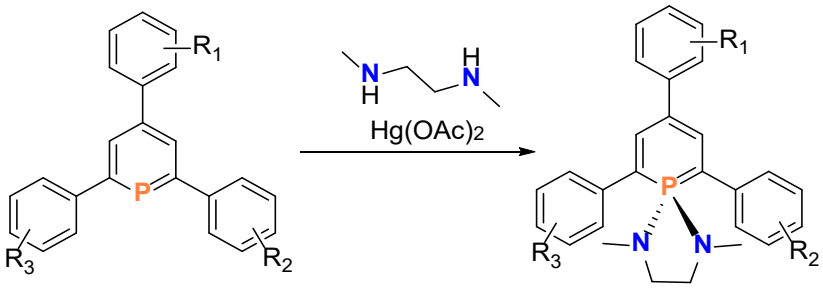

Scheme 17: Synthesis of fluorescent λ^5-phosphinines.

λ^3-Phosphinines can also be oxidized with phosphorus pentachloride under irradiation with UV light. This leads to 1,1'-dichloro-λ^5-phosphinines which are especially useful intermediate compounds for the preparation of λ^5-phosphinines with alkyl- and aryl-substituents at the phosphorus atom (Scheme 18).[78,79] More specific information can be found in Chapter 5.

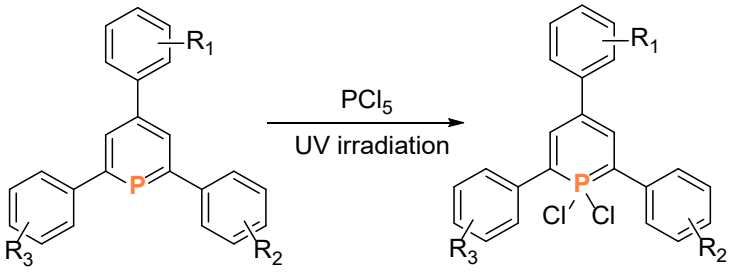

Scheme 18: Synthesis of λ^5-phosphinines with PCl_5 under UV light irradiation.

Some λ^5-phosphinines show pronounced thermal stability and intensive fluorescence, which are necessary features required for the construction of light emitting devices, such as organic light-emitting diodes (OLEDs).[77] For the first time, λ^5-phosphinines with fluorescence quantum yields of up to 42 % were reported by the group of Müller and were applied as luminescent emitting materials in novel OLED devices (Figure 7).

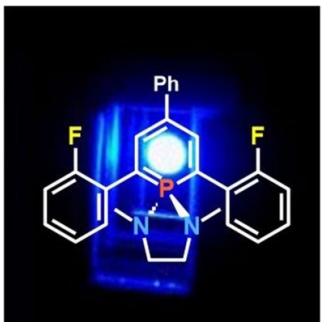

Figure 7: Application of fluorescent λ^5-phosphinines in an organic light-emitting diode device.

Phosphabarrelenes are accessible by reacting λ^3-phosphinines with alkynes *via* [4+2] cycloaddition reaction (Scheme 20). The pyridylfunctionalized 1-phosphabarrelene **25** undergoes a rather selective di-π-methane rearrangement in the coordination sphere of a metal center under UV light, which leads to the formation of chelating 5-phosphasemibullvalene derivatives and their respective transition-metal complexes. These compounds are promising for the application as ligand in transition-metal-mediated transformations and homogeneous catalysis.[80-84]

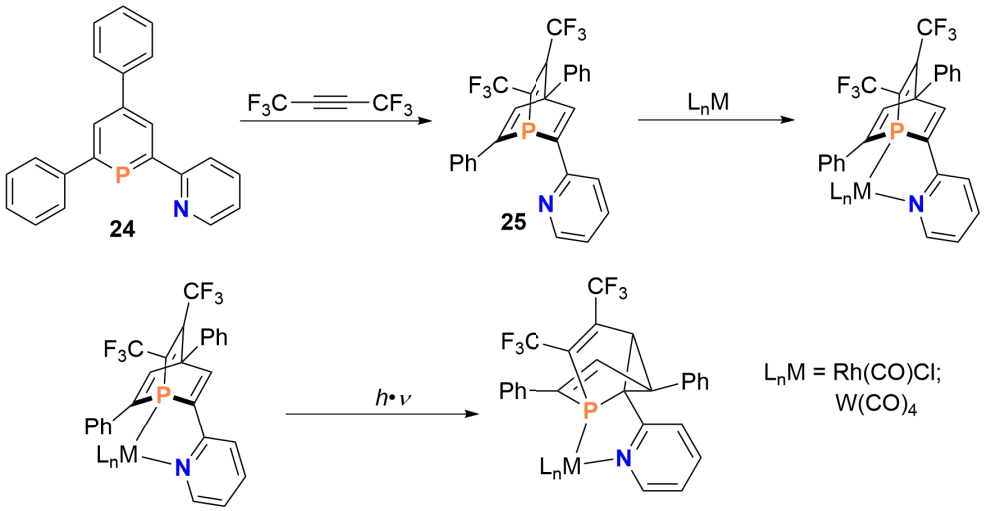

Scheme 19: Synthesis of phosphasemibullvalene.

Overall, the distinctive reactivity of phosphinines compared to classical P(III) compounds can be attributed to the inherent weak nucleophilicity and basicity of the phosphorus atom. However, the nucleophilicity and basicity of phosphinines can be significantly enhanced by the introduction of strong electron-donating groups. This broadens the scope of those phosphorus heterocycles for the preparation of hitherto unknown phosphinine-based compounds as well as for the applications. This is the focus of this work.

1.7 Motivation

For the use of $\lambda^3\sigma^2$-phosphinines in more applied research fields, their specific functionalization is particularly important in order to modify their stereo-electronic properties. Amino- or $SiMe_3$-groups can significantly enhance the basicity and nucleophilicity of the phosphorus atoms in phosphinines, which allows them to exhibit a significantly different reactivity and coordination chemistry compared to the parent phosphinine. In this respect, the synthesis of functionalized phosphinines and their further exploration in applications are imperative.

Phosphinine borane adducts: As already mentioned, $\lambda^3\sigma^2$-phosphinines are extremely weak bases and very poor nucleophiles. They were widely explored as ligands in coordination chemistry. However, there is still little known about the reactivity of

phosphinines towards main group elements and main group-based Lewis acids. According to DFT calculations by Erhardt and Frenking, the bond dissociation of a phosphinine-borane adduct is about 70% compared with that in the pyridine-borane adduct.[118] Based on this calculated value, the synthesis of phosphinine-borane adducts seems promising. Furthermore, Nöth and Deberitz reported the formation of the **1**-BH_3 adduct, based on the decrease in the vapor pressure upon adding B_2H_6 to **1** at low temperatures. However, the equilibrium shifted again to the starting materials at room temperature.[70] Due to the higher nucleophilicity of $SiMe_3$-substituted phosphinines, it was worthwhile to investigate the reaction between phosphinines and boranes in more detail.[34,121]

Phosphinine selenides: Phosphinine sulfides were reported by Mathey and co-works in 1984.[72] They are more stable than phosphinine oxide and display a high reactivity in cycloaddition reactions. However, contrary to phosphinine sulfides, phosphinine selenides are still unknown. The selenation of phosphinines is rather challenging due to the intrinsic low basicity and nucleophilicity of the phosphorus atom, which hinders the reaction with selenium species. Böttcher and co-workers confirmed that 2,6-bis($SiMe_3$)-pyridine is much more basic than the parent pyridine.[119] Therefore, the systematic investigation on the influence of $SiMe_3$-groups on the gas phase basicity of the corresponding phosphinines and their reactivity towards selenium were started.

3-*N,N*-Dimethylaminophosphinine derivatives: After the successful synthesis of 2,4,6-triphenylphosphinine and the parent phosphinine, several synthetic routes for the introduction of different functional groups into specific positions of the phosphorus heterocycle to modify their stereoelectronic properties and coordination abilities were developed (see Chapter 1.2). A series of donor-functionalized phosphinines have been reported in literature, however, the phosphorus-containing aniline derivatives remained elusive until recently.[67,68] Theoretical calculations showed that the electronic properties of phosphorus-containing aniline derivatives differ significantly from the parent phosphinine.[68] Therefore, it was envisaged to explore the synthetic access,

reactivity, and coordination chemistry of novel aminofunctionalized phosphinines in more detail.

λ^5-phosphinines: The group of Müller has synthesized a variety of fluorescent λ^5-phosphinines which show a maximum quantum yields of 42 % in solution.[6,77] However, the work mainly involved the modification of the substituents at 4-position and 2,6-positions of the phosphorus heterocycle. Research on effects of the substituents at the phosphorus atom on the optical properties of λ^5-phosphinines are still scarce.[6,77,95] Furthermore, the fluorescence emission of λ^5-phosphinines has been reported mainly in blue to green region and such compounds with red fluorescence emission in solution were yet unknown. Therefore, it was envisaged to further clarify the effects of the substitution pattern to the photophysical and photochemical properties of λ^5-phosphinines.

Chapter 2

Phosphinine Borane Adducts

2.1 Borane Adducts of Aromatic Phosphorus Heterocycles: Synthesis, Crystallographic Characterization and Reactivity of a Phosphinine-$B(C_6F_5)_3$ Lewis Pair

Jinxiong Lin,[a†] Friedrich Wossidlo,[a†] Nathan T. Coles,[a,b] Manuela Weber,[a] Simon Steinhauer,[a] Tobias Böttcher,[*c] Christian Müller[*a]

†: These authors have contributed equally.

a: J. Lin, Dr. F. Wossidlo, Dr. N. T. Coles, M. Weber, Dr. S. Steinhauer, Prof. Dr. C. Müller

Institut für Chemie und Biochemie, Freie Universität Berlin

Fabeckstr. 34/36, 14195 Berlin, Germany

b: Dr. N. T. Coles

School of Chemistry, University of Nottingham, University Park Campus

Nottingham, NG7 2RD, United Kingdom

c: Priv.-Doz. Dr. T. Böttcher

Institut für Anorganische und Analytische Chemie, Universität Freiburg

Albertstrasse 21, 79104 Freiburg, Germany

This article was published and is reprinted with permission from Wiley-VCH:

J. Lin, F. Wossidlo, N. T. Coles, M. Weber, S. Steinhauer, T. Böttcher, C. Müller, *Chem.Eur. J.* **2022**, *28,* e2021041.

DOI: 10.1002/chem.202104135

Author contributions: This project was designed by Prof. Dr. C. Müller, J. Lin, and Dr. F. Wossidlo. Dr. F. Wossidlo synthesized and characterized the first phosphinine borane adducts. Further applications of phosphinine borane adducts were carried out by J. Lin. Single crystals, except for phosphinine borane adducts, were obtained by J. Lin. The single crystal X-ray diffraction analyses were carried out by Dr. N. Coles and M. Weber. NMR experiments were conducted by J. Lin and Dr. F. Wossidlo. Theoretical calculations were performed by Dr. T. Böttcher. The paper was written by Prof. C. Müller and J. Lin. Estimated own contribution: ~ 75 %.

Chemistry–A European Journal
Research Article
doi.org/10.1002/chem.202104135
Chemistry Europe
European Chemical Societies Publishing
www.chemeurj.org

Borane Adducts of Aromatic Phosphorus Heterocycles: Synthesis, Crystallographic Characterization and Reactivity of a Phosphinine-$B(C_6F_5)_3$ Lewis Pair

Jinxiong Lin[+],[a] Friedrich Wossidlo.[+],[a] Nathan T. Coles,[a, b] Manuela Weber,[a] Simon Steinhauer,[a] Tobias Böttcher,*[c] and Christian Müller*[a]

In memory of Professor Paul C. J. Kamer.

Abstract: A phosphinine-borane adduct of a Me_3Si-functionalized phosphinine and the Lewis acid $B(C_6F_5)_3$ has been synthesized and characterized crystallographically for the first time. The reaction strongly depends on the nature of the substituents in the α-position of the phosphorus heterocycle. In contrast, the reaction of B_2H_6 with various substituted phosphinines leads to an equilibrium between the starting materials and the phosphinine–borane adducts that is determined by the Lewis basicity of the phosphinine. The novel phosphinine borane adduct (**6**-$B(C_6F_5)_3$) shows rapid and facile insertion and [4+2] cycloaddition reactivity towards phenylacetylene. A hitherto unknown dihydro-1-phosphabarrelene is formed with styrene. The reaction with an ester provides a new, facile and selective route to 1-*R*-phosphininium salts. These salts then undergo a [4+2] cycloaddition in the presence of Me_3Si–C≡CH and styrene to cleanly form unprecedented derivatives of 1-*R*-phosphabarrelenium salts.

Introduction

Tertiary phosphines (PR_3) readily react with various electrophilic species. For instance, they can be protonated and also form phosphine-borane adducts upon reaction with boranes (BR_3).[1] Boranes are particularly important as protecting groups for phosphines, especially for the synthesis of P-stereogenic compounds, as they can easily be removed afterwards by reaction with amines or more basic phosphines.[2] In recent years, the interaction of phosphines with boranes has been widely explored in the context of "frustrated Lewis pairs" (FLPs).[3] The reactivity of phosphines towards boranes is typically related to the pronounced basicity and nucleophilicity of phosphines, but steric factors on both the donor and the acceptor site also play a significant role.[3,4]

In contrast to classical phosphines, λ^3-phosphinines (phosphabenzenes) are extremely weak bases and very poor nucleophiles. This can be attributed to the rather high 3 s character of the phosphorus lone pair in C_5H_5P, which is much higher than the value found for the nitrogen lone pair in pyridine C_5H_5N (64% 3 s vs. 29% 2 s character).[5] Nevertheless, phosphinines are very good π-acceptors due to an energetically low-lying LUMO.[6] Thus, they readily form coordination compounds particularly with late transition metals in low oxidation states.[5,7] On the other hand, little is known about the reactivity of phosphinines towards main group-based Lewis acids. Reed and co-worker succeeded in protonating the phosphorus atom in 2,4,6-tris-*t*Bu-λ^3-phosphinine with the in situ generated, non-oxidizing superacid $H[CHB_{11}Me_5Cl_6]$ to afford the salt $[H(C_5H_2{}^tBu_3P)][CHB_{11}Me_5Cl_6]$ (**1**-H, Figure 1).[8]

Recently we have shown direct methylation of phosphinine **2** by using the strong alkylating reagent $[(CH_3)_2Cl]^+[Al(OTeF_5)_4]^-$ (**2**-CH_3).[9] According to DFT calculations by Erhardt and Frenking, the bond dissociation energy of a phosphinine–borane adduct is about 70% that of a pyridine-borane adduct (25.8 vs. 35.6 kcal mol^{-1}).[10] Based on this calculated value, the formation of phosphinine-borane adducts should consequently be possible. As a first indication, Nöth and Deberitz observed a decrease in the vapor pressure upon adding B_2H_6 to 2,4,6-triphenylphosphinine (**3**) at low temperatures.[11] This indicated the formation of the adduct **3**-BH_3 (Figure 1). At room temperature, however, the equilibrium shifted again to the starting materials. Even though this observation was mentioned in a

[a] J. Lin,[+] Dr. F. Wossidlo.,[+] Dr. N. T. Coles, M. Weber, Dr. S. Steinhauer, Prof. Dr. C. Müller
Freie Universität Berlin, Institut für Chemie und Biochemie
Fabeckstr. 34/36, 14195 Berlin (Germany)
E-mail: c.mueller@fu-berlin.de
[b] Dr. N. T. Coles
School of Chemistry, University of Nottingham
University Park Campus, Nottingham, NG7 2RD (UK)
[c] Priv.-Doz. Dr. T. Böttcher
Institut für Anorganische und Analytische Chemie
Universität Freiburg
Albertstrasse 21, 79104 Freiburg (Germany)
E-mail: tobias.boettcher@ac.uni-freiburg.de
[+] These authors have contributed equally to this manuscript.

Supporting information for this article is available on the WWW under https://doi.org/10.1002/chem.202104135

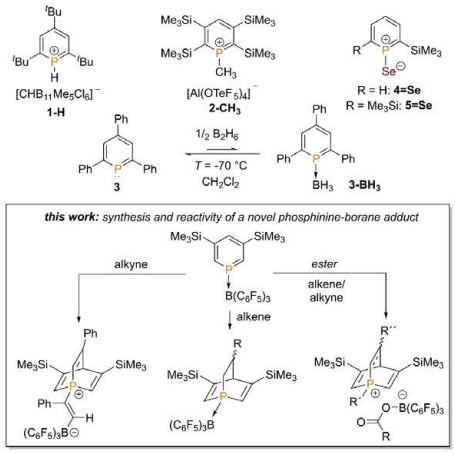

Figure 1. Reactivity of phosphinines towards Lewis acids and selenium, and a brief summary of this work.

footnote almost 50 years ago, no additional reports on adduct formations of phosphinines with boranes, or other main group compounds have been published since, even though borane adducts with five-membered aromatic phosphorus heterocycles are known.[12] In this respect, we recently found that the basicity and nucleophilicity of phosphinines can be increased significantly by introducing σ-donating Me_3Si substituents to the aromatic phosphorus heterocycle.[13] This allowed for the synthesis and characterization of the first phosphinine selenides (**4**=Se, **5**=Se).[14] These results prompted us to investigate the reaction between phosphinines and boranes in more detail and in this work we report the first preparation, crystallographic characterization and reactivity of a phosphinine-borane adduct.

Results and Discussion

As mentioned above, the presumed existence of a phosphinine-borane adduct (**3**-BH_3) is based solely on the observed reduction of the vapor pressure when adding B_2H_6 to 2,4,6-triphenylphosphinine **3** (Figure 1). In order to obtain more conclusive data and to verify the assumption, we first decided to repeat this experiment. Diborane was condensed into a solution of **3** in dichloromethane at $T=-70\,^{\circ}C$. In order to shift the equilibrium more to the side of the product, an excess of diborane was used and the solution was investigated by means of low-temperature NMR spectroscopy. At $T=-70\,^{\circ}C$, the $^{31}P\{^1H\}$ NMR spectrum of the reaction mixture shows a second, yet rather small, signal at $\delta=163.1$ ppm (cf. $\delta=179.0$ ppm for **3**). The equilibrium of the reaction is clearly located on the side of the starting materials, even though a large excess of diborane was used. This is also confirmed by the ^{11}B NMR spectrum of the solution. Even if the experiment corroborates the evidence for the existence of a phosphinine-borane adduct, any subsequent isolation and characterization of the phosphinine–borane adduct remained unsuccessful due to its low concentration (ratio **3**/**3**-$BH_3\approx20:1$). We anticipated that the higher basicity and nucleophilicity of Me_3Si-substituted phosphinines could shift the equilibrium in favor of the sought-after products. Therefore, phosphinines **4** and **5** were reacted with a slight excess of diborane (Scheme 1).[13,15] Analogous to the reaction of **3** with B_2H_6, the reaction mixture was kept at temperatures below $T=-70\,^{\circ}C$ and investigated by means of low-temperature NMR spectroscopy. For both reactions a new, broad signal can be observed in the $^{31}P\{^1H\}$ NMR spectra, which is slightly shifted to higher field when compared to the starting material (**4**: $\delta=230.7$ ppm; **4**-BH_3: $\delta=209.4$ ppm; **5**: $\delta=256.4$ ppm; **5**-BH_3: $\delta=226.0$ ppm).

Much to our delight, phosphinine **5** shows the highest conversion (**5**-BH_3/**5**=98:2), while phosphinine **4** forms considerably less of the phosphinine–borane adduct (**4**-BH_3/**4**=88:12, Figure 2a).

This is perfectly in line with our assumption that the more basic phosphinine **5** should shift the equilibrium more to the

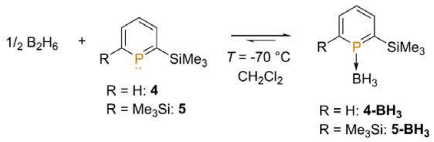

Scheme 1. Reaction of phosphinines **4** and **5** with diborane.

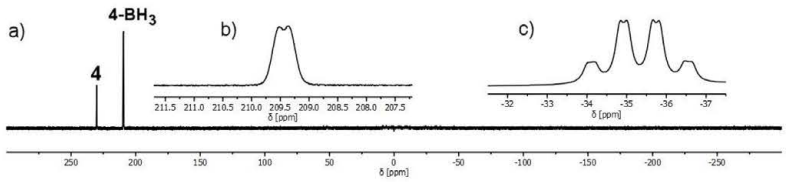

Figure 2. a) $^{31}P\{^1H\}$ NMR spectrum of the reaction of **4** with B_2H_6. b) Enlargement of the signal of **4**-BH_3. c) ^{11}B NMR spectrum of **4**-BH_3.

right side of the reaction equation (see above and Scheme 1). We noticed, however, that increasing the temperature to room temperature only had a marginal influence on the position of the equilibrium. In the case of the reaction of **4** with B_2H_6, a splitting of the new signal in the $^{31}P\{^1H\}$ NMR spectrum into a doublet ($^1J_{(P,B)} = 18$ Hz) can be observed (Figure 2b). As ^{11}B has a nuclear spin of $^3/_2$, splitting of the $^{31}P\{^1H\}$ NMR signal into a quartet is to be expected. Our observation might thus be due to a significant broadening of these signals. In the ^{11}B NMR spectra of the reaction mixtures, a new signal at $\delta = -34.6$ (**5**-BH_3) or -35.3 ppm (**4**-BH_3) can be observed in addition to the signal for excess diborane. The chemical shifts are in good agreement with values typically found for phosphine-borane adducts. Moreover, the ^{11}B signal for **4**-BH_3 shows a quartet, caused by the coupling to the three ^1H atoms. This signal is additionally split into a doublet by coupling to the ^{31}P atom with $^1J_{(B,P)} = 18$ Hz. The same coupling constant is also found in the $^{31}P\{^1H\}$ NMR spectrum (Figure 2c). This confirms the existence of a phosphinine–borane adduct. The ^1H NMR spectra of the reaction mixtures show that the aromatic protons are somewhat more strongly shielded than in the free phosphinines. The signals of the borane protons can be found at $\delta =$ 1.5 ppm.

As B_2H_6 is highly reactive, we also attempted to use the commercially available $BH_3 \cdot SMe_2$ adduct as a borane source for the reaction with **4**. In this case, we could also observe the formation of **4**-BH_3, however, the equilibrium of the reaction was clearly located on the side of the starting material, even when using a large excess of $BH_3 \cdot SMe_2$. This can most likely be attributed to a competition between dimethylsulfide and the phosphinine to form an adduct with the Lewis acidic borane. Once again, this clearly shows the low basicity and nucleophilicity of phosphinines compared to classical phosphines.

During the course of our NMR investigations, we noticed that a subsequent reaction took place with the initially formed phosphinine–borane adducts **4**-BH_3 and **5**-BH_3, even at $T = -70\,^\circ C$, which made crystallization and further characterization of **4**-BH_3 and **5**-BH_3 impossible. While warming the NMR samples up to room temperature, a colorless, viscous oil formed inside the NMR tube and within a few weeks, a slightly yellow solid formed. Additionally, when the adducts were stored at low temperatures, a colorless solid formed over time, which turned into a pale yellow solid as the final product after a few months. In the ^{11}B NMR spectrum only a large number of very broad signals can be detected while the $^{31}P\{^1H\}$ NMR spectra showed mainly a very broad signal at $\delta = 21.4$ ppm. Boranes are frequently used in the hydroboration of double bonds and the hydroboration of phospha-alkenes has previously been reported.[16] It is therefore reasonable to assume that the subsequent hydroboration of the P=C double bond in **4**-BH_3 and **5**-BH_3 slowly takes place, while insoluble polymers are finally formed (Scheme 2). According to quantum chemical calculations by Ermolaeva and Ionkin as well as experimental work by Yoshifuji et al. on the reaction of phospha-alkenes with BH_3, we suggest that the regioisomer **5**(H)-BH_2, shown in Scheme 2, is initially formed.[17,18] The chemical shift of $\delta = -21.4$ ppm, observed during the further conversion of **5**-BH_3, is

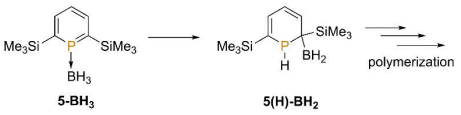

Scheme 2. Potential hydroboration of the P=C double bond in **5**-BH_3 and subsequent polymerization.

in line with the chemical shift of $\delta = -6.4$ ppm reported by Yoshifuji et al. for the product of the hydroboration of a phospha-alkene, which subsequently dimerized.[18] Moreover, Arbuzov and co-workers reported polymerization reactions with hydroborated phospha-alkenes.[16] This finding could explain the formation of the insoluble solid in the reaction mixtures of **4**-BH_3 and **5**-BH_3, which could not be further characterized thus far.

In order to avoid hydroboration of the P=C double bond, we decided to use the strong Lewis acid $B(C_6F_5)_3$ in combination with phosphinines **3**–**5** in CH_2Cl_2 at room temperature. However, no reaction could be observed as judged by $^{31}P\{^1H\}$ NMR spectroscopy (Scheme 3a).

Apparently, formation of the adduct between phosphinines **3**–**5** and the sterically demanding $B(C_6F_5)_3$ is hindered by the bulky phenyl and Me_3Si substituents at the α-position of the phosphinine. We therefore considered the reaction of phosphinine **6**, which contains Me_3Si substituents at the 3,5-positions of the ring, with $B(C_6F_5)_3$ in CH_2Cl_2 at room temperature. Compound **6** was recently reported by us and its gas phase basicity was calculated to be higher than that of unsubstituted phosphinine C_5H_5P, but lower than for **5**, which contains Me_3Si groups at the 2,6-positions.[14]

Nevertheless, we were delighted to detect only one signal in the $^{31}P\{^1H\}$ NMR spectrum of the reaction mixture, which is shifted upfield with respect to the starting material ($\delta = 176.6$ vs. 206.4 ppm). The ^1H, ^{19}F and ^{11}B NMR spectra also indicate the successful and quantitative conversion of **6** to the phosphinine–borane adduct **6**-$B(C_6F_5)_3$ (Scheme 3b).

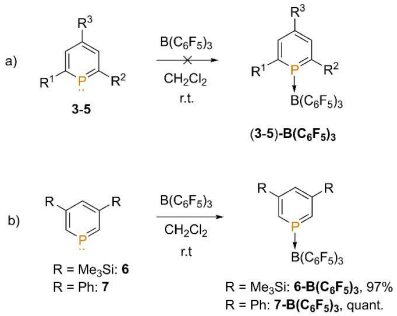

Scheme 3. Reaction of phosphinines **3**–**5** with $B(C_6F_5)_3$.

We considered that the high Lewis acidity of $B(C_6F_5)_3$ might also allow the formation of adducts with less basic phosphinines, such as 3,5-diphenylphosphinine (**7**). Gratifyingly, the quantitative formation of **7**-$B(C_6F_5)_3$ was also observed upon reaction of **7** with $B(C_6F_5)_3$ in CH_2Cl_2 at room temperature ($^{31}P\{^1H\}$ NMR: $\delta = 182.7$ ppm). As already anticipated, these results clearly show that steric factors play a significant role in the interaction between phosphinines and boranes with strong Lewis acidic properties.

Crystals of **6**-$B(C_6F_5)_3$, suitable for X-ray diffraction, were obtained by slow evaporation of a solution of the phosphinine–borane adduct in a mixture of dichloromethane and *n*-pentane and the molecular structure of the first crystallographically characterized phosphinine-borane adduct, along with selected bond lengths, angles and distances are depicted in Figure 3.

The P(1)–B(1) distance of 2.042 Å is shorter than in the corresponding triphenylphosphine adduct $Ph_3P{\rightarrow}B(C_6F_5)_3$ (2.181 Å).[19] Figure 3 clearly shows that sterically demanding substituents in the α-position of the phosphorus heterocycle, such as Me_3Si or Ph groups, would indeed prevent any adduct formation. Interestingly, a closer look at the solid-state structure of **6**-$B(C_6F_5)_3$ reveals that F(5) is located directly above the phosphorus atom. One of the electron lone pair of F(5) points directly towards the LUMO of the phosphinine, while the distance between F(5) and P(1) is 2.868 Å, which is shorter than the sum of the van der Waals radii (3.34 Å).[20] Additionally, the boron-phosphorus bond is slightly tilted out of the plane of the phosphinine ring (Figure 3b). These observations could indicate a significant fluorine–phosphorus interaction, which might stabilize the adduct further. However, the NMR spectra do not show such an interaction at room temperature nor at $T = -70\,^{\circ}C$, as all *ortho*-fluorine atoms remain magnetically equivalent.

In order to gain more insight into a possible interaction between P(1) and F(5), the electron density distributions were calculated for **6**-$B(C_6F_5)_3$, and the results are depicted in Figure 4 as Laplacian plots through the atoms P(1), B(1) and F(5). This indicates that a bond-critical point (red arrow) can be detected between P(1) and F(5), however, the value of 0.098 e Å^{-3} is very low. In comparison, the value for the bond critical point between P(1) and B(1) is 0.678 e Å^{-3}. We therefore suggest that the presence of a bond-critical point between P(1) and F(5) should not be over interpreted.

Instead, we propose on the basis of the calculations and the charges of the atoms that the fluorine–phosphorus interaction can rather be attributed as an electrostatic effect. This is best visualized in the electrostatic potential plot of **6**-$B(C_6F_5)_3$, in which the green, negatively polarized fluorine atom (F5) is directly positioned above the red, positively polarized phosphorus atom (Figure 5, left). For comparison, the electrostatic potential plot of the pyridine–$B(C_6F_5)_3$ adduct was also calculated (Figure 5 right). In this case, a higher electron density can be observed at the heteroatom of the ring due to the higher electronegativity of nitrogen, compared to phosphorus. Consequently, the fluorine atom is positioned above the C–N

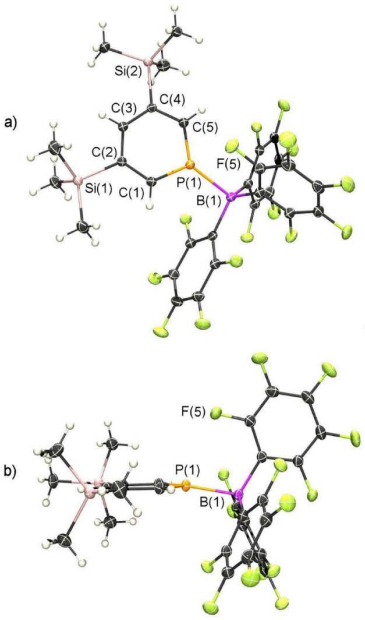

Figure 3. a) Top and b) side views of the Molecular structure of **6**-$B(C_6F_5)_3$ in the crystal. Displacement ellipsoids are shown at the 50% probability level. Selected bond lengths [Å] and angles [°]: P(1)–B(1): 2.0415(12); P(1)–C(1): 1.7046(11); P(1)–C(5) 1.1.7082(10); P(1)···F(5) 2.8679(8); C(1)–P(1)–C(5): 106.87(5); B(1)–P(1)–C(3): 168.36(4); Σ(C–B–C): 338.14(9).

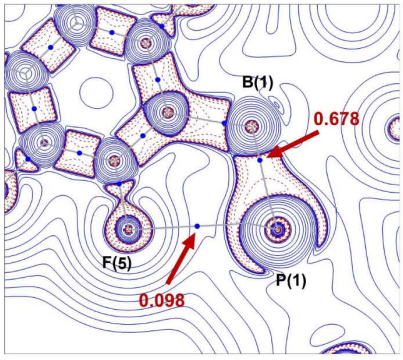

Figure 4. 2D contour plot of the Laplacian of the electron density $\nabla^2\rho(r)$ in the P(1)–B(1)–F(5) plane of **6**-$B(C_6F_5)_3$. Red dashed contours indicate regions of local charge accumulation ($\nabla^2\rho(r) < 0$); Blue contours indicate regions of local charge depletion ($\nabla^2\rho(r) > 0$). Bond paths are shown as gray lines. Bond critical points (BCPs) shown as blue dots. The red arrows indicate the electron density $\rho(r)$ [e A^{-3}] for the BCPs.

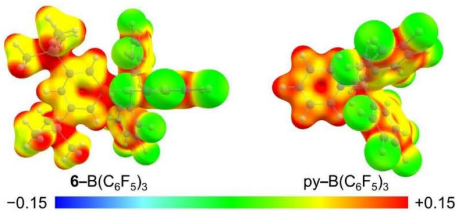

Figure 5. Electrostatic potential of **6**-$B(C_6F_5)_3$ (left) and pyridine-$B(C_6F_5)_3$ (right) calculated at the B3LYP-D3(BJ)/def2-TZVPP level of theory. The electrostatic potential [a.u.] is mapped onto electron density isosurfaces of 0.02 e au^{-3}.

bond. The $B(C_6F_5)_3$ moiety shows the expected propeller-like geometry with no unusually short N–F contacts.

As expected, we found that the phosphorus-boron interaction in such Lewis pairs is rather weak, due to the low basicity and nucleophilicity of the aromatic phosphorus heterocycle (see above). The calculated bond dissociation enthalpy for the reaction $LB + B(C_6F_5)_3 \rightarrow LB–B(C_6F_5)_3$ (LB = Lewis base) is $\Delta H° = -54.9\ kJ \cdot mol^{-1}$ for **6**-$B(C_6F_5)_3$, which is almost half the value obtained for the triphenylphosphine adduct $Ph_3P–B(C_6F_5)_3$ ($\Delta H° = -110.2\ kJ \cdot mol^{-1}$).

Based on our observations and due to the strong polarization of the phosphorus heterocycle caused by the interaction with the Lewis acid, we anticipated that **6**-$B(C_6F_5)_3$ might exhibit a pronounced reactivity particularly towards unsaturated substrates. Previous studies have shown that activated alkynes can react with certain phosphinines, phosphinine–metal complexes, 1-methylphosphininium salts, phosphinine-sulfides and phosphinine-selenides to form 1-phosphabarrelene derivatives.[14,21–23] This orbital controlled [4+2] cycloaddition reaction proceeds by a 1,4-addition of the dienophile across the phosphorus heterocycle. Again, this process is facilitated by increasing the polarization of the aromatic phosphinine, for example, by P coordination to a metal center or by oxidation to a formal P(V) derivative. In this respect, we first considered the reaction between **6**-$B(C_6F_5)_3$ and the less reactive phenylacetylene. So far, no 1-phosphabarrelene derivatives, generated from this dienophile and the corresponding phosphorus heterocycle, have been reported to date. Much to our delight, upon addition of excess PhC≡CH, we could observe a quantitative and selective reactivity at room temperature to a new compound (**9**) after 100 min. The product shows a single resonance at $\delta = -18.3$ ppm in the $^{31}P\{^1H\}$ NMR spectrum. However, its analysis by high resolution mass spectrometry indicates that **9** is not only a simple borane adduct of a 1-phosphabarrelene. The crystallographic characterization reveals that next to a regioselective cycloaddition of phenylacetylene to the phosphinine ring, a further insertion of PhC≡CH into the P→B bond occurred and the zwitterionic alkenyl-phosphabarrelenium borate salt **9** had been formed (Scheme 4 and Figure 6).

The regioselective activation of terminal alkynes both by frustrated and classical Lewis acid/phosphine pairs has been

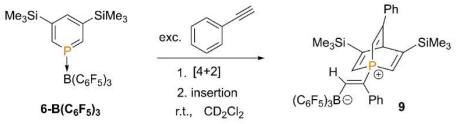

Scheme 4. Reaction of **6**-$B(C_6F_5)_3$ with excess phenylacetylene.

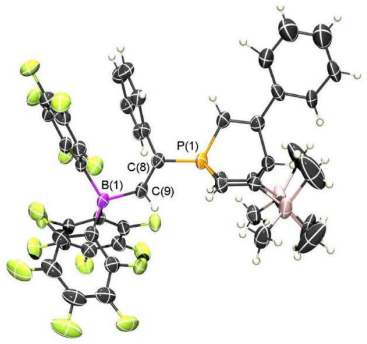

Figure 6. Molecular structure of **9** in the crystal. Displacement ellipsoids are shown at the 50 % probability level for one orientation of the 1-phosphabarrelene moiety. Selected bond lengths [Å]: P(1)–C(8): 1.767(4); C(8)–C(9): 1.344(6); C(9)–B(1): 1.626(6).

reported in literature before. Nevertheless, the formation of phosphonium alkynyl borate salts (R_3PH^+ $PhC{\equiv}C–B(C_6F_5)_3^-$) is also observed in this case, resulting from deprotonation of the alkyne by the basic phosphine.[24] By performing the reaction of **6**-$B(C_6F_5)_3$ with PhC≡CH in a 1:1 ratio, additional information on the mechanism of the product formation could be obtained. Figure 7 shows the $^{31}P\{^1H\}$ NMR spectra of the reaction mixture at $t = 10$ and 80 min after addition of the alkyne to the phosphinine–borane adduct.

Interestingly, a transient intermediate (**8**) can be observed during the course of the reaction, which fully converts to **9** when access phenylacetylene is applied. In the 1:1 reaction, the ratio between the starting material **6**-$B(C_6F_5)_3$, **8** and the product

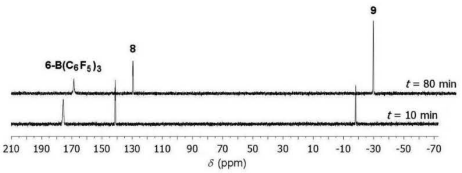

Figure 7. $^{31}P\{^1H\}$ NMR spectra for the reaction of **6**-$B(C_6F_5)_3$ with PhC≡CH at a 1:1 ratio.

9 remains constant after $t = 80$ min. The chemical shift of **8** at $\delta = 140.0$ ppm in the $^{31}P\{^1H\}$ NMR spectrum is characteristic for a phosphininium salt (see below). We therefore anticipate that intermediate **8** is a zwitterionic alkenyl-phosphininium borate salt, which is first generated by insertion of PhC≡CH into the dative P→B bond (Scheme 5). Intermediate **8** further reacts rapidly in a [4 + 2] cycloaddition reaction with PhC≡CH to form the final product **9** (Scheme 5). As a matter of fact, 1-*R*-phosphininium salts readily react with alkynes to 1-*R*-phosphabarrelenium salts even at low temperature.[22d,25] Cycloaddition reactions at highly polarized Te/B-heterocycles have also been observed by Stephan et al.[26] By means of ^{31}P NMR spectroscopy we can further rule out that **8** is the 1-*H*-phosphininium salt, which might be generated by deprotonation of phenylacetylene.

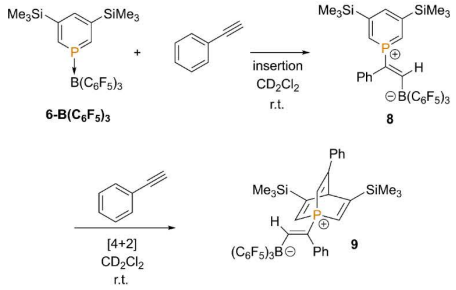

Scheme 5. Reaction of **6**-$B(C_6F_5)_3$ with excess phenylacetylene.

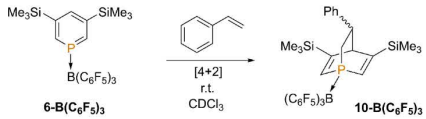

Scheme 6. Reaction of **6**-$B(C_6F_5)_3$ with styrene.

As cycloaddition reactions of C=C double bonds to six-membered aromatic phosphorus heterocycles are unprecedented in the literature, we subsequently treated **6**-$B(C_6F_5)_3$ with styrene (Scheme 6).

Again, we could observe the rapid, quantitative and selective conversion of **6**-$B(C_6F_5)_3$ to a new product, which shows a single resonance at $\delta = -38.0$ ppm in the $^{31}P\{^1H\}$ NMR spectrum. Crystals of the product, suitable for X-ray diffraction were obtained by slow evaporation of the solvent. The result of the X-ray crystal structure analysis is depicted in Figure 8 along with selected bond lengths and angles and unambiguously confirms that a racemic mixture of the cycloaddition product **10**-$B(C_6F_5)_3$ had been formed. This compound represents the first example of a dihydro-1-phosphabarrelene derivative. It is interesting to note that only one regioisomer is formed in the conversion of **6**-$B(C_6F_5)_3$ with styrene. In **10**-$B(C_6F_5)_3$, the phenyl group of the former styrene substrate is pointing away from the $B(C_6F_5)_3$ moiety, most likely due to steric effects during the [4 + 2] cycloaddition step, as this reaction is orbital controlled.[22,23]

Motivated by these initials results, we attempted to apply **6**-$B(C_6F_5)_3$ in typical frustrated Lewis-pair reactions.[27] As styrene derivatives react with diaryl-substituted esters in the presence of the FLP system $R_3P/B(C_6F_5)_3$ to form substituted olefins, we decided to treat **6**-$B(C_6F_5)_3$ first with ester **11** (Scheme 7).[28]

Much to our surprise, the reaction of **6**-$B(C_6F_5)_3$ with **11** in $CDCl_3$ proceeds instantaneously. The NMR spectroscopic analysis of the reaction mixture reveals again the selective and quantitative formation of a single, new species. This compound shows a resonance at $\delta = 156.8$ ppm in the ^{31}P NMR spectrum, which is corroborated in the corresponding ^1H NMR spectrum with a coupling constant of $^2J_{P,H} = 27.0$ Hz to the alkyl CH. This is in line with the presence of the 1-*R*-phosphininium salt **12**, as the $^{31}P\{^1H\}$ NMR signal of the related 1-methyl-phosphininium cation can be observed at $\delta = 160.2$ ppm.[9,21] Most intriguingly,

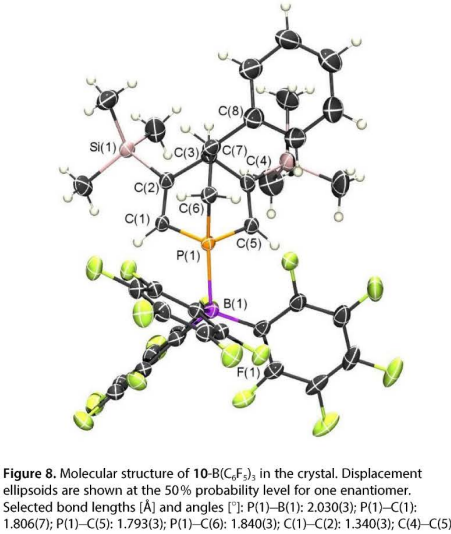

Figure 8. Molecular structure of **10**-$B(C_6F_5)_3$ in the crystal. Displacement ellipsoids are shown at the 50% probability level for one enantiomer. Selected bond lengths [Å] and angles [°]: P(1)–B(1): 2.030(3); P(1)–C(1): 1.806(7); P(1)–C(5): 1.793(3); P(1)–C(6): 1.840(3); C(1)–C(2): 1.340(3); C(4)–C(5): 1.341(4); C(6)–C(7): 1.559(4). C(1)–P(1)–C(5): 100.21(12); C(1)–P(1)–C(6): 98.04(12); C(5)–P(1)–C(6): 100.54(12).

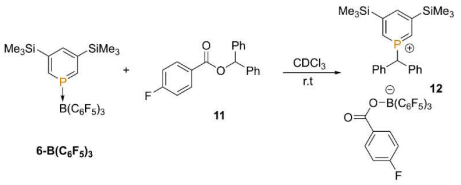

Scheme 7. Study of the reactivity of **6**-$B(C_6F_5)_3$ towards ester **11**.

phosphininum salts can currently only be prepared in a multistep synthesis, or alternatively, with the very strong methylation reagent $[(CH_3)_2Cl]^-[Al(OTeF_5)_4]^-$ due to the low nucleophilicity of the phosphorus atom (see above, Figure 1).[9,21,29] Our first results, depicted in Scheme 8, thus impressively show that various novel phosphininium salts might be easily formed by making use of phosphinine–borane adducts in combination with aromatic alkyl esters. To this end, 1-*R*-phosphininium salts can be generated and further explored, which are otherwise synthetically inaccessible. However, at this point, we do not have any insight into the reaction mechanism of this surprisingly fast quaternization reaction, which can occur either through a single-electron (radical) or a two-electron transfer mechanism during the C–O bond scission reaction.[28]

Subsequently, we added styrene to **11** and observed again the spontaneous formation of a single species, which shows a signal at $\delta = -6.4$ ppm in the $^{31}P\{^1H\}$ NMR spectrum. The same immediate reactions occurs, when **6** was mixed with $B(C_6F_5)_3$, **11** and styrene in an equimolar ratio with $CHCl_3$ as solvent. However, we could not detect any signals of the substituted olefin **13** by means of ^1H NMR spectroscopy (Scheme 8).

Crystals, suitable for X-ray diffraction were obtained of the reaction product **14** by slow evaporation of the solvent. The result of the X-ray crystal structure analysis is depicted in Figure 8 along with selected bond lengths and angles.

Interestingly, crystallographic characterization of **14** (Figure 9) reveals the first example of a dihydro-1-*R*-phosphabarrelenium salt. The compound forms by a fast and regioselective [4 + 2] cycloaddition of styrene to the aromatic 1-*R*-phosphininium heterocycle. It should be mentioned that the reaction of a related 1-methyl-1-phospha-7-bora-norbornadiene with phenylacetylene has recently been described by us.[30]

Finally, we also converted rapidly, quantitatively and selectively a mixture of **6**, ester **11** and $Me_3Si{-}C{\equiv}CH$ towards the corresponding 1-*R*-phosphabarrelenium salt **15** (Scheme 8), which we could also characterize crystallographically (Figure 10).

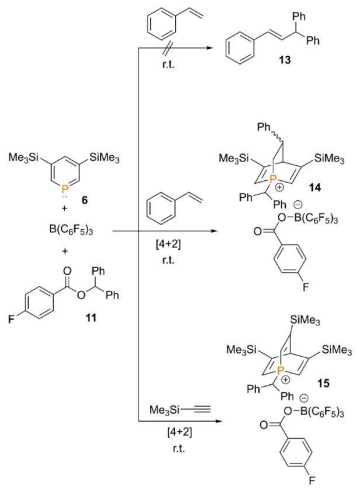

Scheme 8. Reaction of **6** with $B(C_6F_5)_3$, ester **11**, styrene and TMS-acetylene.

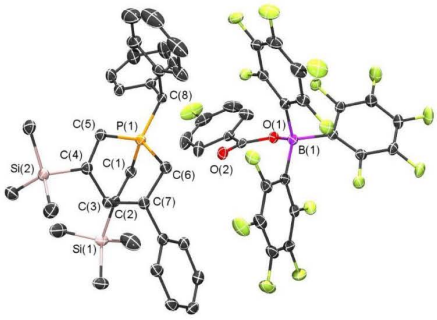

Figure 9. Molecular structure of **14** in the crystal. Displacement ellipsoids are shown at the 50% probability level. Hydrogen atoms and co-crystallized THF are omitted for clarity. Selected bond lengths [Å]: P(1)–C(1): 1.783(2); P(1)–C(8): 1.8199(19); P(1)–C(5): 1.779(2); P(1)–C(6): 1.821(2); C(1)–C(2): 1.347(3); C(2)–C(3): 1.525(3); C(3)–C(4): 1.533(3); C(4)–C(5): 1.341(3); B(1)–O(1): 1.514(2).

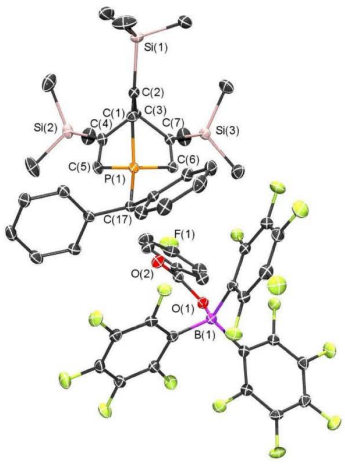

Figure 10. Molecular structure of **15** in the crystal. Displacement ellipsoids are shown at the 50% probability level. Hydrogen atoms are omitted for clarity. Selected bond lengths [Å] and angles [°]: P(1)–C(17): 1.8235(19); P(1)–C(1): 1.7951(19); P(1)–C(5): 1.7873(19); P(1)–C(6): 1.792(2); C(1)–C(2): 1.342(3); C(2)–C(3): 1.558(3); C(4)–C(5): 1.339(3); C(6)–C(7): 1.338(3); B(1)–O(1): 1.510(2). C(5)–P(1)–C(6): 100.35(9); C(5)–P(1)–C(1): 99.68(9); C(1)–P(1)–C(6): 101.00(9).

Conclusion

In conclusion, we could demonstrate that the equilibrium of the reaction between 2,4,6-triphenylphosphinine and B_2H_6 is almost exclusively located on the side of the starting materials, even at low temperature. In contrast, more basic Me_3Si-substituted phosphinines lead to a shift of the equilibrium towards the products, although complete conversion to phosphinine–borane adducts is still not achieved. This demonstrates that Me_3Si-substituted phosphinines are still rather weak Lewis bases. Moreover, hydroboration of the P=C double bond is observed with B_2H_6, which presumably leads to the formation of polymeric species. The use of the much stronger, yet more sterically demanding, Lewis acid $B(C_6F_5)_3$ reveals a strong influence of the α substituents of the aromatic phosphorus heterocycle on the formation of a discrete adduct. Phosphinines with Ph or Me_3Si substituents in the *ortho* position of the phosphinine prevent any reaction with $B(C_6F_5)_3$, whereas 3,5-bis(trimethylsilyl)phosphinine as well as 3,5-diphenylphosphinine undergo complete conversion to the phosphinine–borane adduct. In the case of 3,5-bis(trimethylsilyl)phosphinine, the product could be characterized crystallographically. The solid-state structure reveals an interaction between the phosphorus atom and one of the fluorine atoms of the Lewis acid; this is supported by theoretical calculations. We could further highlight that the novel phosphinine–borane adduct shows distinct insertion and subsequent [4+2] cycloaddition reactivity towards phenylacetylene. This results in a zwitterionic alkenyl-phosphabarrelenium borate salt that is formed selectively and quantitatively. With styrene, the borane adduct of a dihydrophosphabarrelene is formed. In the presence of an ester, the Lewis pair forms 1-*R*-phosphininium salts. This route significantly improves upon the previous multistep synthesis, as this procedure is performed at room temperature in a fast, facile, and selective manner. The cationic heterocycle was then shown to readily undergo a [4+2] cycloaddition reaction with styrene ultimately forming the first example of a dihydro-1-*R*-phosphabarrelenium salt. The [4+2] cycloaddition of the 1-*R*-phosphininium salt generated in situ with TMS-acetylene quantitatively affords the corresponding 1-*R*-phosphabarrelenium salt. The results presented herein highlight how the phosphinine–borane adduct **6**-$B(C_6F_5)_3$ apparently mimics frustrated Lewis-pair reactivity. Our results provide fascinating new perspectives for the future, particularly with respect to the activation of small molecules and the synthesis of adducts of phosphinines with other main group elements and compounds. Experiments in this direction are currently being pursued in our laboratories.

Experimental Section

Experimental details are given in the Supporting Information.

Deposition Numbers 2067304 (for **6**-$B(C_6F_5)_3$), 2121299 (for **9**), 2067303 (for **13**) and 2121300 (for **14**) contain the supplementary crystallographic data for this paper. These data are provided free of charge by the joint Cambridge Crystallographic Data Centre and Fachinformationszentrum Karlsruhe Access Structures service.

Acknowledgements

Funding by the Freie Universität Berlin and the Deutsche Forschungsgemeinschaft DFG (project no. 2100302201) is gratefully acknowledged. The authors thank the Scientific Computing Service of the Freie Universität Berlin (https://doi.org/10.17169/refubium-26754) for the use of high-performance computing resources. Dr. Stephen Argent is thanked for his input on the solution of compound **9**. Open Access funding enabled and organized by Projekt DEAL.

Conflict of Interest

The authors declare no conflict of interest.

Data Availability Statement

The data that support the findings of this study are available in the supplementary material of this article.

Keywords: crystallography · density functional calculations · heterocycles · phosphinine · phosphorus

[1] J. M. Brunel, B. Faure, M. Maffei, *Coord. Chem. Rev.* **1998**, *178–180*, 665.
[2] a) A. B. Burg, R. I. Wagner, *J. Am. Chem. Soc.* **1953**, *75*, 3872; b) M. Ohff, J. Holz, M. Quirmbach, A. Börner, *Synthesis* **1998**, 1391.
[3] See for example: a) D. W. Stephan, G. Erker, *Angew. Chem. Int. Ed.* **2015**, *54*, 6400; b) D. W. Stephan, *Science* **2016**, *354*, aaf7229-1; c) N. Li, W.-X. Zhang, *Chin. J. Chem.* **2020**, *38*, 1360.
[4] A. Staubitz, A. P. M. Robertson, M. E. Sloan, I. Manners, *Chem. Rev.* **2010**, *110*, 4023.
[5] P. Le Floch, *Coord. Chem. Rev.* **2006**, *250*, 627.
[6] a) J. Waluk, H.-P. Klein, A. J. Ashe, J. Michl, *Organometallics* **1989**, *8*, 2804; b) C. Batich, E. Heilbronner, V. Hornung, A. J. Ashe, D. T. Clark, U. T. Cobley, D. Kilcast, I. Scanlan, *J. Am. Chem. Soc.* **1973**, *99*, 928.
[7] a) P. Le Floch, F. Mathey, *Coord. Chem. Rev.* **1998**, *178–180*, 771; b) N. Mézailles, F. Mathey, P. Le Floch, *Prog. Inorg. Chem.* **2001**, 455; c) P. Le Floch, *Coord. Chem. Rev.* **2006**, *250*, 627–681; d) N. T. Coles, A. S. Abels, J. Leitl, R. Wolf, H. Grützmacher, C. Müller, *Coord. Chem. Rev.* **2021**, *433*, 213729.
[8] Y. Zhang, F. S. Tham, J. F. Nixon, C. Taylor, J. C. Green, C. A. Reed, *Angew. Chem. Int. Ed.* **2008**, *47*, 3801.
[9] L. Fischer, F. Wossidlo, D. S. Frost, N. T. Coles, S. Steinhauer, S. Riedel, C. Müller, *Chem. Commun.* **2021**, *57*, 9522.
[10] S. Erhardt, G. Frenking, *Chem. Eur. J.* **2006**, *12*, 4620.
[11] K. Dimroth, *Top. Curr. Chem.* **1973**, *38*, 1.
[12] a) M. Scheibitz, J. W. Bats, M. Bolte, M. Wagner, *Eur. J. Inorg. Chem.* **2003**, 2049; b) G. Frison, F. Mathey, A. Sevin, *J. Phys. A* **2002**, *106*, 5653; c) Y. Panova, A. Khristolyubova, N. Zolotareva, V. Sushev, V. Galperin, R. Rumyantcev, G. Fukin, A. Kornev, *Dalton Trans.* **2021**, *50*, 5890.
[13] a) M. H. Habicht, F. Wossidlo, M. Weber, C. Müller, *Chem. Eur. J.* **2016**, *22*, 12877; b) M. H. Habicht, F. Wossidlo, T. Bens, E. A. Pidko, C. Müller, *Chem. Eur. J.* **2018**, *24*, 944.
[14] F. Wossidlo, N. T. Coles, S. Steinhauer, T. Böttcher, C. Müller, *Chem. Eur. J.* **2021**, *27*, 12788.
[15] N. Avarvari, P. Le Floch, F. Mathey, *J. Am. Chem. Soc.* **1996**, *118*, 11978.
[16] A. S. Ionkin, S. N. Ignatév, V. M. Nekhoroshkov, J. J. Efremov, B. A. Arbuzov, *Phosphorus Sulfur Silicon Relat. Elem.* **1990**, *53*, 1.
[17] L. V. Ermolaeva, A. S. Ionkin, *J. Mol. Struct.* **1992**, *276*, 25.

[18] M. Yoshifuji, H. Takahashi, K. Toyota, *Heteroat. Chem.* **1999**, *10*, 187.
[19] H. Jacobsen, H. Berke, S. Döring, G. Kehr, G. Erker, R. Fröhlich, O. Meyer, *Organometallics* **1999**, *18*, 1724.
[20] M. Mantina, A. C. Chamberlin, R. Valero, C. J. Cramer, D. G. Truhlar, *J. Phys. Chem. A* **2009**, *113*, 5806.
[21] A. Moores, L. Ricard, P. Le Floch, *Angew. Chem.* **2003**, *115*, 5090.
[22] a) G. Märkl, F. Lieb, *Angew. Chem. Int. Ed.* **1968**, *7*, 733; b) N. Mézailles, L. Ricard, F. Mathey, P. Le Floch, *Eur. J. Inorg. Chem.* **1999**, 2233; c) E. Fuchs, M. Keller, B. Breit, *Chem. Eur. J.* **2006**, *12*, 6930; d) A. Moores, T. Cantat, L. Ricard, N. Mézailles, P. Le Floch, *New J. Chem.* **2007**, *31*, 1493; e) M. Rigo, E. R. M. Habraken, K. Bhattacharyya, M. Weber, A. W. Ehlers, N. Mézailles, J. C. Slootweg, C. Müller, *Chem. Eur. J.* **2019**, *25*, 8769.
[23] M. Bruce, M. Papke, A. W. Ehlers, M. Weber, D. Lentz, N. Mézailles, J. C. Slootweg, C. Müller, *Chem. Eur. J.* **2019**, *25*, 14332.
[24] a) M. A. Dureen, D. W. Stephan, *J. Am. Chem. Soc.* **2009**, *131*, 8396; b) M. A. Dureen, C. C. Brown, D. W. Stephan, *Organometallics* **2010**, *29*, 6594.
[25] F. Wossidlo, *Ph.D. thesis*, Freie Universität Berlin (Germany), **2021**.
[26] For cycloaddition/cycloreversions at Te/B-heterocycles see: F. A. Tsao, L. Cao, S. Grimme, D. W. Stephan, *J. Am. Chem. Soc.* **2015**, *137*, 13264.
[27] a) D. W. Stephan, *Acc. Chem. Res.* **2015**, *48*, 306; b) T. C. Johnstone, G. N. J. H. Wee, D. W. Stephan, *Angew. Chem. Int. Ed.* **2018**, *57*, 5881.
[28] a) Y. Soltani, A. Dasgupta, T. A. Gazis, D. M. C. Ould, E. Richards, B. Slater, K. Stefkova, V. Y. Vladimirov, L. C. Wilkins, D. Willcox, R. L. Melen, *Cell Rep. Phys. Sci.* **2020**, 100016, 1; b) A. Dasgupta, K. Stefkova, R. Rabaahmadi, B. F. Yates, N. J. Buurma, A. Ariafard, E. Richards, R. L. Melen, *J. Am. Chem. Soc.* **2021**, *143*, 4451.
[29] T. N. Dave, H. Kaletsch, K. Dimroth, *Angew. Chem. Int. Ed. Engl.* **1984**, *23*, 989.
[30] J. Leitl, A. R. Jupp, E. R M. Habraken, V. Streitferdt, P. Coburger, D. J. Scott, R. M. Gschwind, C. Müller, J. C. Slootweg, R. Wolf, *Chem. Eur. J.* **2020**, *26*, 7788.

Manuscript received: November 17, 2021
Accepted manuscript online: December 30, 2021
Version of record online: January 20, 2022

Chemistry–A European Journal

Supporting Information

Borane Adducts of Aromatic Phosphorus Heterocycles: Synthesis, Crystallographic Characterization and Reactivity of a Phosphinine-$B(C_6F_5)_3$ Lewis Pair

Jinxiong Lin, Friedrich Wossidlo., Nathan T. Coles, Manuela Weber, Simon Steinhauer, Tobias Böttcher,* and Christian Müller*

Table of Contents

1. DFT Calculations

DFT calculations

The quantum chemical calculations were performed with TURBOMOLE 7.5[1] using the B3LYP[2] functional with def2-TZVPP[3] basis set and D3[4](BJ)[5] dispersion correction. Vibrational frequencies were calculated using the AOFORCE[6] module. All optimized structures represent true minima without imaginary vibrational frequencies. The calculations of the electrostatic potential plot and the QTAIM analysis on **6-B(C_6F_5)$_3$** were performed using the non-hydrogen atom coordinates obtained by the crystal structure determination and using reoptimized coordinates for the hydrogen atoms on the B3LYP-D3(BJ)/def2-TZVPP level of theory. The wfn file was generated with TURBOMOLE from this structure. QTAIM calculations were carried out using the MultiWFN 3.6 program package.[7] The electrostatic potential plots were created using the Chemcraft 1.8 program package.[8]

Table S1. Energies used to calculate $\Delta H°$. E_{vrt} = sum of translational, rotational and vibrational energy including zero point energy.

Compound (symmetry)	E_{SCF} [H]	E_{vrt} [kJ mol^{-1}]	$H°$ [kJ mol^{-1}]
6 (C_s)	−1352.08854560	805.01	−3549100.31
Ph_3P (C_3)	−1036.16407705	760.12	−2719685.67
$B(C_6F_5)_3$ (D_3)	−2208.35807223	480.05	−5797560.49
6-$B(C_6F_5)_3$ (C_1)	−3560.46951909	1292.72	−9346715.74
Ph_3P-$B(C_6F_5)_3$ (C_3)	−3244.56724693	1250.84	−8517356.37

2. Experimental Procedures

General Remarks

All reactions were performed under argon in oven-dried glassware using modified Schlenk techniques unless otherwise stated. All common solvents and chemicals were commercially available and were used without further purification. All dry or deoxygenated solvents were prepared using standard techniques or were used from a MBraun solvent purification system. Diborane[9], 1-methyl-phosphininium salt (**2**-CH_3)[10] 2,4,6-triphenylphosphinine (**3**)[11], 2-trimethylsilylphosphinine (**4**)[12], 2,6-bis(trimethylsilyl)phosphinine (**5**)[13], 2,3,5,6-tetrakis(trimethyl-silyl)phosphinine[13], 3,5-diphenylphosphinine (**7**)[14] and benzhydryl 4-fluorobenzoate (**11**)[15] were prepared according to literature procedures.

The ^{1}H, $^{1}H\{^{11}B\}$, ^{11}B, ^{19}F, $^{13}C\{^{1}H\}$, $^{29}Si\{1H\}$, $^{31}P\{^{1}H\}$ and ^{31}P NMR spectra were recorded on a JEOL ECX400 (400 MHz), Bruker Avance600 (600 MHz) and Bruker Avance700 (700 MHz) spectrometer and all chemical shifts are reported relative to the residual resonance in the deuterated solvents. The APCI-Quadrupole-Mass spectrometry measurements were performed on an expressionL, *Advion*. High resolution mass spectrometry (HRMS) was performed on a Agilent 6210 ESI-TOF. Element analyses were performed on a VARIO EL, *Elementar*.

3,5-Bis(trimethylsilyl)phosphinine (6)

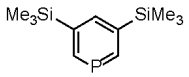

6 was prepared using a modified literature procedure.[13] $HCl{\cdot}Et_2O$ (2 M, 0.6 mL, 1.2 mmol, 4.8 eq.) was added to 2,3,5,6-tetrakis(trimethylsilyl)phosphinine (97 mg, 0.25 mmol, 1 eq.) in diethyl ether (2.4 mL) and was stirred at room temperature overnight. After removal of the solvent in vacuum, the crude product was filtrated over a short silica plug with *n*-pentane (20 mL) as the eluent. The product **5** was isolated as colorless liquid (45 mg, 0.19 mmol, 76%).

^{1}H NMR (401 MHz, Dichlormethane-d_2): δ = 9.02 (dd, $^{2}J_{H,P}$ = 38.4 Hz, $^{4}J_{H,H}$ = 0.8 Hz, 2H, *ortho*-H), 7.92 (dt, $^{4}J_{H,P}$ = 3.7 Hz, $^{4}J_{H,H}$ = 0.8 Hz, 1H, *para*-H), 0.32 (s, 18H, -$SiMe_3$) ppm.

$^{13}C\{^{1}H\}$ NMR (101 MHz, Dichlormethane-d_2): δ = 160.5 (d, $^{1}J_{C,P}$ = 56.8 Hz), 146.0 (d, $^{3}J_{C,P}$ = 12.4 Hz), 138.0 (d, $^{2}J_{C,P}$ = 25.0 Hz), -1.2 (s) ppm.

$^{29}Si\{^{1}H\}$ NMR (80 MHz, Dichlormethane-d_2): δ = -1.9 (d, $^{3}J_{Si,P}$ = 3.7 Hz) ppm.

^{31}P NMR (162 MHz, Dichlormethane-d_2): δ = 200.3 (td, $J_{H,P}$ = 38.4, 3.7 Hz) ppm.

LRMS: APCI (m/z). Calculated $[M+H]^+$: 241.1, Observed: 241.1.

Elemental analysis: Calculated for $C_{11}H_{21}PSi_2$: C 54.95%, H 8.80%, Observed: C 54.59%, H 8.84%.

General method: diborane addition to phosphinines

The corresponding phosphinine were dissolved in dichloromethane-d_2 (0.7 mL) and the solution degassed *via* freeze-pump-thaw. After addition of diborane *via* condensation the samples were warmed up to T = -78 °C and NMR spectra were recorded at low temperature (T = -70 °C).

A) 2,4,6-Triphenylphosphinine borane adduct (3-BH_3)

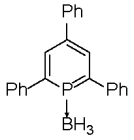

2,4,6-Triphenylphosphinine (**3**, 28 mg, 86 µmol), phosphinine:BH_3 = 1:4, conversion: 4%.

$^{31}P\{^1H\}$ NMR (162 MHz, Dichlormethane-d_2, T = -70 °C): δ = 167.8 (s) ppm.

B) 2-Trimethylsilylphosphinine borane adduct (4-BH_3)

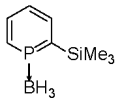

2-Trimethylsilylphosphinine (**4**, 98 mg, 0.58 mmol), phosphinine:BH_3 = 1:1, conversion: 88%.

^1H NMR (401 MHz, Dichlormethane-d_2): δ = 8.36 (dd, $J_{H,P}$ = 18.1 Hz, $J_{H,H}$ = 10.2 Hz, 1H), 8.16 (dd, $J_{H,P}$ = 26.6 Hz, $J_{H,H}$ = 8.2 Hz, 1H), 7.99 (ddd, $J_{H,P}$ = 21.6 Hz, $J_{H,H}$ = 10.1, 8.4 Hz, 1H), 7.55 (q, $J_{H,P}$ = 7.3 Hz, $J_{H,H}$ = 7.3 Hz, 1H), 1.59 (q, $^1J_{H,B}$ = 104.6 Hz, 3H, -B*H*$_3$), 0.45 (s, 9H, -*TMS*) ppm.

^{11}B NMR (128 MHz, Dichlormethane-d_2): δ = -35.3 (qd, $^1J_{H,B}$ = 104.8 Hz, $^1J_{B,P}$ = 25.1 Hz) ppm.

$^{31}P\{^1H\}$ NMR (162 MHz, Dichlormethane-d_2): δ = 209.4 (d, $^1J_{B,P}$ = 25.6 Hz) ppm.

C) 2,6-Bis(trimethylsilyl)phosphinine borane adduct (5-BH_3)

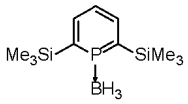

2,6-Bis(trimethylsilyl)phosphinine (**5**, 122 mg, 0.51 mmol), phosphinine:BH_3 = 1:1.3, conversion: 98%.

$^1H\{^{11}B\}$ NMR (401 MHz, Dichlormethane-d_2): δ = 8.11 (dd, $^3J_{H,P}$ = 25.6 Hz, $^3J_{H,H}$ = 8.1 Hz, 2H, *meta*-H), 7.46 (q, $^4J_{H,P}$ = 7.7 Hz, $^3J_{H,H}$ = 7.7 Hz, 1H, *para*-H), 1.66 (d, $^2J_{H,P}$ = 20.0 Hz, 3H, -BH_3), 0.45 (s, 18H, -*TMS*) ppm.

^{11}B NMR (128 MHz, Dichlormethane-d_2): δ = -34.3 (q, $^{1}J_{H,B}$ = 96.0 Hz) ppm.

^{13}C{^{1}H} NMR (101 MHz, Dichlormethane-d_2): δ = 154.2 (d, $J_{C,P}$ = 17.4 Hz), 143.2 (d, $J_{C,P}$ = 18.6 Hz), 126.4 (d, $J_{C,P}$ = 45.3 Hz), -0.1 (d, $J_{C,P}$ = 2.8 Hz) ppm.

^{29}Si{^{1}H} NMR (79 MHz, Dichlormethane-d_2): δ = 1.1 (d, $^{2}J_{Si,P}$ = 16.7 Hz) ppm.

^{31}P{^{1}H} NMR (162 MHz, Dichlormethane-d_2): δ = 226.0 (d, $^{1}J_{B,P}$ = 19.8 Hz) ppm.

2-Trimethylsilylphosphinine (4) with BH_3·SMe_2

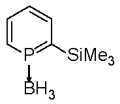

2-Trimethylsilylphosphinine (**4**, 70 mg, 0.42 mmol, 1 eq.) was dissolved in dichloromethane-d_2 (0.7 mL) and BH_3·SMe_2 (158 mg, 2.08 mmol, 5eq.) was added. The NMR spectra were recorded at room temperature and show a conversion of 21%

^{11}B NMR (128 MHz, Dichlormethane-d_2): δ = -35.3 (q, $^{1}J_{H,B}$ = 102.6 Hz) ppm.

^{31}P{^{1}H} NMR (162 MHz, Dichlormethane-d_2): δ = 208.2 (s) ppm.

Follow-up reaction of 2,6-bis(trimethylsilyl)phosphinine borane adduct (5(H)-BH_2)

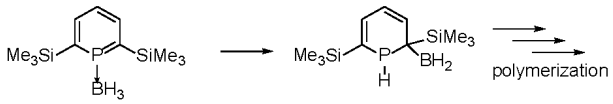

A sample of 2,6-bis(trimethylsilyl)phosphinine borane adduct (**5**-BH_3) was kept at room temperature after recording the NMR spectra. After the formation of a colorless viscous oil (one day) an NMR spectrum was recorded.

^{31}P{^{1}H} NMR (162 MHz, Dichlormethane-d_2): δ = -21.4 (s) ppm.

After an additional two weeks a pale solid precipitated, which could not be dissolved in common solvents (pentane, toluene, benzene, acetonitrile, tetrahydrofuran, dichloromethane, acetone).

A second sample stored at T = -80 °C formed a colorless solid after a week and after two months also formed a slightly yellow, insoluble solid.

General method: $B(C_6F_5)_3$ addition to phosphinines

The corresponding phosphinine (0.150 mmol, 1 eq.), $B(C_6F_5)_3$ (76.8 mg, 0.150 mmol, 1 eq.) and dichlormethane-d_2 (0.7 mL) were added to a J-Young NMR tube and NMR spectra were recorded at room temperature. If conversion was observed, crystals were grown by slow evaporation of the solvent.

A) 2,4,6-Triphenylphosphinine $B(C_6F_5)_3$ adduct (3-$B(C_6F_5)_3$)

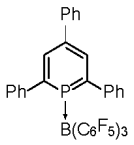

No conversion was observed.

B) 2-Trimethylsilylphosphinine $B(C_6F_5)_3$ adduct (4-$B(C_6F_5)_3$)

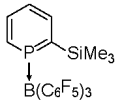

No conversion was observed.

C) 2,6-Bis(trimethylsilyl)phosphinine $B(C_6F_5)_3$ adduct (5-$B(C_6F_5)_3$)

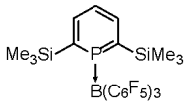

No conversion was observed.

D) 3,5-Bis(trimethylsilyl)phosphinine $B(C_6F_5)_3$ adduct (6-$B(C_6F_5)_3$)

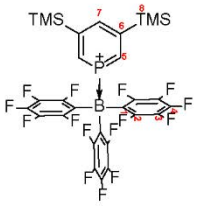

Full conversion was observed. Product **6-$B(C_6F_5)_3$** was isolated as colorless crystals (109 mg, 0.145 mmol, 97%).

^{1}H NMR (401 MHz, Dichlormethane-d_2): δ = 8.43 (d, $^2J_{H,P}$ = 22.9 Hz, 2H, *ortho*-H), 7.98 (d, $^4J_{H,P}$ = 8.5 Hz, 1H, *para*-H), 0.31 (s, 18H, -*TMS*) ppm.

^{11}B NMR (128 MHz, Dichlormethane-d_2): δ = -9.6 (s) ppm.

^{13}C{^{1}H} NMR (151 MHz, Dichlormethane-d_2) δ 154.43 (d, J = 20.8 Hz, *C6*), 148.46 (dt, $^1J_{C,F}$ = 242.6, 13.2 Hz, *C2*), 142.35 – 140.36 (m, *C4*), 140.19 (d, J = 18.1 Hz, *C5*), 138.97 (d, J = 44.9 Hz, *C7*), 138.77 – 136.76 (m, *C3*), -1.55 (s, *C8*) ppm. C1 could not be located.

^{19}F NMR (377 MHz, Dichlormethane-d_2): δ = -129.4 (s, 2F), -156.0 (t, $J_{F,F}$ = 20.1 Hz, 1F), -163.7 (t, $J_{F,F}$ = 21.8 Hz, 2F) ppm.

^{31}P{^{1}H} NMR (162 MHz, Dichlormethane-d_2): δ = 176.6 (s) ppm.

Element Analysis: calculated for $C_{29}H_{21}BF_{15}PSi_2$: C 46.29%, H 2.89%; found: 46.47%, H 3.12%.

E) 3,5-Diphenylphosphinine $B(C_6F_5)_3$ adduct (7-$B(C_6F_5)_3$)

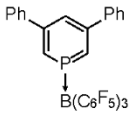

Full conversion was observed. Product **7-$B(C_6F_5)_3$** was isolated as a pale yellow solid (114 mg, 0.150 mmol, quant.).

^{1}H NMR (401 MHz, Dichlormethane-d_2): δ = 8.42 (dd, $^{2}J_{H,P}$ = 20.4 Hz, $^{4}J_{H,H}$ = 1.2 Hz, 2H, *ortho*-H), 8.08 (dt, $^{2}J_{H,P}$ = 6.5 Hz, $^{4}J_{H,H}$ = 1.4 Hz, 1H, *para*-H), 7.63 (dd, $J_{H,H}$ = 8.0, 1.3 Hz, 4H, -Ph), 7.58-7.42 (m, 6H, -Ph) ppm.

^{11}B NMR (128 MHz, Dichlormethane-d_2): δ = -5.1 (s) ppm.

^{19}F NMR (377 MHz, Dichlormethane-d_2): δ = -128.9 (d, $J_{F,F}$ = 15.1 Hz, 2F), -154.5 (t, $J_{F,F}$ = 19.1 Hz, 1F), -162.9 (td, $J_{F,F}$ = 23.6, 7.9 Hz, 2F) ppm.

^{31}P{^{1}H} NMR (162 MHz, Dichlormethane-d_2): δ = 182.7 (s) ppm.

Reaction of 5-B(C6F5)3 with Phenylacetylene (9).

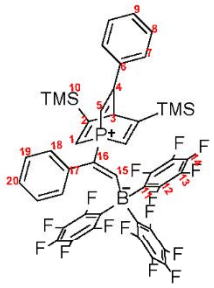

3,5-TMS-Phosphinine (12 mg, 0.05 mmol, 1.0 eq.) and tris(pentafluorophenyl)borane (25 mg, 0.05 mmol, 1.0 eq.) were mixed in DCM (0.2 mL) in a J-Young NMR tube. To the resulting colourless solution, phenylacetylene (14 mg, 0.15 mmol, 3 eq.) in DCM (0.3 ml) was added. The solvent slowly evaporated in glovebox after overnight reaction. The rest solids were washed with toluene and then dissolved in DCM for recrystallization (30 mg, 0.032 mmol, 63%).

^{1}H NMR (600 MHz, Dichlormethane-d_2): δ 8.87 (d, $^{2}J_{H,B}$ = 37.7 Hz, 1H, *CH*), 7.47 (s, 5H, *Ph*), 7.24 – 7.18 (m, 3H, *Ph*), 7.18 (dd, $^{2}J_{H,P}$ = 24.1, 1.2 Hz, 2H, PC*H*), 7.09 – 7.05 (m, 2H, *Ph*), 6.63 (dd, $^{2}J_{H,P}$ = 22.4, 2.2 Hz, 1H, PC*H*), 6.42 (q, J = 1.6 Hz, 1H, C*H*), 0.19 (s, 18H, -*TMS*) ppm.

^{11}B{^{19}F} NMR (129 MHz, Dichlormethane-d_2) δ -15.84 (d, J = 18.2 Hz) ppm.

^{11}B{^{1}H} NMR (129 MHz, Dichlormethane-d_2) δ -15.83 (d, J = 18.2 Hz) ppm.

^{11}B NMR (129 MHz, Dichlormethane-d_2) δ -15.84 (d, J = 18.3 Hz) ppm.

$^{13}C\{^1H\}$ NMR (151 MHz, Dichlormethane-d_2) δ 183.87 (dd, $^1J_{C,B}$ = 101.1, $^2J_{C,P}$ = 49.5 Hz, *C15*), 173.84 (d, $^2J_{C,P}$ = 10.1 Hz, *C2*), 168.28 (d, $^3J_{C,P}$ = 5.1 Hz, *C6*), 148.53 (d, $^1J_{C,F}$ = 237.0 Hz, *C12*), 139.94 – 138.04 (m, *C14*), 136.94 (d, $^1J_{C,F}$ = 264.9 Hz, *C13*), 136.07 (d, $^2J_{C,P}$ = 12.6 Hz, *C4*), 135.37 (d, $^2J_{C,P}$ = 15.7 Hz, *C17*), 131.68 (d, $^1J_{C,P}$ = 55.2 Hz, *C1*), 131.30 (s, *Ar*), 129.75 (s, *Ar*), 128.84 (s, *C20*), 128.73 (d, $^3J_{C,P}$ = 5.7 Hz, *C18*), 128.56 (d, $^4J_{C,P}$ = 3.1 Hz, *C19*), 126.00 (s, *Ar*), 124.57 – 123.27 (m, *C11*), 117.47 (d, $^1J_{C,P}$ = 69.7 Hz, *C16*), 113.40 (d, $^1J_{C,P}$ = 73.8 Hz, *C5*), 61.30 (s, *C3*), 60.94 (s, *C3'*), -1.70 (s, *C10*) ppm.

^{19}F NMR (377 MHz, Dichlormethane-d_2) δ -131.85 (d, $J_{F,F}$ = 23.3 Hz, 2F), -162.35 (t, $J_{F,F}$ = 20.3 Hz, 1F), -166.60 – -166.83 (m, 2F).

$^{31}P\{1H\}$ NMR (162 MHz, Dichlormethane-d_2) δ -17.14 (d, 18.0 Hz).

HRMS: ESI (m/z): Calculated: $[M]Na^+$: 979.1605, Observed: 979.1665.

Reaction of 5-$B(C_6F_5)_3$ with styrene (10-$B(C_6F_5)_3$)

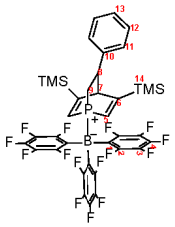

3,5-TMS-Phosphinine (12 mg, 0.05 mmol, 1.0 eq.) and tris(pentafluorophenyl)borane (25 mg, 0.05 mmol, 1.0 eq.) were mixed in DCM (0.2 ml) in a J-Young NMR tube. To the resulting colourless solution, styrene (3 eq.) in DCM (0.3 mL) was added. The solution was left to react at room temperature overnight. Once complete, all volatiles were removed under high vacuum. Crystals were acquired by slow evaporation of a DCM solution (38 mg, 0.044 mmol, 88 %). Crystals were acquired by slow evaporation of toluene solution in glovebox.

^1H NMR (700 MHz, Chloroform-d_1) δ 7.33 – 7.29 (m, 2H, -*Ph*), 7.29 – 7.23 (m, 1H, -*Ph*), 6.97 (dd, *J* = 7.9, 1.5 Hz, 2H, -*Ph*), 6.57 (d, $^2J_{H,P}$ = 32.0 Hz, 1H, PC*H*), 6.36 (d, $^2J_{H,P}$ = 33.0 Hz, 1H, PC*H*), 4.51 (dd, *J* = 2.6, 1.2 Hz, 1H, C*H*), 2.94 – 2.90 (m, 1H, PCH_2CHCH), 1.91 – 1.72 (m, 2H, CH_2), 0.25 (d, *J* = 1.1 Hz, 9H, -*TMS*), -0.26 (d, *J* = 1.1 Hz, 9H, -*TMS*) ppm.

$^{11}B\{^1H\}$ NMR (129 MHz, Chloroform-d_1) δ -16.86 ppm.

$^{13}C\{^1H\}$ NMR (176 MHz, Chloroform-d_1) δ 170.30 (d, $^2J_{C,P}$ = 9.3 Hz, *C6*), 168.47 (d, $^2J_{C,P}$ = 9.1 Hz, *C6'*), 148.64 (d, $^1J_{C,F}$ = 239.7 Hz, *C2*), 140.29 (d, $^1J_{C,F}$ = 252.5 Hz, *C4*), 137.40 (dt, $^2J_{C,P}$ = 250.9, 16.2 Hz, *C3*), 129.95 (d, $^1J_{C,P}$ = 39.1 Hz, *C5*), 129.09 (s, *Ar*), 127.93 (s, *Ar*), 127.71 (d, *J* = 2.8 Hz, *Ar*), 126.37 (s, *Ar*), 54.15 (s, *C7*), 53.85 (s, *C7'*), 40.91 (d, $^2J_{C,P}$ = 10.0 Hz, *C8*), 23.33 (d, $^1J_{C,P}$ = 29.7 Hz, *C9*), -2.11 (s, *C14*), -2.46 (s, *C14*) ppm. C1 could not be located. C10-13 could not be clearly identified due to inequivalence of the aryl groups.

^{19}F NMR (376 MHz, Chloroform-d_1) δ -130.36 (dt, $^3J_{F,F}$ = 23.8, 8.5 Hz, *o*-BCF), -155.63 (d, $^3J_{F,F}$ = 4.1 Hz, *p*-BCF), -162.90 (ddd, $^3J_{F,F}$ = 23.2, 19.8, 8.5 Hz, *m*-BCF) ppm.

$^{31}P\{^1H\}$ NMR (162 MHz, Chloroform-d_1) δ -38.12 ppm.

Element Analysis: Calculated for $C_{29}H_{21}BF_{15}PSi_2$: C 51.88 %, H 3.41 %; found: 51.36 %, H 4.01 %.

Reaction of 6-B(C_6F_5)$_3$ with benzhydryl 4-fluorobenzoate (12)

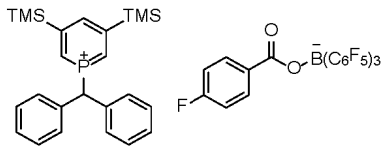

3,5-TMS-Phosphinine (24 mg, 0.1 mmol, 1.0 eq.) and tris(pentafluorophenyl)borane (51 mg, 0.1 mmol, 1.0 eq.) were mixed in Chloroform (0.2 mL) in a J-Young NMR tube. To the resulting colourless solution, benzhydryl 4-fluorobenzoate (31 mg, 0.1 mmol, 1.0 eq.) in chloroform (0.3 mL) was added and the corresponding phosphininium salt form immediately at room temperature. This compound is highly reactive and decomposes within 1 hour at room temperature. Spectroscopic yield 100%.

^1H NMR (401 MHz, Chloroform-d_1) δ 8.10 (d, $^4J_{H,P}$ = 11.1 Hz, 1H, *para*-H), 8.02 (d, $^2J_{H,P}$ = 13.2 Hz, 2H, *ortho*-H), 7.70 (dd, *J* = 8.7, 5.7 Hz, 2H, *Ar*), 7.56 – 7.48 (m, 6H, *Ar*), 7.34 (ddd, *J* = 8.4, 2.6, 1.4 Hz, 4H, *Ar*), 6.99 (d, $^2J_{H,P}$ = 26.9 Hz, 1H, PhC*H*Ph), 6.93 – 6.87 (m, 2H), 0.31 (s, 18H, *-TMS*) ppm.

^{19}F NMR (376 MHz, Chloroform-d_1) δ -112.53 (t, *J* = 7.7 Hz, *F-Ar*), -135.15 (d, $^3J_{F,F}$ = 23.4 Hz, *o*-BCF), -165.27 (d, $^3J_{F,F}$ = 19.8 Hz, *p*-BCF), -169.09 (t, $^3J_{F,F}$ = 22.1 Hz, *m*-BCF) ppm.

$^{31}P\{^1H\}$ NMR (162 MHz, Chloroform-d_1) δ 155.42 ppm.

Reaction of 5-B(C_6F_5)$_3$ with benzhydryl 4-fluorobenzoate and styrene (14)

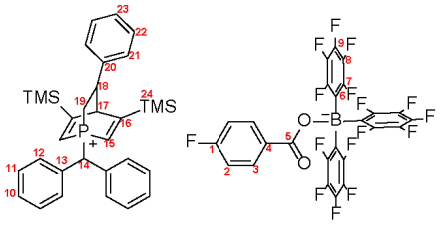

3,5-TMS-Phosphinine (24 mg, 0.1 mmol, 1.0 eq.) and tris(pentafluorophenyl)borane (51 mg, 0.1 mmol, 1.0 eq.) were mixed in THF (0.2 ml) in a J-Young NMR tube. To the resulting colourless solution, benzhydryl 4-fluorobenzoate (31 mg, 0.1 mmol, 1.0 eq.) in THF (0.3 mL) was added followed by styrene (12 mg, 0.1 mmol, 1.2 eq.). The solution was left to react at room temperature for 1 hour. Once complete, all volatiles were removed under high vacuum. The residue was dissolved in chloroform and crystals were acquired *via* slow evaporation of a chloroform solution (105 mg, 0.085 mmol, 85%).

^{1}H NMR (700 MHz, THF-d_8): δ 8.05-8.02 (m, 2H, F-*Ar*), 7.61 – 7.57 (m, 4H, *Ar*), 7.52 – 7.43 (m, 6H, *Ar*), 7.31 – 7.26 (m, 3H, *Ar*), 7.21 (app. dq, *J* = 29.3, 1.3 Hz, 1H, PC*H*), 7.11 (app. dq, *J* = 30.8, 1.2 Hz, 1H, PC*H*), 7.02 – 6.97 (m, 4H, *Ar*/F-*Ar*), 6.02 (d, $^2J_{H,P}$ = 19.4 Hz, 1H, PC*H*Ph$_2$), 4.85 (dt, *J* = 2.5, 1.5 Hz 1H, C*H*), 3.38 (m, 4H, *THF*), 3.16 (m, 1H, PCH$_2$C*H*CH), 2.38 (dddd, *J* = 14.2, 12.9, 10.1, 1.3 Hz, 1H, PCH_2), 2.28 (dddd, *J* = 14.2, 12.9, 4.8, 1.3 Hz, 1H, PCH_2), 1.60 (m, 4H, *THF*), δ 0.30 (s, 9H, *TMS*), -0.21 (s, 9H, *TMS*) ppm. Protic THF was found to be contained within the crystal structure by X-ray diffractometry.

^{11}B NMR (128 MHz, THF-d_8): δ -6.4 ppm.

^{13}C{^{1}H} NMR (176 MHz, THF-d_8): δ 179.7 (d, $^2J_{C,P}$ = 8.1, *C16*), 178.2 (d, $^2J_{C,P}$ = 9.0, *C16'*), 166.9 (s, *C5*), 165.7 (d, $^1J_{C,F}$ = 248.5 Hz, *C1*), 149.3 (m, $^1J_{C,F}$ = 240.1 Hz, *C7*), 141.6 (d, $^3J_{C,P}$ = 4.5 Hz, *C20*), 139.5 (m, $^1J_{C,F}$ = 242.9 Hz, *C9*), 137.5 (m, $^1J_{C,F}$ = 246.0, *C8*), 134.3 (d, $^2J_{C,P}$ = 4.5 Hz, *C13*), 134.1 (d, $^2J_{C,P}$ = 4.5 Hz, *C13'*), 133.0 (d, $^3J_{C,F}$ = 8.9 Hz, *C3*), 131.02 (s, *Ar*), 130.99 (s, *C4*), 130.98 (s, *Ar*), 130.39 (s, *Ar*), 130.37 (s, *Ar*), 130.36 (s, *Ar*), 130.24 (s, *Ar*), 130.19 (s, *Ar*), 130.14 (s, *Ar*), 130.12 (s, *Ar*), 130.10 (s, *Ar*), 129.2 (s, *Ar*), 128.54 (s, *Ar*), 124.1 (d, $^1J_{C,P}$ = 56.2 Hz, *C15'*), 121.4 (d, $^1J_{C,P}$ = 55.4 Hz, *C15*), 115.1 (d, $^2J_{C,F}$ = 21.5 Hz, *C2*), 71.5 (s, *THF*), 55.9 (d, $^2J_{C,P}$ = 56.9 Hz, *C17*), 43.6 (d, $^1J_{C,P}$ = 41.2 Hz, *C14*), 41.0 (d, $^2J_{C,P}$ = 9.1 Hz, *C18*), 27.8 (s, *THF*), 23.1 (d, *J* = 46.0 Hz, *C19*), -2.58 (s, *C24*), -2.66 (s, *C24'*) ppm. C6 could not be located. C10-12 and C21-23 could not be clearly identified due to inequivalence of the aryl groups.

^{19}F NMR (376 MHz, Dichlormethane-d_2): δ -110.3 (m, *F-Ar*), -134.7 (d, $^3J_{F,F}$ = 20.3 Hz, *o*-BCF), -162.5 (t, $^3J_{F,F}$ = 20.4 Hz, *p*-BCF), -166.8 (m, *m*-BCF) ppm.

$^{31}P\{^1H\}$ NMR (162 MHz, THF-d_8): δ -6.4 ppm.

HRMS: ESI (m/z). Positive mode: Calculated $[M_1]^+$: 511.2401, Observed: 511.2440. Negative mode: Calculated $[M_2]^-$ 651.0054, Observed: 651.0000.

Reaction of 5-B(C_6F_5)$_3$ with ester and Trimethylsilylacetylene (15)

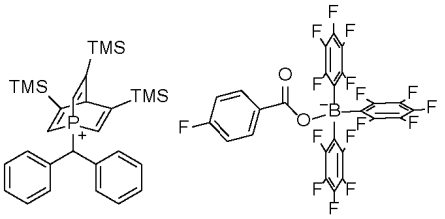

3,5-TMS-Phosphinine (12 mg, 0.05 mmol, 1.0 eq.) and tris(pentafluorophenyl)borane (25 mg, 0.05 mmol, 1.0 eq.) were mixed in DCM (0.2 mL) in a J-Young NMR tube. To the resulting colourless solution, Trimethylsilylacetylene (7.4 mg, 0.075 mmol, 1.5 eq.) was added followed by benzhydryl 4-fluorobenzoate (0.05 mmol, 1.0 eq.) in DCM (0.3 mL). The solution was left to react at room temperature for 3 hours. Once complete, all volatiles were removed under high vacuum. Crystals were acquired by dissolving the residue in a mixture of DCM and *n*-Hexane (48 mg, 0.041 mmol, 83%).

^1H NMR (700 MHz, Dichlormethane-d_2) δ 8.05 – 8.02 (m, 2H, F-*Ph*), 7.53 – 7.46 (m, 6H, *Ar*), 7.43 – 7.40 (m, 4H, *Ar*), 7.02 (dd, $^2J_{H,P}$ = 29.9, 1.5 Hz, 2H, PC*H*) 7.03 – 7.00 (m, 3H, *Ar*), 6.54 (q, *J* = 1.5 Hz, 1H, *Ar*), 5.88 (d, $^2J_{H,P}$ = 17.6 Hz, 1H, C*H*), 0.21 (s, 27H, -*TMS*) ppm.

$^{11}B\{^1H\}$ NMR (129 MHz, Dichlormethane-d_2) δ -4.47 ppm.

$^{13}C\{^1H\}$ NMR (176 MHz, Dichlormethane-d_2) δ 175.69 (d, $^2J_{C,P}$ = 11.1 Hz, *C16*), 167.17 (s, *C5*), 165.21 (d, $^1J_{C,F}$ = 249.0 Hz, *C1*), 148.49 (dt, $^1J_{C,F}$ = 239.9, 6.2 Hz, *C7*), 139.01 (dt, $^1J_{C,F}$ = 245.2, 13.8 Hz, *C9*), 136.95 (ddd, $^1J_{C,F}$ = 246.1, 22.8, 12.1 Hz, *C8*), 132.79 (d, $^2J_{C,P}$ = 4.6 Hz, *C13*), 132.33 (d, $^3J_{C,F}$ = 9.0 Hz, C3), 131.91 (d, $^4J_{C,F}$ = 2.7 Hz, *C4*), 130.71 (s, *C11*), 130.10 (d, $^3J_{C,P}$ = 2.7 Hz, *C12*), 129.08 (s, *C10*), 126.93 (d, $^1J_{C,P}$ = 52.7 Hz, *C15*), 114.99 (d, $^2J_{C,F}$ = 21.4 Hz, *C2*), 62.40 (s, *C17*), 62.10 (s, *C17'*), 42.07 (d, $^1J_{C,P}$ = 40.9 Hz, *C14*), -1.66 (s, *C18*) ppm. C6 could not be located.

^{19}F NMR (377 MHz, Dichlormethane-d_2) δ -110.44 – -110.65 (m, *F*-Ar), -134.60 – -134.87 (m, *o*-BCF), -162.76 (t, $^3J_{F,F}$ = 20.4 Hz, *p*-BCF), -166.78 – -167.11 (m, *m*-BCF) ppm.

$^{31}P\{^1H\}$ NMR (162 MHz, $CDCl_2$-d_2) δ -13.81 ppm.

HRMS: ESI (m/z). Positive mode: Calculated $[M_1]^+$: 505.2327, Observed: 505.2626. Negative mode: Calculated $[M_2]^-$ 651.0054, Observed: 651.0117.

3. NMR Spectra

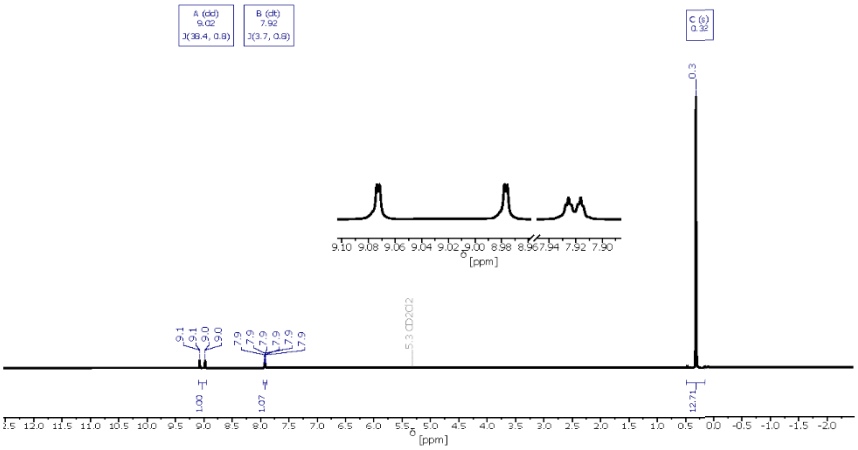

Figure S1: ^{1}H NMR spectrum of 3,5-bis(trimethylsilyl)phosphinine (**6**) in CD_2Cl_2.

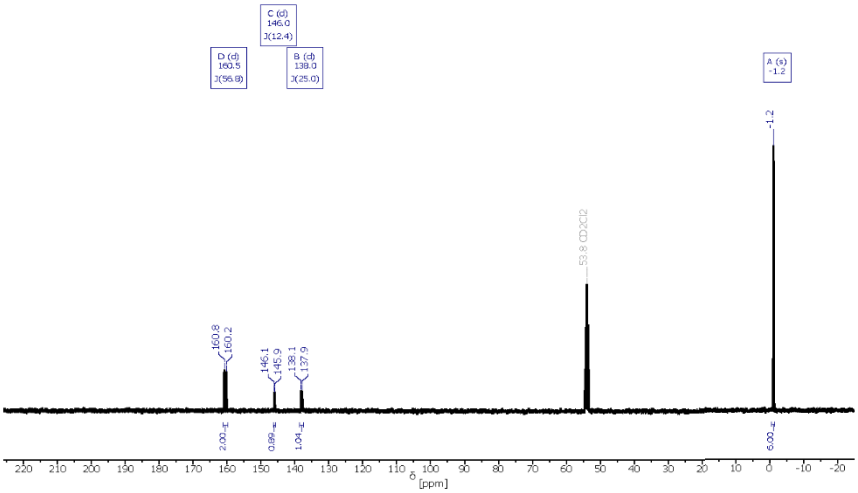

Figure S2: $^{13}C\{^{1}H\}$ NMR spectrum of 3,5-bis(trimethylsilyl)phosphinine (**6**) in CD_2Cl_2.

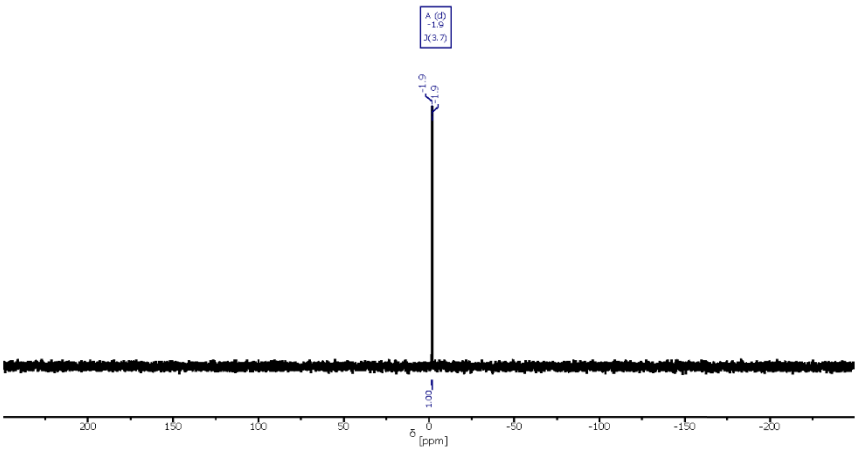

Figure S3: $^{29}Si\{^{1}H\}$ NMR spectrum of 3,5-bis(trimethylsilyl)phosphinine (**6**) in CD_2Cl_2.

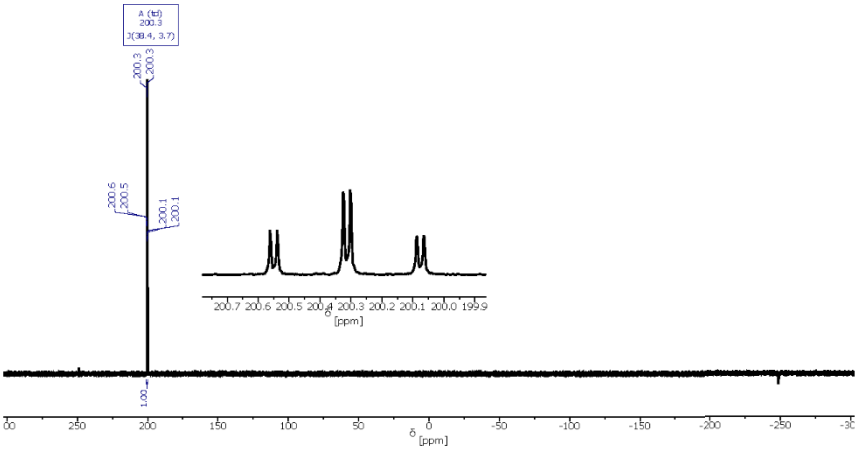

Figure S4: ^{31}P NMR spectrum of 3,5-bis(trimethylsilyl)phosphinine (**6**) in CD_2Cl_2.

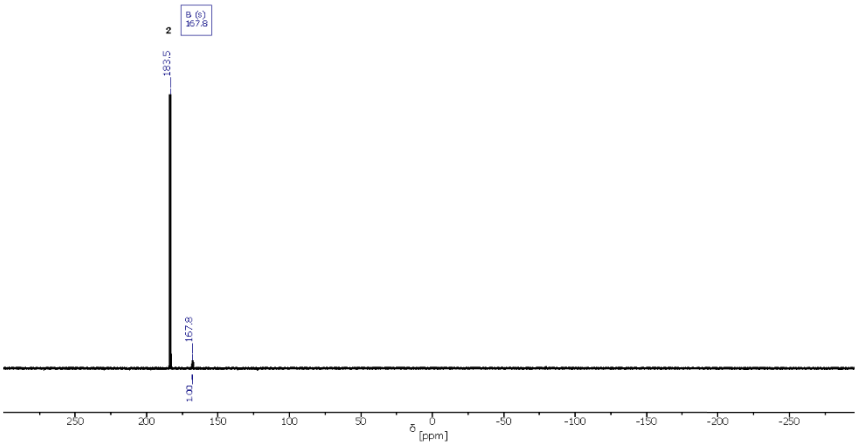

Figure S5: $^{31}P\{^1H\}$ NMR spectrum at T = -70 °C of 2,4,6-triphenylphosphinine borane adduct (**3-BH$_3$**) in CD_2Cl_2.

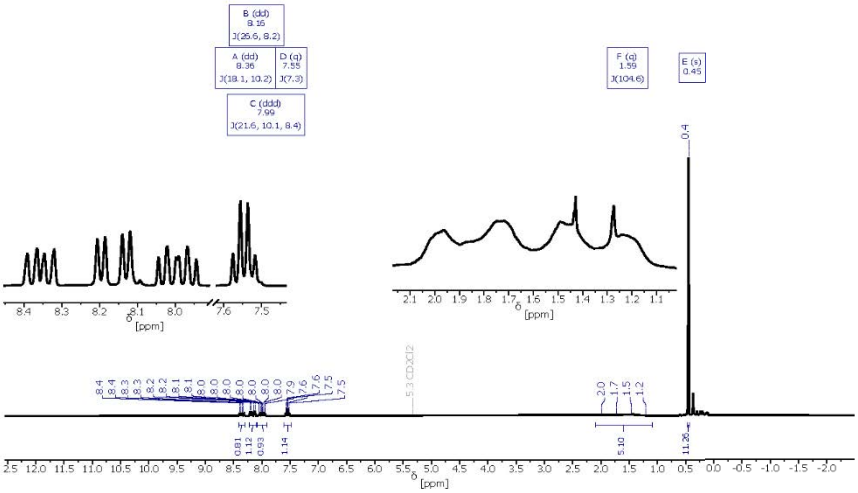

Figure S6: ^{1}H NMR spectrum of 2-trimethylsilylphosphinine borane adduct (**4**-BH_3) in CD_2Cl_2.

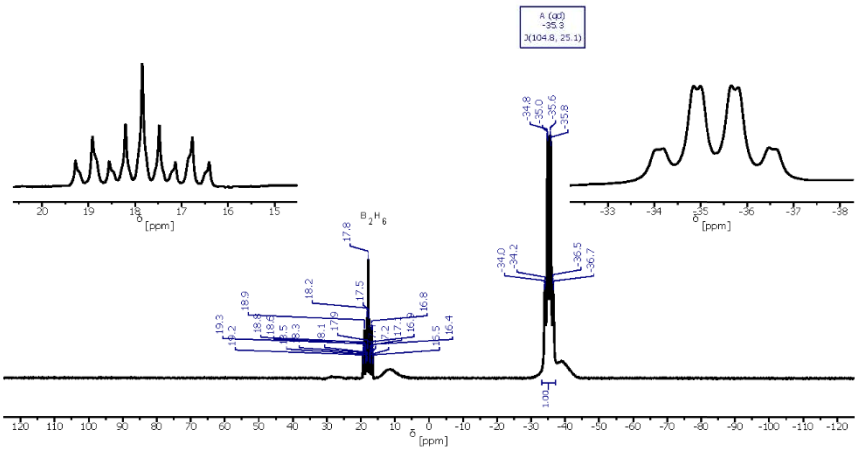

Figure S7: ^{11}B NMR spectrum of 2-trimethylsilylphosphinine borane adduct (**4**-BH_3) in CD_2Cl_2.

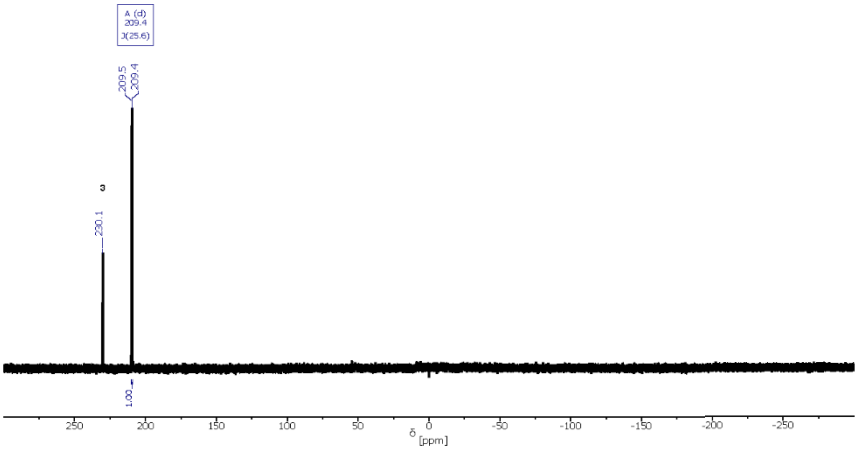

Figure S8: $^{31}P\{^{1}H\}$ NMR spectrum of 2-trimethylsilylphosphinine borane adduct (**4**-BH_3) in CD_2Cl_2.

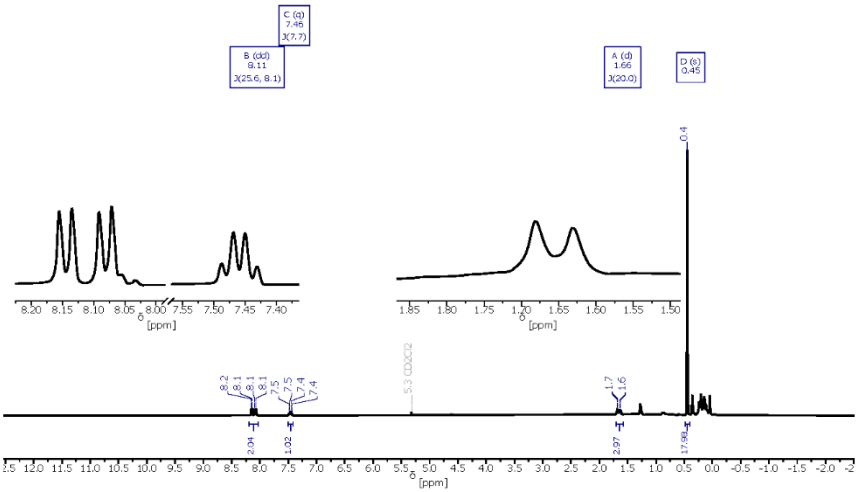

Figure S9: $^{1}H\{^{11}B\}$ NMR spectrum of 2,6-bis(trimethylsilyl)phosphinine borane adduct (**5**-BH_3) in CD_2Cl_2.

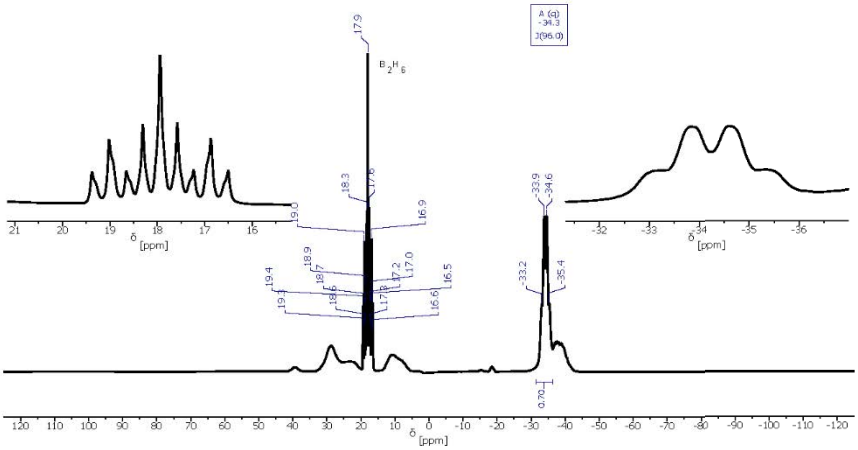

Figure S10: ^{11}B NMR spectrum of 2,6-bis(trimethylsilyl)phosphinine borane adduct (**5**-BH_3) in CD_2Cl_2.

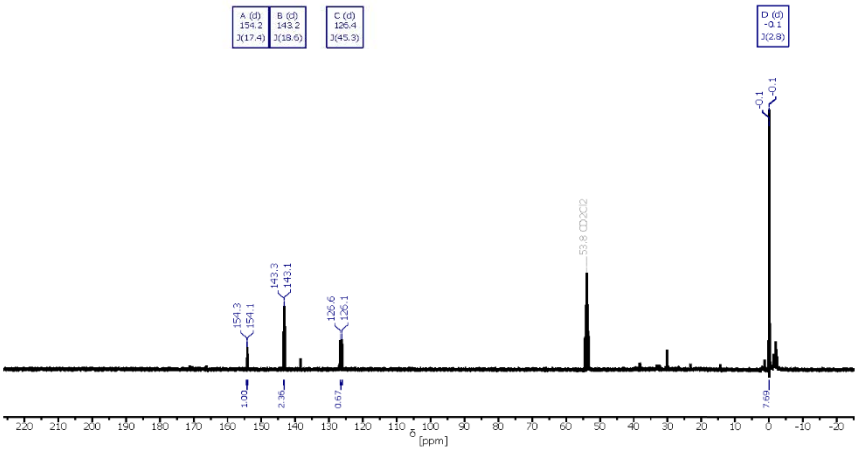

Figure S11: $^{13}C\{^1H\}$ NMR spectrum of 2,6-bis(trimethylsilyl)phosphinine borane adduct (**5**-BH_3) in CD_2Cl_2.

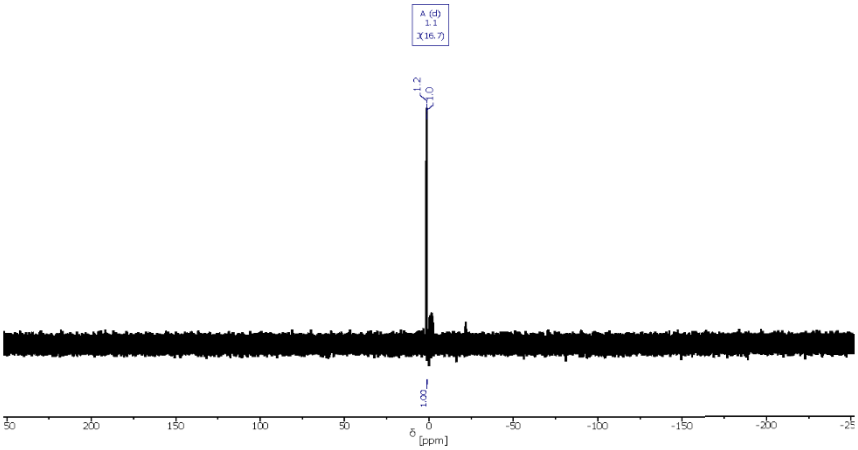

Figure S12: $^{29}Si\{^{1}H\}$ NMR spectrum of 2,6-bis(trimethylsilyl)phosphinine borane adduct (**5**-BH_3) in CD_2Cl_2.

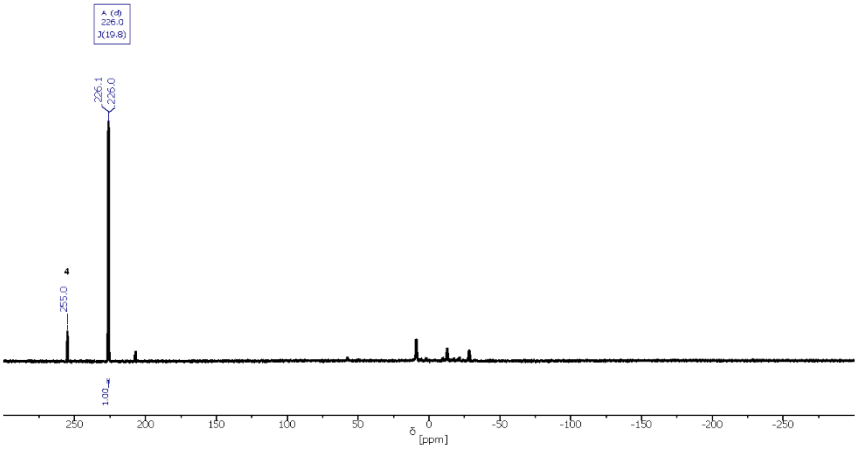

Figure S13: $^{31}P\{^{1}H\}$ NMR spectrum of 2,6-bis(trimethylsilyl)phosphinine borane adduct (**5**-BH_3) in CD_2Cl_2.

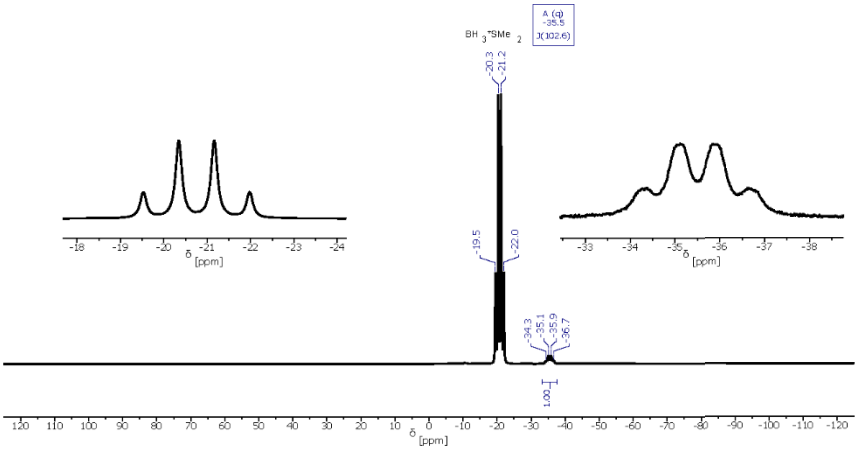

Figure S14: ^{11}B NMR spectrum of 2-trimethylsilylphosphinine (**4**) with $BH_3{\cdot}SMe_2$ in CD_2Cl_2.

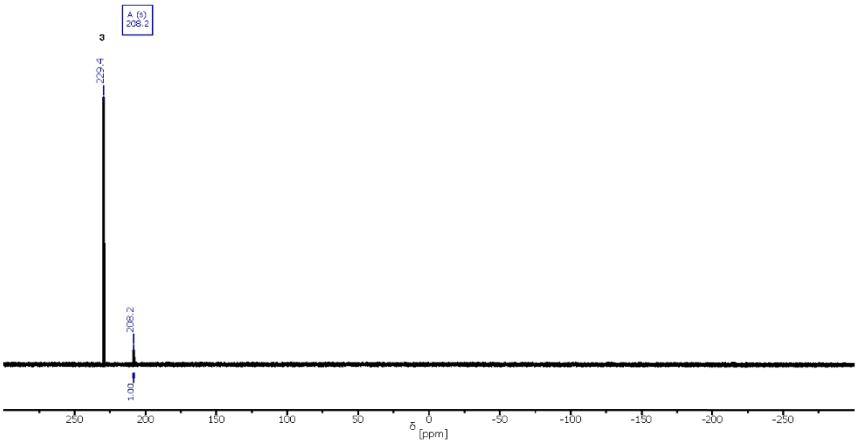

Figure S15: $^{31}P\{^1H\}$ NMR spectrum of 2-trimethylsilylphosphinine (**4**) with $BH_3{\cdot}SMe_2$ in CD_2Cl_2.

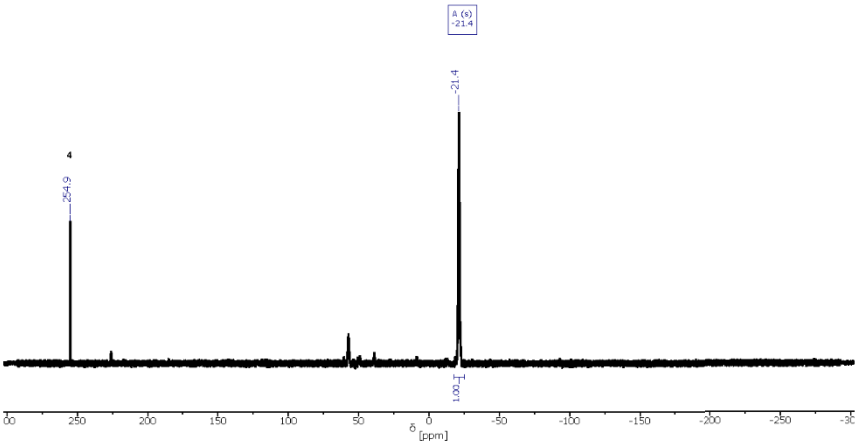

Figure S16: $^{31}P\{^{1}H\}$ NMR spectrum of the follow-up product of 2,6-bis(trimethylsilyl)phosphinine borane adduct (**5-BH$_3$**) in CD_2Cl_2.

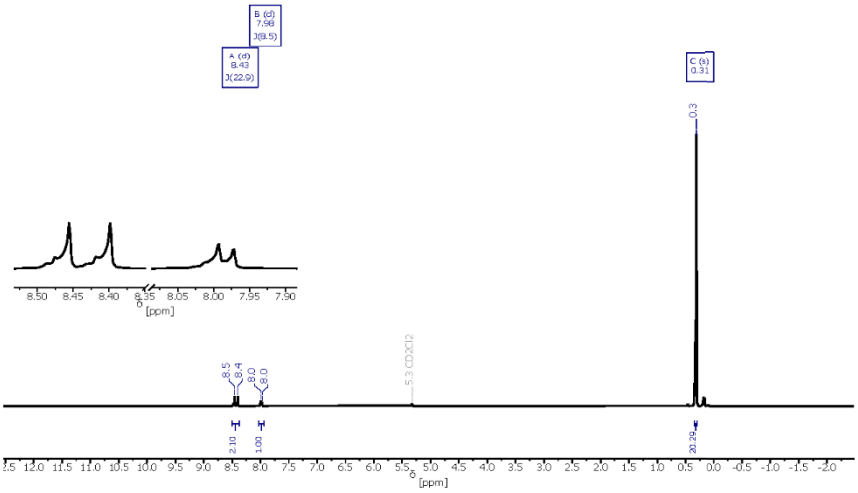

Figure S17: ^{1}H NMR spectrum of 3,5-bis(trimethylsilyl)phosphinine $B(C_6F_5)_3$ adduct (**6-B(C_6F_5)$_3$**) in CD_2Cl_2.

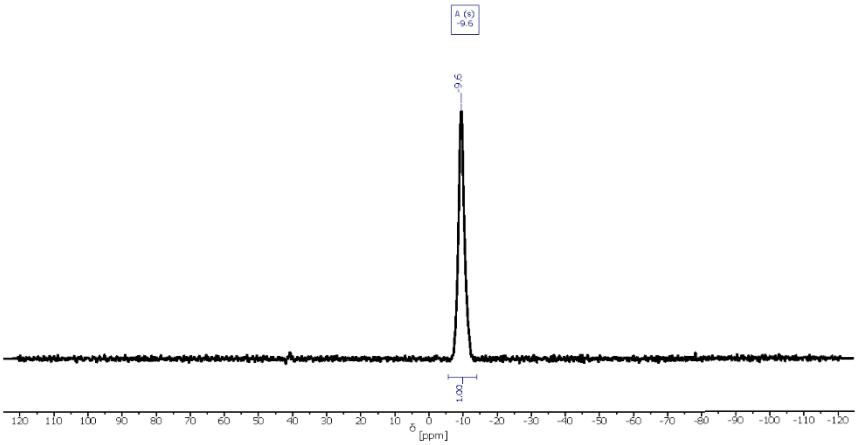

Figure S18: $^{11}B\{^1H\}$ NMR spectrum of 3,5-bis(trimethylsilyl)phosphinine $B(C_6F_5)_3$ adduct (**6-B(C_6F_5)$_3$**) in CD_2Cl_2.

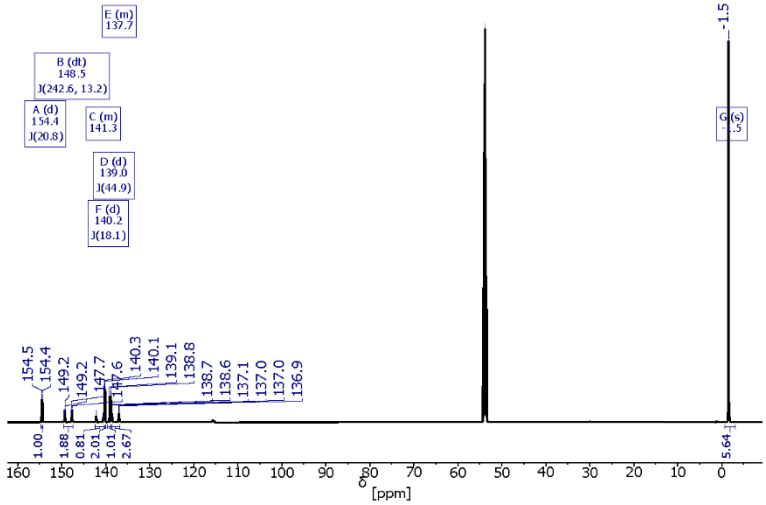

Figure S19: $^{13}C\{^1H\}$ NMR spectrum of 3,5-bis(trimethylsilyl)phosphinine $B(C_6F_5)_3$ adduct (**6-B(C_6F_5)$_3$**) in CD_2Cl_2.

22

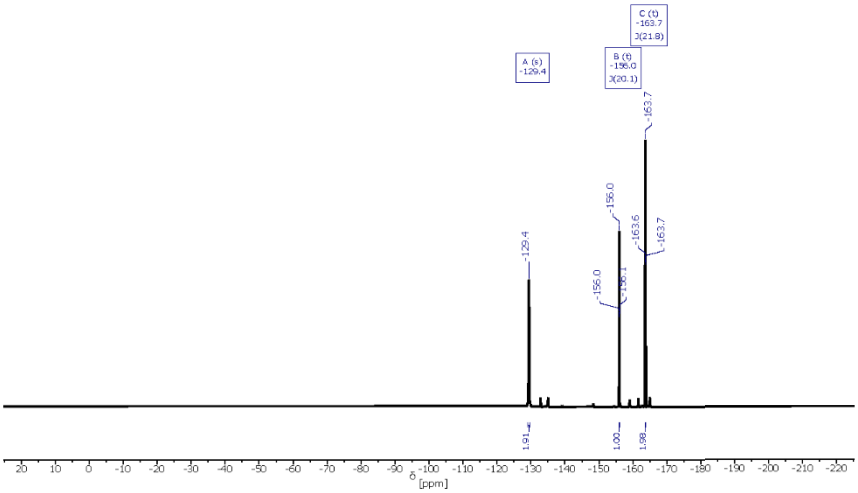

Figure S20: ^{19}F NMR spectrum of 3,5-bis(trimethylsilyl)phosphinine $B(C_6F_5)_3$ adduct (**6-B(C_6F_5)$_3$**) in CD_2Cl_2.

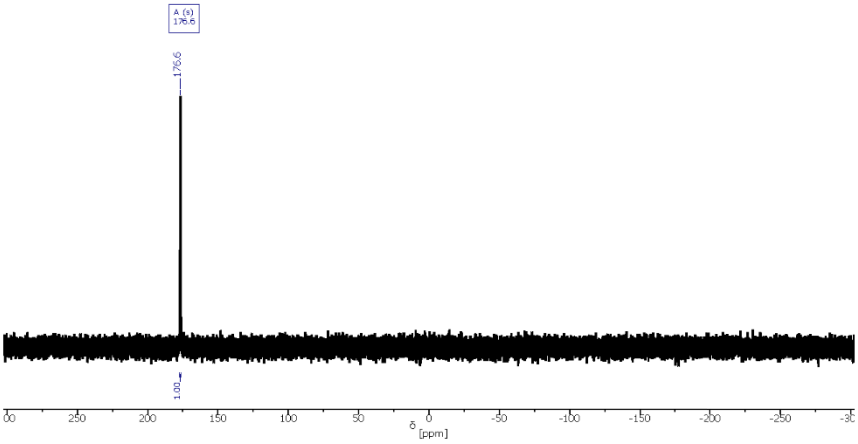

Figure S21: $^{31}P\{^1H\}$ NMR spectrum of 3,5-bis(trimethylsilyl)phosphinine $B(C_6F_5)_3$ adduct (**6-B(C_6F_5)$_3$**) in CD_2Cl_2.

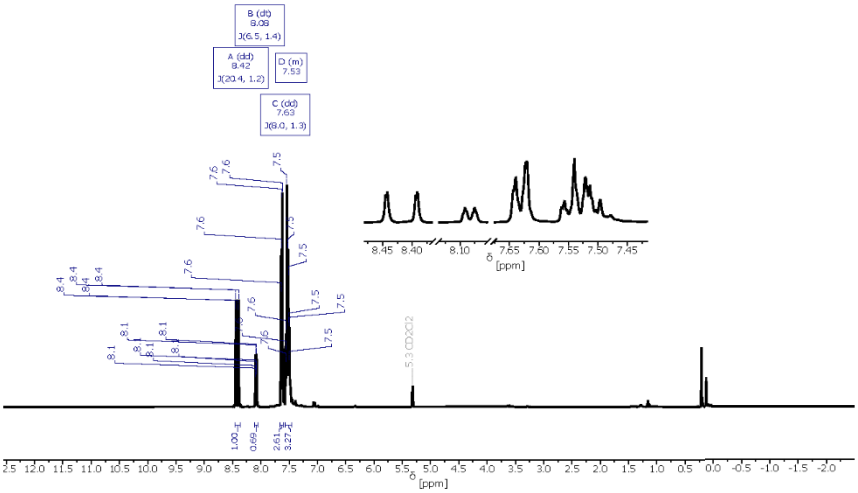

Figure S22: ^{1}H NMR spectrum of 3,5-diphenylphosphinine $B(C_6F_5)_3$ adduct (**7-B(C_6F_5)$_3$**) in CD_2Cl_2.

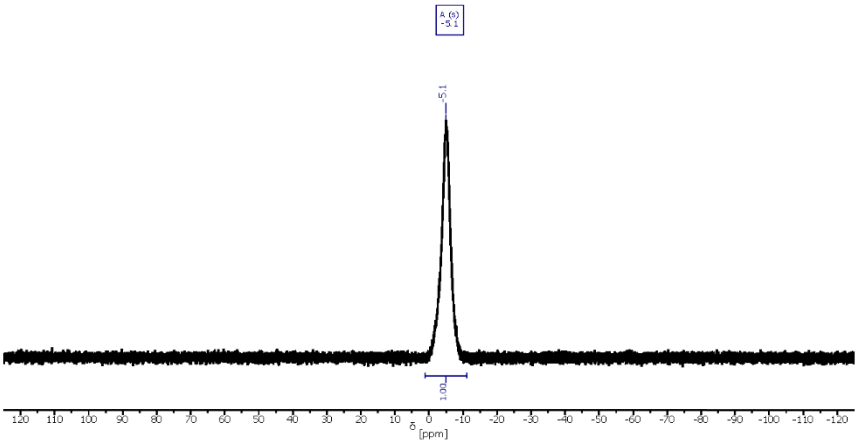

Figure S23: ^{11}B NMR spectrum of 3,5-diphenylphosphinine $B(C_6F_5)_3$ adduct (**7-B(C_6F_5)$_3$**) in CD_2Cl_2.

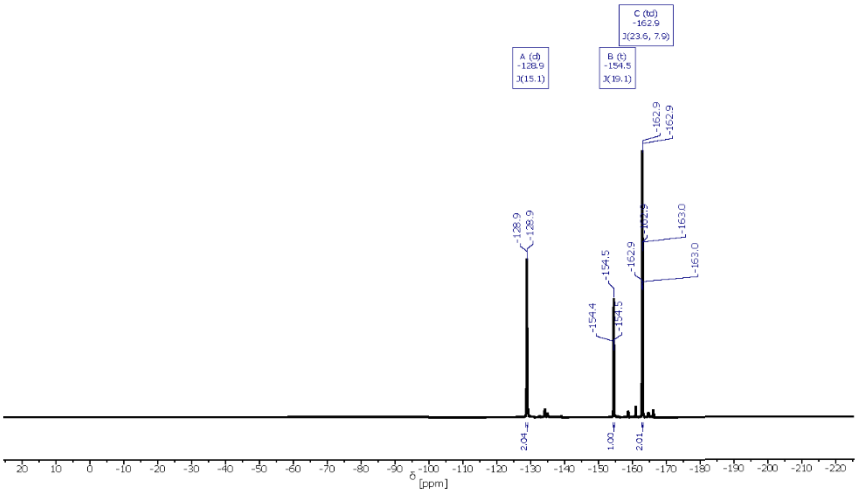

Figure S24: ^{19}F NMR spectrum of 3,5-diphenylphosphinine $B(C_6F_5)_3$ adduct (**7-B(C_6F_5)$_3$**) in CD_2Cl_2.

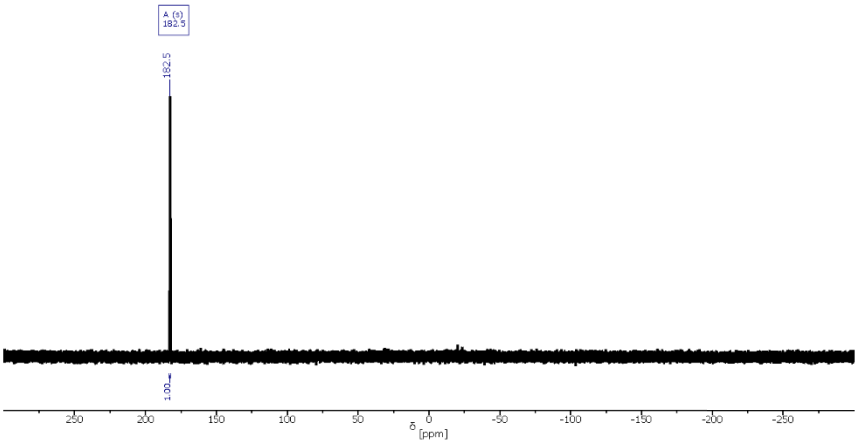

Figure S25: ^{31}P NMR spectrum of 3,5-diphenylphosphinine $B(C_6F_5)_3$ adduct (**7-B(C_6F_5)$_3$**) in CD_2Cl_2.

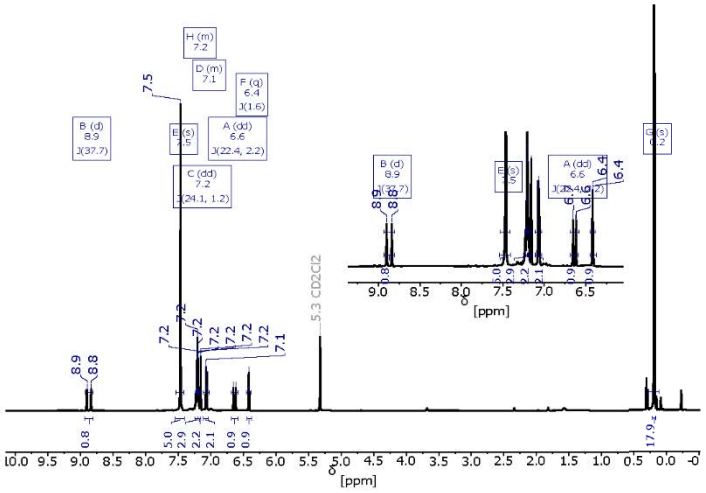

Figure S26: ^{1}H NMR spectrum of **9** in DCM d_2.

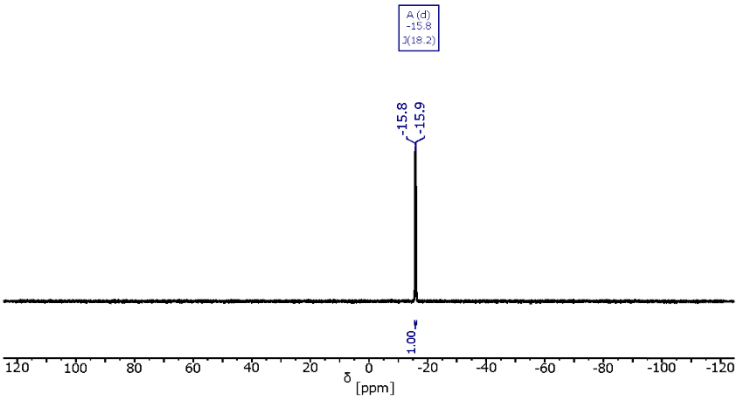

Figure S27: ^{11}B{^{19}F} NMR spectrum of **9** in DCM d_2.

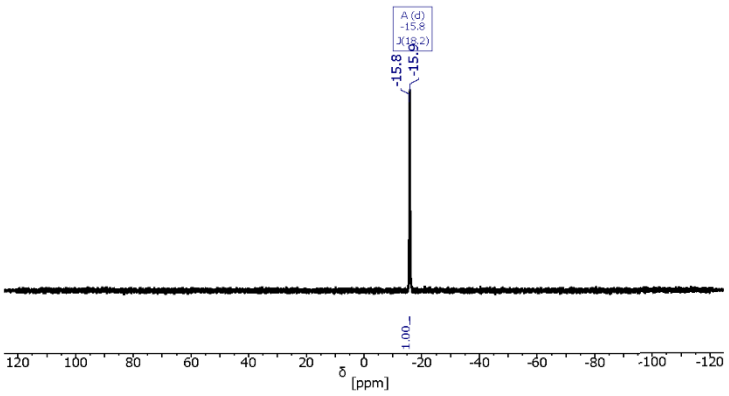

Figure S28: $^{11}B\{^{1}H\}$ NMR spectrum of **9** in DCM d_2.

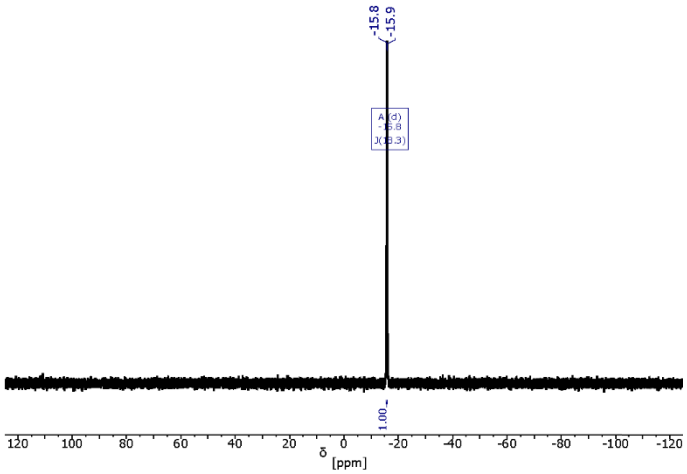

Figure S29: ^{11}B NMR spectrum of **9** in DCM d_2.

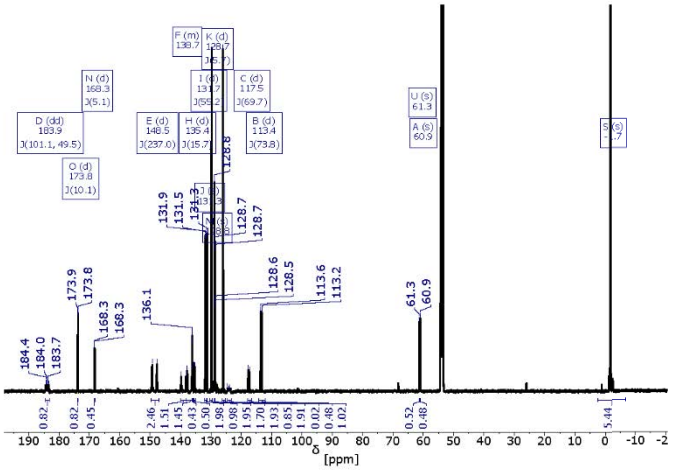

Figure S30: $^{13}C\{^{1}H\}$ NMR spectrum of **9** in DCM d_2.

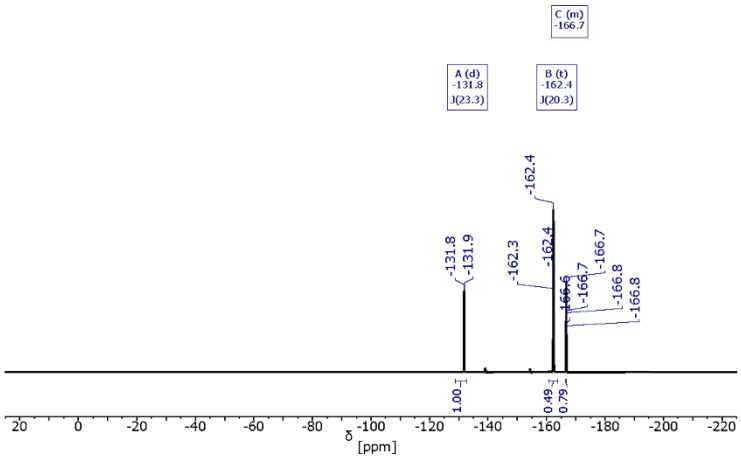

Figure S31: ^{19}F NMR spectrum of **9** in DCM d_2.

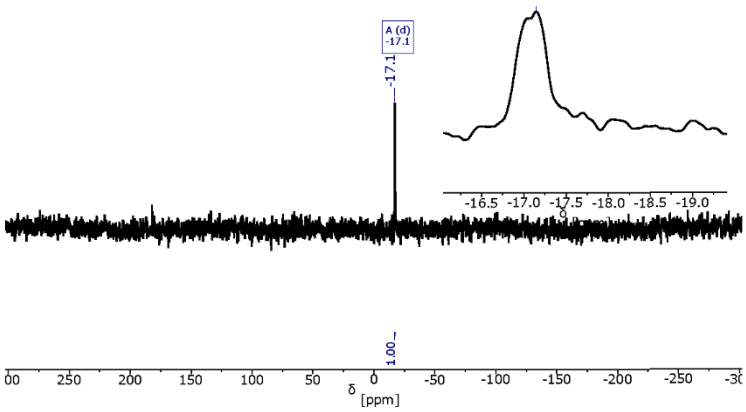

Figure S32: $^{31}P\{^{1}H\}$ NMR spectrum of **9** in DCM d_2.

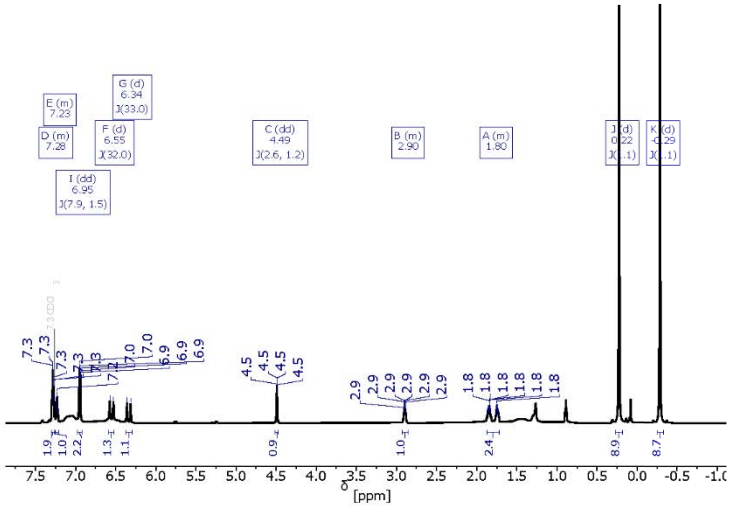

Figure S33: ^{1}H NMR spectrum of **10-B(C_6F_5)$_3$** in Chloroform-d_1.

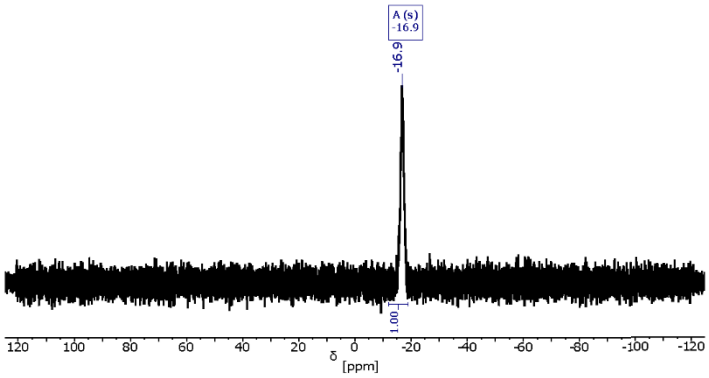

Figure S34: $^{11}B\{^{1}H\}$ NMR spectrum of **10-B(C_6F_5)$_3$** in Chloroform-d_1.

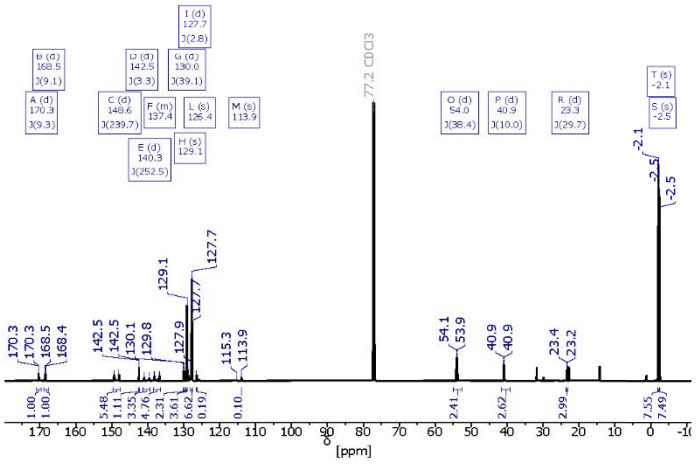

Figure S35: $^{13}C\{^{1}H\}$ NMR spectrum of **10-B(C_6F_5)$_3$** in Chloroform-d_1.

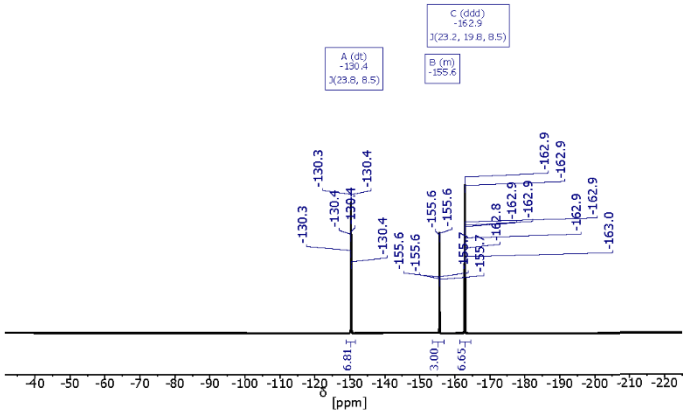

Figure S36: ^{19}F NMR spectrum of **10**-$B(C_6F_5)_3$ in Chloroform-d_1.

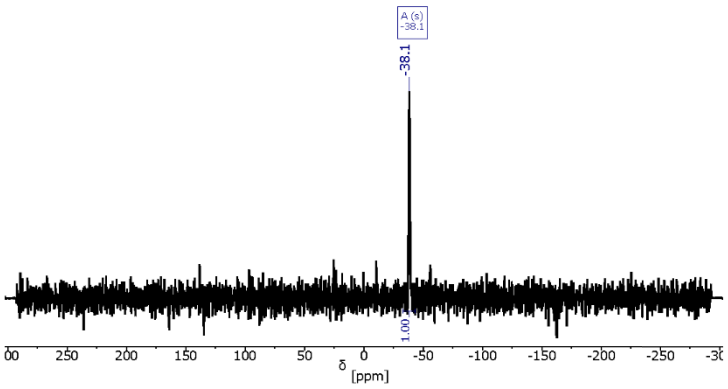

Figure S37: $^{31}P\{^1H\}$ NMR spectrum of **10**-$B(C_6F_5)_3$ in Chloroform-d_1.

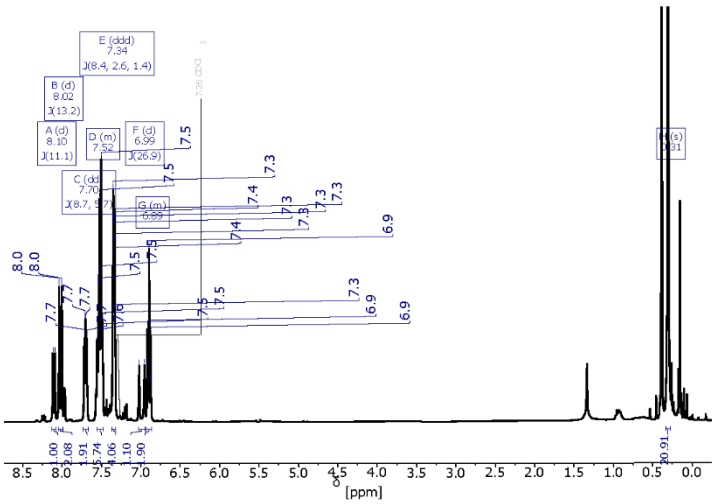

Figure S38: ^{1}H NMR spectrum of **12** in Chloroform d_1.

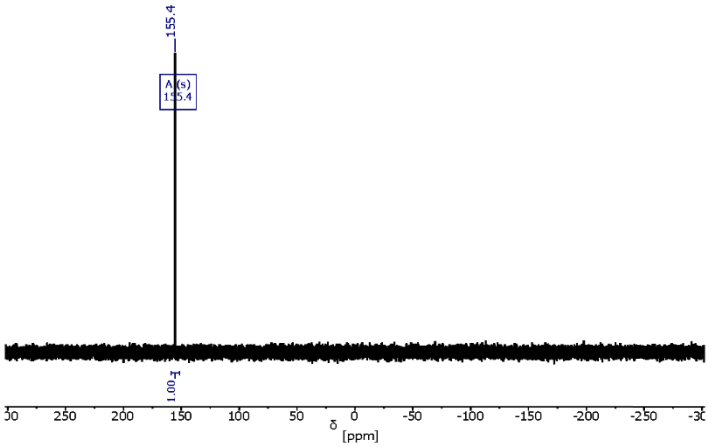

Figure S39:^{31}P{^{1}H} NMR spectrum of **12** in Chloroform d_1.

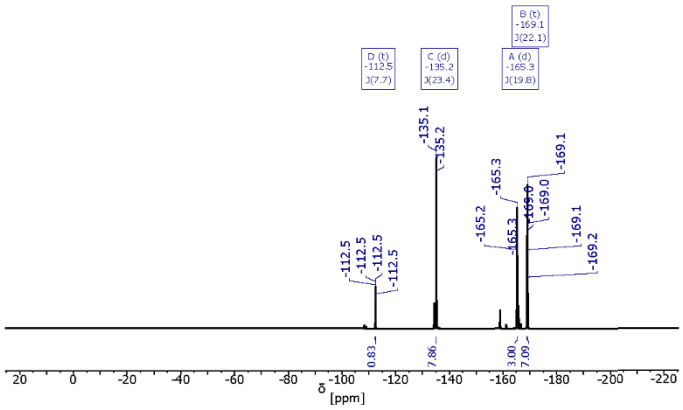

Figure S40:[19]F NMR spectrum of **12** in Chloroform d_1.

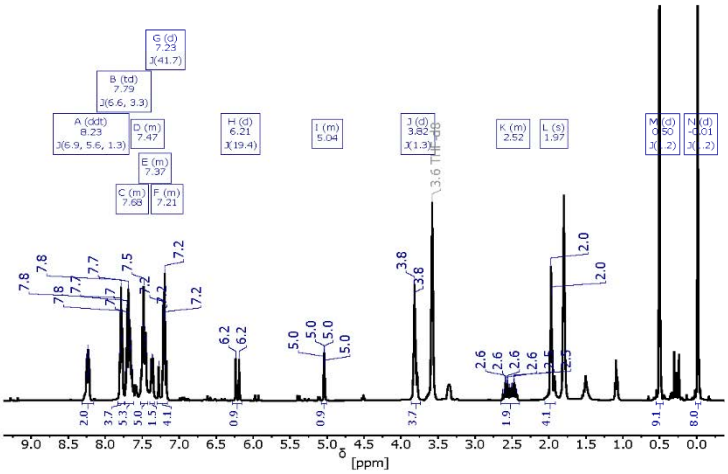

Figure S41: [1]H NMR spectrum of **14** in THF-d_8.

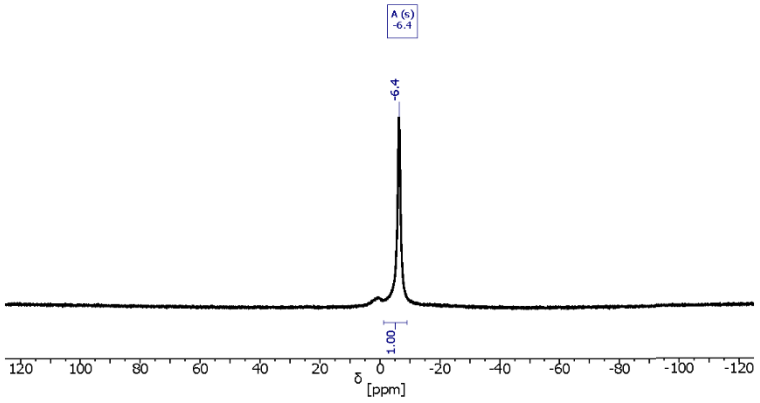

Figure S42: ^{11}B NMR spectrum of **14** in THF-d_8.

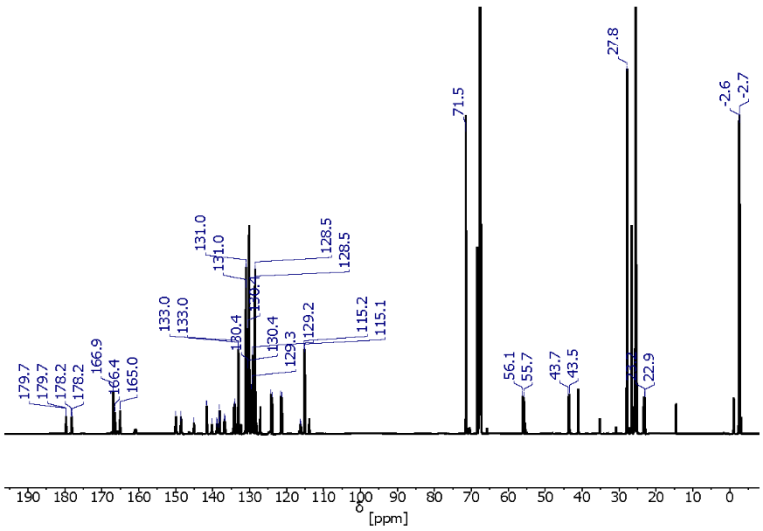

Figure S43: ^{13}C{^{1}H} NMR spectrum of **14** in THF-d_8.

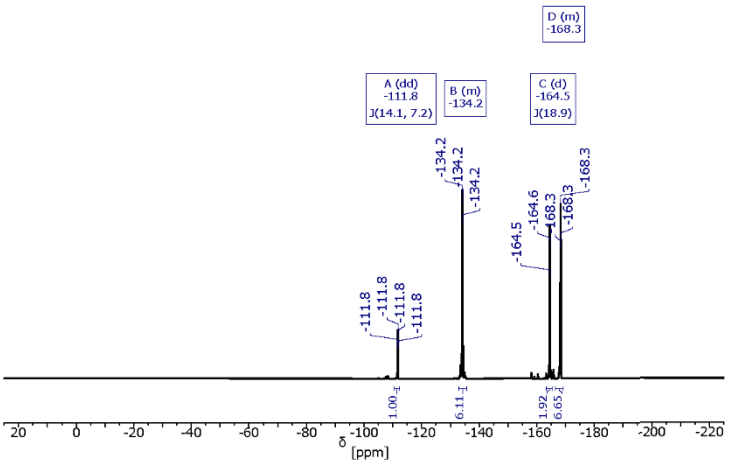

Figure S44: ^{19}F NMR spectrum of **14** in CD_2Cl_2.

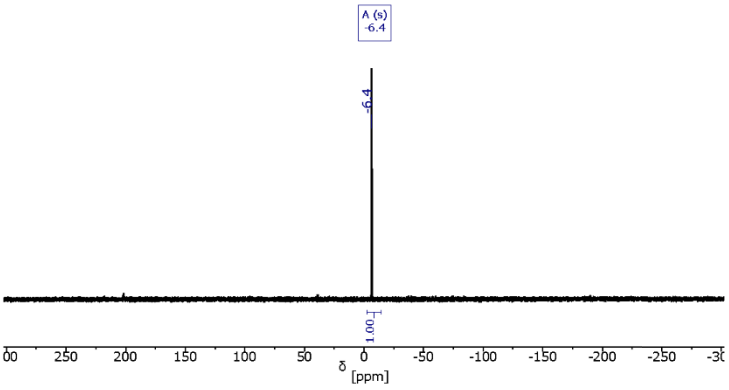

Figure S45: $^{31}P\{^1H\}$ NMR spectrum of **14** in THF-d_8.

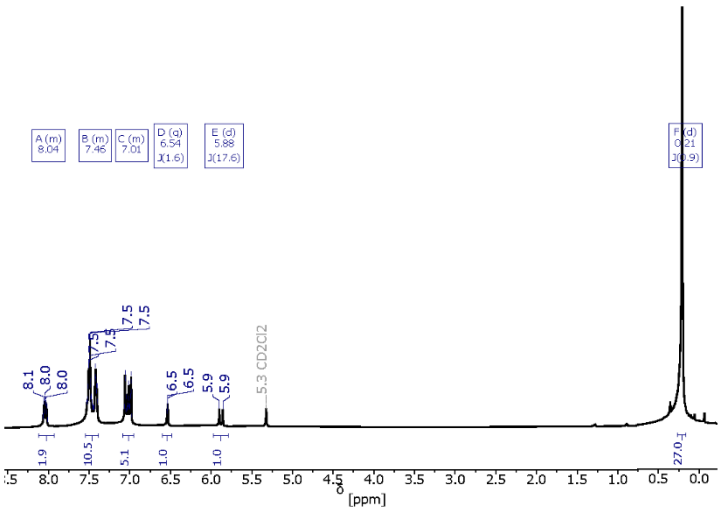

Figure S46: ^{1}H NMR spectrum of **15** in DCM-d_2.

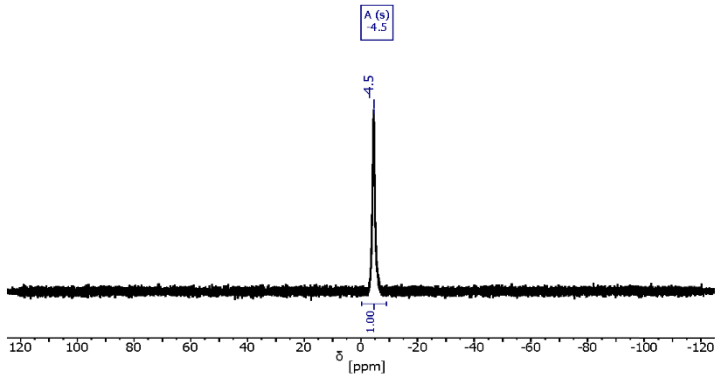

Figure S47: $^{11}B\{^{1}H\}$ NMR spectrum of **15** in DCM-d_2.

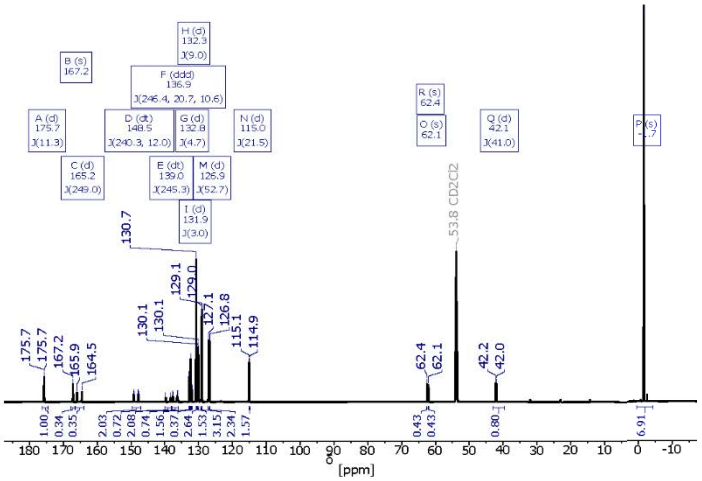

Figure S48: $^{13}C\{^{1}H\}$ NMR spectrum of **15** in DCM-d_2.

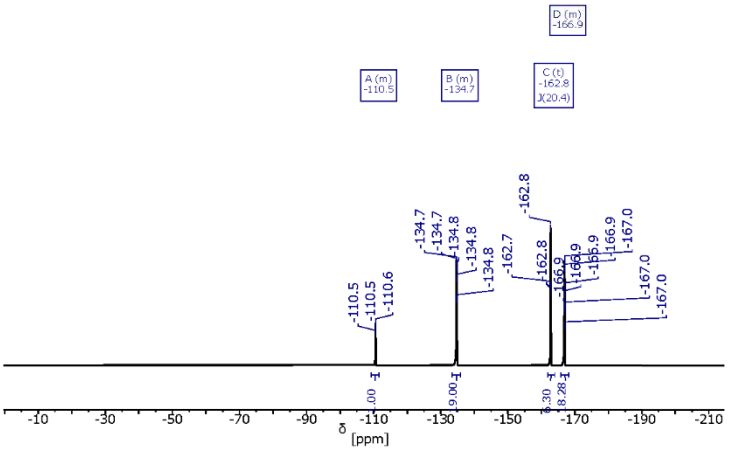

Figure S49: ^{19}F NMR spectrum of **15** in DCM-d_2.

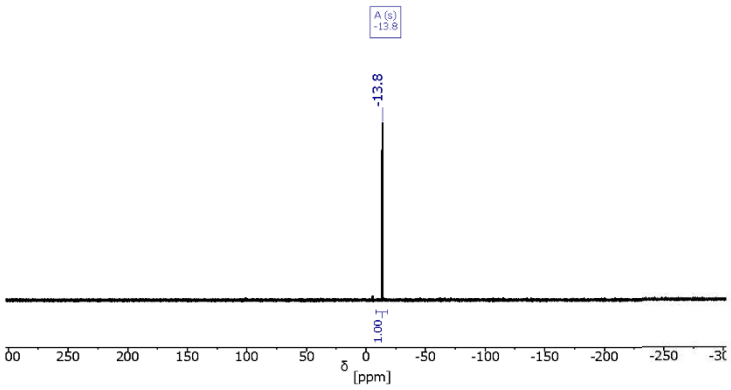

Figure S50: $^{31}P\{^{1}H\}$ NMR spectrum of **15** in DCM-d_2.

4. Crystallographic Details

Low-temperature x-ray diffraction data was collected on a Bruker D8 Venture fitted with a PhotonII CMOS Detector. The data collection was executed with Mo K_α radiation ($\lambda = 0.71073$ Å) from an $I\mu S$ micro-source, performing ϕ-and ω-scans. The structure was solved by dual-space methods using SHELXT[16] and refined against F^2 on all data by full-matrix least squares with SHELXL-2018[17] following established refinement strategies[18]. The program Olex2[19] was also used to aid in the refinement of the structures. All non-hydrogen atoms were refined anisotropically, all hydrogen atoms were included into the model at geometrically calculated positions and refined using a riding model. The isotropic displacement parameters of all hydrogen atoms were fixed to 1.2 times the U value of the atoms they are linked to (1.5 times for methyl groups). Selected crystallographic can be found in **Table S1** below. The supplementary crystallographic data can be found in the CCDC with the following deposit numbers 2079366 (**6-B(C$_6$F$_5$)$_3$**), 2129188 (**9**), 2121299 (**10-B(C$_6$F$_5$)$_3$**), 2094934 (**14**), 2121300 (**15**). These data can be obtained free of charge from The Cambridge Crystallographic Data Centre *via* www.ccdc.cam.ac.uk/data_request/cif.

Table S1- Selected crystallographic data

	6-B(C_6F_5)$_3$	**9**	**10- B(C_6F_5)$_3$**
CCDC number	2079366	2129188	2121299
Empirical formula	$C_{29}H_{21}BF_{15}PSi_2$	$C_{45}H_{33}BF_{15}PSi_2$	$C_{37}H_{29}BF_{15}PSi_2$
Formula weight	752.42	956.67	856.56
Temperature/K	100	101.3	101.9
Crystal system	Triclinic	Monoclinic	Monoclinic
Space group	$P\bar{1}$	$P2_1/c$	$C2/c$
a/Å	11.6244(10)	14.3921(11)	34.5304(18)
b/Å	12.2966(10)	18.3419(14)	11.6897(6)
c/Å	13.6947(11)	17.0817(14)	20.4603(10)
α/°	105.213(3)	30	90
β/°	102.936(3)	108.262(4)	96.274(2)
γ/°	112.880(3)	30	90
Volume/Å^3	1619.2(2)	4282.1(6)	8209.3(7)
Z	2	4	8
Reflections collected	55490	45482	66006
Independent reflections (R_{int})	9961 (0.0385)	8163 (0.0585)	8376 (0.0552)
R1 [I>=2σ (I)]	0.0328	0.0929	0.0582
wR_2 (all data)	0.0867	0.1996	0.1656

	14	**15**
CCDC number	2094934	2121300
Empirical formula	$C_{61}H_{52}BF_{16}O_3PSi_2$	$C_{54}H_{46}BF_{16}O_2PSi_3$
Formula weight	1234.98	1156.96
Temperature/K	99.9	102.4
Crystal system	Monoclinic	Orthorhombic
Space group	$P2_1/n$	$P2_12_12$
a/Å	13.4712(6)	19.2802(3)
b/Å	20.9562(9)	21.0118(4)
c/Å	20.5720(9)	13.4419(3)
α/°	90	90
β/°	92.549(2)	90
γ/°	90	90
Volume/Å^3	5801.8(4)	5445.47(18)

Z	4	4
Reflections collected	120663	129159
Independent reflections (R_{int})	11861 (0.0516)	16603 (0.0526)
R1 [I>=2σ (I)]	0.0469	0.0308
wR_2 (all data)	0.1126	0.0730

Additional refinement details for 9:

The crystal contains one molecule per asymmetric unit which exhibits 3-fold rotational disorder of the phenyl and two silyl groups. The model was allowed to refine freely with the sum of free variables 2, 3 and 4 constrained to a total of 2 (SUMP) to reflect that there are two silyl moieties. In addition to this relatively strong DFIX restraints were used for the Si-C and C-C bonds of the disordered silyl and phenyl groups bound to the central barrelene core. Tphenyl groups were constrained to be regular hexagons (AFIX 66) with additional FLAT restraints to prevent bending of the phenyl moieties relative to the barrelene core. Thermal restraints (RIGU, SIMU) were applied to all disordered atoms and thermal constraints (EADP) were employed to Si1A/C10A and Si1B/C10B where the atoms are close together/partially overlapping.

Additional refinement details for 10- $B(C_6F_5)_3$:

The crystal was found to contain one equivalent of phosphinine-borane adduct and disordered solvent. It was not possible to adequately model the solvent and so SQUEEZE was implemented. SQUEEZE was used to remove electrons equating to 0.85 equivalents of DCM per ASU.

Additional refinement details for 14:

The crystal was found to contain one equivalent of the synthesized salt in addition to an equivalent of disordered THF. The THF was modelled in a 60:40 ratio with both parts requiring angle, distance and thermal restraints. The restraints were introduced using the Fragment DB add-on through the Olex2 interface.

5. Cartesian Coordinates of the Calculated Structures in Ångström

6, C_s

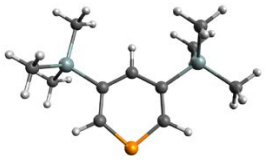

C	-1.1725946	-0.9031352	0.0000000
C	-1.1917553	-2.3011100	0.0000000
P	0.1840883	-3.3513583	0.0000000
C	1.4639305	-2.1781151	0.0000000
C	1.3154943	-0.7927013	0.0000000
C	0.0400701	-0.2086333	0.0000000
Si	-2.8223687	0.0189391	0.0000000
Si	2.8174783	0.3552452	0.0000000
C	-2.5259071	1.8734189	0.0000000
C	-3.7837923	-0.4745054	-1.5362452
C	-3.7837923	-0.4745054	1.5362452
C	4.3993853	-0.6535986	0.0000000
C	2.7455783	1.4367467	-1.5351895
C	2.7455783	1.4367467	1.5351895
H	-2.1570883	-2.7996630	0.0000000
H	2.4692327	-2.5857364	0.0000000
H	-0.0096955	0.8747891	0.0000000
H	-3.4793376	2.4056812	0.0000000
H	-1.9703598	2.1939755	0.8832270
H	-1.9703598	2.1939755	-0.8832270
H	-4.7621769	0.0099823	-1.5600353
H	-3.9454412	-1.5532999	-1.5717534
H	-3.2447332	-0.1910796	-2.4419362
H	-3.9454412	-1.5532999	1.5717534
H	-3.2447332	-0.1910796	2.4419362
H	-4.7621769	0.0099823	1.5600353
H	5.2672789	0.0090062	0.0000000
H	4.4714985	-1.2911580	0.8829344
H	4.4714985	-1.2911580	-0.8829344
H	3.5834916	2.1365725	-1.5623147
H	1.8238008	2.0206038	-1.5648657
H	2.7830287	0.8306479	-2.4420900
H	1.8238008	2.0206038	1.5648657
H	2.7830287	0.8306479	2.4420900
H	3.5834916	2.1365725	1.5623147

$B(C_6F_5)_3$, D_3

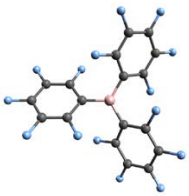

C	2.3040491	0.9255891	0.7364603
C	1.5607391	0.0000000	0.0000000
C	2.3040491	-0.9255891	-0.7364603
C	3.6880144	-0.9338955	-0.7570667
C	4.3831931	0.0000000	0.0000000
C	3.6880144	0.9338955	0.7570667
C	-1.0352299	-3.6608619	0.7570667
C	-2.1915966	-3.7959566	0.0000000
C	-2.6527845	-2.7269664	-0.7570667
C	-1.9536083	-1.5325705	-0.7364603
C	-0.7803696	-1.3516397	0.0000000
C	-0.3504409	-2.4581596	0.7364603
B	-0.0000000	0.0000000	0.0000000
C	-1.9536083	1.5325705	0.7364603
C	-2.6527845	2.7269664	0.7570667
C	-2.1915966	3.7959566	0.0000000
C	-1.0352299	3.6608619	-0.7570667
C	-0.3504409	2.4581596	-0.7364603
C	-0.7803696	1.3516397	0.0000000
F	1.6817440	1.8408783	1.4916941
F	1.6817440	-1.8408783	-1.4916941
F	4.3574490	-1.8234429	-1.4893890
F	5.7101703	0.0000000	0.0000000
F	4.3574490	1.8234429	1.4893890
F	-0.5995767	-4.6853829	1.4893890
F	-2.8550852	-4.9451526	0.0000000
F	-3.7578723	-2.8619401	-1.4893890
F	-2.4351194	-0.5359938	-1.4916941
F	0.7533754	-2.3768722	1.4916941
F	-2.4351194	0.5359938	1.4916941
F	-3.7578723	2.8619401	1.4893890
F	-2.8550852	4.9451526	0.0000000
F	-0.5995767	4.6853829	-1.4893890
F	0.7533754	2.3768722	-1.4916941

PPh_3, C_3

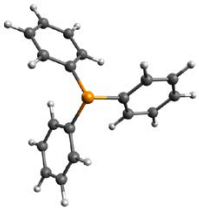

C	1.3806168	-0.8950538	-0.6131993
C	1.7583797	-2.1232418	-1.1651625
C	2.7801131	-2.8730625	-0.5984139
C	3.4559101	-2.3954819	0.5200680
C	3.0996238	-1.1686272	1.0672404
C	2.0667401	-0.4243875	0.5074212
C	0.9595915	2.5844224	-1.1651625
C	1.0980886	3.8441798	-0.5984139
C	0.3465931	4.1906469	0.5200680
C	-0.5377511	3.2686666	1.0672404
C	-0.6658398	2.0020432	0.5074212
C	0.0848309	1.6431761	-0.6131993
P	0.0000000	-0.0000000	-1.4316152
C	-2.5618728	-2.1000394	1.0672404
C	-1.4009004	-1.5776557	0.5074212
C	-1.4654477	-0.7481223	-0.6131993
C	-2.7179712	-0.4611806	-1.1651625
C	-3.8782017	-0.9711173	-0.5984139
C	-3.8025032	-1.7951650	0.5200680
H	1.2448629	-2.4922271	-2.0445522
H	3.0555956	-3.8243084	-1.0343928
H	4.2587561	-2.9736871	0.9577625
H	3.6235535	-0.7893963	1.9349403
H	1.7936694	0.5250901	0.9454935
H	1.5359005	2.3241964	-2.0445522
H	1.7841505	4.5583777	-1.0343928
H	0.4459106	5.1750345	0.9577625
H	-1.1281395	3.5327875	1.9349403
H	-1.3515760	1.2908182	0.9454935
H	-2.4954140	-2.7433913	1.9349403
H	-0.4420934	-1.8159083	0.9454935
H	-2.7807634	0.1680306	-2.0445522
H	-4.8397461	-0.7340692	-1.0343928
H	-4.7046666	-2.2013474	0.9577625

6–$B(C_6F_5)_3$, C_1

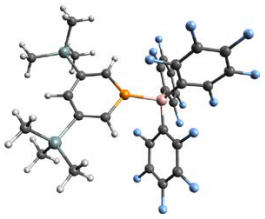

P	-0.2178311	-0.1962506	0.1373221
Si	1.0462474	2.2669124	-3.3835634
Si	-1.4839851	3.8628577	1.4616093
F	-1.7446672	-1.1344868	2.6229848
F	2.6780403	-0.8859794	0.9519176
F	0.2731965	-3.9085467	-1.8024346
F	2.4125724	-3.3699228	2.1945798
F	-2.6320504	-1.3796527	-0.5440069
F	0.0074853	-4.9153005	1.1821295
F	4.8006451	-1.1486608	-0.6449076
F	-1.4895650	-1.2010150	5.2817402
F	2.3928787	-4.1462823	-3.3635979
F	-2.0642783	-6.5888320	0.8846774
F	2.6390084	-3.4265804	4.8346807
F	-4.4257510	-5.6812456	-0.1319090
F	0.7104627	-2.3489819	6.4241658
F	4.6853950	-2.7788819	-2.8264708
F	-4.6675721	-3.0595499	-0.8382560
C	-1.2138616	-3.0684637	0.3552839
C	1.3822981	-2.4252316	-0.2982738
C	-0.7688118	2.4470450	0.4140836
C	0.3513783	-2.1826820	2.2699613
C	-0.8125864	1.1628690	0.9677904
H	-1.2414147	1.0063448	1.9466597
C	-0.2249403	2.6832956	-0.8521647
H	-0.2250689	3.7094163	-1.1999233
C	1.4366478	-2.7836157	2.9022782
C	-0.6187563	-1.6852171	3.1344224
C	2.5798959	-1.7406908	-0.0840025
C	-1.1440625	-4.4171245	0.6975334
C	0.3320116	1.7223339	-1.7093456
C	1.3705775	-3.2254071	-1.4382736
C	0.3856488	0.3790709	-1.3466028
H	0.8305791	-0.3449061	-2.0138754
C	-0.5236967	-1.7179779	4.5151648
C	-2.4336570	-2.6623474	-0.1643323

C	-2.1957685	-5.3040804	0.5451563
C	1.5721567	-2.8432236	4.2835085
C	-3.3980664	-4.8469167	0.0240338
C	3.6325658	-2.6673398	-2.0184153
C	0.5905581	-2.3015839	5.0980180
C	3.6889361	-1.8428755	-0.9034524
C	-3.3010232	3.5000336	1.7449616
H	-3.8476446	3.4656694	0.8010860
H	-3.7574574	4.2697091	2.3706397
H	-3.4418760	2.5401564	2.2448438
C	2.4649895	-3.3609271	-2.2859860
C	-1.2668714	5.4869147	0.5508711
H	-0.2151024	5.7093001	0.3624593
H	-1.6727633	6.3046272	1.1497569
H	-1.7924419	5.4903626	-0.4056827
C	-0.5600936	3.8914144	3.0928340
H	-0.6583194	2.9431105	3.6240827
H	-0.9502096	4.6758048	3.7445069
H	0.5041205	4.0787543	2.9406821
C	1.9593244	0.8202231	-4.1496467
H	2.7653445	0.4644042	-3.5050636
H	2.4075957	1.1216755	-5.0982834
H	1.2954726	-0.0208283	-4.3576368
C	2.2205541	3.6969915	-3.0782572
H	1.7127714	4.5432085	-2.6123600
H	2.6507212	4.0482395	-4.0183669
H	3.0417229	3.3988725	-2.4243924
C	-0.3787366	2.8112730	-4.4743649
H	-1.0785780	1.9915045	-4.6448773
H	-0.0174339	3.1529365	-5.4464762
H	-0.9337703	3.6330342	-4.0180902
C	-3.5162623	-3.5148614	-0.3344242
B	0.0931730	-2.1518959	0.6612909

Ph_3P–$B(C_6F_5)_3$, *C_3*

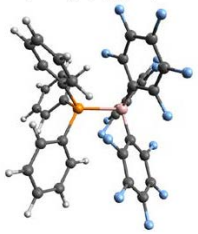

C	1.6542974	0.1857267	1.5315751

C	2.7129953	-0.6232521	1.1059864
C	3.9725687	-0.4840150	1.6713146
C	4.1944674	0.4632104	2.6640189
C	3.1457808	1.2643002	3.0974870
C	1.8823293	1.1271485	2.5368686
C	-0.8167455	2.6611489	1.1059864
C	-1.5671151	3.6823529	1.6713146
C	-2.4983856	3.4009102	2.6640189
C	-2.6678064	2.0921760	3.0974870
C	-1.9173039	1.0665707	2.5368686
C	-0.9879928	1.3398002	1.5315751
P	-0.0000000	-0.0000000	0.7851377
C	-0.4779743	-3.3564761	3.0974870
C	0.0349746	-2.1937192	2.5368686
C	-0.6663046	-1.5255269	1.5315751
C	-1.8962498	-2.0378968	1.1059864
C	-2.4054536	-3.1983379	1.6713146
C	-1.6960818	-3.8641205	2.6640189
H	2.5595539	-1.3597016	0.3357204
H	4.7820928	-1.1135411	1.3279428
H	5.1794416	0.5763574	3.0961646
H	3.3080725	2.0021322	3.8713604
H	1.0785602	1.7596696	2.8805930
H	-0.1022408	2.8964895	0.3357204
H	-1.4266915	4.6981844	1.3279428
H	-3.0888609	4.1973493	3.0961646
H	-3.3879336	1.8638087	3.8713604
H	-2.0631987	0.0542257	2.8805930
H	0.0798611	-3.8659409	3.8713604
H	0.9846385	-1.8138953	2.8805930
H	-2.4573131	-1.5367879	0.3357204
H	-3.3554013	-3.5846433	1.3279428
H	-2.0905807	-4.7737067	3.0961646
C	2.3269391	1.2329541	-1.3293840
C	1.5686974	0.1692462	-1.8125338
C	2.2775685	-0.6907455	-2.6501552
C	3.6322679	-0.5470091	-2.9268120
C	4.3416847	0.5076215	-2.3784773
C	3.6738122	1.4174564	-1.5748601
C	-0.6093529	-3.8903429	-1.5748601
C	-1.7312292	-4.0138200	-2.3784773
C	-2.2898577	-2.8721317	-2.9268120
C	-1.7369874	-1.6270594	-2.6501552
C	-0.6377772	-1.4431549	-1.8125338
C	-0.0956999	-2.6316654	-1.3293840

B	0.0000000	0.0000000	-1.4092757
C	-2.2312391	1.3987113	-1.3293840
C	-3.0644593	2.4728865	-1.5748601
C	-2.6104555	3.5061985	-2.3784773
C	-1.3424101	3.4191408	-2.9268120
C	-0.5405811	2.3178050	-2.6501552
C	-0.9309202	1.2739087	-1.8125338
F	1.7353608	2.1743961	-0.5640474
F	1.6778116	-1.7200765	-3.2717167
F	4.2541078	-1.4158464	-3.7293136
F	5.6423010	0.6539338	-2.6301683
F	4.3322684	2.4516362	-1.0435175
F	-0.0429550	-4.9776726	-1.0435175
F	-2.2548272	-5.2133430	-2.6301683
F	-3.3532129	-2.9762422	-3.7293136
F	-2.3285357	-0.5929892	-3.2717167
F	1.0154019	-2.5900646	-0.5640474
F	-2.7507627	0.4156685	-0.5640474
F	-4.2893134	2.5260364	-1.0435175
F	-3.3874738	4.5594091	-2.6301683
F	-0.9008949	4.3920887	-3.7293136
F	0.6507241	2.3130657	-3.2717167

Pyridine-B(C_6F_5)$_3$, C_1

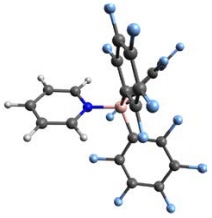

N	-0.6786860	-0.9735356	1.0786847
F	-0.8215574	-2.2675284	-1.5368270
F	-2.0412245	-2.2827021	-3.9102029
F	-2.7081831	0.0664048	-5.1302354
F	-2.1242905	2.4255802	-3.9065019
F	-0.9290900	2.4754189	-1.5506493
F	1.8710163	1.5414572	-1.5159911
F	4.1955201	0.7482687	-2.5691492
F	5.0922298	-1.7955659	-2.1638914
F	3.5947682	-3.5250995	-0.6806038
F	1.2876965	-2.7727575	0.3679682
F	2.4083942	1.4248918	1.3019569
F	2.2772980	3.6338350	2.7559716

F	-0.1143961	4.8405072	3.2511010
F	-2.4018765	3.7590610	2.2323208
F	-2.2995851	1.5473413	0.7415820
C	0.0142519	-1.2582884	2.1960484
H	1.0183269	-0.8672125	2.2425404
C	-0.5255322	-2.0036214	3.2198208
H	0.0711326	-2.2141563	4.0944613
C	-1.8303519	-2.4682934	3.0993584
H	-2.2797656	-3.0559298	3.8876932
C	-2.5457095	-2.1579325	1.9543665
H	-3.5653162	-2.4854362	1.8182664
C	-1.9401313	-1.4055634	0.9643529
H	-2.4639983	-1.1200278	0.0685401
C	-0.8514702	0.0988176	-1.3886554
C	-1.1494972	-1.0750145	-2.0798104
C	-1.7725182	-1.1162768	-3.3161808
C	-2.1104639	0.0747135	-3.9398821
C	-1.8144879	1.2723167	-3.3099952
C	-1.1962778	1.2669112	-2.0655430
C	1.4773760	-0.5493735	-0.4845107
C	2.2746482	0.2822431	-1.2703959
C	3.4771290	-0.1044778	-1.8345565
C	3.9364990	-1.3983698	-1.6319614
C	3.1744313	-2.2709925	-0.8758571
C	1.9705394	-1.8394407	-0.3312657
C	0.0637205	1.4151277	0.8717253
C	1.1922960	1.9843766	1.4502604
C	1.1545258	3.1307798	2.2356341
C	-0.0588402	3.7445408	2.4955343
C	-1.2198843	3.1922594	1.9743312
C	-1.1321289	2.0518927	1.1959979
B	0.0234635	0.0308510	-0.0058507

6-B(C_6F_5)$_3$_HOPT

(Non-hydrogen atom coordinates were taken from the crystal structure of **6-B(C_6F_5)$_3$**. The geometry of the hydrogen atom coordinates was optimized).

P	-0.2944551	-0.2411762	-0.0318976
Si	1.1827649	2.4562828	-3.3267886
Si	-1.5737081	3.7810848	1.4118744
F	-1.8242491	-1.1647812	2.5029084
F	2.6349549	-0.8682352	0.6890484
F	0.2398269	-4.1954572	-1.7119086
F	2.4736859	-3.1311312	2.1585034
F	-2.7836301	-1.5769182	-0.5297406
F	0.0820159	-4.8873022	1.2584124

F	4.7699199	-1.3325312	-0.8369346
F	-1.5158311	-0.9901542	5.1464824
F	2.3647099	-4.6253562	-3.2029176
F	-1.9294691	-6.6623562	1.1842734
F	2.7409159	-2.9604912	4.7788884
F	-4.3681931	-5.9266982	0.2195434
F	0.7788099	-1.9114552	6.3275694
F	4.6605859	-3.2037842	-2.8312806
F	-4.7569311	-3.3688202	-0.6264656
C	-1.2474071	-3.1459022	0.3694544
C	1.3224689	-2.5182532	-0.3944166
C	-0.8265441	2.3961228	0.3549414
C	0.3368379	-2.0770252	2.1716644
C	-0.9245151	1.0823778	0.8371034
H	-1.4218189	0.8827100	1.7733326
C	-0.1857131	2.6862608	-0.8587726
H	-0.1426970	3.7288422	-1.1475648
C	1.4645909	-2.5493742	2.8333294
C	-0.6459811	-1.5847632	3.0259194
C	2.5295809	-1.8261542	-0.2591536
C	-1.1120221	-4.4694782	0.7950024
C	0.3961209	1.7606768	-1.7432816
C	1.3300379	-3.4490542	-1.4313556
C	0.4058349	0.3911998	-1.4570266
H	0.8688515	-0.3066374	-2.1401433
C	-0.5249641	-1.4995102	4.4037124
C	-2.5103291	-2.8250852	-0.1049416
C	-2.1301141	-5.4049102	0.7527414
C	1.6258169	-2.4898622	4.2101394
C	-3.3644231	-5.0331982	0.2652454
C	3.5991979	-2.9815332	-2.0516806
C	0.6290679	-1.9609732	4.9976904
C	3.6492009	-2.0351172	-1.0432026
C	-3.3601251	3.3603368	1.7354134
H	-3.9344234	3.2990963	0.8094896
H	-3.8267816	4.1180022	2.3686473
H	-3.4566807	2.4016831	2.2481859
C	2.4305459	-3.6911712	-2.2387646
C	-1.4257431	5.3786158	0.4621234
H	-0.3862366	5.6494816	0.2693544
H	-1.8753585	6.1991882	1.0250001
H	-1.9446724	5.3180920	-0.4962465
C	-0.6500171	3.8047068	3.0304904
H	-0.7348621	2.8400526	3.5345871
H	-1.0535382	4.5632904	3.7044294

H	0.4121312	4.0120273	2.8899294
C	1.7394229	1.0203768	-4.3833406
H	2.4947146	0.4134342	-3.8802314
H	2.1788584	1.3757481	-5.3172771
H	0.9010661	0.3709906	-4.6423864
C	2.5947369	3.5606118	-2.8091856
H	2.2410448	4.3633589	-2.1594499
H	3.0695417	4.0236735	-3.6767791
H	3.3604625	3.0061338	-2.2643381
C	-0.1099741	3.4729438	-4.1956056
H	-0.9777911	2.8699500	-4.4683909
H	0.2916759	3.9116192	-5.1116606
H	-0.4612275	4.2936763	-3.5677085
C	-3.5601051	-3.7375152	-0.1648006
B	0.0423339	-2.1654532	0.5615894

6. References

[1] a) M. Von Arnim, R. Ahlrichs, *J. Comput. Chem.* **1998**, *19*, 1746-1757. b) O. Treutler, R. Ahlrichs, *J. Chem. Phys.* **1995**, *102*, 346-354.

[2] a) C. Lee, W. Yang, R. G. Parr, *Phys. Rev. B* **1988**, *37*, 785-789. b) A. D. Becke, *J. Chem. Phys.* **1993**, *98*, 1372-1377. c) A. D. Becke, *J. Chem. Phys.* **1993**, *98*, 5648-5652. doi: 10.1063/1.464913.

[3] F. Weigend, R. Ahlrichs, *Phys. Chem. Chem. Phys.* **2005**, *7*, 3297-3305.

[4] S. Grimme, J. Antony, S. Ehrlich, H. Krieg, *J. Chem. Phys.* **2010**, *132*, 154104.

[5] S. Grimme, S. Ehrlich, L. Goerigk, *J. Comput. Chem.* **2011**, *32*, 1456-1465.

[6] a) P. Deglmann, F. Furche, R. Ahlrichs, *Chem. Phys. Lett.* **2002**, *362*, 511-518. b) P. Deglmann, F. Furche, *J. Chem. Phys.* **2002**, *117*, 9535-9538.

[7] T. Lu, F. Chen, *J. Comput. Chem.* **2012**, *33*, 580-592.

[8] Chemcraft - graphical software for visualization of quantum chemistry computations. https://www.chemcraftprog.com

[9] H.-J. Becher, *Handbuch der Präparativen Anorganischen Chemie*, 3. Edition, (Ed.: G. Brauer), Ferdinand Enke Verlag, **1975**.

[10] L. Fischer, F. Wossidlo, D. S. Frost, N. T. Coles, S. Steinhauer, S. Riedel, C. Müller, *Chem. Commun.* **2021**, *57*, 9522.

[11] B. Breit, R. Winde, T. Mackewitz, R. Paciello, K. Harms, *Chem. Eur. J.* **2001**, *7*, 3106–3121.

[12] M. H. Habicht, F. Wossidlo, T. Bens, E. A. Pidko, C. Müller, *Chem. Eur. J.* **2018**, *24*, 944-952.

[13] N. Acarvari, P. Le Floch, F. Mathey, *J. Am. Chem. Soc.* **1996**, *118*, 11978-11979.

[14] M. Blug, O. Piechaczyk, M. Fustier, N. Mézailles, P. Le Floch, *J. Org. Chem.* **2008**, *73*, 3258-3261.

[15] Y. Soltani, A. Dasgupta, T. Gazis, D. Ould, E. Richards, B. Slater, K. Stefkova, V. Vladimirov, L. Wilkins, D. Willcox, R. Melen, *Cell Rep. Phys. Sci.* **2020**, *1*, 100016-100025.

[16] G. M. Sheldrick, *Acta Cryst.* **2015**, *A71*, 3-8.

[17] G. M. Sheldrick, *Acta Cryst. C.* **2015**, *71*, 3-8.

[18] P. Müller, *Crystallogr. Rev.* **2009**, *15*, 57-83.

[19] O. V. Dolomanov, L. J. Bourhis, R. J. Gildea, J. A. K. Howard, H. Puschmann, *J. Appl. Cryst.* **2009**, *42*, 339-341.

Chapter 3

Phosphinine Selenide

3.1 Phosphinine Selenide: Noncovalent Interactions with Organoiodines and Elemental Iodine, and Reactivity towards Potassium Cyanide

Jinxiong Lin,[a] Nathan T. Coles,[a,b] Manuela Weber,[a] Christian Müller*[a]

a: J. Lin, Dr. N. T. Coles, M. Weber, Prof. Dr. C. Müller

Institut für Chemie und Biochemie, Freie Universität Berlin

Fabeckstr. 34/36, 14195 Berlin, Germany

b: Dr. N. T. Coles

School of Chemistry, University of Nottingham, University Park Campus

Nottingham, NG7 2RD, United Kingdom

This article was published and is reprinted with permission from Wiley-VCH:

J. Lin, N. T. Coles, M. Weber, C. Müller, *ChemPlusChem* **2022**, e202200284.

DOI: 10.1002/cplu.202200284

Author contributions: This project was designed by Prof. Dr. C. Müller and J. Lin. All reactions were performed by J. Lin. All single crystals were obtained by J. Lin. The single crystal X-ray diffraction analyses were carried out by Dr. N. T. Coles and M. Weber. NMR experiments were conducted by J. Lin. The paper was written by J. Lin and corrected by Prof. Dr. C. Müller and Dr. N. T. Coles.

Estimated own contribution: ~ 75 %.

ChemPlusChem

Research Article
doi.org/10.1002/cplu.202200284

Chemistry Europe
European Chemical Societies Publishing

www.chempluschem.org

Special Collection

Phosphinine Selenide: Noncovalent Interactions with Organoiodines and Elemental Iodine, and Reactivity towards Potassium Cyanide

Jinxiong Lin,[a] Nathan T. Coles,[a, b] Manuela Weber,[a] and Christian Müller*[a]

Dedicated to Prof. László Nyulászi on the occasion of his 65th birthday

A co-crystalline adduct consisting of a phosphinine selenide and an organohalide was obtained by slow evaporation of the solvent from a mixture of 2,6-bis(trimethylsilyl)phosphinine selenide and 1,4-diiodotetrafluorobenzene (1,4-TFDIB). The crystallographic characterization of the product shows π-π stacking, F···H hydrogen bonding between 1,4-TFDIB and the phosphinine selenide, as well as F···F interactions between 1,4-TFDIB molecules. Moreover, the phosphorus heterocycle could be crystallized with diiodine to form a 1:1 adduct. The $d_{(I-I)}$ distance in this compound is 2.8475(3) Å, which is shorter than the corresponding one in triphenylphosphine selenide diiodide, reflecting the weaker net-donor power of the phosphinine selenide towards diiodine. The phosphinine selenide could also be used as a selenium transfer reagent to generate KSeCN from KCN.

Introduction

Since the first synthesis of phosphine selenides ($R_3P{=}Se$, R = alkyl, aryl), a vast amount of reports concerning their application in several fields of chemical research have been published in literature.[1] In general, trivalent phosphines readily react with grey selenium to form quantitatively phosphine selenides, which are thermodynamically and kinetically rather stable compounds.[2] Consequently, the selenium atom can be used as a protecting group, which can be removed again by different methods.[3] Moreover, the ^1J coupling between the ^{31}P and ^{77}Se nucleus provides valuable information on the basicity of the trivalent phosphorus atom, which is of fundamental importance when applying organophosphorus compounds as ligands in homogeneous catalysis.[4] Interestingly, the selenium atom in triphenylphosphine selenide ($Ph_3P{=}Se$, **1**) shows a high affinity towards organoiodines, which often results in the formation of co-crystalline adducts with non-covalent halogen bonding interactions. Pennington and co-workers have reported on cocrystals, that display halogen bonding, by combining **1** with 1,2-diiodotetrafluorobenzene (1,2-TFDIB), 1,4-diiodotetrafluorobenzene (1,4-TFDIB, **2**), and tetraiodoethylene (TIE), respectively (Scheme 1). In this way finite adducts, chains and two-dimensional layers could be assembled.[5] 1,4-TFDIB has been extensively investigated as a tool in cocrystal formation as the polarizable iodine atoms attached to the aromatic ring lead to the presence of σ-holes. This, in turn, facilitates the formation of halogen bonds. On the other hand, π-hole is generated at the π-surface of the aryl-ring, due to the presence of highly electronegative fluorine atoms, that cause an electron-deficient core.[6] Halogen bonding as a non-covalent interaction is a

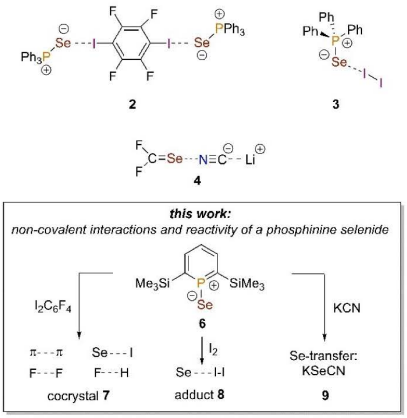

Scheme 1. Adducts of $Ph_3P{=}Se$ with 1,4-TFDIB (**2**) and I_2 (**3**). Interaction of LiCN with $F_2C{=}Se$ (**4**) and brief summary of this work.

[a] J. Lin, Dr. N. T. Coles, M. Weber, Prof. Dr. C. Müller
Institut für Chemie und Biochemie
Freie Universität Berlin
Fabeckstr. 34/36, 14195 Berlin (Germany)
E-mail: c.mueller@fu-berlin.de
[b] Dr. N. T. Coles
School of Chemistry
University of Nottingham
University Park Campus, NG7 2RD Nottingham (UK)

Supporting information for this article is available on the WWW under https://doi.org/10.1002/cplu.202200284

Part of a Special Collection: "From Light to Heavy: Advancing the Chemistry of Pnictogen Compounds"

valuable instrument in understanding the association of molecules in a crystalline environment.[7] This topic recently attracted a lot of attention, for instance, for the synthesis of diverse crystalline forms,[8] the development of photoluminescent materials,[9] the construction of stoichiomorphic donor-acceptor aggregates and the exploration of the nature and energetics of intermolecular interactions.[10,11]

Besides the formation of halogen bonding using organoiodine compounds, phosphine selenides can also form charge-transfer complexes with dihalogens. The first examples were reported by Zingaro and co-workers in 1960, who showed that $R_3P{=}Se$ (R = alkyl or aryl) can form 1:1 adducts with I_2 (**3**), IBr and ICl in CCl_4.[12] Godfrey and co-workers characterized crystallographically several phosphine selenide dihalides and showed, that the donor power of the selenium atom in $R_3P{=}Se$ towards diiodine is sensitive to the nature of the R groups.[13]

Also, chalcogen bonds with nitrogen bases are known. This type of noncovalent Se···N interaction plays a prominent role with respect to molecular recognition, biological systems as well as crystal engineering.[14] In this case, the σ-hole at the selenium atom can interact with the lone pair of nitrogen-based compounds (**4**, Scheme 1).[15]

Our group recently reported on the first synthesis of a phosphinine selenide (**6**, Scheme 1).[16] In contrast to classical phosphines, the selenation of phosphinines is rather challenging as the phosphorus atom in the aromatic phosphorus heterocycle shows a very weak basicity along with a poor nucleophilicity. These characteristics severely hindered the reaction with grey selenium. However, the electronic properties of phosphinines can be drastically influenced by introducing strongly electron-donating Me_3Si-substituents to the heterocyclic ring. In this way, it was possible to react the bis-$SiMe_3$-substituted phosphinine **5** with red selenium to the corresponding phosphinine selenide, albeit the desired product could finally not be characterized crystallographically. Interestingly and similar to **4** (Scheme 1), the phosphinine selenide **6** is expected to be a multifunctional molecule, with a σ-hole at the selenium atom, a π-hole at the phosphorus atom (energetically low-lying LUMO) as well as two lone-pairs perpendicular to one another with a high *p*-character at the selenium atom. This is also reflected in the corresponding electrostatic potential plot of **6** (Figure 1) and indicates that the phosphinine selenide should have the potential to form adducts with organoiodine compounds as well as with halogens and nitrogen bases and that the formation of co-crystalline adducts can be expected.[16] These qualitative considerations prompted us to investigate the reactivity of phosphinine selenide **6** towards organoiodines, dihalogens as well as CN^- in more detail.

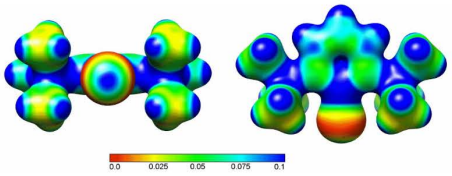

Figure 1. Electrostatic potential plot of **6** calculated at B3LYP–D3/def2-TZVP level of theory. The electrostatic potential (in a.u.) is mapped on electron density isosurfaces of 0.02 e/au^3 (in accordance to ref. [16]).

Results and Discussion

As 1,3,5-trifluoro-2,4,6-triiodobenzene (TFTIB), 1,2-TFDIB, 1,4-TFDIB, as well as TIE have been used successfully in the formation of co-crystals with $Ph_3P{=}Se$ and Ph_3P before,[5,8] we started a systematic study these organoiodines in combination with phosphinine selenide **6**. At first, an equimolar solution of TFTIB and **6** in different solvents (see Supporting Information) was prepared at $T = -30\,^{\circ}C$ and the solvent was slowly evaporated at room temperature. Colorless crystals were obtained, which turned out to be the starting material TFTIB. With 1,2-TFDIB and TIE, only viscous oils were obtained with **6**. When using a combination of 1,4-TFDIB and **6** in deuterated dichloromethane as solvent, the ^{31}P NMR spectrum of the mixture shows a signal at δ(ppm) = 168.4 with ^{77}Se-satellites, which is identical to the pure phosphinine selenide **6**.[16] However, when using a mixture of dichloromethane and *n*-pentane, single crystals, suitable for X-ray diffraction, could be obtained by slow evaporation of the solvent mixture.

The crystallographic characterization of the product **7** reveals indeed the presence of a co-crystalline adduct that crystallizes in the centrosymmetric monoclinic space group $P2_1/c$. The unit cell consists of four molecules 1,4-TFDIB and four molecules of **6** (Figure 2), while the asymmetric unit contains two half molecules of crystallographically different molecules of 1,4-TFDIB. Figure 2 represents the first structurally characterized phosphinine selenide.

The P(1)–Se(1) bond length of 2.083(1) Å is slightly shorter than the one found in the co-crystalline product of 1,4-TFDIB and $Ph_3P{=}Se$ (2.127(2) and 2.107(2) Å).[5] As expected, the Se atom lies very close to the axis defined by the P(1) and C(3) atoms (Se(1)–P(1)–C(3): 178.64°), while the phosphorus heterocycle is essentially planar with a P(1)–C(1)–C(2)–C(3) torsion angle of 0.2°. This situation may contribute to π-π stacking. In fact, the phosphorus heterocycle and the closest 1,4-TFDIB

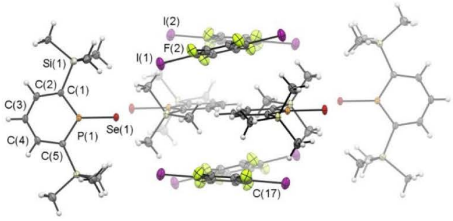

Figure 2. Molecular structure of phosphinine selenide···1,4-TFDIB adduct **7** in the crystal (unit cell). Displacement ellipsoids are shown at the 50% probability level. Selected bond lengths (Å) and angles (°): Se(1)–P(1): 2.083(1), P(1)–C(1): 1.721(5), P(1)–C(5): 1.715(5), C(1)–C(2): 1.414(7), C(2)–C(3): 1.387(8), C(3)–C(4): 1.390(8), C(4)–C(5): 1.396(7), C(1)–P(1)–C(5): 111.8(3).

molecule show nearly an offset-stacked geometry with *d*(C17···centroid(**6**) = 3.852 Å and *d*(C3-centroid(1,4-TFDIB) = 3.634 Å. The C–C bond distances in the phosphinine selenide are very similar to the ones observed in a 2,6-bis-Si$(CH_3)_3$-substituted phosphinine sulphide, reported by Le Floch and co-workers.[17] The same is observed for the P(1)–C(1) and P(1)–C(5) bond lengths (1.721(5) and 1.715(5) Å, respectively) as well as for the C(1)–P(1)–C(5) angle of 111.75°.

A closer look to the packing of the molecules in the crystal of **7** reveals further distinct features (Figure 3). The iodine atoms of one of the 1,4-TFDIB molecules show potential I(2)···Se(1) contacts to two different phosphinine selenides, with an interatomic distance of $d_{(I···Se)}$ = 3.8730(7) Å (Figure 3, blue dotted line). This value is significantly longer than the one found for the cocrystal consisting of Ph_3P=Se and 1,4-TFDIB ($d_{(I···Se)}$ = 3.4944(11), 3.6841(12), 3.4224(13) Å) and almost equal to the sum of the van der Waals radii of selenium and iodine (3.91 Å).[5,18] The second molecule of 1,4-TFDIB has a distance of I(1)···Se(1) of 4.0216(7) Å, which is clearly outside the sum of the van-der-Waals radii and is not to be considering interacting. Moreover, the P=Se···I angle is with 130.69(4)° considerably larger than the one found in Ph_3P=Se···1,4-TFDIB (113.01(7)°, 88.90(6)°, and 112.60(7)°). The C(17)–I(2)–Se(1) angle of 143.71° deviates substantially from linearity. Consequently, only a weak interaction of the selenium atom with the σ-hole of 1,4-TFDIB should be considered. The four fluorine atoms of 1,4-TFDIB form short F···F contacts of 2.692(6) and 2.757(6) Å with neighboring 1,4-TFDIB molecules (Figure 3, red dotted lines), as well as two F···H hydrogen bonds with adjacent phosphinine selenides ($d_{(F···H)}$ = 2.579 Å and 2.623 Å, Figure 3, green dotted lines). Overall we assume that the co-crystal **7** is primarily held together by F···F and F···H interactions as well as π-π stacking, with only slight contributions by Se···I contacts.

It is well known that Ph_3P=Se can form charge-transfer (CT) adducts when combined with stoichiometric amounts of an appropriate dihalogen or interhalide compounds.[13] Upon addition of Br_2 to **6** in dichloromethane, however, the formation of several products was observed by means of $^{31}P\{^1H\}$ NMR spectroscopy, even at T = −30 °C. We anticipate that the rather reactive bromine reacted unselectively with the unsaturated phosphorus heterocycle. The same was observed when the interhalide compounds IBr and ICl, respectively, were used. Nevertheless, when I_2 was added to **6** at room temperature in dichloromethane, the $^{31}P\{^1H\}$ NMR spectrum revealed a single resonance at δ(ppm) = 162.0, which is only slightly shifted compared to the starting material (δ(ppm) = 170.3). Additionally, the $^1J_{P,Se}$ coupling constant decreased numerically from 883 Hz to 833 Hz. Much to our delight, the slow evaporation of the solvent at T = −30 °C afforded large dark red crystals, which were suitable for single crystal X-ray diffraction.

The crystallographic characterization reveals, that an I_2 adduct of **6** has indeed been formed. The molecular structure of the new compound (**8**) and its packing in the solid state is depicted in Figure 4, along with selected bond lengths and angles.

The I(1)–I(2) bond length in **8** is with 2.8475(3) Å slightly shorter compared to Ph_3P=Se···I_2, while the distance $d_{(Se···I)}$ is with 2.8585(3) Å somewhat longer than in the triphenylphos-

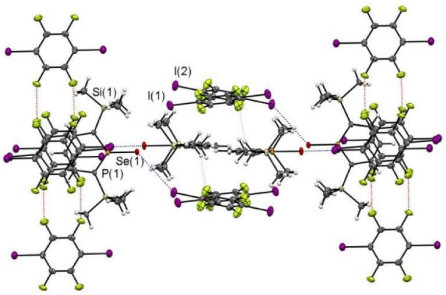

Figure 3. Overview of molecular packing in the cocrystal of **7**. 1,4-TFDIB molecule is involved in I···Se interactions (blue), short F···H contacts with two neighboring phosphinine selenides (green), and short F···F short contacts with neighboring 1,4-TFDIB molecules (red).

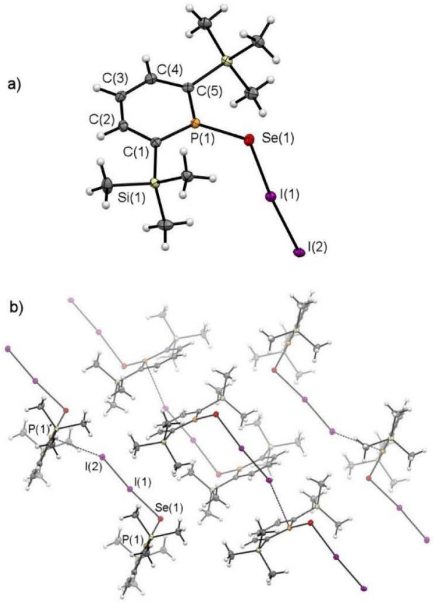

Figure 4. Molecular structure of phosphinine selenide-diiodide adduct **8** in the crystal and packing of **8** in the solid state. Displacement ellipsoids are shown at the 50% probability level. Prime (') donates a symmetry equivalent atom generated using the following equation: 1 + x, + y, + z. Selected bond lengths (Å) and angles (°): I(1)–Se(1): 2.8585(3), I(1)–I(2): 2.8475(3), Se(1)–P(1): 2.1243(6), P(1)–C(1): 1.709(2), P(1)–C(5): 1.705(2), C(1)–C(2): 1.401(2), C(2)–C(3): 1.395(2), C(3)–C(4): 1.395(3), C(4)–C(5): 1.399(2), I(2)–P(1)': 3.6853(5). Se(1)–I(1)–I(2): 174.500(15); I(1)–Se(1)–P(1): 105.85(2), C(1)–P(1)–C(5): 113.81(8).

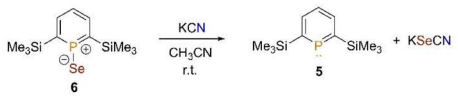

Scheme 2. Reaction of phosphinine selenide **6** with KCN in acetonitrile.

phine derivative ($d_{(I\text{–}I)}$: 2.881(2) Å; $d_{(Se\text{–}I)}$: 2.803(3) Å; $d_{(I\text{–}I)}$ in I_2: 2.71 Å). This can be attributed to the smaller polarization of the Se(1)–I(1) bond in **8**. Moreover, the P(1)–Se(1)–I(1) bond angle in **8** is with 105.85(2)° very similar with respect to $Ph_3P{=}Se{\cdots}I_2$ (106.0(1)°). This is in line with the donation of electron density from one of the non-bonding *p*-orbitals at the selenium atom to the σ-hole of the I_2 molecule. The Se(1)–I(1)–I(2) moiety is essentially linear (174.500(15)°), which is consistent with other crystallographically characterized charge-transfer complexes of diiodine (Scheme 1).[13]

Additionally, the P(1)–Se(1) bond in **8** is with 2.1243(6) Å considerably longer with respect to **7** (2.083(1) Å). Also this observation is in line with earlier computational studies on phosphinine selenides, which show, that the two non-bonding *p*-orbitals at the selenium atom are involved in backdonation to σ*(P–C) and π*(P–C) orbitals.[16] Consequently, also the bond lengths P(1)–C(5) (1.705(2) Å) and P(1)–C(1) (1.709(2) Å) are shorter in **8** with respect to **7** (1.721(5), 1.715(5) Å).

Additionally, I(2) has a short contact of 3.6853(5) Å to the phosphorus atom P(1)' of a neighbouring phosphinine selenide (Figure 4b), which is significantly shorter than the sum of the van-der-Waals radii of these atoms. This is perfectly in line with the presence of a formal positive charge at the phosphorus atom.

As the σ-hole at the selenium atom of **6** (Figure 1) is in fact larger than the corresponding one in $Ph_3P{=}Se$, we anticipated that the rather nucleophilic CN^- anion might form a strong Se···NCK bond. Compound **6** was thus reacted with KCN in acetonitrile at room temperature (Scheme 2).

Upon slow evaporation of the solvent, single crystals, suitable for X-ray diffraction, were obtained. Much to our surprise, we found that KSeCN had been formed, rather than the expected adduct of the type **6**···NCK (Figure S10). This polymorph of KSeCN can be found in the Cambridge Crystallographic Data Center.[19] Apparently, **6** serves as a very good selenium-transfer reagent, rather than participating in non-covalent interactions.

Conclusion

In conclusion, we have structurally characterized for the first time the phosphinine selenide (**6**) in form of a co-crystalline adduct with the organoiodine 1,4-TFDIB (**7**). The molecular structure of **7** in the solid state is stabilized by several non-bonding interactions, including π-π stacking, hydrogen bonding, F–F– and Se–I interactions. This demonstrates that phosphinine selenides can be used efficiently as a multifunctional molecule for crystal design. Moreover, we could show that the phosphinine selenide also forms an adduct with diiodine *via* interaction of one of the selenium lone-pairs with the σ-hole at the I_2 molecule, as confirmed by single crystal X-ray diffraction. The iodine molecule shows an additional contact with the phosphorus atom of a neighboring phosphinine selenide, which carries a formal positive charge. Moreover, it turned out that the phosphinine selenide acts as an efficient selenium transfer reagent as it reacts selectively with KCN towards KSeCN.

Experimental Section

General Remarks: All reactions were performed under argon in oven-dried glassware using modified Schlenk techniques unless otherwise stated. All common solvents and chemicals were commercially available and were used without further purification. All dry or deoxygenated solvents were prepared using standard techniques or an MBraun solvent purification system. 2,6-Bis(trimethylsilyl)phosphinine selenide (**6**) was prepared according to the literature.[16] The ^1H, $^{13}C\{^1H\}$, ^{19}F, $^{29}Si\{^1H\}$, ^{31}P, $^{31}P\{^1H\}$ and $^{77}Se\{^1H\}$ NMR spectra were recorded on a JEOL ECX400 (400 MHz) and a Bruker Avance 600 (600 MHz) spectrometer and all chemical shifts are reported relative to the residual resonance in the deuterated solvents. The HRMS ESI mass spectra were measured on an Agilent 6210 ESI-TOF.

Single crystal X-ray diffraction: Low-temperature and room-temperature X-ray diffractometry was performed on a Bruker-AXS X8 Kappa Duo diffractometer with *IμS* micro-sources, performing ϕ- and ω-scans. The data were collected using a Photon 2 CPAD detector with Mo K_α radiation ($\lambda = 0.71073$ Å). The structures were solved by dual-space methods using SHELXT[20] and refined against F^2 on all data by full-matrix least squares with SHELXL-2017[21] following established refinement strategies[22]. The program Olex2[23] was also used for refinement. All non-hydrogen atoms were refined anisotropically. All hydrogen atoms were included into the model at geometrically calculated positions and refined using a riding model. The isotropic displacement parameters of all hydrogen atoms were fixed to 1.2 times the *U*-value of the atoms they are linked to (1.5 times for methyl groups). Details of the data quality and a summary of the residual values of the refinements are listed in table S2. Tables S3–S8 provide all bond lengths and angles for the obtained structures (Supporting Information).

Preparation of 7: Phosphinine selenide **6** (32 mg, 0.1 mmol) was dissolved in dichloromethane (2 mL) at $T = -30$ °C. Subsequently, 1,4-TFDIB (40 mg, 0.1 mmol) was added to the solution. Another 2 mL of *n*-pentane was layered on the dichloromethane solution. The co-crystalline adduct **7** was obtained after the solution was evaporation at $T = -30$ °C. ^1H NMR (400 MHz, C_6D_6) δ 7.47 (dd, $^3J_{H,P} = 42.7$, $^3J_{H,H} = 8.1$ Hz, 2H, *meta-H*), 6.64 (q, $^4J_{H,P} = 8.0$ Hz, 1H, *para-H*), 0.43 (s, 18H, –Si*Me*$_3$) ppm. $^{13}C\{^1H\}$ NMR (101 MHz, CD_2Cl_2) δ 148.6–147.8 (m, $C_6F_4I_2$), 146.1 (d, $^3J_{C,P} = 15.1$ Hz, *meta-C*-C_5H_3P), 145.5 (d, $^4J_{C,P} = 14.6$ Hz, *para-C*-C_5H_3P), 120.0 (d, $^2J_{C,P} = 52.2$ Hz, *ortho-C*-C_5H_3P), 73.5–73.2 (m, $C_6F_4I_2$), −1.0 (d, $J = 2.8$ Hz, –Si*Me*$_3$) ppm. ^{31}P NMR (162 MHz, CD_2Cl_2) δ 168.39 (td, $J_{H,P} = 43.1$, 7.6 Hz, $^1J_{P\text{–}Se} = 883.5$ Hz) ppm. $^{31}P\{^1H\}$ NMR (162 MHz, C_6D_6) δ 170.3 (s, $^1J_{P\text{–}Se} = 883.5$ Hz) ppm. ^{19}F NMR (377 MHz, CD_2Cl_2) δ −114.6 ppm. $^{77}Se\{^1H\}$ NMR (76 MHz, CD_2Cl_2) δ −28.0 (d, $^1J_{P\text{–}Se} = 878.8$ Hz).

Preparation of 8: Phosphinine selenide **6** (32 mg, 0.1 mmol) was dissolved in dichloromethane (1 mL) at $T = -30$ °C and I_2 (25 mg, 0.1 mmol) was added to the solution. The dichloromethane solution was stored in the freezer at $T = -30$ °C and red crystals were obtained after the solvent slowly evaporated. Product yield: 92%

(0.09 mmol, 51.6 mg). ^{1}H NMR (600 MHz, CD_2Cl_2) δ 7.94 (dd, $^{1}J_{H,P}$ = 44.4, $^{2}J_{H,H}$ = 8.1 Hz, 2H, *meta-H*), 7.27 (q, $^{3}J_{H,P}$ = 8.2 Hz, 1H, *para-H*), 0.49 (s, 18H, $-SiMe_3$) ppm. $^{13}C\{^{1}H\}$ NMR (151 MHz, CD_2Cl_2) δ 148.5 (d, $^{3}J_{C,P}$ = 13.0 Hz, *para-C*), 146.8 (d, $^{2}J_{C,P}$ = 16.4 Hz, *C2*, *meta-C*), 122.4 (d, $^{1}J_{C,P}$ = 54.5 Hz, *ortho-C*), −0.7 (d, *J* = 2.9 Hz, $-SiMe_3$) ppm. $^{31}P\{^{1}H\}$ NMR (243 MHz, CD_2Cl_2) δ 162.0 (s, $^{1}J_{P-Se}$ = 832.5 Hz) ppm. HR-ESI MS (m/z): 573.5846 (Calculated: 573.8169) $[M]^+$.

Synthesis of KSeCN: Phosphinine selenide **6** (32 mg, 0.1 mmol) was dissolved in acetonitrile (1 mL) and KCN (6.5 mg, 0.1 mmol) was added to the solution at room temperature. After stirring for 2 hours, the solvent was slowly evaporated to afford dark red crystals in quantitative yield. (14 mg). The free phosphinine **6** could be detected as a viscous oil at the bottom of the vial.

Acknowledgements

Funding by Freie Universität Berlin, the Deutsche Forschungsgemeinschaft DFG (Project-Nr 2100302201) as well as the China Scholarship Council is gratefully acknowledged. Open Access funding enabled and organized by Projekt DEAL.

Conflict of Interest

The authors declare no conflict of interest.

Data Availability Statement

The data that support the findings of this study are available from the corresponding author upon reasonable request.

Keywords: co-crystals · noncovalent interactions · phosphorus · σ-holes · selenium

[1] For recent examples, see a) M. L. Kelty, A. J. McNeece, J. W. Kurutz, A. S. Filatov, J. S. Anderson, *Chem. Sci.* **2022**, *13*, 4377–4387; b) W. P. Teh, D. C. Obenschain, B. M. Black, F. E. Michael, *J. Am. Chem. Soc.* **2020**, *142*, 16716–16722; c) T. Zheng, J. R. Tabor, Z. L. Stein, F. E. Michael, *Org. Lett.* **2018**, *20*, 6975–6978; d) S. Konishi, T. Iwai, M. Sawamura, *Organometallics* **2018**, *37*, 1876–1883; e) M. J. Poller, N. Burford, K. Karaghiosoff, *Chem. Eur. J.* **2018**, *24*, 85–88.
[2] T. Murai, T. Kimura, *Curr. Org. Chem.* **2006**, *10*, 1963–1973.
[3] a) M. Bollmark, J. Stawinski, *Chem. Commun.* **2001**, *8*, 771–772; b) R. Rodriguez, H. Liu, *J. Am. Chem. Soc.* **2012**, *134*, 1400–1403.
[4] J. A. Gillespie, E. Zuidema, P. W. Van Leeuwen, P. C. Kamer, *Phosphorus (III) ligands in homogeneous catalysis: design and synthesis*, (Eds: P. C. Kamer, P. W. Van Leeuwen), John Wiley & Sons, **2012**, Ch. 1.
[5] a) H. D. Arman, E. R. Rafferty, C. A. Bayse, W. T. Pennington, *Cryst. Growth Des.* **2012**, *12*, 4315–4323; b) A. J. Peloquin, C. D. McMillen, S. T. Iacano, W. T. Pennington, *ChemPlusChem* **2021**, *86*, 549–557.
[6] a) H. Wang, W. Wang, W. J. Jin, *Chem. Rev.* **2016**, *116*, 5072–5104; b) T. Sakurai, M. Sundaralingam, G. Jeffrey, *Acta Crystallogr.* **1963**, *16*, 354–363.
[7] A. Hasija, D. Chopra, *Cryst. Growth Des.* **2020**, *20*, 6272–6282.
[8] K. Lisac, F. Topić, M. Arhangelskis, S. Cepić, P. A. Julien, C. W. Nickels, A. J. Morris, T. Friščić, D. Cinčić, *Nat. Commun.* **2019**, *10*, 1–10.
[9] R. Bhowal, S. Biswas, D. P. A. Saseendran, A. L. Koner, D. Chopra, *CrystEngComm* **2019**, *21*, 1940–1947.
[10] T. Salzillo, M. Masino, G. Kociok-Köhn, D. Di Nuzzo, E. Venuti, R. G. Della Valle, D. Vanossi, C. Fontanesi, A. Girlando, A. Brillante, *Cryst. Growth Des.* **2016**, *16*, 3028–3036.
[11] a) R. Lee, A. J. Firbank, M. R. Probert, J. W. Steed, *Cryst. Growth Des.* **2016**, *16*, 4005–4011; b) M. Singh, D. Chopra, *Cryst. Growth Des.* **2018**, *18*, 6670–6680.
[12] R. A. Zingaro, E. A. Meyers, *Inorg. Chem.* **1962**, *1*, 771–774.
[13] S. M. Godfrey, S. L. Jackson, C. A. McAuliffe, R. G. Pritchard, *J. Chem. Soc. Dalton Trans.* **1997**, 4499–4502.
[14] a) Y. Feng, D. Rainteau, C. Chachaty, Z. W. Yu, C. Wolf, P. J. Quinn, *Biophys. J.* **2004**, *86*, 2208–2217; b) F. G. Wu, N. N. Wang, Z. W. Yu, *Langmuir* **2009**, *25*, 13394–13401.
[15] X. Guo, X. An, Q. Li, *J. Phys. Chem. A* **2015**, *119*, 3518–3527.
[16] F. Wossidlo, D. S. Frost, J. Lin, N. T. Coles, K. Klimov, M. Weber, T. Böttcher, C. Müller, *Chem. Eur. J.* **2021**, *27*, 12788–12795.
[17] A. Moores, T. Cantat, L. Ricard, N. Mézailles, P. Le Floch, *New J. Chem.* **2007**, *31*, 1493–1498.
[18] S. Nyburg, C. Faerman, *Acta Crystallogr. Sect. B* **1985**, *41*, 274–279.
[19] A. Shlyaykher, M. Ehmann, A. J. Karttunen, F. Tambornino, CCDC 2080510: Experimental Crystal Structure Determination, **2021**, DOI: 10.5517/ccdc.csd.cc27ty78.
[20] G. M. Sheldrick, *Acta Crystallogr. Sect. A* **2015**, *71*, 3–8.
[21] G. M. Sheldrick, *Acta Crystallogr. Sect. C* **2015**, *71*, 3–8.
[22] P. Müller, *Crystallogr. Rev.* **2009**, *15*, 57–83.
[23] O. v. Dolomanov, L. J. Bourhis, R. J. Gildea, J. A. K. Howard, H. Puschmann, *J. Appl. Crystallogr.* **2009**, *42*, 339–341.

Manuscript received: August 18, 2022
Revised manuscript received: September 20, 2022
Accepted manuscript online: September 30, 2022

ChemPlusChem

Supporting Information

Phosphinine Selenide: Noncovalent Interactions with Organoiodines and Elemental Iodine, and Reactivity towards Potassium Cyanide

Jinxiong Lin, Nathan T. Coles, Manuela Weber, and Christian Müller*

Contents

1. Experimental details

Table S1: Method and list of solvents used for crystallization experiments.

Experiment number	Solvent used for crystallization	Method	Result
Phosphinine selenide (**6**)+TFTIB			
1.	Acetonitrile	Slow evaporation (r. t.)	Single crystal of TFTIB and grey selenium
2.	Dichloromethane	Slow evaporation (-30 °C)	Single crystal of TFTIB and viscous oil
3.	Dichloromethane and *n*-Pentane	Diffusion and then Slow evaporation (-30 °C)	Single crystal of TFTIB and viscous oil
4.	Dichloromethane and diethyl ether	Layering of solvents and then slow evaporation (-30 °C)	Single crystal of TFTIB and viscous oil
6+1,2-F_4DIB			
1	Dichloromethane	Slow evaporation (-30 °C)	viscous oil
2	Tetrahydrofuran	Slow evaporation (r. t.)	viscous oil
3	Dichloromethane and *n*-Pentane	Layering of solvents and then slow evaporation (-30 °C)	viscous oil
4	*n*-hexane	Slow evaporation (r. t.)	viscous oil
6+TIE			
1	Dichloromethane	Slow evaporation (-30 °C)	Aggregates
2	Dichloromethane and *n*-Pentane	Layering of solvents and then slow evaporation (-30 °C)	Aggregates
6+1,4-F4DIB			
1	Dichloromethane	Slow evaporation (-30 °C)	viscous oil
2	Dichloromethane and *n*-Pentane	Slow evaporation (r. t.)	Co-crystal
3	Acetonitrile	Slow evaporation (r. t.)	Grey selenium and viscous oil

2. NMR spectra

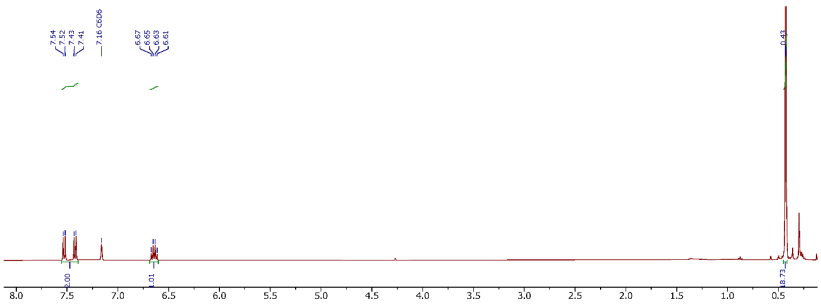

Figure S1: ^{1}H NMR spectrum of **7** in C_6D_6.

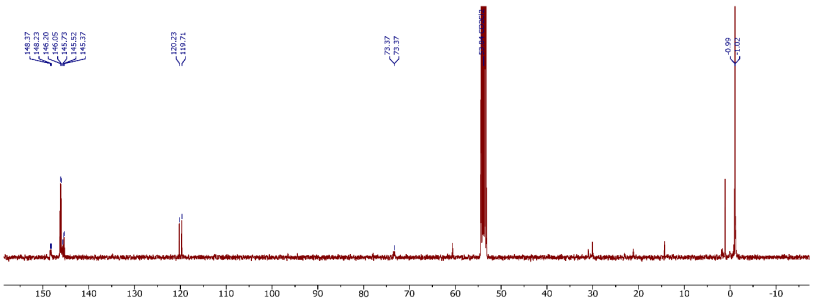

Figure S2: $^{13}C\{^{1}H\}$ NMR spectrum of **7** in CD_2Cl_2.

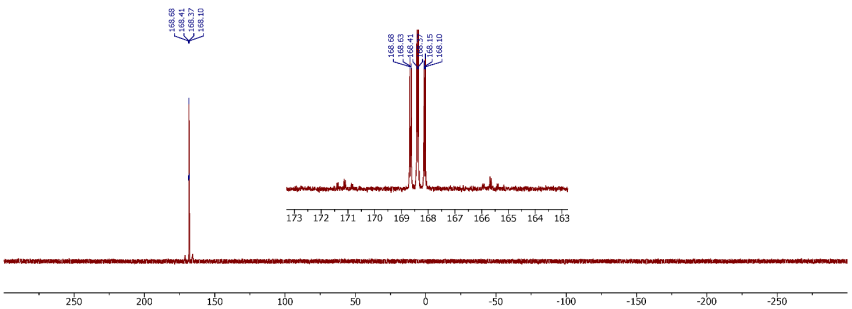

Figure S3: ^{31}P NMR spectrum of **7** in CD_2Cl_2.

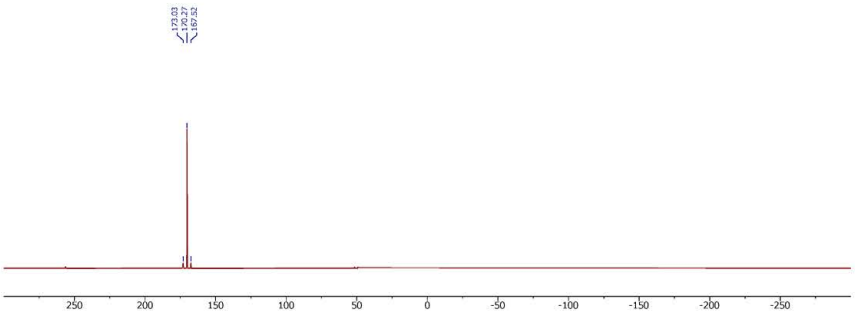

Figure S4: $^{31}P\{^{1}H\}$ NMR spectrum of **7** in C_6D_6.

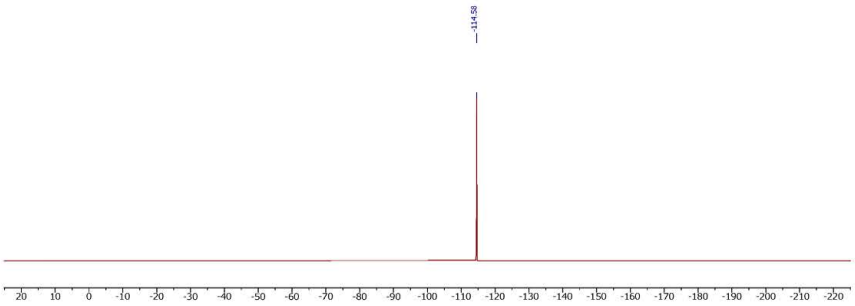

Figure S5: ^{19}F NMR spectrum of **7** in CD_2Cl_2.

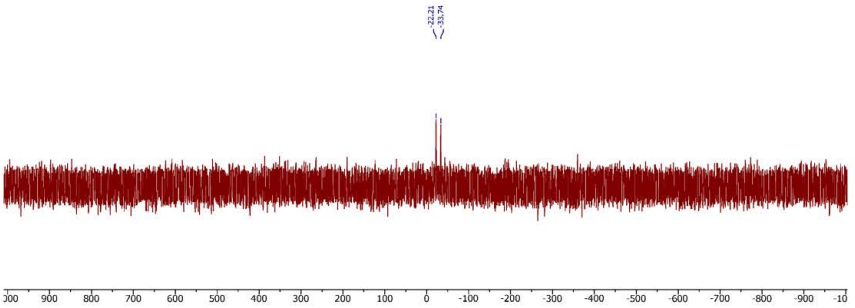

Figure S6: $^{77}Se\{^{1}H\}$ NMR spectrum of **7** in CD_2Cl_2.

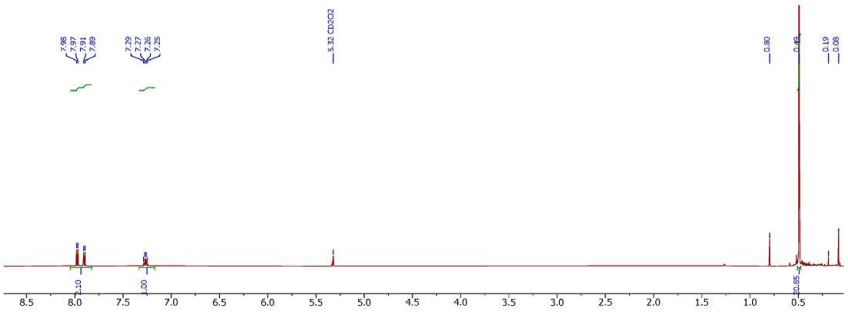

Figure S7: ^{1}H NMR spectrum of **8** in CD_2Cl_2.

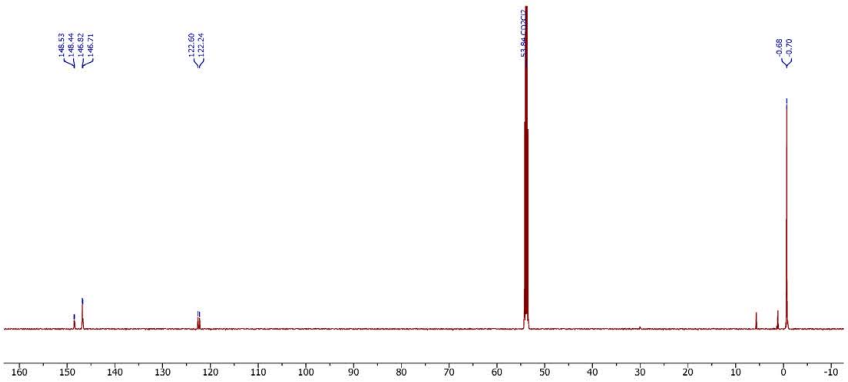

Figure S8: $^{13}C\{^{1}H\}$ NMR spectrum of **8** in CD_2Cl_2.

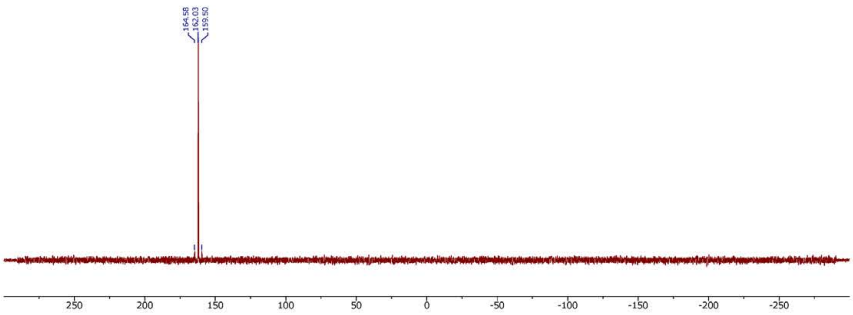

Figure S9: $^{31}P\{^{1}H\}$ NMR spectrum of **8** in CD_2Cl_2.

3. Crystallographic details

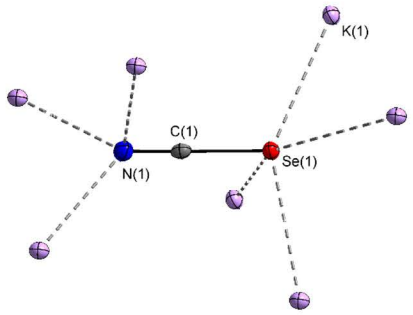

Figure S10. Molecular structure of KSeCN in the crystal. Displacement ellipsoids are shown at the 50 % probability level. Selected bond lengths (Å) and angles (°): Se(1)-C(1): 1.808(1); Se(1)-K(1): 3.3374(3); 3.8096(3); 3.3892(4); 3.4396(3), K(1)-N(1): 2.867(1); 2.810(1); 3.007(1), N(1)-C(1): 1.160(2). C(1)-Se(1)-K(1): 98.45(4); 128.58(4); 80.27(4); 112.44(4).

This polymorph of KSeCN can be found in the Cambridge Crystallographic Data Center (Figure S10).[1]

The structures were solved by dual-space methods using SHELXT[2] and refined against F^2 on all data by full-matrix least squares with SHELXL-2017[3] following established refinement strategies[4]. The program Olex2[5] was also used to aid in the refinement. All non-hydrogen atoms were refined anisotropically. All hydrogen atoms were included into the model at geometrically calculated positions and refined using a riding model. The isotropic displacement parameters of all hydrogen atoms were fixed to 1.2 times the *U*-value of the atoms they are linked to (1.5 times for methyl groups). Details of the data quality and a summary of the residual values of the refinements are listed in **Table S2** below. Tables **S3**, **S5**, **S7** give all bond lengths for the structures and **S4**, **S6**, **S8** give all angles for the structures.

Table S2 – Selected crystallographic data for **7**, **8** and KSeCN.

Sample name	**7**	**8**	KSeCN
CCDC number	2201270	2201271	2201272
Empirical formula	$C_{17}H_{21}F_4I_2PSeSi_2$	$C_{11}H_{21}I_2PSeSi_2$	CKNSe
Formula Weight	721.25	573.19	144.08
Temperature / K	100.0	102	294.0
Crystal system	Monoclinic	Monoclinic	Monoclinic
Space group	$P2_1/c$	$P2_1/c$	$P2_1/n$
a/Å	10.2800(2)	9.6576(2)	4.4153(2)
b/Å	10.1004(2)	15.7829(3)	7.5083(3)
c/Å	23.2591(4)	12.3940(2)	11.7238(7)
α/°	90	90	90
β/ °	90.2792(6)	90.4417(6)	100.168(2)
γ/ °	90	90	90
Volume/Å^3	2415.01(8)	1889.10(6)	382.56(3)
Z	4	4	4
Reflections collected	58835	62088	15784
Independent reflections (R_{int})	5927 (0.0497)	5730 (0.0340)	1673 (0.0375)

R_1 [I>2σ (I)]	0.0446	0.0173	0.0189
wR_2 (all data)	0.1016	0.0407	0.0331

Additional refinement details for **7**: Refined as a 2-component twin. Twin was found using the twinning tool COSET in WINGX2014. This generated a new hkl file which was refined against.

Table S3-List of bond lengths for **7**.

Atom1	Atom2	Length/ Å	Atom1	Atom2	Length/ Å
I2	C17	2.082(5)	C13	C14	1.376(9)
F3	C15	1.349(8)	Se1	P1	2.083(1)
F4	C16	1.342(8)	P1	C1	1.721(5)
C15	C16	1.36(1)	P1	C5	1.715(5)
C15	C17	1.370(9)	Si1	C1	1.879(5)
C16	C17	1.394(9)	Si1	C6	1.863(7)
C17	C15	1.370(9)	Si1	C7	1.856(7)
I2	C17	2.082(5)	C13	C14	1.376(9)
F3	C15	1.349(8)	C14	C12	1.39(1)
F4	C16	1.342(8)	I1	C13	2.078(7)
C15	C16	1.36(1)	F1	C12	1.343(8)
C16	C17	1.394(9)	F2	C14	1.343(7)
I1	C13	2.078(7)	C12	C13	1.377(9)
F1	C12	1.343(8)	Si1	C8	1.856(7)
F2	C14	1.343(7)	Si2	C5	1.897(6)
C12	C13	1.377(9)	Si2	C9	1.867(6)
C12	C14	1.39(1)	Si2	C10	1.851(7)
C2	C3	1.387(8)	Si2	C11	1.855(7)
C3	C4	1.390(8)	C1	C2	1.414(7)
C4	C5	1.396(7)			

Table S4-List of angles for **7**.

Atom1	Atom2	Atom3	Angle/°	Atom1	Atom2	Atom3	Angle/°
F3	C15	C16	119.0(6)	C12	C14	F2	117.7(6)
F3	C15	C17	119.6(6)	C12	C14	C13	121.3(6)
C16	C15	C17	121.3(6)	F2	C14	C13	120.9(6)
F4	C16	C15	119.0(6)	Se1	P1	C1	123.4(2)
F4	C16	C17	119.6(5)	Se1	P1	C5	124.9(2)
C15	C16	C17	121.3(6)	C1	P1	C5	111.8(3)
I2	C17	C16	121.0(4)	C1	Si1	C6	107.6(3)
I2	C17	C15	121.6(4)	C1	Si1	C7	110.0(3)
C16	C17	C15	117.3(5)	C1	Si1	C8	109.1(3)
C17	C15	F3	119.6(6)	C6	Si1	C7	108.4(3)
C17	C15	C16	121.3(6)	C6	Si1	C8	109.7(3)
F3	C15	C16	119.0(6)	C7	Si1	C8	111.9(3)
F4	C16	C15	119.0(6)	C5	Si2	C9	107.0(3)
F4	C16	C17	119.6(5)	C5	Si2	C10	108.6(3)
C15	C16	C17	121.3(6)	C5	Si2	C11	110.3(3)
C15	C17	I2	121.6(4)	C9	Si2	C10	110.4(3)

C15	C17	C16	117.3(5)	C9	Si2	C11	108.6(3)
I2	C17	C16	121.0(4)	C10	Si2	C11	111.8(3)
F1	C12	C13	120.5(6)	P1	C1	Si1	122.7(3)
F1	C12	C14	118.7(6)	P1	C1	C2	115.3(4)
C13	C12	C14	120.8(6)	Si1	C1	C2	122.0(4)
I1	C13	C12	121.0(5)	C1	C2	C3	126.9(5)
I1	C13	C14	121.1(5)	C2	C3	C4	123.3(5)
C12	C13	C14	117.9(6)	C3	C4	C5	126.2(5)
F2	C14	C13	120.9(6)	P1	C5	Si2	121.6(3)
F2	C14	C12	117.7(6)	P1	C5	C4	116.6(4)
C13	C14	C12	121.3(6)	Si2	C5	C4	121.7(4)
C14	C12	F1	118.7(6)	I1	C13	C14	121.1(5)
C14	C12	C13	120.8(6)	C12	C13	C14	117.9(6)
F1	C12	C13	120.5(6)	I1	C13	C12	121.0(5)

Table S5-List of bond lengths for **8**.

Atom1	Atom2	Length/ Å	Atom1	Atom2	Length/Å
I1	Se1	2.8585(3)	Si1	C8	1.860(2)
I1	I2A	2.843(2)	Si2	C5	1.906(2)
Se1	P1	2.1249(6)	Si2	C9	1.865(2)
P1	C1	1.708(2)	Si2	C10	1.863(2)
P1	C5	1.705(2)	Si2	C11	1.861(2)
Si1	C1	1.909(2)	C1	C2	1.402(2)
Si1	C6	1.856(2)	C2	C3	1.394(3)
Si1	C7	1.863(2)	C3	C4	1.394(3)
C4	C5	1.400(3)			

Table S6-List of angles for **8**.

Atom1	Atom2	Atom3	Angle/°	Atom1	Atom2	Atom3	Angle/°
Se1	I1	I2A	174.36(4)	C9	Si2	C11	110.62(9)
I1	Se1	P1	105.85(2)	C10	Si2	C11	111.98(9)
Se1	P1	C1	123.73(6)	P1	C1	Si1	124.1(1)
Se1	P1	C5	122.31(6)	P1	C1	C2	114.9(1)
C1	P1	C5	113.81(9)	Si1	C1	C2	121.0(1)
C1	Si1	C6	106.88(8)	C1	C2	H2	117
C1	Si1	C7	106.35(9)	C1	C2	C3	126.0(2)
C1	Si1	C8	111.19(8)	C2	C3	C4	124.3(2)
C6	Si1	C7	110.48(9)	C3	C4	C5	125.9(2)
C6	Si1	C8	108.65(9)	P1	C5	Si2	123.4(1)
C7	Si1	C8	113.11(9)	P1	C5	C4	115.1(1)
C5	Si2	C9	107.05(8)	Si2	C5	C4	121.5(1)
C5	Si2	C10	108.02(8)	C9	Si2	C10	109.64(9)
C5	Si2	C11	109.38(8)				

Table S7-List of bond lengths for KSeCN.

Atom1	Atom2	Length/ Å	Atom1	Atom2	Length/ Å
Se1	C1	1.808(1)	K1	N1	3.007(1)
Se1	K1	3.3374(3)	K1	C1	3.174(1)
Se1	K1	3.8096(3)	N1	C1	1.160(2)
Se1	K1	3.3892(4)	N1	K1	2.810(1)
Se1	K1	3.4396(3)	N1	K1	3.007(1)
K1	N1	2.867(1)	C1	K1	3.174(1)
K1	Se1	3.8096(3)	Se1	K1	3.3374(3)
K1	Se1	3.3374(3)	Se1	K1	3.8096(3)
K1	Se1	3.3892(4)	Se1	K1	3.3374(3)
K1	Se1	3.4396(3)	K1	N1	2.867(1)
K1	N1	2.810(1)	K1	N1	2.867(1)
N1	C1	1.160(2)			

Table S8-List of bond angles for KSeCN.

Atom1	Atom2	Atom3	Angle/°	Atom1	Atom2	Atom3	Angle/°
C1	Se1	K1	98.45(4)	Se1	K1	C1	169.26(3)
C1	Se1	K1	128.58(4)	Se1	K1	N1	155.47(3)
C1	Se1	K1	80.27(4)	Se1	K1	N1	83.76(2)
C1	Se1	K1	112.44(4)	Se1	K1	C1	102.81(2)
K1	Se1	K1	75.99(1)	N1	K1	N1	98.68(3)
K1	Se1	K1	98.70(1)	N1	K1	C1	85.26(3)
K1	Se1	K1	148.35(1)	N1	K1	C1	21.42(3)
K1	Se1	K1	150.95(1)	K1	N1	C1	135.5(1)
K1	Se1	K1	89.35(1)	K1	N1	K1	91.43(4)
K1	Se1	K1	80.56(1)	K1	N1	K1	108.12(4)
N1	K1	Se1	145.99(3)	C1	N1	K1	128.1(1)
N1	K1	Se1	133.39(3)	C1	N1	K1	87.42(9)
N1	K1	Se1	83.65(3)	K1	N1	K1	98.68(4)
N1	K1	Se1	68.87(2)	Se1	C1	N1	179.6(1)
N1	K1	N1	88.57(4)	Se1	C1	K1	108.83(5)
N1	K1	N1	71.88(3)	N1	C1	K1	71.16(9)
N1	K1	C1	88.06(3)	K1	Se1	K1	98.70(1)
Se1	K1	Se1	75.99(1)	K1	Se1	K1	89.35(1)
Se1	K1	Se1	66.43(1)	K1	Se1	K1	148.35(1)
Se1	K1	Se1	118.60(1)	K1	Se1	K1	75.99(1)
Se1	K1	N1	75.00(3)	Se1	K1	Se1	112.96(1)
Se1	K1	N1	139.12(2)	Se1	K1	Se1	66.43(1)
Se1	K1	C1	119.19(2)	Se1	K1	Se1	75.99(1)
Se1	K1	Se1	112.96(1)	Se1	K1	Se1	71.48(1)
Se1	K1	Se1	71.48(1)	N1	K1	N1	88.57(4)
Se1	K1	N1	133.05(3)	N1	K1	C1	21.42(3)
Se1	K1	N1	80.49(2)	N1	K1	N1	71.88(3)
Se1	K1	C1	77.72(2)	C1	K1	N1	88.06(3)
Se1	K1	Se1	80.56(1)	K1	N1	K1	91.43(4)
Se1	K1	N1	87.72(3)	K1	N1	K1	108.12(4)

Se1	K1	N1	154.44(3)	K1	N1	C1	87.42(9)
K1	C1	N1	71.16(9)	K1	N1	C1	135.5(1)

4. References

[1] A. Shlyaykher, M. Ehmann, A. J. Karttunen, F. Tambornino, CCDC 2080510: *Experimental Crystal Structure Determination*, **2021**, DOI: 10.5517/ccdc.csd.cc27ty78.

[2] G. M. Sheldrick, *Acta Crystallogr. A* **2015**, *71*, 3–8.

[3] G. M. Sheldrick, *Acta Crystallogr. C* **2015**, *71*, 3–8.

[4] P. Müller, *Crystallogr. Rev.* **2009**, *15*, 57–83.

[5] O. v. Dolomanov, L. J. Bourhis, R. J. Gildea, J. A. K. Howard, H. Puschmann, *J. Appl. Crystallogr.* **2009**, *42*, 339–341.

Chapter 4

3-*N*,*N*-Dimethylaminophosphinine derivative

4.1 How to Shrink the Ring: Phospholenes from Phosphabenzenes *via* Selective Ring Contraction

Jinxiong Lin,[a] Nathan. T. Coles,[a,b] Lea Dettling,[a] Luca Steiner,[c] J. Felix Witte,[c] Beate Paulus,[c] Christian Müller*[a]

a: J. Lin, Dr. N. T. Coles, L. Dettling, Prof. Dr. C. Müller

Institut für Chemie und Biochemie, Freie Universität Berlin

Fabeckstr. 34/36, 14195 Berlin, Germany

b: Dr. N. T. Coles

School of Chemistry, University of Nottingham, University Park Campus

Nottingham, NG7 2RD, United Kingdom

c: L. Steiner, Dr. J. F. Witte, Prof. Dr. B. Paulus

Institut für Chemie und Biochemie, Freie Universität Berlin

Arnimallee 22, 14195 Berlin, Germany

Submitted for publication

Author contributions: This project was designed by J. Lin and Prof. Dr. C. Müller. All reactions were performed by J. Lin. All single crystals were obtained by J. Lin. The single crystal X-ray diffraction analyses were carried out by Dr. N. T. Coles. NMR experiments were conducted by J. Lin. Theoretical calculations were performed by L. Dettling, L. Steiner, Dr. F. Steiner, Prof. Dr. B. Paulus. The paper was written by J. Lin and was corrected by Dr. N. T. Coles, Prof. B. Paulus, Prof. C. Müller.

Estimated own contribution: ~ 70 %.

RESEARCH ARTICLE

How to Shrink the Ring: Phospholenes from Phosphabenzenes *via* Selective Ring Contraction

Jinxiong Lin,[a] Nathan T. Coles,[a,b] Lea Dettling,[a] Luca Steiner,[c] J. Felix Witte,[c] Beate Paulus,[c] and Christian Müller*[a]

[a] J. Lin, Dr. N. T. Coles, L. Dettling, Prof. Dr. C. Müller
Freie Universität Berlin
Institut für Chemie und Biochemie
Fabeckstrasse 34/36, 14195 Berlin (Germany)
E-mail: c.mueller@fu-berlin.de
[b] Dr. N. T. Coles
School of Chemistry
University of Nottingham
University Park, NG7 2RD
[c] L. Steiner, Dr. J. F. Witte. Prof. Dr. B. Paulus
Freie Universität Berlin
Institut für Chemie und Biochemie
Arnimallee 22, 14195 Berlin (Germany)

Supporting information for this article is given via a link at the end of the document.

Abstract: A 3-aminofunctionalized phosphabenzene was synthesized and structurally characterized. The pyramidalized nitrogen atom of the dimethylamino substituent indicates only a weak interaction between the lone pair of the nitrogen atom and the aromatic phosphorus heterocycle, resulting in somewhat basic character. It turned out that the amino-group can indeed be protonated by HCl. In contrast to pyridines, however, the phosphabenzene-ammonium salt undergoes a selective ring contraction to form a hydroxylphospholene oxide in the presence of additional water. Combining experimental work and quantum chemical calculations, a rational mechanism for this hitherto unknown conversion is proposed.

Introduction

λ^3,σ^2-phosphinines, also known as phosphabenzenes or phosphorines, are intriguing aromatic phosphorus heterocycles which are currently undergoing a renaissance within coordination chemistry, small molecule activation, catalysis and molecular materials science.[1-3] However, for their use in more applied research fields, their specific functionalization is particularly important in order to modify their stereo-electronic properties and coordination abilities. Phosphinines with additional donor-substituents at the 2-position of the heterocycle (**A**, Chart 1) are relatively rare. Small bite-angle phosphinines (Do = PR_2), for example, have been used successfully as chelating ligands in several catalytic reactions.[4] Grützmacher and co-workers have accessed sodium salts of phosphinine-2-ols (Do = OH).[5] The anionic phosphinine-2-olate (Do = ONa) acts as a 4e-donor and bridges a cationic $[Au(PPh_3)]^+$ and a neutral [AuCl] fragment.[6] We have recently reported the first 2-*N*,*N*-dimethylaminophosphinine **B**. Natural Resonance Theory calculations revealed resonance structures with two lone-pairs at the phosphorus atom (**B´**), contributing substantially to the electronic ground state of this compound. Accordingly, **B**/**B´** forms coordination polymers with $CuBr{\cdot}S(CH_3)_2$, in which the phosphorus atom of the phosphinine heterocycle bridges two Cu(I) centres in a rare μ_2-P-4e coordination mode in the solid state, exhibiting the first example for this bonding motif for a neutral substituted phosphinine.[7] Stimulated by these results, we anticipated to synthesize a 3-aminofunctionalized phosphinine (**C**) with the aim to investigate the influence of an amino group in 3-position on the electronic properties and the reactivity of the corresponding phosphorus heterocycle. We report here an unusual ring contraction of **C** in the presence of hydrochloric acid and water and the selective formation of a hydroxylphospholene oxide (**D**, Chart 1).

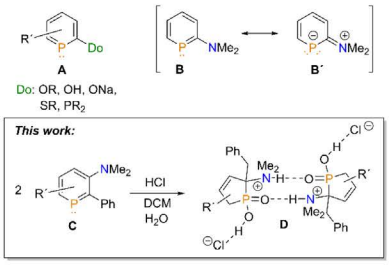

Chart 1. 2-Donor-substituted phosphinines and pictorial summary of this work.

Results and Discussion

While **B** was prepared *via* the 2-pyrone route, we found that the 3-*N*,*N*-dimethylaminophosphinine derivative **3** can easily be synthesized using a method developed by Mathey and co-workers.[8] The precursor 1,3,2-diazaphosphinine (**1**) was sequentially reacted with 1-(trimethylsilyl)propyne to afford azaphosphinine **2** and subsequently with *N*,*N*-dimethyl-phenylacetylene at elevated temperatures in toluene (Scheme 1).

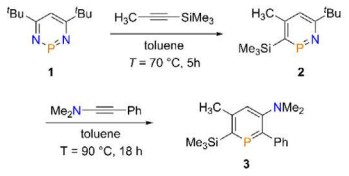

Scheme 1. Synthesis of the 3-*N*,*N*-dimethylaminofunctionalized phosphinine **3**.

A single resonance at δ(ppm) = 244.0 was found for product **3** in the $^{31}P\{^{1}H\}$ NMR spectrum. The chemical shift is remarkably different compared to the one observed for the previously synthesized phosphinine **B** (δ(ppm) = 127.0). This already indicates, that the electronic properties of **3** vary significantly from its regioisomer. Crystals of **3** suitable for single crystal X-ray diffraction were obtained by slow evaporation of the solvent from a solution of **3** in *n*-hexanes and the molecular structure of this compound in the solid state is depicted in Figure 1, along with selected bond lengths and angles.

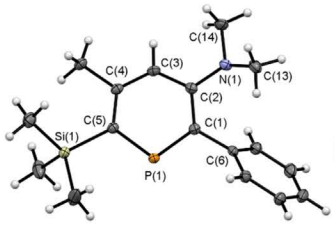

Figure 1. Molecular structure of **3** in the crystal. Displacement ellipsoids are shown at the 50% probability level. Selected bond lengths (Å) and angles (°): P(1)-C(1): 1.7369(8), P(1)-C(5): 1.7333(8), N(1)-C(2): 1.4059(10), C(1)-C(2): 1.4151(11), C(2)-C(3): 1.4104(11), C(3)-C(4): 1.3960(12), C(4)-C(5): 1.4115(11). C(1)-P(1)-C(5): 105.33(4), C(2)-N(1)-C(14): 118.06(7), C(2)-N(1)-C(13): 117.58(7), C(13)-N(1)-C(14): 110.26(7).

The crystallographic characterization of **3** shows, that the N(1)-C(4) bond length of 1.406(1) Å is closer to a C-N single bond (1.47 Å) than to a double bond (1.28 Å).[9] Moreover, the nitrogen atom of the dimethylamino substituent in **3** is pyramidalized (Σ∢(CNC) = 345.9°), in contrast to the bonding observed for **B**/**B´** in a Cu(I) complex, in which the phosphinine serves as a ligand. The twist angle of best plane through the NMe_2 group versus the phosphinine ring has been calculated as 28.30(5)°. For **3**, this might hint to only a weak electronic interaction between the nitrogen lone pair and the π-accepting phosphorus heterocycle.
As shown by us recently, an *N*,*N*-dimethylamino-group in the 2-position of the parent phosphinine induces accumulation of negative charge (red) in the ring of the π-system, as visualized by the electrostatic potential (ESA) map of **B**/**B´** (Figure 2, left).[7] In this case, the ring is even more negative than the nitrogen substituent, in full accordance with the π-accepting character of the aromatic phosphorus heterocycle. Accordingly, the basicity of **B**/**B´** is also reduced with respect to *N*,*N*-dimethylaniline, as shown by a decrease of the computed gas phase basicities (220 kcal/mol for **B**/**B´** vs. 225 kcal/mol for $C_6H_5N(CH_3)_2$).

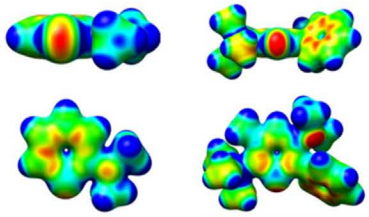

Figure 2. Electrostatic potential maps for **B**/**B´** (left) and **3** (right). Parameters: r(red): 0.000, yellow: 0.025, green: 0.050, light blue: 0.075, blue 0.100. The electrostatic potential (in a.u.) is mapped on electron density isosurfaces of 0.02 e/au^3. The calculations were performed at a B3LYP-D3/def2-TZVP level.[7]

In contrast, according to the electrostatic potential map of **3**, we found a large concentration of electrons close to the nitrogen atom, suggesting the presence of a lone pair that is not part of the aromatic phosphorus heterocycle (Figure 2, right). Interestingly, this effect is clearly caused by the steric demand of the phenyl-group in the 2-position of **3**. In fact, the parent phosphinine, substituted in 3-position by an *N*,*N*-dimethylamino group (**3´**), shows again a fully planar nitrogen atom (see Figure S29). Consequently, because the lone pair of the nitrogen atom in **3** shows only weak interaction with the aromatic system, the amino substituent should provide a stronger basic character than the one in **B**/**B´**. This is also confirmed by the calculated gas phase basicity of this compound (225 kcal/mol for **3** *versus* 220 kcal/mol for **B**/**B´**).[10]
We thus anticipated, that the amine functionality in **3** can easily be protonated, in contrast to **B**/**B´**. Upon addition of a slight excess of HCl/Et_2O to **3**, a precipitate is formed instantaneously. Based on the ^{1}H and ^{31}P NMR data, the protonated species **4** is formed initially, with the $SiMe_3$-substituent still located in the *ortho*-position of the heterocycle. The signal of this pronated species **4** can be found at δ(ppm) = 252.3 in the $^{31}P\{^{1}H\}$ NMR spectrum. However, during the process of recrystallizing **4** from hot acetonitrile, protodesilylation occurs, resulting in phosphinine **5** (Scheme 2).

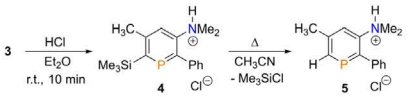

Scheme 2. Synthesis of protonated phosphinines **4** and **5**.

Compound **5** shows a single resonance at δ(ppm) = 212.7 in the $^{31}P\{^{1}H\}$ NMR spectrum. The crystallographic characterization of **5** (Figure 3) displays indeed the presence of an ammonium group in the 3-position of the phosphinine as well as a Cl^- counter anion, and clearly shows that protodesilylation had occurred.

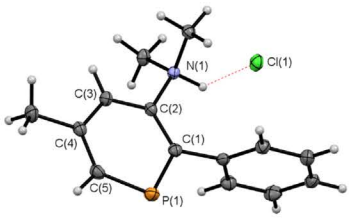

Figure 3. Molecular structure of **5** in the crystal. Displacement ellipsoids are shown at the 50% probability level. Selected bond lengths (Å) and angles (°): P(1)-C(1): 1.7445(13), P(1)-C(5): 1.7230(14), C(1)-C(2): 1.3886(17), C(2)-C(3): 1.3942(16), C(3)-C(4): 1.3940(17), C(4)-C(5): 1.3902(18), N(1)-C(2): 1.4824(15); C(1)-P(1)-C(5): 102.13(6).

Surprisingly, when stirring the suspension containing the white precipitate for a prolonged time at room temperature in an open reaction vessel, a clear solution is formed overnight at room temperature. The $^{31}P\{^1H\}$ NMR spectrum shows that a new compound had formed selectively, which exhibits a single signal at δ(ppm) = 53.0. Remarkably, this chemical shift is not in the usual range found for a phosphinine, which indicates that there is no λ^3,σ^2-phosphinine present anymore.[11] Crystals of the product (**6**, Scheme 3) suitable for X-ray diffraction were obtained from a concentrated solution of **6** in a mixture of dichloromethane and *n*-hexane. The molecular structure of **6** in the solid state is depicted in Figure 4, along with selected bond lengths and angles.

Much to our surprise, the crystallographic characterization of **6** reveals that the product consists of two phospholene oxide moieties bridged by an additional oxygen atom. The amine functionalities of both five-membered phosphorus heterocycles are protonated, with the chloride counter anion bridging the two ammonium groups by hydrogen bonding. The second counter anion is a rare hydrogen dichloride anion $[Cl(HCl)]^-$, which is located on the unit cell with the bond lengths matching those previously reported in literature.[12]

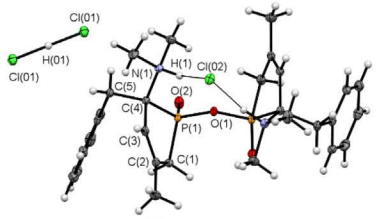

Figure 4. Molecular structure of **6** in the crystal. Displacement ellipsoids are shown at the 50% probability level. Selected bond lengths (Å) and angles (°): P(1)-C(1): 1.7956(13), P(1)-C(4): 1.8629(12), P(1)-O(1): 1.6307(6), P(1)-O(2): 1.4687(9), N(1)-C(4): 1.5225(15), N(1)-H(1): 0.980, C(1)-C(2): 1.5137(18), C(2)-C(3): 1.3381(18), C(3)-C(4): 1.5110(17), C(4)-C(5): 1.5542(16). C(1)-P(1)-C(4): 95.89(6), P(1)-O(2)-P(1): 121.92(8).

The P(1)-C(1) (1.80 Å) and P(1)-C(4) (1.86 Å) bond lengths are consistent with those of reported phospholenes.[13] In general, hydrogen dichloride salts tend to liberate HCl readily with some of them being rather unstable toward moisture and oxygen.[14] **6**, however, is air- and moisture stable in solution and in the solid state. While ring expansion reactions from phospholes to phosphinines and a ring contraction from 1,3,5-triphosphinines to a triphosphole have been reported in literature before, the here presented results are the first case of a ring contraction reaction from a 1-phosphinine to a hydroxylphospholene oxide.[15,16]

To clarify the role of water in this reaction (see also Figure S25 and S26), a dry solution of HCl/Et_2O was reacted with a solution of **3** in diethylether and monitored by means of NMR spectroscopy. Again, a precipitate was formed immediately and no resonance could be observed in the $^{31}P\{^1H\}$ spectrum anymore. The white precipitate is, however, soluble in CD_3CN and the NMR spectra verified the formation of the protonated species **4**. When dichloromethane was used as a solvent, the first step in the protonation of **3** with HCl/Et_2O is again the formation of **4**. A prolonged reaction time leads to a new, yet unknown transient intermediate with a resonance at δ(ppm) = 75.0 in the $^{31}P\{^1H\}$ NMR spectrum. Finally, protodesilylation occurs and **5** is formed quantitatively. Apparently, the presence of water is indeed essential for the ring contraction to occur, while in the absence of water only protonation, followed by protodesilylation, occurs.[17]

Consequently, we attempted the reaction of **4** with an aqueous HCl solution in dichloromethane. The main product showed a resonance at δ(ppm) = 56.0 in the $^{31}P\{^1H\}$ NMR spectrum after stirring the reaction mixture for overnight. The chemical shift of this species is similar to the one recorded for the oxygen bridged dimer **6**, however, not identical. According to NMR spectroscopic analysis, it was identified as compound **7-TMS**. Recrystallization of this species from a hot isopropanol solution afforded crystals suitable for X-ray diffraction and the molecular structure of **7** (Scheme 3) is depicted in Figure 5, along with selected bond lengths and angles.

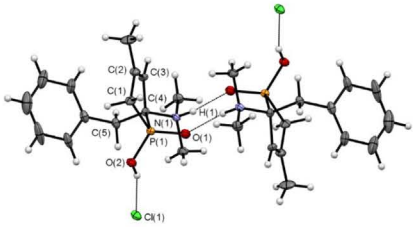

Figure 5. Molecular structure of **7** in the crystal. Displacement ellipsoids are shown at the 50% probability level. Selected bond lengths (Å) and angles (°): P(1)-C(1): 1.786(3), P(1)-C(4): 1.863(3), P(1)-O(1): 1.483(3), P(1)-O(2): 1.550(3), N(1)-C(4): 1.533(4), N(1)-H(1): 0.93(5), C(1)-C(2): 1.515(5), C(2)-C(3): 1.333(5), C(3)-C(4): 1.507(5), C(4)-C(5): 1.548(5); C(1)-P(1)-C(4): 95.78(16).

The crystallographic characterization of **7** shows that the product consists again of a five-membered phosphorus heterocycle. In contrast to **6**, however, a hydroxyphospholene oxide is present, that forms hydrogen bonding to a second molecule, *via* the –P=O and $-N(H)Me_2$ moieties.

Moreover, protodesilylation occurred during the reaction or the crystallization process, respectively. The dissolved crystals show

a signal in the $^{31}P\{^{1}H\}$ NMR spectrum at δ(ppm) = 47.0. Formally, **7** is the hydrolyzed product of the oxygen-bridged dimer **6** (Scheme 3).

In order to get insight into the mechanism of the formation of **7-TMS** (respectively **7**), calculations based on Grimme´s PBEh-3c composite method[18] and the PBE0-D3(BJ)[19] level of DFT were carried out (see supporting information). Based on the computational results, the NMR monitoring experiments as well as the crystallographic data, we propose the following mechanism for the ring contraction in the presence of water (Scheme 4). The first step is the protonation of the amino substituent by HCl, forming **4** as the first intermediate (**int.1**).

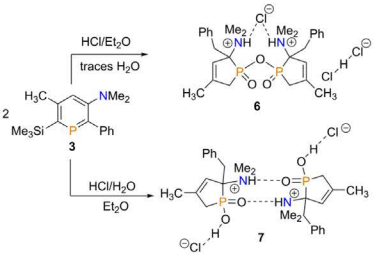

Scheme 3. Formation of oxygen-bridged phospholene oxide **6** and hydroxylphospholene oxide **7**.

This step is exergonic by -69.5 kJ/mol and fully consistent with the NMR experiments. A proton migration forming a racemic mixture of **int.2** occurs, which is energetically feasible under the applied reaction conditions (+22.3 kJ /mol). Subsequently, we propose the addition of water to the reactive P=C bond in **int.2** to give a trivalent hydroxyphosphine species (HOPCH(Ph)R), that tautomerizes to **int.3**. Overall, this process is also exergonic by -101.9 kJ/mol. A related tautomerism reaction at a phosphinine has been reported in the literature before.[20] Moreover, metal complexes of phosphinines also readily add H_2O across the P=C double bond.[21]

In the presence of a second water molecule, **int.3** is in equilibrium with the phosphinic acid derivate **int.4** (+8.7 kJ/mol). **Int.4** can transform into tautomer **int.5** (+32.0 kJ/mol). Such a process is known in literature.[22] The formation of **Int.5** is crucial in order to reach the transition state of the rate-determining step (RDS). The phosphorus atom in **int.5**, having a rather strong nucleophilicity, can react with electrophilic C=N$^+$ moieties intermolecularly to form a new P-C bond. The formation of the P-C bond (+33.3 kJ/mol) in the transition state (**TS**) can be specified as a 5-exo-trig reaction, which is allowed according to the Baldwin rules.[23] The ring formation from **TS** to **int.6** is associated with a significant decrease in free energy by -63.2 kJ/mol. The last step is a proton transfer, which is a significantly exergonic reaction (-50.3 kJ/mol), to form the final product **7-TMS**. The whole reaction sequence is exergonic by -187.0 kJ/mol and the energy barrier of the RDS (**int.3**→**TS**) is 76.0 kJ/mol. The protodesilylation to **7** presumably proceeds in the presence of excess HCl during the recrystallization process.

In order to get additional experimental proof for our proposed mechanism, we sought to incorporate deuterium into the products by using DCl/D_2O. The reaction between DCl/D_2O and **3** in dichloromethane was again stirred in a Schlenk flask overnight. The product (**7-*d***) was recrystallized from hot isopropanol. For compound **7-*d*** several signals (see Figure S22) can be detected as broad resonances due to ^{2}D-^{13}C coupling in the $^{13}C\{^{1}H\}$ NMR spectrum compared to that of compound **7**.

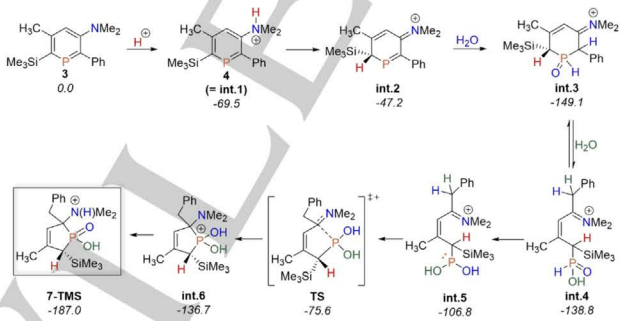

Scheme 4. Proposed reaction mechanism for the reaction of **3** with HCl in the presence of water. **7-TMS** is the main product; Relative Gibbs free Energies (in kJ/mol) are given below the compound name; Int.: intermediate. Calculated at the PBE0-D3(BJ) level of theory. Note: only the diastereomer **int.3** is shown as **int.3'** is located at higher energy (-146.4 kJ/mol) and therefore not considered for the mechanism.

Moreover, compound **7d** shows a chemical shift (δ(ppm) = 47.5) similar to compound **7** in the $^{31}P\{^{1}H\}$ NMR spectrum. By means of 2D and HMQC NMR experiments, the D-atoms were assigned to the positions depicted in Scheme 5, which supports the proposed mechanism. Moreover, the crystallographic characterization of **7-*d*** showed the same molecular structure in the solid state as determined for **7**.

It is clear, that the here observed unusual ring contraction reaction can only proceed because the special electronic properties of phosphinines, in combination with the particular reactivity of low-coordinate organophosphorus species, allows sequential

reactions at the aromatic phosphorus heterocycle. This is in clear contrast to functionalized pyridines.

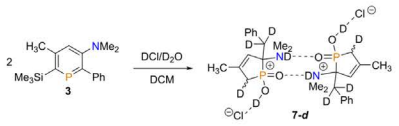

Scheme 5. Formation of **7-*d*** by reaction of **3** with DCl/D_2O.

Conclusion

In summary, we have synthesized and structurally characterized a new 3-aminofunctionalized phosphinine by a series of [4+2] cycloaddition/cycloreversion reactions, starting from 1,3,2-diazaphosphinine, 1-(trimethylsilyl)propyne and *N*,*N*-dimethylphenylacetylene. The steric demand of the phenyl group in α-position of the heterocycle causes a weak electronic interaction between the nitrogen lone-pair and the aromatic phosphorus heterocycle, as evidenced by a substantial pyramidalization of the nitrogen atom. This allows for protonation of the dimethylamino substituent by hydrochloric acid. Remarkably, in the presence of water, the protonated phosphinine undergoes a hitherto unknown, selective ring contraction to form a hydroxylphospholene oxide, which participates in hydrogen bonding and forms a dimer in the solid state. DFT-based calculations and deuterium labeling experiments were performed to get insight into the reaction mechanism. The experimental results are fully consistent with the calculations and the proposed reaction pathway. Overall, we could show for the first time that a phosphinine can undergo a selective and quantitative ring contraction reaction. The special electronic properties of phosphinines in combination with the particular reactivity of low-coordinate organophosphorus species allow for sequential reactions at the aromatic phosphorus heterocycles, in contrast to functionalized pyridines.

Experimental Section

All experimental and computational details can be found in the Supporting Information. CCDC-2181743(3), 2181744(5), 2181745(6), 2181746(6) contains the supplementary crystallographic data for this paper. These data can be obtained free of charge from The Cambridge Crystallographic Data Centre via www.ccdc.cam.ac.uk/data_request/cif.

Acknowledgements

Funding by the Deutsche Forschungsgemeinschaft (grant PA 1360/16-1) and the China Scholarship Council are gratefully acknowledged. The authors thank the computing facilites of the Freie Universität Berlin (Zentrale Einrichtung für Datenverarbeitung) for providing computational resources.

Keywords: phosphorus heterocycles • phospholene • phosphinic acid • X-ray crystallography • DFT calculations

[1] N. T. Coles, A. S. Abels, J. Leitl, R. Wolf, H. Grützmacher, C. Müller, *Coord. Chem. Rev.* **2021**, *433*, 213729-213756.

[2] a) F. Knoch, F. Kremer, U. Schmidt, U. Zenneck, P. Le Floch, F. Mathey, *Organometallics* **1996**, *15*, 2713-2719; b) P. Le Floch, *Coord. Chem. Rev.* **2006**, *250*, 627-681; c) C. Müller, D. Vogt, *Dalton Trans.* **2007**, 5505-5523; d) C. Müller, D. Vogt in *Catalysis and Material Science Applications*, *Vol. 36* (Eds.: M. Peruzzini, L. Gonsalvi), Springer, Berlin, **2011**, pp. 151-183; e) M. Rigo, E. R. Habraken, K. Bhattacharyya, M. Weber, A. W. Ehlers, N. Mézailles, J. C. Slootweg, C. Müller, *Eur. J. Chem.* **2019**, *25*, 8769-8779.

[3] G. Pfeifer, F. Chahdoura, M. Papke, M. Weber, R. Szűcs, B. Geffroy, D. Tondelier, L. Nyulászi, M. Hissler, C. Müller, *Eur. J. Chem.* **2020**, *26*, 10534-10543.

[4] a) R. Newland, M. F. Wyatt, R. Wingad, S. M. Mansell, *Dalton Trans.* **2017**, *46*, 6172-6176; b) R. J. Newland, M. P. Delve, R. L. Wingad, S. M. Mansell, *New J. Chem.* **2018**, *42*, 19625-19636; c) R. J. Newland, J. M. Lynam, S. M. Mansell, *Chem. Commun.* **2018**, *54*, 5482-5485; d) R. J. Newland, A. Smith, D. M. Smith, N. Fey, M. J. Hanton, S. M. Mansell, *Organometallics* **2018**, *37*, 1062-1073.

[5] X. Chen, S. Alidori, F. F. Puschmann, G. Santiso‐Quinones, Z. Benkő, Z. Li, G. Becker, H. F. Grützmacher, H. Grützmacher, *Angew. Chem. Int. Ed.* **2014**, *53*, 1641-1645.

[6] Y. Hou, Z. Li, Y. Li, P. Liu, C.-Y. Su, F. Puschmann, H. Grützmacher, *Chem. Sci.* **2019**, *10*, 3168-3180.

[7] S. Giese, K. Klimov, A. Mikeházi, Z. Kelemen, D. S. Frost, S. Steinhauer, P. Müller, L. Nyulászi, C. Müller, *Angew. Chem. Int. Ed.* **2021**, *60*, 3581-3586.

[8] N. Avarvari, P. Le Floch, F. Mathey, *J. Am. Chem. Soc.* **1996**, *118*, 11978-11979.

[9] F. H. Allen, O. Kennard, D. G. Watson, L. Brammer, A. G. Orpen, R. Taylor, *J. Chem. Soc., Perkin Trans. 2* **1987**, S1-S19.

[10] F. Wossidlo, D. S. Frost, J. Lin, N. T. Coles, K. Klimov, M. Weber, T. Böttcher, C. Müller, *Chem. Eur. J.* **2021**, *27*, 12788-12795.

[11] M. H. Habicht, F. Wossidlo, T. Bens, E. A. Pidko, C. Müller, *Eur. J. Chem.* **2018**, *24*, 944-952.

[12] D. Mootz, W. Poll, H. Wunderlich, H. G. Wussow, *Chem. Ber.* **1981**, *114*, 3499-3504.

[13] a) F. Leca, C. Lescop, L. Toupet, R. Réau, *Organometallics* **2004**, *23*, 6191-6201; b) R.-M. L. Mercado, C. Zhang, H. Zhang, P. Wisian-Neilson, *Phosphorus Sulfur Silicon Relat. Elem.* **2015**, *190*, 2194-2206.

[14] a) R. Kohle, W. Kuchen, W. Peters, *Z. anorg. allg. Chem.* **1987**, *551*, 179-190; b) J. L. Atwood, S. G. Bott, A. W. Coleman, K. D. Robinson, S. B. Whetstone, C. M. Means, *J. Am. Chem. Soc.* **1987**, *109*, 8100-8101; c) B. H. Ward, G. E. Granroth, K. A. Abboud, M. W. Meisel, D. R. Talham, *Chem. Mater.* **1998**, *10*, 1102-1108; d) K. Nikitin, H. Müller‐Bunz, J. Muldoon, D. G. Gilheany, *Eur. J. Chem.* **2017**, *23*, 4794-4802.

[15] a) J. Grundy, F. Mathey, *Angew. Chem.* **2005**, *117*, 1106-1108; b) H. Wang, C. Li, D. Geng, H. Chen, Z. Duan, F. Mathey, *Eur. J. Chem.* **2010**, *16*, 10659-10661; c) P. Tokarz, P. M. Zagórski, *Chem. Heterocycl. Compd.* **2017**, *53*, 858-860.

[16] a) S. B. Clendenning, P. B. Hitchcock, J. F. Nixon, L. Nyulászi, *Chem. Commun.* **2000**, 1305-1306; b) S. B. Clendenning, P. B. Hitchcock, M. F. Lappert, P. G. Merle, J. F. Nixon, L. Nyulászi, *Chem. Eur. J.* **2007**, *13*, 7121-7128.

[17] M. Blug, O. Piechaczyk, M. Fustier, N. Mézailles, P. Le Floch, *J. Org. Chem.* **2008**, *73*, 3258-3261.

[18] S. Grimme, J. G. Brandenburg, C. Bannwarth, A. Hansen, *J. Chem. Phys.* **2015**, *143*, 054107.

[19] a) J. P. Perdew, M. Ernzerhof, K. Burke, *J. Chem. Phys.* **1996**, *105*, 9982; b) S. Grimme, J. Antony, S. Ehrlich, H. Krieg, *J. Chem. Phys.* **2010**, *132*, 154104; c) S. Grimme, S. Ehrlich, L. Goerigk, *J. Comput. Chem.* **2011**, *32*, 1456.

[20] M. Doux, N. Mézailles, L. Ricard, P. Le Floch, *Eur. J. Inorg. Chem.* **2003**, 3878.

[21] a) B. Schmid, L. M. Venanzi, A. Albinati, F. Mathey, *Inorg. Chem.* **1991**, *30*, 4693; b) I. de Krom, E. A. Pidko, M. Lutz, C. Müller, *Chem. Eur. J.*, 2013, **19**, 7523; d) R. J. Newland, M. P. Delve, R. L. Wingad, S. M. Mansell, *New J. Chem.* **2018**, *42*, 19625.

[22] a) D. Vincze, P. Ábrányi-Balogh, P. Bagi, G. Keglevich, *Molecules* **2019**, *24*, 3859–3871; b) L. Davis, M. Putri, C. Meyer, C. Durant, *Tetrahedron Lett.* **2014**, *55*, 3100–3103; c) D. Akbayeva, M. Varia, S. S. Costantini, M Peruzzini, P. Stoppioni, *Dalton Trans.* **2006**, *2*, 389–395.

[23] J. Baldwin, *J. Chem. Soc., Chem. Commun.* **1976**, *18*, 734–736.

How to Shrink the Ring: Phospholenes from Phosphabenzenes *via* Selective Ring Contraction

Jinxiong Lin, Nathan T. Coles, Lea Dettling, Luca Steiner, J. Felix Witte, Beate Paulus, and Christian Müller

CONTENTS

1. Experimental Procedures

1.1 General Remarks

All reactions were performed under argon in oven-dried glassware using modified Schlenk techniques unless otherwise stated. All common solvents and chemicals were commercially available and were used without further purification. All dry or deoxygenated solvents were prepared using standard techniques or were used from a MBraun solvent purification system. N,N-dimethyl-2-phenylethyn-1-amine and 1,3,2-diazaphosphinines were prepared according to literature[1][2]. The ^{1}H, ^{19}F, $^{13}C\{^{1}H\}$, $^{31}P\{^{1}H\}$ and ^{31}P NMR spectra were recorded on a *JEOL* ECX400 (400 MHz) spectrometer and a Bruker Avance 600 (600 MHz), and all chemical shifts are reported relative to the residual resonance in the deuterated solvents. The HRMS ESI mass spectra were measured on an Agilent 6210 ESI-TOF. Low-temperature x-ray diffractometry was performed on a Bruker-AXS X8 Kappa Duo diffractometer with *IμS* micro-sources, performing ϕ- and ω-scans. Data was collected using a Photon 2 CPAD detector with Mo K_α radiation (λ = 0.71073 Å). The structures were solved by dual-space methods using SHELXT[3] and refined against F^2 on all data by full-matrix least squares with SHELXL-2017[4] following established refinement strategies[5]. The program Olex2[6] was also used to aid in the refinement. All non-hydrogen atoms were refined anisotropically. All hydrogen atoms were included into the model at geometrically calculated positions and refined using a riding model. The isotropic displacement parameters of all hydrogen atoms were fixed to 1.2 times the U-value of the atoms they are linked to (1.5 times for methyl groups). Details of the data quality and a summary of the residual values of the refinements are listed in **Table S1** below. Tables **S2**, **S4**, **S6** and **S8** give all bond lengths for the structures, and **S3**, **S5**, **S7** and **S9** give all angles for the structures.

1.2 Synthesis details

1.2.1 Synthesis of 3

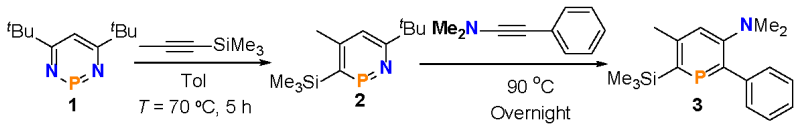

Scheme S1: Synthesis of **3**.

1 equiv. of 1-(trimethylsilyl)-prop-1-yne (0.22 g, 2.0 mmol) was added to a solution of 1,3,2-diazaphosphinine (2.0 mmol, 0.13 M) in toluene (15 mL). The mixture was heated at T = 70 °C for 5 hours after which complete formation of the 1,2-monoazaphosphinine was observed by ^{31}P NMR spectroscopy (δ = 297.9 ppm). Next, 2 equiv. of N, N-dimethyl-2-phenylethyn-1-amine

(0.58 g, 4 mmol) were then added to the mixture and heated at T = 90 °C for overnight. The solution was then cooled to room temperature and the product purified by column chromatography (silica) using an eluent of *n*-hexane : ethyl acetate (9:1). Yield: 78 % (471 mg, 1.56 mmol).

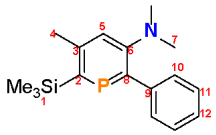

^{1}H NMR (400 MHz, C_6D_6) δ 7.65 (d, $^{1}J_{H,H}$ = 7.8 Hz, 2H, *1-Ph*), 7.24 (t, $^{1}J_{H,H}$ = 7.5 Hz, 2H, *-Ph*), 7.11 (td, $^{1}J_{H,H}$ = 7.4, 1.3 Hz, 1H, *-Ph*), 6.78 (br. s, 1H, C_5HP), 2.45 (s, 3H, *-Me*), 2.33 (s, 6H, -NMe_2), 0.48 (d, $^{4}J_{H,P}$ = 1.8 Hz, 9H, *-TMS*) ppm.

^{13}C{^{1}H} NMR (151 MHz, C_6D_6) δ 156.8 (d, $^{1}J_{C,P}$ = 88 Hz, *C8*), 156.3 (d, $^{1}J_{C,P}$ = 106 Hz, *C2*), 155.9 (d, $^{2}J_{C,P}$ = 10 Hz, *C6*), 149.7 (d, $^{2}J_{C,P}$ = 13 Hz, *C3*), 143.7 (d, $^{2}J_{C,P}$ = 24 Hz, *C9*), 129.3 (d, $^{3}J_{C,P}$ = 11 Hz, *C10*), 128.7 (s, *C11*), 126.6 (s, *C12*), 122.9 (d, $^{3}J_{C,P}$ = 16Hz, *C5*), 42.6 (s, *C7*), 26.3 (d, $^{4}J_{C,P}$ = 3 Hz, *C4*), 1.5 (d, $^{3}J_{C,P}$ = 11 Hz, *C1*) ppm.

^{31}P{^{1}H} NMR (162 MHz, C_6D_6) δ 244 ppm.

HR-ESI MS (*m/z*): 302.1506 (calculated: 302.1489) $[M+H]^+$.

Element analysis: calculated for $C_{17}H_{24}NPSi$: C: 67.74%, H: 8.03%, N: 4.65%; found: C: 67.79%, H: 9.519%, N: 4.672%.

1.2.2 Synthesis of 4

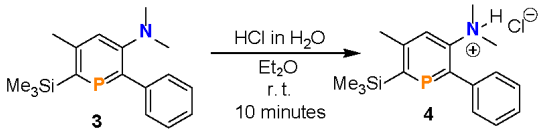

Scheme S2: Synthesis of protonated phosphinine (**4**).

3 (36 mg, 0.12 mmol) was dissolved in 2 mL Et_2O at room temperature and 0.1 mL HCl in water (0.24 mmol, 2.4 M) was added to the Schlenk flask. A white precipitate was formed immediately, after which the reaction was stirred for an additional 10 minutes. All solvents were removed by syringe and the residual solid was washed with Et_2O. Yield: 75% (30 mg, 0.09 mmol).

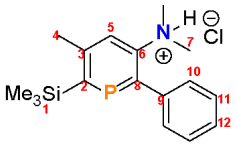

^{1}H NMR (400 MHz, CD_3CN) δ 7.68 – 7.00 (m, 6H, C_5HP & *1-Ph*), 3.26 – 2.82 (m, 1H, -*H*NMe_2), 2.68 (s, 6H, -*N*Me_2), 2.50 (s, 3H, -*Me*), 0.43 (s, 9H, *TMS*) ppm.

^{31}P{^{1}H} NMR (142 MHz, CD_3CN) δ 252 ppm.

Compound **4** is not stable as protodesilylation slowly proceeds in solution. Therefore, **4** was not fully characterized.

1.2.3 Synthesis of 5

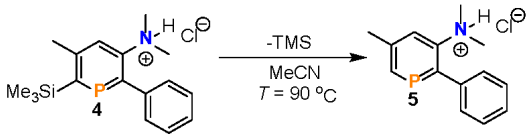

Scheme S3: Recrystallization for protodesilylation.

4 (34 mg, 0.1 mmol) was dissolved in refluxing MeCN (0.5 mL) for recrystallization. This resulted in protodesilylation. Yield: 72% (19 mg, 0.07 mmol).

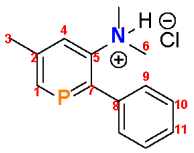

^{1}H NMR (700 MHz, CD_3CN) δ 7.51 – 7.41 (m, 5H, *-Ph*), 7.41 – 7.37 (m, 2H, C_5H_2P), 2.75 – 2.66 (m, 6H, -*N*Me_2), 2.52 (d, $^{4}J_{H,P}$ = 1.5 Hz, 3H, *-Me*), 2.58-2.37 (m, 1H, -*H*NMe_2) ppm.

^{13}C{^{1}H} NMR (176 MHz, CD_3CN) δ 158.9 (d, $^{1}J_{C,P}$ = 54 Hz, *C7*), 146.8 (d, $^{2}J_{C,P}$ = 14 Hz, *C5*), 142.5 (d, $^{2}J_{C,P}$ = 12 Hz, *C8*), 132.0 (d, $^{1}J_{C,P}$ = 88 Hz, *C1*), 130.3 (d, $^{3}J_{C,P}$ = 10 Hz, *C9*), 129.4 (s, *C10*), 128.3 (s, *C11*), 125.5 (d, $^{2}J_{C,P}$ = 25 Hz, *C2*), 125.0 (s, *C4*), 44.8 (s, *C6*), 24.7 (d, $^{3}J_{C,P}$ = 3 Hz, *C3*) ppm.

^{31}P{^{1}H} NMR (142 MHz, CD_3CN) δ 213 ppm.

HR-ESI MS (*m/z*): 230.1104 (calculated: 230.1094) $[M]^+$.

1.2.4 Synthesis of 6

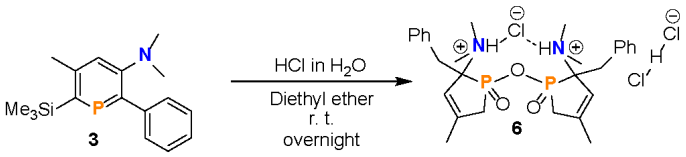

Scheme S4: Synthesis of **6**.

3 (36 mg, 0.12 mmol) was dissolved in Et_2O (3 mL) at room temperature and 0.1 mL HCl in water (0.24 mmol, 2.4 M) was added to the Schlenk flask. The reaction was stirred for overnight before removing all volatiles *in vacuo*. The residual solid was washed with Et_2O. Yield: 40 % (30 mg, 0.05 mmol).

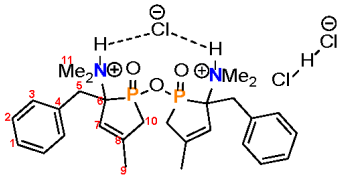

^{1}H NMR (700 MHz, D_2O) δ 7.68 – 6.67 (m, 10H, *Ph*), 5.72 (d, $^3J_{H,P}$ = 24.7 Hz, 2H, C_4HP), 3.33 (d, $^3J_{H,P}$ = 11.6 Hz, 4H, -CH_2), 3.01 (s, 9 H, -NMe_2), 2.72 (s, 3H, -NMe_2), 2.06 (s, 2H, -HNMe_2), 2.00 (m, 4H, CH_2), 1.76 (s, 6H, -*Me*) ppm.

^{13}C{^{1}H} NMR (176 MHz, D_2O) δ 145.0 (d, $^2J_{C,P}$ = 9 Hz, *C8*), 134.0 (t, $^3J_{C,P}$ = 5 Hz, *C4*), 131.3 (s, *C3*), 128.3 (s, *C1*), 127.4 (s, *C2*), 121.9 (d, $^2J_{C,P}$ = 17 Hz, *C7*), 71.3 (d, $^1J_{C,P}$ = 86 Hz, *C6*), 40.8 (s, *C11*), 39.3 (s, *C11'*) 35.1 (d, $^2J_{C,P}$ = 14 Hz, *C5*), 35.1 (d, $^1J_{C,P}$ = 192 Hz, *C10*), 20.4 (d, $^3J_{C,P}$ = 12 Hz, *C9*) ppm.

^{31}P{^{1}H} NMR (162 MHz, D_2O) δ 53 ppm.

^{31}P NMR (162 MHz, D_2O) δ 53 (t, $^2J_{H,P}$ = 11 Hz) ppm.

HR-ESI MS (*m/z*): 531.2596 (calculated: 531.2542) $[(M+OH)]^+$.

1.2.5 Synthesis of 7

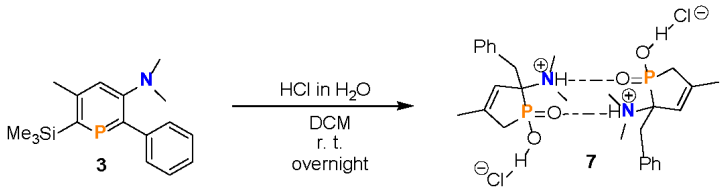

Scheme S5: Synthesis of 7.

3 (72 mg, 0.24 mmol) was dissolved in DCM (3 mL) at room temperature and HCl in water (0.3 mL, 0.72 mmol, 2.4 M) was added to the Schlenk flask. The reaction was stirred for overnight before removing all volatiles *in vacuo*. A crystal suitable for single crystal X-ray diffraction was obtained by slowly cooling a hot solution of the crude solid in isopropanol. Yield: 87 % (63 mg, 0.21 mmol).

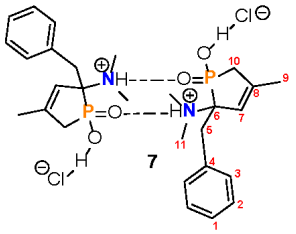

^{1}H NMR (400 MHz, D_2O) δ 7.55 – 7.11 (m, 5H, -*Ph*), 5.69 (d, $^{3}J_{H,P}$ = 25.3 Hz, 1H, *CH*), 3.29 (d, $^{3}J_{H,P}$ = 12.6 Hz, 2H, -CH_2), 2.96 (d, $^{4}J_{H,P}$ = 3.4 Hz, 6H, -NMe_2), 2.67 (s, 1H, -O*H*), 2.05-1.96 (m, 1H, -*H*NMe_2), 1.96 (m, 2 H, CH_2), 1.72 (s, 3H, -CH_3) ppm.

^{13}C{^{1}H} NMR (151 MHz, D_2O) δ 145.0 (d, $^{2}J_{C,P}$ = 9 Hz, *C8*), 134.0 (d, $^{3}J_{C,P}$ = 4 Hz, *C4*), 131.3 (s, *C3*), 128.3 (s, *C1*), 127.4 (s, *C2*), 121.9 (d, $^{2}J_{C,P}$ = 16 Hz, *C7*), 71.3 (d, $^{1}J_{C,P}$ = 86 Hz, *C6*), 40.8 (s, *C11*), 39.3 (s, *C11'*), 35.3 (d, $^{1}J_{C,P}$= 95 Hz, *C10*), 35.2 (s, *C5*), 20.4 (d, $^{3}J_{C,P}$ = 12 Hz, *C9*) ppm.

^{31}P{^{1}H} NMR (162 MHz, D_2O) δ 47 ppm.

^{31}P NMR (162 MHz, D_2O) δ 47 (t, $^{2}J_{H,P}$ = 25 Hz) ppm.

HR-ESI MS (*m/z*): 266.1306 (calculated: 266.1304) $[M]^+$.

1.2.6 Synthesis of 7-TMS-*d*

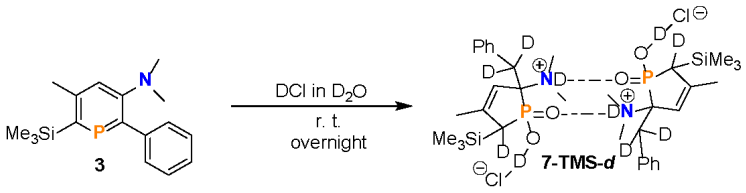

Scheme S6: Synthesis of 7-TMS-***d***.

Method 1: **3** (72 mg, 0.24 mmol) was dissolved in DCM (3 mL) at room temperature and DCl in D_2O (0.2 mL, 2.4 M) was added to the Schlenk flask. The reaction was stirred for overnight before removing the DCM phase by syringe. The water phase containing the product **7-TMS-*d*** was washed with 0.2 mL DCM, after which all volatiles were evaporated under *vacuum* to obtain the pure product. Yield: 62 % (56 mg, 0.15 mmol).

Method 2: **3** (72 mg, 0.24 mmol) was dissolved in MeCN or THF (0.5 mL) at room temperature in an NMR tube and DCl in D_2O (0.2 mL, 2.4 M) was added. This reaction was allowed to stand at room temperature for approximately 5 days. Almost all starting material was converted to the product directly. Yield: 88 % (80 mg, 0.21 mmol). The product was recrystallized from isopropanol without further purification.

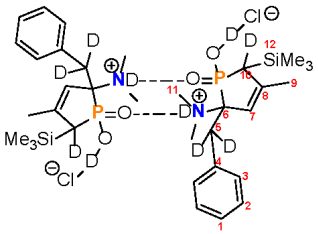

^{1}H NMR (400 MHz, CD_3CN) δ 7.43 – 7.14 (m, 5H, -*Ph*), 5.74 (d, $^{3}J_{H,P}$ = 27.1 Hz, 1H, *CH*), 3.00 (s, 6H, -N*Me*$_2$), 1.66 (s, 3H, -*Me*), 0.04 (d, *J* = 5.6 Hz, 9H, -*TMS*) ppm.

^{13}C{^{1}H} NMR (151 MHz, CD_3CN) δ 144.0 (s, *C8*), 133.8 (s, *C4*), 132.1 (s, *C3*), 128.5 (d, $^{2}J_{C,P}$ = 14 Hz, *C7*), 127.9 (s, *C2*), 122.9 (s, *C1*), 71.7 (d, $^{1}J_{C,P}$ = 90 Hz, *C6*), 41.7-41.4 (m, *C11*), 40.3-40.0 (m, *C11'*), 35.7-34.7 (broad peak due to D-C coupling, *C10* and *C5*), 20.5 (s, *C9*), 0.8 (s, *C12*).

^{29}Si{^{1}H}-DEPT NMR (80 MHz, CD_3CN) δ 8 ppm.

^{31}P{^{1}H} NMR (162 MHz, CD_3CN) δ 55 ppm.

1.2.7 Synthesis of 7-*d*

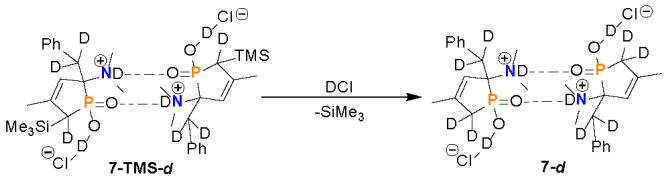

Scheme S7: Recrystallization for protodesilylation.

Protodesilylation of 7-TMS-***d*** in solution occurs under strong acid conditions. All volatiles were removed *in vacuo* after the reaction was completed. The residual solid was dissolved in refluxing isopropanol (0.5 mL) and subsequently recrystallized. Yield: 90% (58 mg, 0.19 mmol).

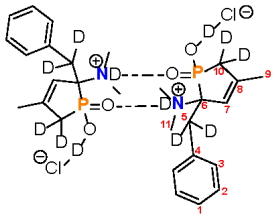

^{1}H NMR (400 MHz, D_2O) δ 7.43 – 7.23 (m, 5H, -*Ph*), 5.67 (dd, $^{3}J_{H,P}$ = 24.9, 1.5 Hz, 1H, C*H*), 2.94 (d, $^{2}J_{H,H}$ = 3.2 Hz, 6H, -N*Me*$_2$), 1.70 (s, 3H, -*Me*) ppm.

^{13}C{^{1}H} NMR (151 MHz, D_2O) δ 145.0 (d, $^{2}J_{C,P}$ = 9 Hz, *C8*), 133.9 (d, $^{3}J_{C,P}$ = 4 Hz, *C4*), 131.3 (s, *C3*), 128.4 (s, *C1*), 127.5 (s, *C2*), 122.0 (d, $^{2}J_{C,P}$ = 17 Hz, *C7*), 71.2 (d, $^{1}J_{C,P}$ = 86 Hz, *C6*), 40.9 (s, *C11*), 39.3 (s, *C11'*), 36.1 – 33.7 (m, broad peak due to D-C coupling, *C10 & C5*), 20.4 (d, $^{3}J_{C,P}$ = 12 Hz, *C9*) ppm.

^{31}P{^{1}H} NMR (162 MHz, D_2O) δ 48 ppm.

1.2.8 Synthesis of 5 by reaction of 3 with HCl-Et_2O in DCM

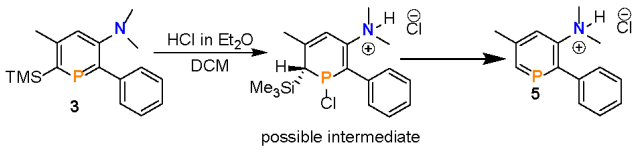

Scheme 10: Reaction of **3** with HCl-ether in DCM solvent.

3 (30 mg, 0.1 mmol) was dissolved in DCM (0.5 mL) at room temperature in an NMR tube and HCl in Et_2O (0.1 mL, 0.2 mmol) was added. The sample was submitted for NMR spectroscopic analyis.

$^{31}P\{^1H\}$ NMR (162 MHz, CH_2Cl_2) δ 217.80 (s), 74.61 (s) ppm.

^{31}P NMR (162 MHz, CH_2Cl_2) δ 217.88 (d, $^2J_{H,P}$ = 39.9 Hz), 74.63 (m) ppm

2. NMR Spectra

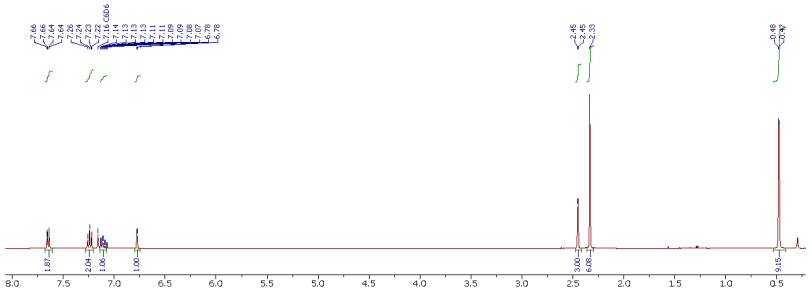

Figure S1 ^{1}H NMR spectrum of **3** in C_6D_6.

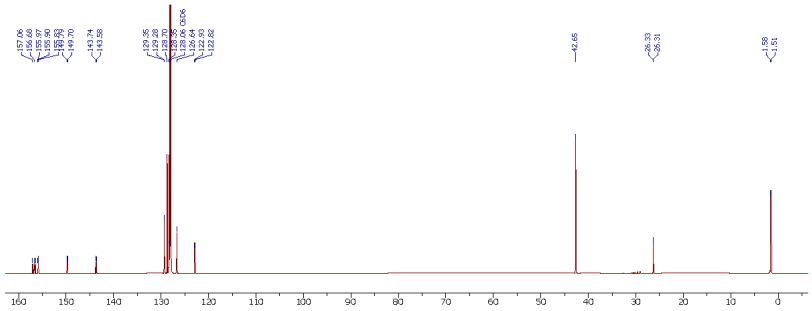

Figure S2 $^{13}C\{^{1}H\}$ NMR spectrum of **3** in C_6D_6.

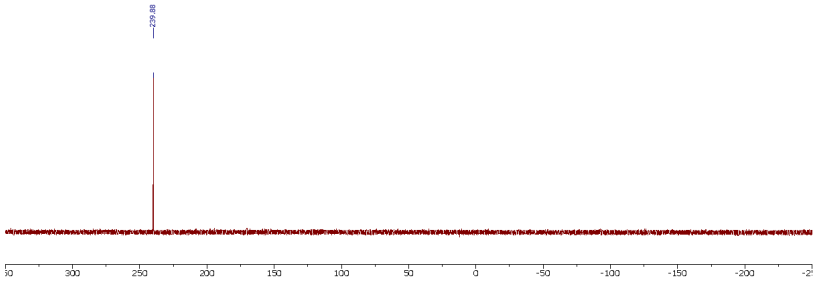

Figure S3 $^{31}P\{^{1}H\}$ NMR spectrum of **3** in CD_2Cl_2.

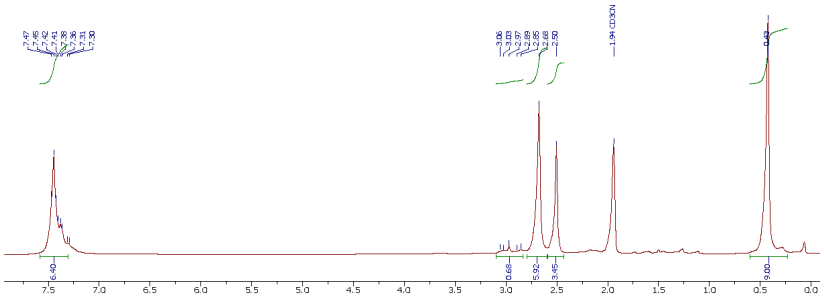

Figure S4 ^{1}H NMR spectrum of **4** in CD_3CN.

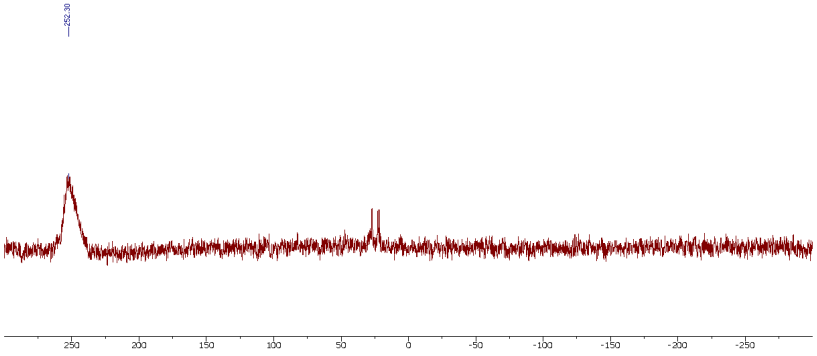

Figure S5 $^{31}P\{^{1}H\}$ NMR spectrum of **4** in CD_3CN.

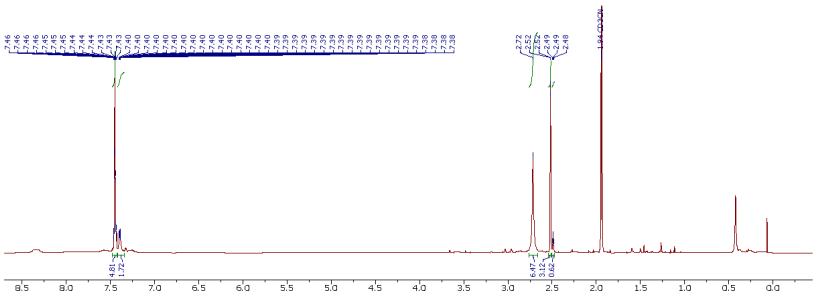

Figure S6 ^{1}H NMR spectrum of **5** in CD_3CN.

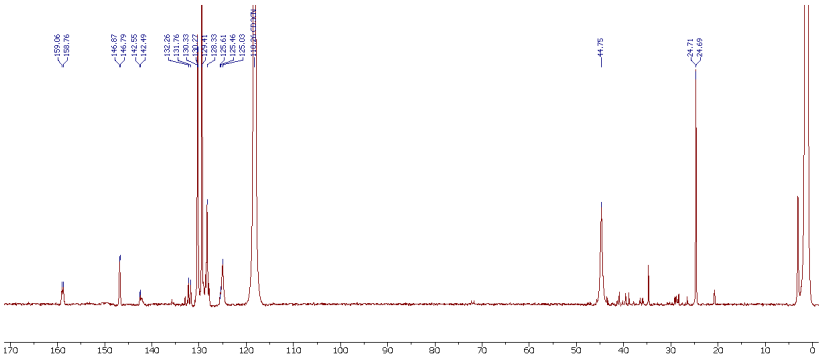

Figure S7 $^{13}C\{^{1}H\}$ NMR spectrum of **5** in CD_3CN.

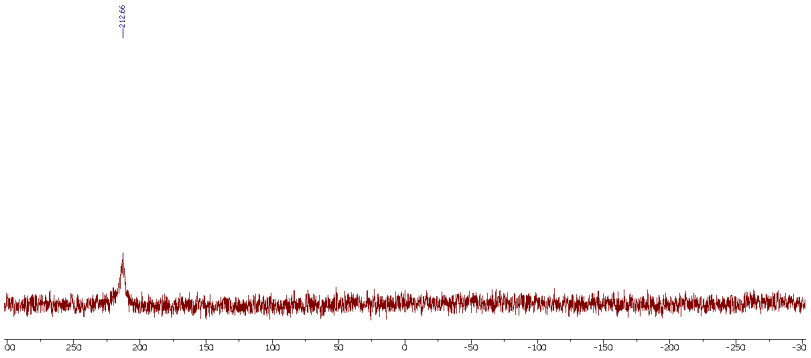

Figure S8 $^{31}P\{^{1}H\}$ NMR spectrum of **5** in CD_3CN.

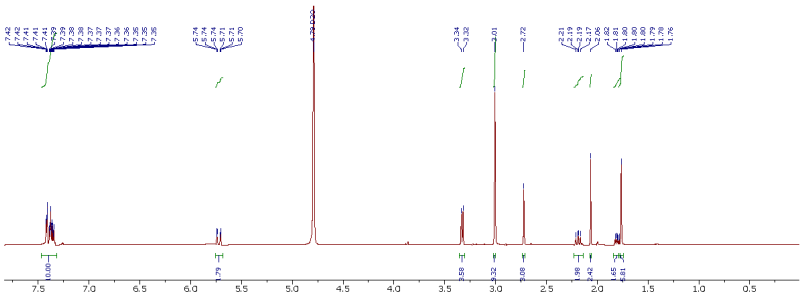

Figure S9 ^{1}H NMR spectrum of **6** in D_2O.

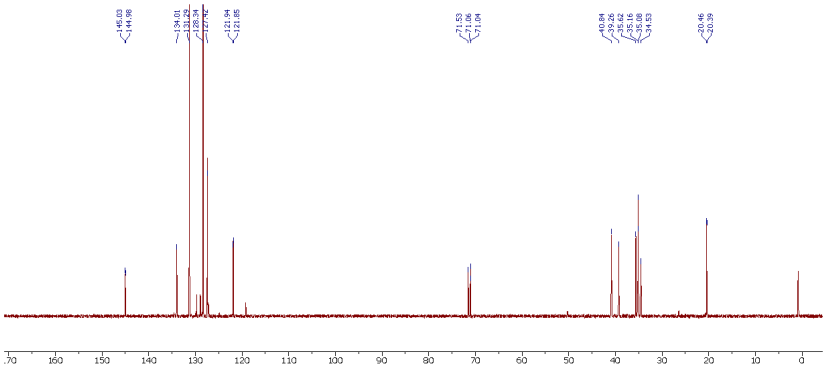

Figure S10 $^{13}C\{^{1}H\}$ NMR spectrum of **6** in D_2O.

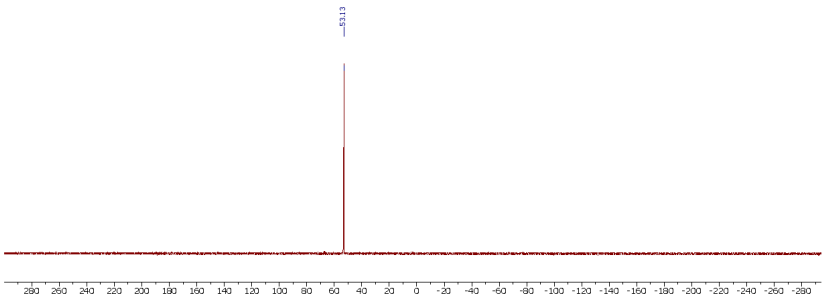

Figure S11 $^{31}P\{^{1}H\}$ NMR spectrum of **6** in D_2O.

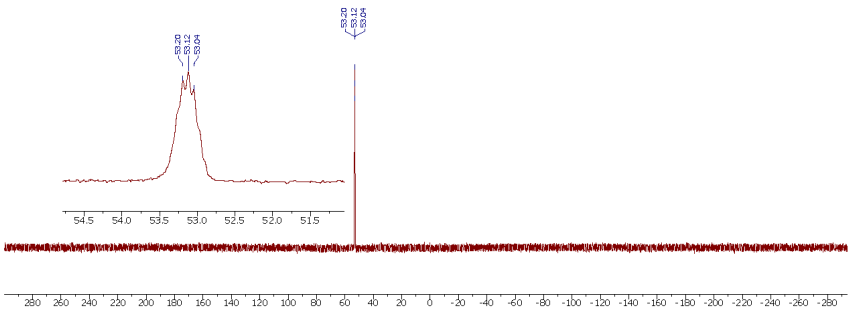

Figure S12 ^{31}P NMR spectrum of **6** in D_2O.

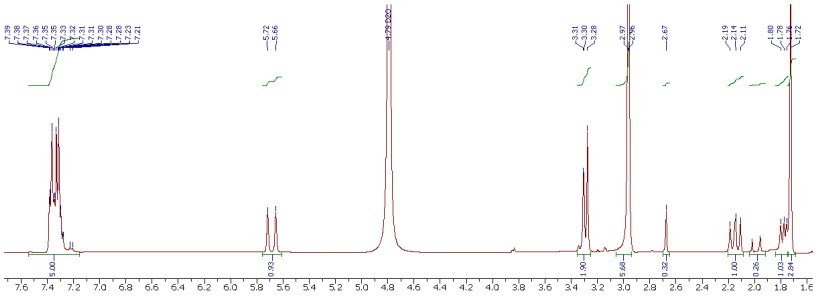

Figure S13 ^{1}H NMR spectrum of **7** in D_2O.

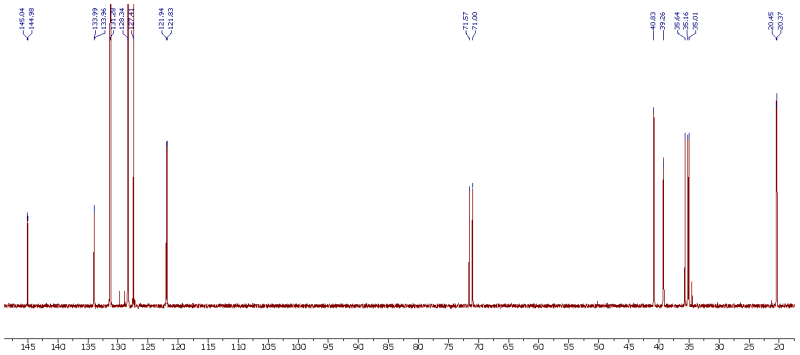

Figure S14 $^{13}C\{^{1}H\}$ NMR spectrum of **7** in D_2O.

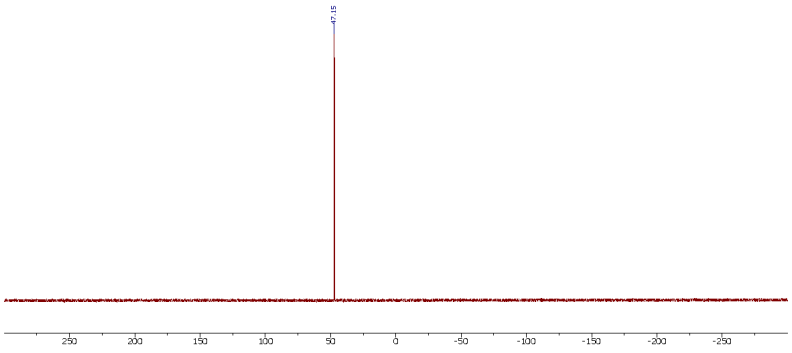

Figure S15 $^{31}P\{^{1}H\}$ NMR spectrum of **7** in D_2O.

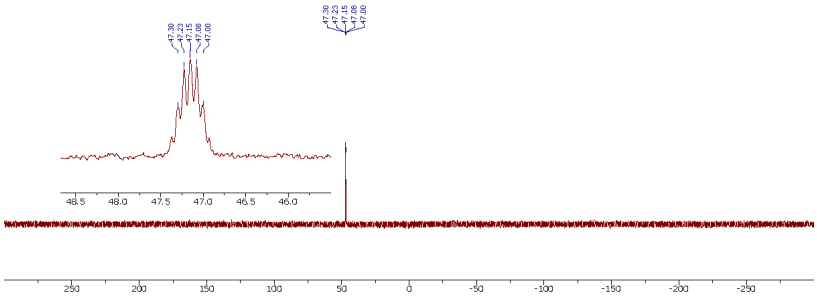

Figure S16 ^{31}P NMR spectrum of **7** in D_2O.

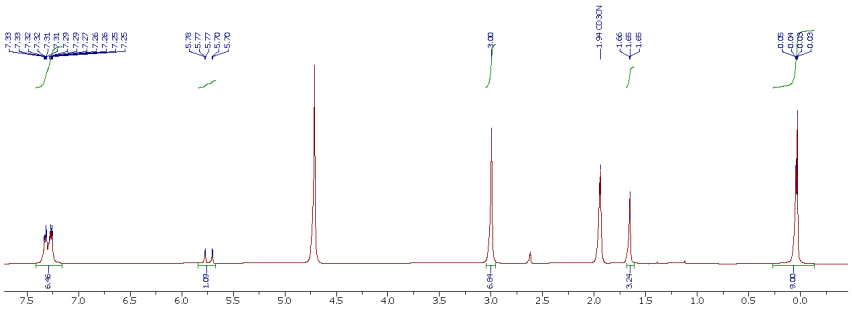

Figure S17 ^{1}H NMR spectrum of **7-TMS-*d*** in CD_3CN.

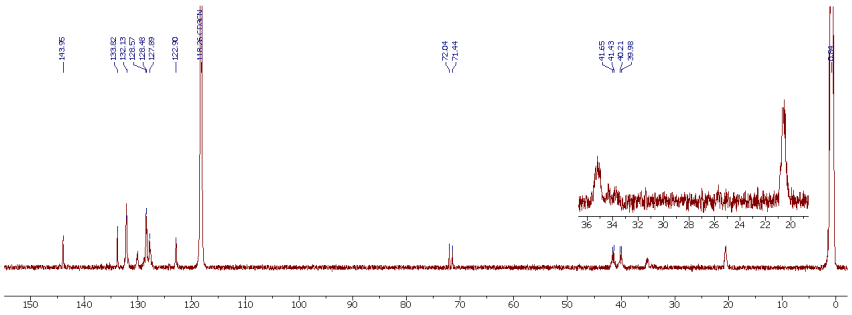

Figure S18 $^{13}C\{^{1}H\}$ NMR spectrum of **7-TMS-*d*** in CD_3CN.

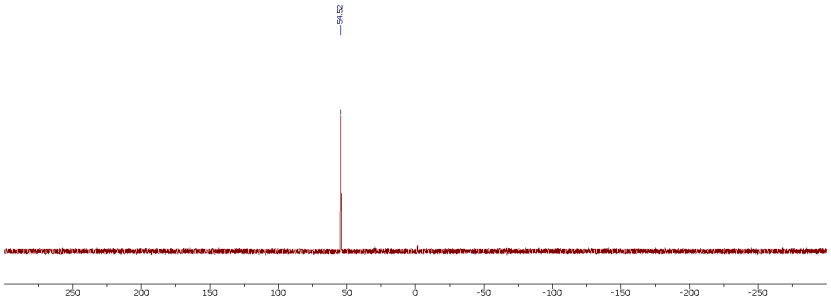

Figure S19 $^{31}P\{^{1}H\}$ NMR spectrum of **7-TMS-*d*** in CD_3CN.

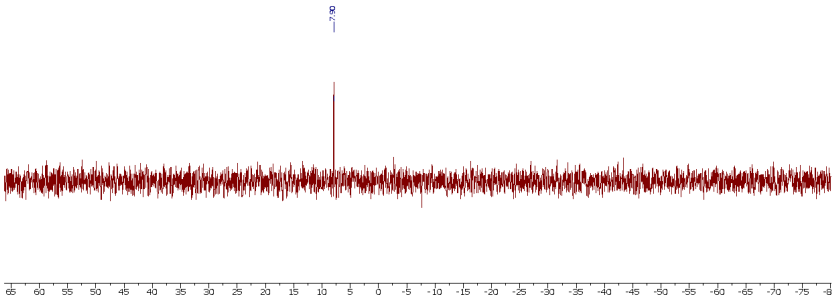

Figure S20 $^{29}Si\{^{1}H\}$ NMR spectrum of **7-TMS-*d*** in CD_3CN.

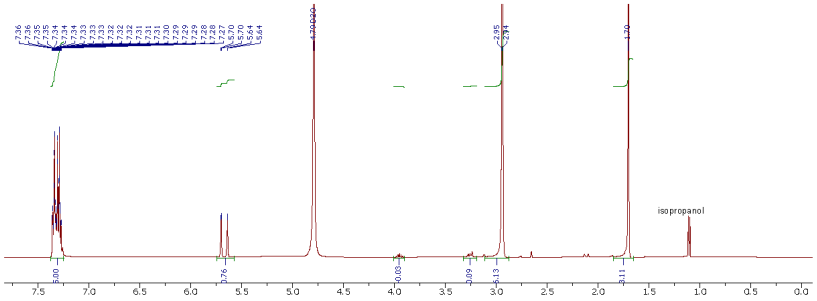

Figure S21 ^{1}H NMR spectrum of **7-*d*** in D_2O.

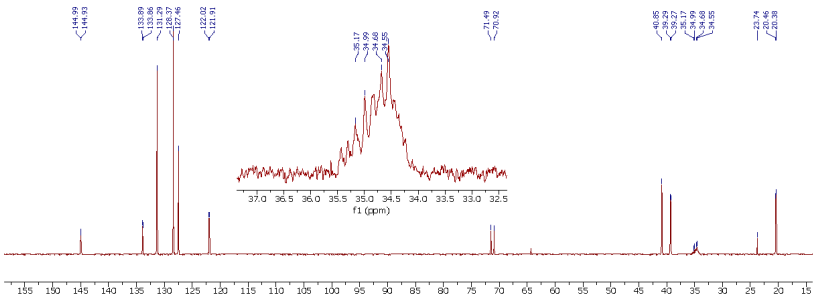

Figure S22 $^{13}C\{^{1}H\}$ NMR spectrum of **7-*d*** in D_2O.

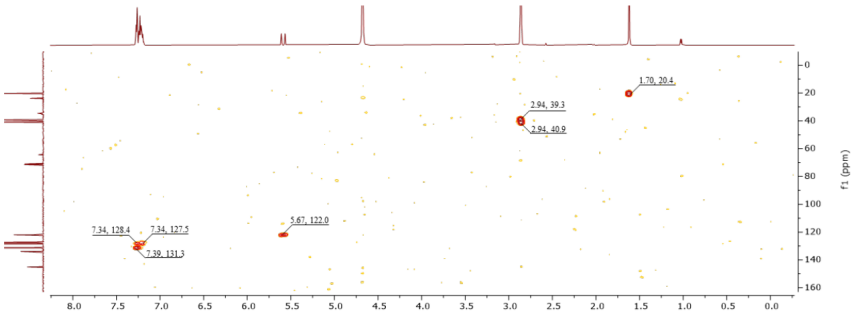

Figure S23 HMQC NMR spectrum of **7-*d*** in D_2O

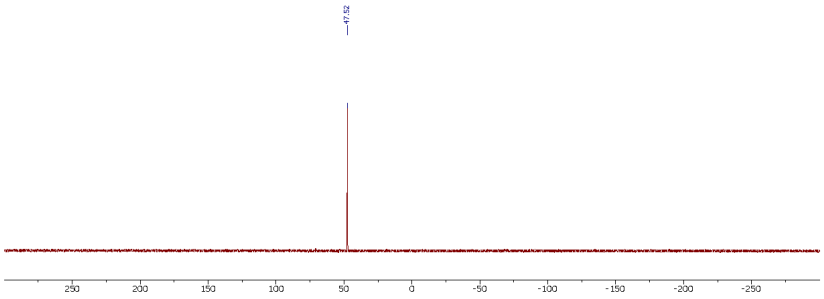

Figure S24 $^{31}P\{^{1}H\}$ NMR spectrum of **7-*d*** in D_2O.

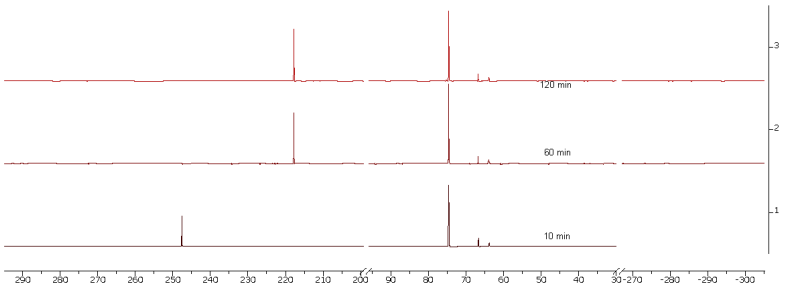

Figure S25 Time elapsed $^{31}P\{^{1}H\}$ NMR spectra for recording the process of **3** with HCl-Et_2O in DCM.

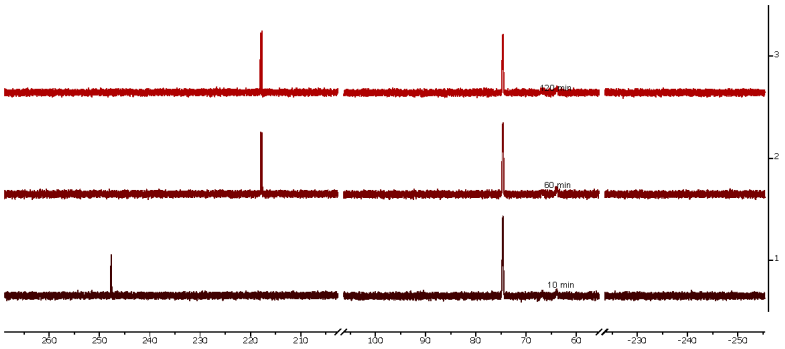

Figure S26 Time elapsed ^{31}P NMR spectra for recording the process of **3** with HCl-Et_2O in DCM.

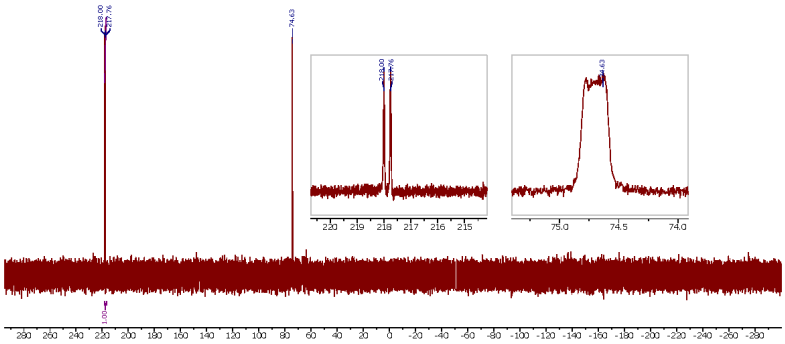

Figure S27 ^{31}P NMR spectrum for the reaction of **3** with HCl-Et_2O in DCM.

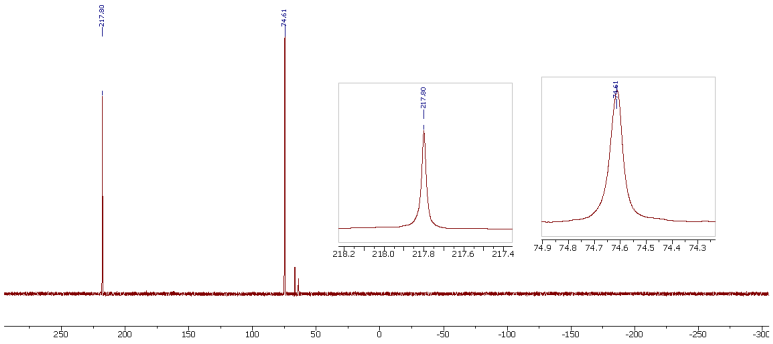

Figure S28 $^{31}P\{^{1}H\}$ NMR spectrum for the reaction of **3** with HCl-Et_2O in DCM.

3. Crystallographic details

The supplementary crystallographic data for **3**, **5**, **6** and **7** can be found in the CCDC with the following deposit numbers CCDC 2181743 (**3**), 2181744 (**5**), 2181745 (**6**) and 2181746 (**7**). These data can be obtained free of charge from www.ccdc.cam.ac.uk/data_request/cif.

Table S1 Selected crystallographic data for **3**, **5**, **6** and **7**.

	3	**5**	**6**	**7**
Sample Name	JL1302	JX0137	JX0136	JX0193
CCDC number	2181743	2181744	2181745	2181746
Empirical formula	$C_{17}H_{24}NPSi$	$C_{14}H_{17}ClNP$	$C_{28}H_{41}Cl_3N_2O_3P_2$	$C_{14}H_{21}ClNO_2P$
Formula Weight	301.43	265.70	621.92	301.74
Temperature/K	100.0	100.0	100.0	100.0
Crystal system	Monoclinic	Orthorhombic	Orthorhombic	Monoclinic
Space group	$P2_1/c$	$Pbca$	$Pbcn$	$P2_1/c$
a/Å	10.1624(4)	12.5647(8)	9.6377(3)	6.6747(5)
b/Å	17.8102(6)	10.1062(8)	12.5777(4)	8.4813(6)
c/Å	10.1967(3)	21.9775(18)	24.6612(6)	27.458(2)
α/°	90	90	90	90
β/°	111.8630(10)	90	90	95.079(3)
γ/°	90	90	90	90
Volume/Å^3	1712.81(10)	2790.7(4)	2989.43(15)	1548.3(2)
Z	4	8	4	4
Reflections collected	53517	58240	46022	34171
Independent reflections (R_{int})	5223 (0.0232)	4258 (0.0546)	4560 (0.0602)	4695 (0.0439)
R_1 [I>2σ (I)]	0.0278	0.0328	0.0312	0.0802
wR_2 (all data)	0.0784	0.0862	0.0787	0.1876

Table S2 List of bond lengths for **3**.

Atom1	Atom2	Length/Å	Atom1	Atom2	Length/Å
P1	C1	1.7333(8)	C2	C6	1.5152(12)
P1	C5	1.7369(8)	C3	C4	1.4104(11)
Si1	C1	1.8866(8)	C4	C5	1.4151(11)
Si1	C13	1.8662(11)	C5	C7	1.4907(11)
Si1	C14	1.8703(11)	C7	C8	1.3994(11)
Si1	C15	1.8731(10)	C7	C12	1.4041(11)
N1	C4	1.4059(10)	C8	C9	1.3973(12)
N1	C16	1.4665(12)	C9	C10	1.3866(14)
N1	C17	1.4568(11)	C10	C11	1.3945(14)
C1	C2	1.4115(11)	C11	C12	1.3903(12)
C2	C3	1.3960(12)			

Table S3 List of bond angles for **3**.

Atom1	Atom2	Atom3	Angle/°	Atom1	Atom2	Atom3	Angle/°
C1	P1	C5	105.33(4)	C2	C3	C4	126.39(7)
C13	Si1	C1	108.37(4)	N1	C4	C3	119.73(7)
C13	Si1	C14	108.17(7)	N1	C4	C5	119.95(7)
C13	Si1	C15	107.22(6)	C3	C4	C5	120.29(7)
C14	Si1	C1	110.48(5)	C4	C5	P1	122.90(6)
C14	Si1	C15	108.99(5)	C4	C5	C7	122.65(7)
C15	Si1	C1	113.44(4)	C7	C5	P1	114.36(6)
C4	N1	C16	117.58(7)	C8	C7	C5	121.46(7)
C4	N1	C17	118.06(7)	C8	C7	C12	118.34(8)
C17	N1	C16	110.26(7)	C12	C7	C5	120.08(7)
P1	C1	Si1	114.15(4)	C9	C8	C7	120.85(8)
C2	C1	P1	120.96(6)	C10	C9	C8	120.12(9)
C2	C1	Si1	124.81(6)	C9	C10	C11	119.70(8)
C1	C2	C6	120.39(7)	C12	C11	C10	120.28(9)
C3	C2	C1	123.14(8)	C11	C12	C7	120.72(8

Table S4 List of bond lengths for **5**.

Atom1	Atom2	Length/Å	Atom1	Atom2	Length/Å
P1	C5	1.7445(13)	C7	C8	1.3950(18)
P1	C1	1.7230(14)	C3	C2	1.3940(17)
N1	C4	1.4824(15)	C2	C1	1.3902(18)
N1	C00A	1.5006(16)	C2	C6	1.5104(18)
N1	C00C	1.5009(16)	C12	C11	1.3974(18)
C4	C5	1.3886(17)	C10	C11	1.3847(19)
C4	C3	1.3942(16)	C10	C9	1.382(2)
C5	C7	1.4969(16)	C8	C9	1.3935(19)
C7	C12	1.3937(18)			

Table S5 List of bond angles for **5**.

Atom1	Atom2	Atom3	Angle/°	Atom1	Atom2	Atom3	Angle/°
C1	P1	C5	102.13(6)	C8	C7	C5	119.97(11)
C4	N1	C00A	112.30(9)	C2	C3	C4	123.43(12)
C4	N1	C00C	111.33(9)	C3	C2	C6	118.48(12)
C00A	N1	C00C	111.37(10)	C1	C2	C3	121.10(11)
C5	C4	N1	118.65(10)	C1	C2	C6	120.42(11)
C5	C4	C3	125.46(11)	C7	C12	C11	120.11(12)
C3	C4	N1	115.87(10)	C9	C10	C11	120.11(12)
C4	C5	P1	121.69(9)	C2	C1	P1	126.17(10)
C4	C5	C7	122.58(11)	C10	C11	C12	120.08(13)
C7	C5	P1	115.73(9)	C9	C8	C7	120.24(13)
C12	C7	C5	120.69(11)	C10	C9	C8	120.18(13)

C12	C7	C8	119.28(11)

Table S6 List of bond lengths for **6**.

Atom1	Atom2	Length/Å	Atom1	Atom2	Length/Å
P1	O1	1.6307(6)	C3	C4	1.5110(17)
P1	O2	1.4687(9)	C4	C5	1.5542(16)
P1	C1	1.7956(13)	C5	C6	1.5117(17)
P1	C4	1.8629(12)	C6	C7	1.3935(17)
N1	C4	1.5225(15)	C6	C11	1.3962(18)
N1	C13	1.4957(16)	C7	C8	1.3882(19)
N1	C14	1.5009(16)	C8	C9	1.388(2)
C1	C2	1.5137(18)	C9	C10	1.3837(19)
C2	C3	1.3381(18)	C10	C11	1.3897(18)
C2	C12	1.4932(18)			

Table S7 List of bond angles for **6**.

Atom1	Atom2	Atom3	Angle/°	Atom1	Atom2	Atom3	Angle/°
O1	P1	C1	102.76(4)	N1	C4	P1	112.28(8)
O1	P1	C4	100.17(5)	N1	C4	C5	109.52(9)
O2	P1	O1	112.02(5)	C3	C4	P1	99.06(8)
O2	P1	C1	122.39(6)	C3	C4	N1	110.34(10)
O2	P1	C4	120.00(5)	C3	C4	C5	112.57(10)
C1	P1	C4	95.89(6)	C5	C4	P1	112.76(8)
P1	O1	P1[1]	121.92(8)	C6	C5	C4	114.42(10)
C13	N1	C4	114.93(10)	C7	C6	C5	119.88(11)
C13	N1	C14	108.93(10)	C7	C6	C11	118.64(12)
C14	N1	C4	113.04(9)	C11	C6	C5	121.48(11)
C2	C1	P1	101.64(8)	C8	C7	C6	120.82(12)
C3	C2	C1	116.33(11)	C9	C8	C7	119.96(12)
C3	C2	C12	124.59(12)	C10	C9	C8	119.81(12)
C12	C2	C1	119.07(12)	C9	C10	C11	120.28(13)
C2	C3	C4	117.90(11)	C10	C11	C6	120.44(12)

Table S8 List of bond lengths for **7**

Atom1	Atom2	Length/ Å	Atom1	Atom2	Length/ Å
P1	O1	1.483(3)	C3	C4	1.507(5)
P1	O2	1.550(3)	C4	C5	1.549(5)
P1	C1	1.786(3)	C5	C6	1.517(5)
P1	C4	1.863(3)	C6	C7	1.389(6)
N1	C4	1.533(4)	C6	C11	1.385(5)
N1	C13	1.494(4)	C7	C8	1.391(6)
N1	C14	1.486(5)	C8	C9	1.381(8)

C1	C2	1.515(5)	C9	C10	1.371(9)
C2	C3	1.332(5)	C10	C11	1.404(7)
C2	C12	1.489(5)			

Table S9 List of bond angles for **7**.

Atom1	Atom2	Atom3	Angle/°	Atom1	Atom2	Atom3	Angle/°
O1	P1	O2	114.86(15)	N1	C4	C5	110.3(3)
O1	P1	C1	114.30(17)	C3	C4	P1	99.1(2)
O1	P1	C4	109.66(15)	C3	C4	N1	110.3(3)
O2	P1	C1	107.78(16)	C3	C4	C5	113.8(3)
O2	P1	C4	112.96(15)	C5	C4	P1	114.7(2)
C1	P1	C4	95.78(16)	C6	C5	C4	113.8(3)
C13	N1	C4	115.1(3)	C7	C6	C5	120.5(3)
C14	N1	C4	113.9(3)	C11	C6	C5	120.7(4)
C14	N1	C13	108.6(3)	C11	C6	C7	118.8(4)
C2	C1	P1	101.7(2)	C6	C7	C8	120.8(4)
C3	C2	C1	116.6(3)	C9	C8	C7	120.2(5)
C3	C2	C12	125.7(3)	C10	C9	C8	119.4(5)
C12	C2	C1	117.6(3)	C9	C10	C11	120.8(5)
C2	C3	C4	117.5(3)	C6	C11	C10	119.9(5)
N1	C4	P1	108.1(2)				

4. DFT calculations

4.1 Methodology

All calculations were performed using the Turbomole program package (Version 7.3).[7] Structure optimizations were carried out employing the PBEh-3c composite method including three body interaction terms[8] and COSMO (ε = ∞) as an implicit solvation model.[9] SCF energies and structural gradients were converged to 10^{-7} a.u. and 10^{-4} a.u., respectively. The exchange correlation functional was integrated using the radial multigrid m4.[10] Electronic energies were calculated at the PBE0-D3(BJ)/def2-TZVP[11] level with COSMO (ε = 9.08, DCM) for implicit solvation.[12] The solvation model (ε = 78.4, H_2O) was applied for H_2O and H_3O^+ single point energies. Normal modes and vibrational frequencies were computed within the rigid-rotor harmonic-oscillator approximation applied to vibrational modes below 100 cm^{-1} at 298.15 K.[13] Furthermore, a concentration correction to the translational partition function (q_{trans}) is used,

$$q_{trans} = \left(\frac{mk_BT}{2\pi}\right)^{\frac{3}{2}} \cdot \frac{V}{n}$$

with the mass (m), Boltzmann constant (k_B), temperature (T), volume (V) and amount of substance (n). Intermediates were assumed to have a concentration of 1M and water is calculated with its initial concentration of 55.6M. Spurious negative frequencies between −100 cm^{-1} and 0 were sign inverted as they arise due to inaccuracies of the COSMO solvation model and contribute to the Gibbs free energy of the respective compound to minimize the error. Relaxed potential energy surface scans were conducted to obtain a reasonable guess for the transition state. The optimized transition state was assessed through a normal mode calculation. The structural gradient is converged to $6 \cdot 10^{-4}$ a. u. and the imaginary mode corresponds to the P-C bond formation with a frequency of -142 cm^{-1}.

4.2 Electrostatic potential maps, mechanism and energy diagram

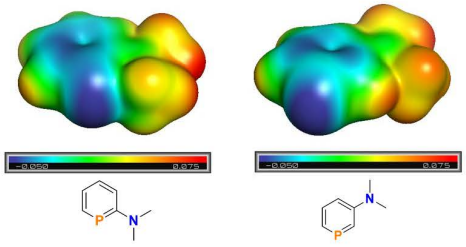

Figure S29. Electrostatic potential maps of 2-dimethylaminophosphinine and 3-dimethylaminophosphinine calculated at the PBE0/def2-TZVP level of DFT, isovalue = 0.02 a.u..

The ring contraction experiment was investigated with the reaction pathways and Gibbs free energy profiles depicted in Figure S31 and S32, respectively

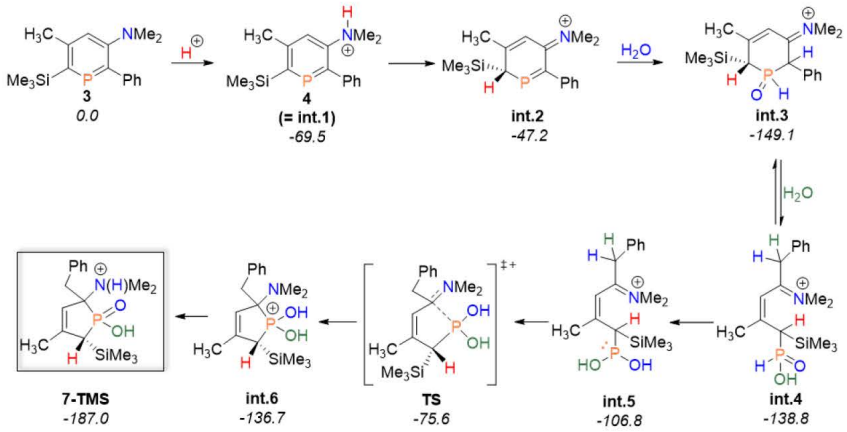

Figure S30 Lewis structures of the reaction pathway. The **7-TMS** is the product formed with reaction. Energies (in kJ/mol), relative to phosphinine **3** (0.0 kJ/mol), are given below the compound name; Int.: intermediate.

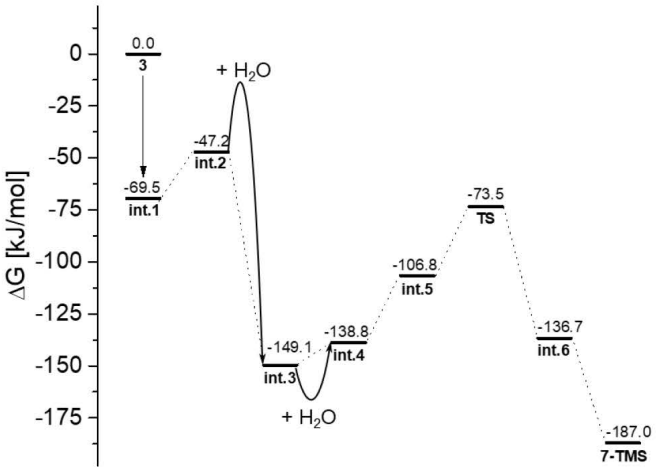

Figure S31 Relative free energies of the compounds shown in the reaction paths.

In the reaction of **3** to **int.1**, the aromaticity of the phosphinine is conserved. It is known that the energy gain of the enamine formation is not high enough to destroy the aromatic system.[14] However, the oxidative addition of H_2O across the activated P=C bond in **int.2** to give a P-OH species with an adjacent CH unit. This compound will tautomerize to **int.3**. This process is exergonic by -101.9 kJ/mol. Furthermore, an equilibrium reaction of **int.3** to **int.4** happens. Their energetic difference amounts to 8.7 kJ/mol which corresponds to an equilibrium constant of $K = e^{\frac{-\Delta G}{RT}} = 33$. The formation of **int.5** is necessary for the formation of the transition state of the RDS. Phosphinic acids are known to tautomerize to form nucleophilic phosphorus species (HP=O↔P-OH).[15] The nucleophile can then react with the electrophilic imide. The transition state of the P-C bond formation can be specified as a 5-exo-trig reaction, which is allowed according to the Baldwin rules.[16] Polar protic solvents stabilize the transition state and decrease the total energy barrier of 75.6 kJ/mol (**int.3** to **TS**), because the amine group can form hydrogen bonds with surrounding water molecules. Our calculations suggest that the intramolecular hydrogen transfer between the POH unit and the nitrogen occurs after the RDS (**int.6** to **7-TMS**), rather than simultaneously. Ring formation (**TS** to **int.6**) and subsequent hydrogen transfer and P=O double bond formation (**int.6** to **7-TMS**) contribute to a significant decrease in free energy of 63.2 kJ/mol and 50.3 kJ/mol, respectively. The overall reaction starting from **int.3** as the most stable compound before the RDS is thus rendered exergonic with ΔG = -37.9 kJ/mol.

All in all, the proposed reaction mechanism serves as a rationale for the outcomes of ring contraction. The computed relative Gibbs free energies of the structures and the energy barrier of the RDS (76 kJ/mol) seem physically sound.

4.3 Calculated structures

"Phosphinine **3**", E_el(SPE) = -3536821.66 kJ/mol, G = 862.25 kJ/mol, neg. freq. (1-3) = 0.0, 0.0, 0.0

C	1.0299750	0.0105888	-1.0678551
C	1.5357904	-1.2851171	-0.9610759
C	2.7960210	-1.6015980	-1.4528295
H	0.9446595	-2.0506681	-0.4727475
P	-1.5823549	-0.6621443	-1.2851133
C	3.5707847	-0.6261375	-2.0624337
C	3.0749719	0.6681570	-2.1778201
H	3.1715204	-2.6121128	-1.3541097
C	1.8190854	0.9844126	-1.6857702

H	4.5533210	-0.8695844	-2.4457438
H	1.4434089	1.9942540	-1.7841393
H	3.6697211	1.4343811	-2.6587850
C	-0.3402415	0.3310383	-0.6020117
C	-3.0673403	0.0083438	-0.7173755
H	2.4121199	1.9985956	1.4622551
C	-0.6084556	1.4174399	0.2508522
H	-4.8739643	2.2810874	-0.2846175
H	-5.1015429	1.0033750	0.8976444
C	-1.9314480	1.7770560	0.5497450
H	-0.4396036	4.0519244	0.5491495
H	-0.3041123	3.5330673	2.2407167
C	-3.0882132	1.1478295	0.1026318
H	-4.2537838	2.4743976	1.3467469
H	-2.0762781	2.6156878	1.2183440
H	-6.3592960	0.9100444	-1.4348138
H	-5.3730112	0.8442155	-2.8941489
H	1.1870164	1.4754138	2.6293522
H	1.5936613	0.4589597	1.2479213
Si	-4.6226582	-0.9140466	-1.2844546
H	-6.6306348	-0.3577169	-2.6215628
C	-4.3960621	1.7538651	0.5425308
C	-5.8574879	0.2357551	-2.1284058
H	-6.2984614	-2.3616299	-0.1555066
H	-5.7853288	-1.0941274	0.9498104
C	-5.4349397	-1.7833623	0.1806301
H	-4.7375809	-2.4774114	0.6533063
H	-3.4579824	-2.9838809	-2.1154851

C	-4.1334814	-2.2373160	-2.5351411
H	-5.0330624	-2.7604126	-2.8682899
H	-3.6536188	-1.8146446	-3.4192175
N	0.4399542	2.1629684	0.7776981
H	1.1295810	4.0281981	1.3421051
C	1.4539408	1.4872786	1.5652959
C	0.1793718	3.5001264	1.2554178

"**int. 1**(= phosphinine **4**)", E_el(SPE) = -3537978.97 kJ/mol, G = 897.46 kJ/mol, neg. freq. (1-3) = -34.31, 0.0, 0.0

C	1.0704792	0.0226310	-1.2164456
C	1.6776134	-1.1853635	-0.8739665
C	2.9665879	-1.4659802	-1.3032960
H	1.1418655	-1.9019094	-0.2640408
P	-1.5956949	-0.6048140	-1.4930536
C	3.6610653	-0.5462263	-2.0780793
C	3.0620479	0.6562061	-2.4274324
H	3.4294163	-2.4049051	-1.0296430
C	1.7714068	0.9397317	-2.0029907
H	4.6664530	-0.7675102	-2.4111940
H	1.2991965	1.8676220	-2.3046133
H	3.5940766	1.3731597	-3.0383458
C	-0.3120918	0.3170680	-0.7657542
C	-3.0262612	0.0018820	-0.7400464
H	1.6375997	2.1213258	2.6090194
C	-0.5744087	1.2744489	0.1938820
H	-4.8182867	2.1807207	0.0962064
H	-4.9718760	0.7514527	1.1069401

C	-1.8342851	1.6141341	0.6603389
H	0.4753622	3.6093961	-0.5306536
H	-0.2779881	3.8996606	1.0534509
C	-3.0155240	1.0248753	0.2222290
H	-4.1028353	2.1568925	1.7001837
H	-1.9179209	2.3829238	1.4189330
H	-6.3901371	0.9218317	-1.0802798
H	-5.4741700	1.1185194	-2.5746278
H	-0.1286045	2.0821873	2.7997767
H	0.7535158	0.5929433	2.3856513
Si	-4.6284291	-0.8656319	-1.3161459
H	-6.6977107	-0.1401667	-2.4462195
C	-4.2932110	1.5514061	0.8157757
C	-5.9118102	0.3831472	-1.8974495
H	-6.1669491	-2.4868007	-0.2464032
H	-5.5897717	-1.3525546	0.9663142
C	-5.2906042	-1.9289859	0.0904606
H	-4.5416668	-2.6546422	0.4119536
H	-3.5048581	-2.7795986	-2.5032187
C	-4.2125171	-1.9921543	-2.7654492
H	-5.1304616	-2.4792297	-3.1029724
H	-3.8034236	-1.4427916	-3.6147511
N	0.5710410	1.9761318	0.8036087
H	1.4919166	3.8623338	0.9087080
C	0.7154657	1.6701826	2.2560999
C	0.5613571	3.4430542	0.5387920
H	1.4129018	1.6083952	0.3502453

"**int. 2**", E_el(SPE) = -3537952.60 kJ/mol, G = 893.43 kJ/mol, neg. freq. (1-3) = -0.0, -0.0, -0.0

C	0.7963424	-0.2400849	-0.7947546
C	1.7535650	-1.1443430	-0.3414700
C	2.9379080	-1.3231521	-1.0441693
H	1.5810050	-1.6950379	0.5751784
P	-1.4508938	-1.4942145	-0.2086692
C	3.1734608	-0.6051666	-2.2077536
C	2.2155553	0.2886969	-2.6718694
H	3.6771574	-2.0233564	-0.6778199
C	1.0319472	0.4674250	-1.9736039
H	4.0973120	-0.7429112	-2.7540554
H	0.2868604	1.1593054	-2.3479240
H	2.3876753	0.8439423	-3.5846239
C	-0.5070235	-0.0941343	-0.0938584
C	-3.0647450	-0.9833766	0.3725172
H	1.6755704	2.5980824	-0.4056283
C	-0.9703247	1.1566448	0.4597650
H	-4.5696447	1.4236753	2.2935258
H	-5.2482231	-0.0914853	1.6718170
C	-2.2684645	1.2452335	1.0590580
H	-1.7888714	3.6321244	0.2133934
H	-0.8970118	3.8215274	1.7406128
C	-3.1892068	0.2477710	1.1282608
H	-4.1027324	-0.1264587	2.9930351
H	-2.4818667	2.1367842	1.6316474
H	-2.9530017	1.4724801	-1.8478240
H	-2.2026007	0.1826866	-2.7971721
H	1.5200885	3.0034402	1.3080983

H	1.6543760	1.3229887	0.8279346
Si	-4.0514092	-0.7201975	-1.3666215
H	-3.7782901	0.8174683	-3.2514175
C	-4.3497189	0.3842039	2.0588920
C	-3.1479829	0.5520766	-2.3998510
H	-6.3458624	-0.0795181	-1.8828140
H	-5.7891043	0.8614729	-0.5048712
C	-5.7780452	-0.1331013	-0.9509251
H	-6.3060740	-0.8182475	-0.2873415
H	-4.4954003	-3.1645807	-1.4980484
C	-4.0975315	-2.4078966	-2.1758524
H	-4.7523123	-2.3716649	-3.0489058
H	-3.1158049	-2.7401384	-2.5146171
N	-0.2154107	2.2532493	0.4859176
H	-0.1646620	4.3028746	0.2074212
C	1.2404252	2.2814366	0.5413818
C	-0.8107203	3.5678288	0.6823509
H	-3.6298491	-1.8179824	0.7983442

"**int. 3**", E_el(SPE) = -3738656.72 kJ/mol, G = 961.23 kJ/mol, neg. freq. (1-3) = -64.71, -0.0, -0.0

C	0.8691009	-0.1812842	-0.9993552
C	1.5163728	-0.3586113	0.2199711
C	2.8560689	-0.7179997	0.2520547
H	0.9862716	-0.2208512	1.1554201
P	-1.5148964	-1.4499935	-1.1119996
C	3.5542781	-0.9185591	-0.9309037
C	2.9071320	-0.7565698	-2.1482518
H	3.3523270	-0.8447508	1.2050628

C	1.5696026	-0.3902240	-2.1832784
H	4.5985671	-1.2003684	-0.9038893
H	1.0734364	-0.2566921	-3.1367636
H	3.4437344	-0.9124082	-3.0747626
C	-0.6056418	0.1578785	-1.0622925
C	-3.0868995	-1.1002775	-0.3056482
H	0.4826900	2.2266739	-1.7796426
C	-1.0412532	1.0946174	0.0330744
H	-4.7125658	-0.7944246	1.8721129
H	-3.3636372	-1.7565229	2.4285062
C	-1.9361081	0.6585598	1.0653131
H	-1.9876668	3.3197424	1.2280522
H	-0.4957198	2.8949987	2.0979147
C	-2.8362074	-0.3512603	0.9460219
H	-3.5193374	-0.0780309	2.9720286
H	-1.9121758	1.1861293	2.0084668
H	-3.0678582	1.9110276	-1.8079305
H	-2.7832552	0.7839609	-3.1495533
H	0.1015401	3.8307328	-1.1661260
H	1.3981411	2.8852843	-0.4165932
Si	-4.3658751	-0.2211018	-1.4798836
H	-4.2902523	1.6722895	-3.0340125
C	-3.6533051	-0.7470564	2.1255203
C	-3.5291903	1.1547577	-2.4457959
H	-6.4508783	1.0083818	-1.0432502
H	-5.3396029	1.2508338	0.2967996
C	-5.7194320	0.5072067	-0.4059159
H	-6.2531891	-0.2560860	0.1617990

H	-4.2396397	-1.9971614	-3.2124599
C	-5.0353011	-1.5458982	-2.6199285
H	-5.5291944	-2.3394717	-2.0568867
H	-5.7694109	-1.1212064	-3.3069007
N	-0.5470181	2.2991815	0.0744482
H	-0.4920638	4.2033267	0.9161867
C	0.4153808	2.8293505	-0.8837486
C	-0.9070729	3.2288045	1.1467145
H	-0.8146759	-2.2246822	-0.1656551
H	-0.8257519	0.6181376	-2.0309953
O	-1.5673478	-2.0192831	-2.4937569
H	-3.5526644	-2.0632383	-0.0685987

"**int. 4**", E_el(SPE) = -3939242.59 kJ/mol, G = 1022.96 kJ/mol, neg. freq. (1-3) = -0.0, -0.0, -0.0

C	0.4640643	0.4419910	-1.6228847
C	1.2250420	-0.4051107	-0.8225810
C	2.3089142	-1.0899792	-1.3549675
H	0.9896287	-0.5406253	0.2258308
P	-1.9904399	-1.9431221	0.1715859
C	2.6422827	-0.9425852	-2.6934856
C	1.8867206	-0.1006851	-3.4982459
H	2.8924202	-1.7411544	-0.7174833
C	0.8082114	0.5885762	-2.9642835
H	3.4873728	-1.4776756	-3.1062690
H	0.2302971	1.2506187	-3.5985813
H	2.1389601	0.0253481	-4.5429605
C	-0.7629931	1.1700159	-1.1262810
C	-3.3445926	-0.7413848	0.1396161

H	1.2099835	2.6585147	-0.6849144
C	-0.8977943	1.4834615	0.3300576
H	-5.3547915	0.8037788	0.9873864
H	-4.6078810	0.1843090	2.4417697
C	-2.1880566	1.4137258	0.9775120
H	-0.3896277	3.2136400	2.6534262
H	-0.5899632	1.4632325	2.9078472
C	-3.2276809	0.5559010	0.8582901
H	-4.4512544	1.9001286	2.0392830
H	-2.3569801	2.2343353	1.6655628
H	-5.2228217	1.6201230	-1.3094693
H	-3.6250586	1.8189720	-2.0196642
H	1.5202860	3.4925277	0.8346615
H	2.1464969	1.8552114	0.5916593
Si	-4.1481217	-0.6135011	-1.6466291
H	-4.9654084	1.2629650	-3.0103485
C	-4.4723708	0.8955608	1.6238458
C	-4.5149903	1.1885022	-2.0184581
H	-6.2250194	-1.6427313	-2.5292270
H	-6.4197084	-1.2217295	-0.8288974
C	-5.7200177	-1.6268726	-1.5620611
H	-5.5026173	-2.6589617	-1.2815353
H	-2.0481251	-0.8092972	-3.0633340
C	-2.9964261	-1.3367629	-2.9464412
H	-2.7726750	-2.3880677	-2.7596129
H	-3.5046029	-1.2833608	-3.9119696
N	0.0890604	2.0123264	0.9913714
H	1.0267366	2.1692238	2.8342163

C	1.3126181	2.5234638	0.3849335
C	0.0181428	2.2272134	2.4337270
O	-1.0752343	-1.6186965	1.4584129
H	-0.8612184	2.1277510	-1.6516864
O	-2.5290193	-3.3255677	0.0409320
H	-4.1349938	-1.3016514	0.6563984
H	-1.0592871	-1.5899674	-0.8126382
H	-1.5021544	-1.7520156	2.3158502
H	-1.6540323	0.6201281	-1.4260258

"**int. 5**", E_el(SPE) = -3939208.26 kJ/mol, G = 1020.63 kJ/mol, neg. freq. (1-3) = -87.96, -42.92, 0.0

C	0.2792969	-0.2203622	-0.3131041
C	0.1921456	-0.3648372	1.0640661
C	1.3472930	-0.3214764	1.8348457
C	2.5804852	-0.1265929	1.2311158
C	2.6730617	0.0328501	-0.1500287
C	1.5141538	-0.0207303	-0.9171997
C	4.0308403	0.2499067	-0.7908228
C	4.4817125	1.6499107	-0.4810298
C	5.2078685	1.9024334	0.7531934
C	6.3390365	1.3000660	1.1733399
C	7.1661731	0.3786720	0.3536616
P	7.5642074	-1.1814430	1.2772783
O	6.0213159	-1.7704882	1.2912706
N	4.0933498	2.6618477	-1.1946010
C	3.1932002	2.5703815	-2.3373629
C	4.4490305	4.0316988	-0.8269955
C	6.8553936	1.6430397	2.5377513

Si	8.7886083	1.2554487	-0.2605851
C	9.1853276	0.5744346	-1.9658183
C	10.2212214	0.9508737	0.9173332
C	8.4284467	3.0943077	-0.4074644
O	8.3059599	-2.0351069	0.0815359
H	1.5680672	0.0748001	-1.9944683
H	-0.6135570	-0.2657914	-0.9228710
H	-0.7701012	-0.5188255	1.5347105
H	3.4789619	-0.1120445	1.8361565
H	1.2893209	-0.4471514	2.9081681
H	2.1902338	2.8658815	-2.0315711
H	6.8053775	0.7702950	3.1936264
H	7.9016588	1.9500017	2.5145560
H	3.7055704	4.4387858	-0.1422723
H	5.4268512	4.0632970	-0.3569633
H	6.2772012	2.4383873	3.0026413
H	4.7837494	2.6757228	1.3851772
H	10.0198602	1.2968522	1.9318916
H	10.4865428	-0.1057275	0.9730802
H	3.5410047	3.2511129	-3.1089258
H	3.1636375	1.5718868	-2.7529980
H	11.1016317	1.4892099	0.5595483
H	9.3117315	3.6133012	-0.7850234
H	8.1598527	3.5559094	0.5438557
H	7.6171524	3.2846805	-1.1126503
H	9.4695179	-0.4776176	-1.9403356
H	8.3387859	0.6789118	-2.6469640
H	10.0217929	1.1269820	-2.3983861

H	4.4691060	4.6406537	-1.7253103
H	4.7310758	-0.4529622	-0.3482168
H	6.6579747	0.1123702	-0.5816064
H	3.9992930	0.0448184	-1.8598111
H	5.8908221	-2.4110945	2.0009063
H	7.8730486	-2.0157641	-0.7833794

"**TS**", E_el(SPE) = -3939174.29 kJ/mol, G = 1019.91 kJ/mol, neg. freq. (1-3) = -142.35, -86.32, -15.21

C	0.4061097	5.0322048	-0.9489917
C	-0.5406964	4.9640965	-1.9612726
C	-1.0290888	3.7271295	-2.3627707
C	-0.5786134	2.5683494	-1.7475896
C	0.3596546	2.6274794	-0.7187396
C	0.8532119	3.8703929	-0.3331622
C	0.8421332	1.3597611	-0.0526799
C	-0.2006526	0.8275381	0.9131798
C	-1.3874381	0.1705023	0.2996038
C	-1.5337243	-1.1167164	-0.0426800
C	-0.4657415	-2.1554138	0.1735074
P	0.6800816	-1.3628525	1.3405959
O	0.0426434	-1.8453556	2.7565116
N	-0.4079928	1.4543260	2.0639486
C	-1.5711937	1.1984989	2.8983127
C	0.5672009	2.3353674	2.6802575
C	-2.8480421	-1.5913497	-0.5791229
Si	0.3799439	-2.8651808	-1.4177431
C	1.4673068	-4.3116864	-0.8897480
C	1.3837753	-1.5493657	-2.3042066

C	-0.9357320	-3.5230671	-2.5886471
O	2.1460180	-2.0421824	1.2248078
H	1.6057886	3.9367261	0.4428020
H	0.8031459	5.9901329	-0.6391373
H	-0.8895629	5.8687988	-2.4419597
H	-0.9571306	1.6084955	-2.0791227
H	-1.7567826	3.6631309	-3.1612962
H	-2.2082943	0.4328740	2.4697519
H	-2.7683220	-1.9070952	-1.6183809
H	-3.1982998	-2.4563468	-0.0130734
H	0.5988850	2.1374822	3.7501669
H	1.5658012	2.1752886	2.2875981
H	-3.6075210	-0.8136245	-0.5241853
H	-2.2300417	0.8403199	0.1577776
H	0.7665031	-0.7025611	-2.6107691
H	2.2147720	-1.1743857	-1.7051983
H	-1.2517324	0.8706990	3.8875701
H	-2.1509757	2.1144262	3.0136524
H	1.8099621	-1.9754056	-3.2149332
H	-0.4475957	-4.1454104	-3.3419982
H	-1.4644060	-2.7319087	-3.1208230
H	-1.6744247	-4.1448320	-2.0811026
H	2.4856941	-4.0115159	-0.6423745
H	1.0516737	-4.8542625	-0.0383440
H	1.5415078	-5.0245548	-1.7130168
H	0.2911695	3.3800055	2.5343289
H	1.0123221	0.5939542	-0.8067706
H	-0.9265165	-3.0413227	0.6330425

H 1.8011291 1.5249677 0.4347333

H 0.4090883 -1.3868335 3.5243872

H 2.1968702 -2.9986080 1.3731659

"**int. 6**", E_el(SPE) = -3939242.51 kJ/mol, G = 1024.97 kJ/mol, neg. freq. (1-3) = -47.38, -0.0, -0.0

C 0.4973329 3.9966830 -0.1714805

C 0.0193837 5.0683987 -0.9135126

C -0.5479108 4.8541168 -2.1618527

C -0.6220727 3.5626511 -2.6670479

C -0.1422073 2.4955164 -1.9216360

C 0.4111969 2.6952317 -0.6577790

C 0.9209142 1.5229569 0.1400409

C -0.1748827 0.7895673 0.9462665

N -0.6546232 1.4413962 2.1750217

C 0.3738140 2.1252840 2.9535833

C -1.3019867 0.3243650 0.0548970

C -1.4203762 -0.9721691 -0.2504075

C -2.4897548 -1.5000445 -1.1454197

C -0.4185953 -1.9501183 0.3359473

Si 0.7266605 -2.8551635 -0.9433317

C -0.3256803 -4.1504283 -1.8006741

P 0.3522191 -0.8837601 1.5414437

O 1.9279936 -0.9584299 1.6417990

O -0.3422950 -0.9922027 2.9473921

C -1.8726199 2.2370564 2.0652559

C 2.0976941 -3.7254056 0.0052489

C 1.4058726 -1.6010335 -2.1586968

H 0.9535955 4.1863688 0.7919591

H	0.0974010	6.0722532	-0.5164530
H	-0.9196863	5.6885425	-2.7421853
H	-0.1922555	1.4944720	-2.3339686
H	-1.0474258	3.3851858	-3.6463101
H	-2.6998697	1.6311159	1.7039174
H	-2.0807126	-1.8098826	-2.1084596
H	-2.9725787	-2.3738636	-0.7058985
H	-0.0123804	2.3036545	3.9558426
H	1.2686705	1.5106444	3.0548705
H	-3.2483377	-0.7436171	-1.3373169
H	-1.9809588	1.0563208	-0.3620458
H	0.6155589	-0.9979746	-2.6099881
H	2.1274124	-0.9257962	-1.6962542
H	-2.1379393	2.5877602	3.0610065
H	-1.7571139	3.1080124	1.4144868
H	1.9245293	-2.1133864	-2.9711267
H	0.3218018	-4.7997768	-2.3937468
H	-1.0680146	-3.7295313	-2.4776819
H	-0.8481057	-4.7812915	-1.0797374
H	2.9509946	-3.0800715	0.2151664
H	1.7453774	-4.1571983	0.9443055
H	2.4761371	-4.5536206	-0.5968963
H	0.6724080	3.0881566	2.5343696
H	1.3657917	0.8028395	-0.5503006
H	-0.9425990	-2.7559053	0.8640879
H	1.7298294	1.8388700	0.7999946
H	-0.7401136	-0.0612130	3.0611017
H	2.3396634	-1.7599259	1.9991345

"**7-TMS**", E_el(SPE) = -3939307.43 kJ/mol, G = 1039.56 kJ/mol, neg. freq. (1-3) = -0.0, 0.0, 0.0

C	0.7110912	0.9315607	-1.5040317
C	0.8972112	-0.2980944	-2.1295524
C	0.7641588	-0.4195112	-3.5067659
H	1.1645765	-1.1639837	-1.5382926
P	-0.9848676	-0.6930937	1.0656394
C	0.4408632	0.6875892	-4.2771299
C	0.2421819	1.9169442	-3.6616316
H	0.9194271	-1.3818072	-3.9772914
C	0.3770480	2.0356754	-2.2861479
H	0.3418059	0.5946452	-5.3508757
H	0.2438096	3.0048742	-1.8202720
H	-0.0099423	2.7872394	-4.2537162
C	0.9698801	1.0982078	-0.0297828
C	-2.5628268	-0.3722467	0.2467677
H	2.2237339	1.3188905	2.3585558
C	-0.2733899	1.0465151	0.8752312
H	-4.6459898	1.5468607	0.4496582
H	-3.7548493	2.8738493	-0.3053247
C	-1.4650860	1.8037743	0.3840271
H	-0.7058807	3.4957279	2.1991299
H	0.5737258	3.2550771	3.3920692
C	-2.5882470	1.1252486	0.1204230
H	-4.2171259	1.4566106	-1.2466841
H	-1.4123266	2.8748696	0.2319085
H	-3.6314619	0.3820100	-3.1018028
H	-1.9040107	0.4621072	-2.7655288

H	1.3644723	1.0657801	3.8867637
H	1.3191350	-0.1805467	2.6288347
Si	-2.9962891	-1.3260634	-1.3916094
H	-2.5444832	-0.8256560	-3.7710318
C	-3.8631117	1.7912292	-0.2714888
C	-2.7460321	-0.2178897	-2.8874723
H	-5.1781262	-2.2792932	-2.1042188
H	-5.4392543	-0.8769117	-1.0734062
C	-4.8178317	-1.7637692	-1.2116760
H	-4.9882818	-2.4233952	-0.3586825
H	-0.9511000	-2.7135151	-1.7703509
C	-2.0019590	-2.9077551	-1.5630319
H	-2.0583296	-3.5335615	-0.6722976
H	-2.4097506	-3.4809789	-2.3988129
N	0.1204966	1.5477437	2.2683923
H	0.9953688	3.3883959	1.6763690
C	1.3388569	0.8887740	2.8162330
C	0.2533629	3.0249817	2.3801651
O	-0.0776028	-1.7996343	0.6693627
H	1.6859822	0.3396115	0.2881338
H	1.4622982	2.0637897	0.1101806
H	-3.3528582	-0.6954012	0.9358846
O	-1.4008575	-0.7094466	2.6338991
H	-1.0118322	-1.4340493	3.1436152
H	-0.6495517	1.2848712	2.8875457

5 References

[1] N. Avarvari, P. Floch, F. Mathyl, *J. Am. Chem. Soc.* **1996**, *118*, 11978–11979.

[2] L. Hong, S. Ahles, M. Strauss, C. Logemann, H. Wegner, *Org. Chem. Front.* **2017**, *4*, 871–875.

[3] G. M. Sheldrick, *Acta Crystallogr. A* **2015**, *71*, 3–8.

[4] G. M. Sheldrick, *Acta Crystallogr. C* **2015**, *71*, 3–8.

[5] P. Müller, *Crystallogr. Rev.* **2009**, *15*, 57–83.

[6] O. v. Dolomanov, L. J. Bourhis, R. J. Gildea, J. A. K. Howard, H. Puschmann, *J. Appl. Crystallogr.* **2009**, *42*, 339–341.

[7] R. Ahlrichs, M. Bär, M. Ha, *Chem. Phys. Lett.* **1989**, *162*, 165-169.

[8] a) S. Grimme, J. Antony, S. Ehrlich, H. Krieg, *J. Chem. Phys.* **2010**, *132*, 154104; b) S. Grimme, S. Ehrlich, L. Goerigk, *J. Comput. Chem.* **2011**, *32*, 1456-1465; c) S. Grimme, J. G. Brandenburg, C. Bannwarth, A. Hansen, *Chem. Phys.* **2015**, *143*, 054107.

[9] a) A. Klamt, G. Schüürmann, *J. Chem. Soc., Perkin trans. II* **1993**, 799-805; b) A. Klamt, *J. Phys. Chem.* **1995**, *99*, 2224-2235; c) A. Klamt, V. Jonas, T. Bürger, J. C. Lohrenz, *J. Phys. Chem. A* **1998**, *102*, 5074-5085; d) A. Schäfer, A. Klamt, D. Sattel, J. C. Lohrenz, F. Eckert, *Phys. Chem. Chem. Phys.* **2000**, *2*, 2187-2193.

[10] R. Ahlrichs, M. Bär, H. Baron, R. Bauernschmitt, S. Böcker, M. Ehrig, K. Eichkorn, S. Elliott, F. Furche, F. Haase, *J. Chem. Phys.* **1995**, *102*, 346-354.

[11] a) O. B-Trott, A. Olson, *J. Comput. Chem.* **2012**, *32*, 174-182; b) P. Blaha, K. Schwarz, G. K. H. Madsen, D. Kvasnicka, J. Luitz, *Techn. Universität Wien, Austria* **2001**; c) C. Adamo, V. Barone, *Chem. Phys. Lett.* **1997**, *274*, 242-250; d) J. Slater, *Phys. Rev.* **1951**, *82*, 538; e) A. D. Sakharov, in *In The Intermissions... Collected Works on Research into the Essentials of Theoretical Physics in Russian Federal Nuclear Center, Arzamas-16*, World Scientific, **1998**, pp. 84-87; f) A. Schäfer, H. Horn, *Phys. Chem. Chem. Phys.* **2005**, *7*, 3297-3305; g) S. Ehrlich, J. Moellmann, W. Reckien, T. Bredow, S. Grimme, *ChemPhysChem* **2011**, *12*, 3414-3420.

[12] a) P. A. M. Dirac, *Proc. Math. Phys. Eng. Sci.* **1929**, *123*, 714-733; b) J. C. Slater, *Phys. Rev.* **1951**, *81*, 385; c) J. P. Perdew, Y. Wang, *Phys. Rev. B* **2018**, *98*, 079904; d) J. P. Perdew, K. Burke, M. Ernzerhof, *Phys. Rev. Lett.* **1996**, *77*, 3865; e) J. P. Perdew, M. Ernzerhof, K. Burke, *J. Chem. Phys.* **1996**, *105*, 9982-9985; f) F. Weigend, R. Ahlrichs, *Phys. Chem. Chem. Phys.* **2005**, *7*, 3297-3305.

[13] S. Grimme, *Chem. Eur. J.* **2012**, *18*, 9955–9964.

[14] a) Y. Li, L. Zhang, S. Luo, *ACS Omega* **2022**, *7*, 6354–6374; b) M. Papke, L. Dettling, J. A. W. Sklorz, D. Szieberth, L. Nyulászi, C. Müller, *Angew. Chem. Int. Ed.* **2017**, *56*, 16484–16489.

[15] a) D. Vincze, P. Ábrányi-Balogh, P. Bagi, G. Keglevich, *Molecules* **2019**, *24*, 3859–3871; b) L. Davis, M. Putri, C. Meyer, C. Durant, *Tetrahedron Lett.* **2014**, *55*, 3100–3103; c) D. Akbayeva, M. Varia, S. S. Costantini, M Peruzzini, P. Stoppioni, *Dalton Trans.* **2006**, *2*, 389–395.

[16] J. Baldwin, *J. Chem. Soc., Chem. Commun.* **1976**, *18*, 734–736.

4.2 Copper(I) and Gold(I) Complexes of 3-Aminofunctionalized Phosphabenzenes: Synthesis and Structural Characterization

Jinxiong Lin,[a] Daniel S. Frost, Nathan. T. Coles,[a,b] Manuela Weber,[a] Christian Müller[*a]

a: J. Lin, Dr. D. Frost, Dr. N. T. Coles, M. Weber, Prof. Dr. C. Müller

Institut für Chemie und Biochemie, Freie Universität Berlin

Fabeckstr. 34/36, 14195 Berlin, Germany

b: Dr. N. T. Coles

School of Chemistry, University of Nottingham, University Park Campus

Nottingham, NG7 2RD, United Kingdom

To be submitted

Author contributions: This project was designed by Prof. Dr. C. Müller and J. Lin. All compounds and complexes were synthesized by J. Lin. All single crystals were obtained by J. Lin. The single crystal X-ray diffraction analyses were carried out by Dr. N. T. Coles and M. Weber. NMR experiments were conducted by J. Lin. Theoretical calculations were performed by Dr. D. S. Frost. The paper was written by J. Lin and was corrected by Dr. N. T. Coles and Prof. Dr. C. Müller.

Estimated own contribution: ~ 70 %.

ARTICLE

Copper(I) and Gold(I) Complexes of 3-Aminofunctionalized Phosphabenzenes: Synthesis and Structural Characterization

Jinxiong Lin,[a] Daniel S. Frost,[a] Nathan T. Coles,[a,b] Manuela Weber[a] and Christian Müller[a*]

Dedicated to Prof. Dr. Sjoerd Harder on the occasion of his 60th birthday

Abstract: A series of 3-aminofunctionalized phosphabenzenes was synthesized and structurally characterized. DFT calculations show that these aromatic phosphorus heterocycles possess stronger π-donor and σ-donor abilities compared to the parent phosphabenzene C_5H_5P. The novel 3-aminofunctionalized phosphabenzenes show a classical terminal σ-coordination mode towards Cu(I). However, the Cu(I) ions shows a rare distorted trigonal planar coordination environment in the corresponding complexes of the type $[(Phosphinine)_2CuBr]_2$. Upon reaction with AuCl·SMe_2, mononuclear phosphinine-Au(I)Cl complexes are formed.

Introduction

Phosphinines (phosphabenzenes, phosphorines), the higher homologues of pyridines, are usually regarded as strong π-acceptor and relatively weak σ donor ligands once coordinated to a metal center. In fact, their particular electronic properties are especially suited for a coordination to late transition metals in low oxidation states.[1] To date, several synthetic routes for the preparation of phosphinines have been reported in literature. Some of them allow the introduction of functional substituents into specific positions of the 6-membered aromatic heterocycle, which is important for the modification of their stereoelectronic ligand properties and coordination abilities.[2,3,4-6]

Recently, we have shown that the basicity and nucleophilicity of the phosphorus lone-pair can be significantly enhanced by introducing σ-donating substituents into the 2-position of the phosphinine ring.[7] This, together with steric factors, can also affect drastically their coordination behaviour towards metal fragments. For instance, the reaction of the parent phosphinine C_5H_5P with CuBr·SMe_2 leads to the infinite CuBr coordination polymer **A**, which consists of repeating $[(C_5H_5P)_2CuBr]$ units (Figure 1). The 2-$SiMe_3$-phosphinine, on the other hand, forms the bromido-bridged dimer **B** of the type $[(L)_2CuBr]_2$ upon reaction with CuBr·SMe_2.[7] Mathey and co-workers investigated the reaction of a phosphinin-2-ol with copper chloride. They observed the formation of the dimeric copper chloride complex **C** containing two σ-P coordinating as well as two μ_2-P-coordinating phosphinines.[8] The corresponding anionic phosphinin-2-olate, reported by Grützmacher and co-workers, acts as a 4e donor and bridges a cationic $[Au(PPh_3)]^+$ as well as a neutral [AuCl] fragment (**D**).[9] More recently, our group synthesized a neutral 2-*N*,*N*-dimethylamino-substituted phosphinine.[10] The strong interaction between the lone-pair of the nitrogen atom of the NMe_2 group and the aromatic system results in a high π-density at the phosphorus atom. As a consequence, the phosphorus-containing derivative of *N*,*N*-dimethyl-aniline acts again as a μ_2-P ligand and forms the coordination polymer **E** when reacted with CuBr·SMe_2.

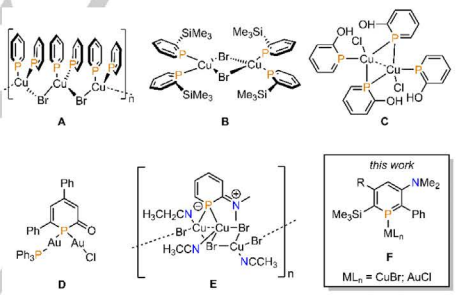

Figure 1: Coordination compounds **A**-**F** of differently substituted phosphinines and brief outline of this work.

We have recently reported on the synthesis, structural characterization and reactivity of the novel 3-*N*,*N*-dimethylaminofunctionalized phosphinine **6** (Scheme 1).[11] This compound shows only a weak interaction between the nitrogen lone pair and the aromatic phosphorus heterocycle, in contrast to observations made for the 2-*N*,*N*-dimethylaminophosphinine derivative (*vide infra*). We report here on our first results concerning the coordination chemistry of this donor-functionalized phosphorus heterocycle towards Cu(I) and Au(I) (**F**, Figure 1).

Results and Discussion

The 3-*N*,*N*-dimethylaminofunctionalized phosphinines **5-7** were synthesised according to a modified literature procedure described by Mathey and co-workers.[12] 1,3,2-diazaphosphinine **1** reacts with 1.2 equiv. of trimethylsilylacetylene derivatives in

[a] J. Lin, Dr. D. S. Frost, Dr. N. T. Coles, M. Weber, Prof. Dr. C. Müller
Institut für Chemie und Biochemie
Freie Universität Berlin
Fabeckstr. 34/36, 14195 Berlin (Germany)
E-mail: c.mueller@fu-berlin.de
[b] Dr. N. T. Coles
School of Chemistry
University of Nottingham
University Park Campus, Nottingham, NG7 2RD (UK)

Supporting information for this article is given via a link at the end of the document.

toluene at *T* = 70 °C first to the corresponding 1,2-azaphosphinines **2**-**4** (Scheme 1). Their formation was monitored by means of $^{31}P\{^{1}H\}$ NMR spectroscopy.[5] After complete conversion of **1** to **2**-**4**, all volatiles were removed under vacuum to prevent further reaction of the slight excess of trimethylsilylacetylenes and 1,2-azaphosphinines at higher temperatures. Compounds **2**-**4** were dissolved in toluene again and then reacted with *N*,*N*-dimethyl-2-phenylethyn-1-amine at *T* = 90 °C to the desired phosphinines **5**-**7** (Scheme 1). Compounds **5**-**7** were easily purified by means of column chromatography.

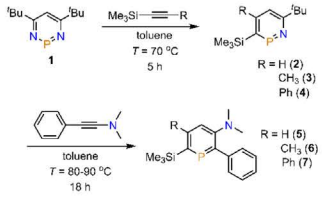

Scheme 1. Synthesis of phosphinines **5**-**7**.

Compounds **5**-**7** show resonances in the $^{31}P\{^{1}H\}$ NMR spectra at δ(ppm) = 237.7, 244.3 and 244.5, respectively. These values are rather different to the one found for 2-*N*,*N*-dimethylaminosphosphinine (δ(ppm) = 127.0).[10] This indicates that the electronic properties of **5**-**7** vary significantly from its regioisomer. Crystals of **5**-**7**, suitable for X-ray diffraction, were obtained by slow evaporation of the solvent from a solution of the phosphinines in *n*-hexanes. The molecular structure of **5** in the crystal is depicted in Figure 2, along with selected bond lengths and angles (for the crystallographic characterization of **6**, see ref. 11; for **7** see supporting information).

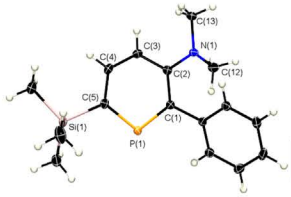

Figure 2. Molecular structure of **5** in the crystal. Displacement ellipsoids are shown at the 50% probability level. Selected bond lengths [Å] and angles [°]: P(1)-C(1): 1.737(1); P(1)-C(5): 1.731(1); C(5)-C(4): 1.397(2); C(4)-C(3): 1.387(2); C(3)-C(2): 1.407(2); C(2)-C(1): 1.419(2); N(1)-C(2): 1.393(2); C(5)-Si(1): 1.875(1). C(5)-P(1)-C(1): 104.68(5); C(12)-N(1)-C(2): 119.48(9); C(2)-N(1)-C(12)-C(13): 144.9(1).

The crystallographic characterization of **5**-**7** reveal similar C-N bond distances of 1.393(1) (**5**), 1.407(1) (**6**) and 1.415(2) Å (**7**). Moreover, the nitrogen atom of the *N*,*N*-dimethylamino-substituent is clearly pyramidalized in all three phosphinines. Consequently, we anticipate that the lone pair of the nitrogen atom only weakly contributes to a conjugation with the aromatic phosphorus heterocycle, in contrast to the situation in 2-*N*,*N*-dimethylamino-phosphinine.[10]

Having synthesized the novel 3-*N*,*N*-dimethylamino-substituted phosphinines **5**-**7**, we were further interested in the electronic ligand properties, particularly with respect to the parent phosphinine C_5H_5P as well as the 2-*N*,*N*-dimethylamino-functionalized regioisomer, recently reported by us.[10] As already demonstrated for phosphinine **6**, we also found a large concentration of electrons close to the nitrogen atom in the electrostatic potential (ESA) maps of **5** and **7**, suggesting the presence of a lone pair that is not part of the aromatic phosphorus heterocycle (Figure 3). This effect is clearly caused by the steric demand of the phenyl-group in the 2-position of **5**-**7**. In fact, both the 2-*N*,*N*-dimethylamino-[10] as well as the 3-*N*,*N*-dimethylamino-substituted phosphinine[11], without any other substituents at the phosphorus heterocycle, show a fully planar nitrogen atom (Figure 3, left).

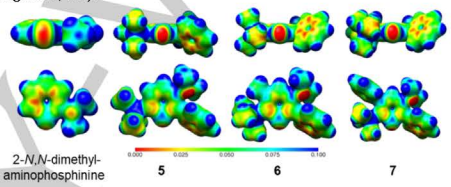

Figure 3: Electrostatic potential maps for 2-*N*,*N*-dimethylaminophosphinine (left) and phosphinines **5**-**7**. The electrostatic potential (in a.u.), color-coded from 0 (red) to 0.1 (blue), is mapped on electron density isosurfaces of 0.02 e/au^3.

Additionally, significant differences can be found in the frontier Kohn-Sham orbitals of the parent phosphinine C_5H_5P, **5** and 2-*N*,*N*-dimethylaminophosphinine (Figure 4).

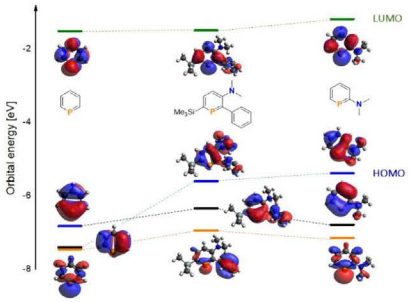

Figure 4: Kohn-Sham orbitals of C_5H_5P (left), **5** and 2-*N*,*N*-dimethyl-aminophosphinine (right). Energy level of lone pair in orange.

While the energy of the LUMO of **5** is similar to the one of C_5H_5P, both are considerably lower in energy than the LUMO in 2-*N*,*N*-dimethylaminophosphinine. This is in line with the reduced π-acceptor property of this compound, due to the efficient electronic interaction between the nitrogen lone pair and the aromatic phosphorus heterocycle (*vide supra*). On the other hand, particularly the presence of the trimethylsilyl-group in 2-position of the ring leads to stronger σ-donor properties of **5**, while the 3-*N*,*N*-dimethylamino-substituent increases at the same time the π-donor capability compared to the parent phosphinine (+ 1.10 eV). However, less than in 2-*N*,*N*-dimethylaminophosphinine due to the strongly reduced interaction of the lone-pair with the phosphorus heterocycle. The fact that the lone-pair in 2-*N*,*N*-dimethylaminophosphinine (HOMO-2) is lower in energy than the one in **5** can be attributed to the electronegative character of the nitrogen atom in close proximity to the phosphorus atom.

Having elucidated qualitatively the steric and electronic features of the novel phosphinines, we were further interested in exploring their coordination properties. Phosphinines are known to react readily with Cu(I) precursors to form a variety of different complexes, including infinite stair-like coordination polymers, infinite chain structures, phosphinine-bridged copper dimers as well as tetranuclear heterocubane clusters and polynuclear architectures.[8,12-16]. We therefore decided to focus first on the coordination chemistry of the novel phosphinines towards Cu(I).

Phosphinines **5**-**7** were reacted with $CuBr{\cdot}S(CH_3)_2$ in THF in a molar ratio of 1:1 (Scheme 2). Only one single resonance at δ(ppm) = 202.8, d(ppm) = 223.0 and δ(ppm) = 224.3 was observed in the corresponding $^{31}P\{^1H\}$ NMR spectra of the reaction products **8**-**10** after the reaction mixtures were stirred for overnight at room temperature. The coordination shift difference of **8** around Δδ(ppm) = -35.0 (-21 (**9**), -21 (**10**)) is indicative for a successful coordination of the phosphinines to Cu(I).

Pale yellow crystals of **8**-**10**, suitable for X-ray diffraction, were obtained by slow evaporation of the solvent from a solution of the coordination compounds in acetonitrile. Complex **8** crystallizes in the triclinic space group *P*-1, while complexes **9** and **10** crystallize in the monoclinic space group $P2_1/c$. The molecular structures of the complexes **8** and **10** in the crystal are depicted in Figures 5 and 6, along with selected bond lengths and angles (for the crystallographic characterization of complex **9**, see supporting information).

The molecular structures of the Cu(I) complexes **8**-**10** in the solid state reveal the formation of a bromide-bridged dimer of the type **[**(phosphinine)CuBr$]_2$. Compounds **8**-**10** show a classical terminal 2e-donation *via* the lone pair of phosphorus to the respective Cu(I) centers. Interestingly, this structural motif has so far never been reported in the chemistry of phosphinine-Cu(I) complexes, as the Cu(I) atom shows a rare distorted trigonal planar coordination environment. This can most likely be attributed to the steric demand of both the $SiMe_3$- and the Ph-group in 2-position of the phosphorus heterocycle. In fact, 2-$SiMe_3$-phosphinine forms a dimer of the type [(Phosphinine$)_2$CuBr$]_2$ with $CuBr{\cdot}S(CH_3)_2$, that shows a distorted tetrahedral coordination environment around the Cu(I) center (**B**, Figure 1).[7] Overall, the P-Cu···Cu-P angles decrease considerably from 166.07° in **8**, to 170.72° in **9** and 176.05° in **10**. Consequently, the P-Cu_2Br_4-P moiety shows a butterfly-like arrangement in **8**, while it is almost planar in **10** (Figure 5). In contrast to the situation in **E** (Figure 1), containing the 2-*N*,*N*-dimethylaminophosphinine as ligand, the nitrogen atoms in **8**-**10** are clearly pyramidalized, while the C(2)-N(1) bond lengths (1.407(5) Å (**8**); 1.379(3) Å (**9**), 1.3800(15) Å (**10**)) are considerably longer (**E**: C(2)-N(1): 1.359(8) Å) This indicates a significant C-N single bond character in the phosphinine ligand in **8**-**10**, which is again in line with a strongly reduced interaction of the nitrogen lone-pair with the π-accepting phosphorus heterocycle.

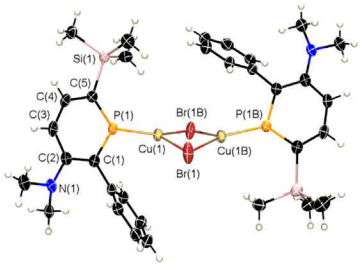

Figure 5. Molecular structure of **8** in the crystal. Displacement ellipsoids are shown at a 50% probability level. Selected bond lengths [Å] and angles [°]: P(1)-C(1): 1.735(4); P(1)-C(5): 1.714(5); Cu(1)-P(1): 2.164(1); Cu(1B)-P(1B): 2.163(1); Br(1B)-Cu(1): 2.3734(9); Br(1)-Cu(1): 2.4142(7); N(1)-C(2): 1.398(6); C(1)-C(2): 1.411(8); C(2)-C(3): 1.413(7); C(3)-C(4): 1.382(7); C(4)-C(5): 1.394(8); C(1)-P(1)-C(5): 108.1(2); Cu(1)-Br(1)-Cu(1B): 76.11(3); Br(1)-Cu(1)-Br(1B): 102.45(3); Cu(1)-Br(1B)-Cu(1B)-Br(1): 12.86(3).

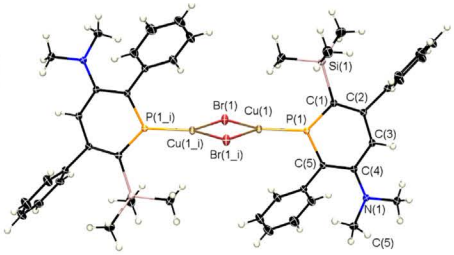

Figure 6. Molecular structure of **10** in the crystal. Displacement ellipsoids are shown at a 50% probability level. Selected bond lengths [Å] and angles [°]: P(1)-C(1): 1.724(1); P(1)-C(5): 1.723(1); Cu(1)-P(1): 2.1792(5); Br(1)-Cu(1): 2.4361(4); N(1)-C(4): 1.380(2); C(1)-C(2): 1.416(1); C(2)-C(3): 1.393(2); C(3)-C(4): 1.413(2); C(4)-C(5): 1.421(2). C(1)-P(1)-C(5): 108.42(6); Cu(1)-Br(1)-Cu(1_i): 77.95(1); Br(1)-Cu(1)-Br(1_i): 102.05(1); Cu(1)-Br(1)-Cu(1_i)-P(1_i): 176.33(2).

The reaction of phosphinines **5**-**7** with $CuBr{\cdot}S(CH_3)_2$ in THF, under formation of the Cu(I)-complexes **8**-**10**, is summarized in Scheme 2.

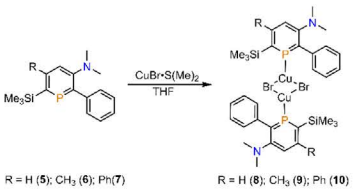

Scheme 2. Synthesis of coordination compounds **8**-**10**.

As phosphinines usually also react readily with Au(I) precursors, we further investigated the coordination chemistry of **5**-**7** towards AuCl·S(CH_3)$_2$.[17]

The reaction of **5** and **7** with the Au(I) precursor in THF affords a yellow solution, while under the same reaction conditions, the formation of black particles, which could not be further analyzed, were observed with phosphinine **2** and AuCl·S(CH_3)$_2$. Complexes **11** and **12** show single resonances at δ(ppm) = 193.2 (**11**) and δ(ppm) = 204.7 (**12**) in the corresponding ^{31}P{^{1}H} NMR spectra.

Crystals, suitable for X-ray diffraction, were obtained by layering *n*-hexanes onto a solution of complexes **11** and **12** in acetonitrile. The coordination compounds crystallize in the monoclinic space group *Cc* and the triclinic space group *P-1*, respectively. The molecular structure of **11** in the crystal is depicted in Figure 7, along with selected bond lengths and angles (for the crystallographic characterization of **12**: see supporting information).

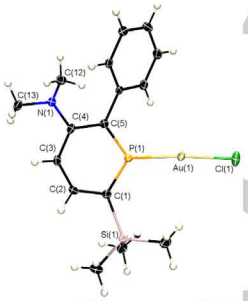

Figure 7. Molecular structure of **11** in the crystal. Displacement ellipsoids are shown at the 50% probability level. Selected bond lengths [Å] and angles [°]: P(1)-C(1): 1.716(5); P(1)-C(5): 1.698(6); C(5)-C(4): 1.396(6); C(4)-C(3): 1.381(8); C(3)-C(2): 1.41(1); C(2)-C(1): 1.426(7); N(1)-C(2): 1.385(7); P(1)-Au(1): 2.213(1); Au(1)-Cl(1): 2.282(1). P(1)-Au(1)-Cl(1): 175.98(5); C(5)-P(1)-C(1): 110.4(2); C(2)-N(1)-C(12)-C(13): 149.9(7).

As expected, both **11** and **12** display an almost linear geometry around the Au(I) center (P(1)-Au(1)-Cl(1): 175.98(5)° for **11**; P(1)-Au(1)-Cl(1): 178.73(3)° for **12**). The phosphorus-Au(I) distances are very similar to the values found for reported phosphinine-AuCl complexes.[17] However, in our case, no aurophilic Au···Au contacts can be found in the unit-cells of **11** and **12**. We anticipate, that the sterically demanding Ph- and $SiMe_3$-substituents in 2-position of the heterocyclic ring prevent a close arrangement of two coordination compounds to form aurophilic interactions. A summary about the reaction of phosphinines **5** and **7** with AuCl·SMe_2 is depicted in Scheme 3.

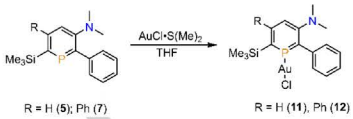

Scheme 3. Synthesis of phosphinine-Au(I) complexes **11** and **12**.

Due to the presence of a $SiMe_3$-group and a donor-functionality, we anticipated that the novel phosphinines provide the possibility for post-synthesis ligand modifications.[11] In fact, $SiMe_3$-substituted phosphinines can be protodesilylated, while amino-functionalized phosphinines can be protonated exclusively at the nitrogen-donor.[11,18] Due to the similarity of the here reported phosphorus heterocycles, we focused exclusively on phosphinine **6**. Indeed, the amine functionality in **6** can easily be protonated by adding a slight excess of HCl/Et_2O. Based on the ^{1}H and ^{31}P NMR spectra, the protonated species **13** is formed quantitatively, with the $SiMe_3$-substituent still located in the *ortho*-position of the heterocycle. The phosphorus resonance of **13** can be found at δ(ppm) = 252.3 in the ^{31}P{^{1}H} NMR spectrum. Upon heating **13** in acetonitrile, protodesilylation occurs, resulting in phosphinine **14**, which shows a signal at δ(ppm) = 212.7 in the ^{31}P{^{1}H} NMR spectrum (Scheme 4).

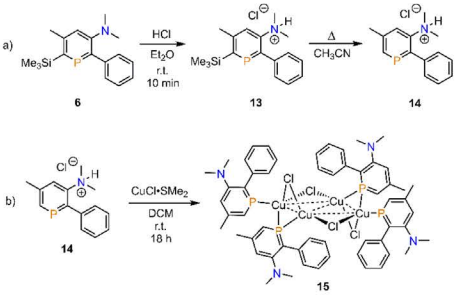

Scheme 4. a) Post-synthesis modification of **6** by protonation and protodesilylation. b) reaction of **14** with a Cu(I) precursor.

So far, we were not able to isolate any Cu(I)- and Au(I)-complexes when reacting the phosphinine-based hydrochloride salt **14** with $CuBr{\cdot}SMe_2$ and $AuCl{\cdot}SMe_2$, respectively.

However, a yellow powder could finally be obtained in high yield, when reacting **14** CuCl·SMe2 instead. The $^{31}P\{1H\}$ NMR shift of the new compound (**15**) occurs at δ(ppm) = 172.8 (Δδ(ppm) = -40) in THF. Crystals of **15**, suitable for single-crystal X-ray diffraction, were obtained from a solution of the complex in a mixture of THF and *n*-hexane at *T* = -30°C. Complex **15** crystallises in the space group *P-1* and the molecular structure of this compound in the crystal is depicted in Figure 8, along with selected bond lengths and angles.

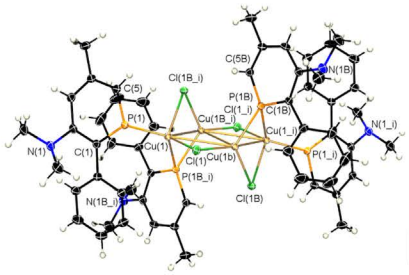

Figure 8: Molecular structure of **15** in the crystal. Displacement ellipsoids are shown at the 50% probability level. Selected bond lengths [Å] and angles [°]. P(1)-Cu(1): 2.2140(4); P(1B_i)-Cu(1): 2.3469(5); P(1B_i)-Cu(1B_i): 2.2503(4); Cu(1)-Cu(1B_i): 2.4586(4); Cu(1B_i)-Cu(1_i): 3.3433(3); Cu(1)-Cl(1B_i): 2.4157(4); Cu(1B_i)-Cl(1B_i): 2.2758(4); Cu(1B_i)-Cl(1_i): 2.2078(5); Cl(1_i)-Cu(1_i): 2.3334(4). C(1)-P(1)-C(5): 106.14(7); C(5B)-P(1B)-C(1B): 106.32(7).

Interestingly, the crystallographic characterization of **15** reveals the presence of a Cu_4-rhombus, which is capped by a total of four chlorido ligands. Additionally, two phosphinine ligands coordinate in the classical σ-coordination mode *via* the phosphorus lone pair to two of the four Cu(I) centers. The other two phosphinine ligands show the rare bridging μ_2-coordination mode and span also two of the four Cu(I) centers. To the best of our knowledge, this type of complex is unprecedented in the coordination chemistry of phosphinines. As **15** is overall neutral, deprotonation of **14** is expected during complex formation and crystallization.

Conclusions

We have synthesized novel 3-*N*,*N*-dimethylaminophosphinines, starting from 1,3,2-diazaphosphinine, substituted acetylenes and *N*,*N*-dimethyl-2-phenylethyn-1-amine. Based on DFT calculations, the phenyl and trimethylsilyl substituents in the donor-functionalized phophinines increase both the σ-donor and the π-donor capacity of the aromatic heterocycles compared to the parent phosphinine C_5H_5P. However, the increase of π-electron density at the phosphorus atom of the novel phosphinines is still weaker than in 2-*N*,*N*-dimethylaminophosphinine due to a much weaker interaction between the lone-pair of the exocyclic nitrogen atom and the aromatic phosphorus heterocycle, as shown by the calculated electrostatic potential maps. The 3-*N*,*N*-dimethylaminophosphinines readily react with $CuBr{\cdot}SMe_2$ to form bromide-bridged dimers of the type $[(phosphinine)CuBr]_2$, which show a rare distorted trigonal planar coordination environment at the Cu(I) centers. In fact, the core of **8** in the solid-state shows a butterfly structure, while the one in **9** and **10** display each a planar, $P\text{-}Cu_2Br_4\text{-}P$ moiety. Upon reaction of the 3-*N*,*N*-dimethylaminophosphinines with $AuCl{\cdot}S(CH_3)_2$, mononuclear phosphinine-Au(I)-complexes were formed quantitatively. The novel phosphinines are prone to post-synthesis ligand modification, as they can easily be protonated exclusively at the nitrogen atom, while protodesilylation occurs in acetonitrile at higher temperature. The formed phosphinine-based hydrochloride salts react with $CuCl{\cdot}SMe_2$ to form a rare Cu_4Cl_4-core containing four differently coordinating phosphinine ligands.

Experimental Section

Experimental details are given in Supporting Information. Deposition Numbers 2214696 (for **5**), 2214697 (for **7**), 2214698 (for **8**), 2214699 (for **9**), 2214700 (for **10**), 2214701 (for **11**), 2214702 (for **12**) contain the supplementary crystallographic data for this paper. These data are provided free of charge by the joint Cambridge Crystallographic Data Centre and Fachinformationszentrum Karlsruhe Access Structures service.

Acknowledgements

The authors express their sincere thanks to Freie Universität Berlin and the China Scholarship Council for funding.

Keywords: Phosphinine • Coordination Chemistry • DFT Calculations • Cu(I) Complexes• Au(I) Complexes

[1] N. T. Coles, A. S. Abels, J. Leitl, R. Wolf, H. Grützmacher, C. Müller, *Coord. Chem. Rev.* **2021**, *433*, 213729.
[2] G. Märkl, *Angew. Chem., Int. Ed. Engl.* **1966**, *5*, 846-847.
[3] A. J. Ashe III, *J. Am. Chem. Soc.* **1971**, *93*, 3293-3295.
[4] W. Rösch and M. Regitz, *Z. Naturforsch. B* **1986**, *41*, 931-934.
[5] N. Avarvari, P. Le Floch and F. Mathey, *J. Am. Chem. Soc.* **1996**, *118*, 11978-11979.
[6] K. Nakajima, S. Takata, K. Sakata and Y. Nishibayashi, *Angew. Chem.* **2015**, *127*, 7707-7711.
[7] M. H. Habicht, F. Wossidlo, T. Bens, E. A. Pidko and C. Müller, *Chem. Eur. J.* **2018**, *24*, 944-952.
[8] Y. Mao, K. M. H. Lim, Y. Li, R. Ganguly and F. Mathey, *Organometallics* **2013**, *32*, 3562-3565.
[9] Y. Hou, Z. Li, Y. Li, P. Liu, C.-Y. Su, F. Puschmann and H. Grützmacher, *Chem. Sci.* **2019**, *10*, 3168-3180.
[10] S. Giese, K. Klimov, A. Mikeházi, Z. Kelemen, D. S. Frost, S. Steinhauer, P. Müller, L. Nyulászi and C. Müller, *Angew. Chem. Int. Ed.* **2021**, *60*, 3581-3586.

[11] J. Lin, N. T. Coles, L. Dettling, L. Steiner, J. F. Witte, B. Paulus, C. Müller, *Chem. Eur. J.* **2022**, under revision.
[12] P. Roesch, J. r. Nitsch, M. Lutz, J. Wiecko, A. Steffen and C. Müller, *Inorg. Chem.* **2014**, *53*, 9855-9859.
[13] X. Chen, Z. Li, F. Yanan and H. Grützmacher, *Eur. J. Inorg. Chem.* **2016**, *2016*, 633-638.
[14] H. Kanter and K. Dimroth, *Tetrahedron Lett.* **1975**, *16*, 541-544.
[15] M. Shiotsuka, T. Tanamachi, T. Urakawa, M. Munakata and Y. Matsuda, *J. Supramol. Chem.* **2002**, *2*, 211-217.
[16] N. Mézailles, P. Le Floch, K. Waschbüsch, L. Ricard, F. Mathey and C. P. Kubiak, *J. Organomet. Chem.* **1997**, *541*, 277-283.
[17] a) J. Moussa, L. M. Chamoreau, H. Amouri, *RSC. Adv.* **2014**, *4*, 11539-11542; b) J. Stott, C. Bruhn, U. Siemeling, *Z. Naturforsch. B* **2013**, *68*, 853-859; c) M. Rigo, L. Hettmanczyk, F. J. L. Heutz, S. Hohloch, M. Lutz, B. Sarkar, C. Müller, *Dalton Trans.* **2017**, *46*, 86-95; d) N. Mézailles, L. Ricard, F. Mathey, P. Floch, *Eur. J. Inorg. Chem.* **1999**, *1999*, 2233-2241; e) M. Rigo, E. R. M. Habraken, K. Bhattacharyya, M. Weber, A. W. Ehlers, N. Mézailles, J. C. Slootweg, C. Müller, *Chem. Eur. J.* **2019**, *25*, 8769-8779.
[18] F. Wossidlo, D. S. Frost, J. Lin, N. T. Coles, K. Klimov, M. Weber, T. Böttcher, C. Müller, *Chem. Eur. J.* **2021**, *27*, 12788-12795.

Copper(I) and Gold(I) Complexes of 3-Aminofunctionalized Phosphabenzenes: Synthesis and Structural Characterization

Jinxiong Lin, Daniel S. Frost, Nathan T. Coles, Manuela Weber and Christian Müller

Contents

1. Experimental Procedures

General Remarks

All reactions were performed under argon in oven-dried glassware using modified Schlenk techniques unless otherwise stated. All common solvents and chemicals were commercially available and were used without further purification. All dry or deoxygenated solvents were prepared using standard techniques or were used from a MBraun solvent purification system. N,N-dimethyl-2-phenylethyn-1-amine, 1,3,2-diazaphosphinines, **6**, **13** and **14** were prepared according to literature[1,2]. The ^{1}H, ^{19}F, $^{13}C\{^{1}H\}$, $^{31}P\{^{1}H\}$ and ^{31}P NMR spectra were recorded on a *JEOL* ECX400 (400 MHz) spectrometer and a Bruker Avance 600 (600 MHz) spectrometer and all chemical shifts are reported relative to the residual resonance in the deuterated solvents. The HRMS ESI mass spectra were measured on an Agilent 6210 ESI-TOF. Low-temperature x-ray diffractometry was performed on a Bruker-AXS X8 Kappa Duo diffractometer with *IμS* micro-sources, performing ϕ-and ω-scans. Data was collected using a Photon 2 CPAD detector with Mo K_α radiation (λ = 0.71073 Å) or Cu K_α radiation (λ = 1.5406 Å). The structures were solved by dual-space methods using SHELXT[3] and refined against F^2 on all data by full-matrix least squares with SHELXL-2017[4] following established refinement strategies[5]. The program Olex2[6] was also used to aid in the refinement. All non-hydrogen atoms were refined anisotropically. All hydrogen atoms were included into the model at geometrically calculated positions and refined using a riding model. The isotropic displacement parameters of all hydrogen atoms were fixed to 1.2 times the U-value of the atoms they are linked to (1.5 times for methyl groups). Details of the data quality and a summary of the residual values of the refinements are listed in **Table S1** below. Tables **S2**, **S4**, **S6**, **S8**, **S10**, **S12**, **S14** and **S16** give all bond lengths for the structures and **S3**, **S5**, **S7**,**S9** ,**S11** , **S13**, **S15** and **S17** give all angles for the structures. Supplementary crystallographic data for **5**, **7**-**12** and **15** can be found in the CCDC with the following deposit numbers CCDC 2214696 (**5**), 2214697 (**7**), 2214698 (**8**), 2214699 (**9**), 2214700 (**10**), 2214701 (**11**) and 2214702 (**12**), 2214703 (**15**). These data can be obtained free of charge from www.ccdc.cam.ac.uk/data_request/cif.

The general method for the synthesis of compounds 5-7.

1 equiv. of (trimethylsilyl)acetylene derivatives (2.0 mmol) was added to a solution of 1,3,2-diazaphosphinines (2.0 mmol) in 15 mL toluene. The mixture was heated to T = 70 °C for 5 hours. The complete formation of the 1,2-monoazaphosphinine was observed by ^{31}P NMR spectroscopy and all volatiles were removed under vacuum. The reaction of residual solids with 2 equiv. of N,N-dimethyl-2-phenylethyn-1-amine (0.58 g, 4 mmol) in 15 mL toluene was heated to T = 90 °C (for compound **1**, T = 80 °C) overnight. At the end of reaction, the solution was removed under vacuum and the product was purified by column chromatography of silica with *n*-hexane/ethyl acetate (9:1).

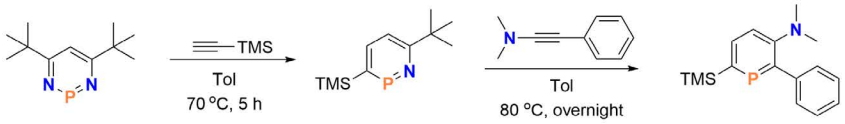

Scheme S1: Synthesis of **5**.

(trimethylsilyl)acetylene derivatives: (trimethylsilyl)acetylene (0.20 g, 2.0 mmol), product yield: 477 mg, 0.17 mmol, 83 %.

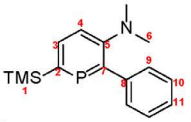

^{1}H NMR (600 MHz, *$CDCl_3$*) δ 7.96 (t, ^{3}J(H,P) = 10.8 Hz, 1H, C_5H_2P), 7.53 (d, J = 7.6 Hz, 2H, *-Ph*), 7.40 (t, J = 7.6 Hz, 2H, *-Ph*), 7.29 (t, J = 7.6 Hz, 1H, *-Ph*), 7.15 (d, ^{4}J(H,P) = 8.7 Hz, 1H, C_5H_2P), 2.63 (s, 6H, *-NMe_2*), 0.36 (s, 9H, *-TMS*) ppm.

^{13}C{^{1}H} NMR (151 MHz, *$CDCl_3$*) δ 159.1 (d, ^{1}J(C,P) = 58.6 Hz, *C7*), 158.3 (d, ^{1}J(C,P) = 72.1 Hz, *C2*), 155.0 (d, ^{2}J(C,P) = 10.8 Hz, *C5*), 143.5 (d, ^{2}J(C,P) = 23.3 Hz, *C8*), 138.9 (d, ^{2}J(C,P) = 12.7 Hz, *C3*), 128.7 (d, ^{3}J(C,P) = 10.6 Hz, *C9*), 128.5 (s, *C11*), 126.6 (s, *C10*), 119.5 (d, ^{3}J(C,P) = 17.6 Hz, *C4*), 42.8 (s, *C6*), 0.2 (d, ^{3}J(C,P) = 5.9 Hz, *C1*) ppm.

^{31}P{^{1}H} NMR (162 MHz, *CD_2Cl_2*) δ 238 ppm.

HR-ESI MS (*m/z*): 288.1461 g/mol (calculated: 288.1332 g/mol) $[M][H]^+$.

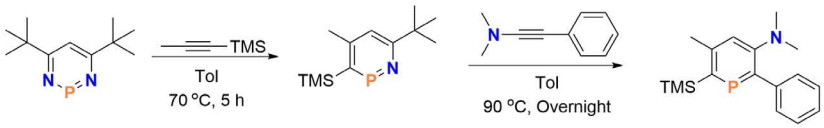

Scheme S2: Synthesis of **6**.

(trimethylsilyl)acetylene derivatives: 1-(trimethylsilyl)-1-propyne (0.22 g, 2.0 mmol), product yield: 470 mg, 0.16 mmol, 78 %.

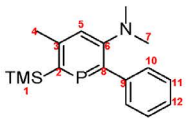

^{1}H NMR (400 MHz, *C_6D_6*) δ 7.65 (d, J = 7.8 Hz, 2H, *-Ph*), 7.24 (t, J = 7.7 Hz, 2H, *-Ph*), 7.11 (td, J = 7.4, 1.3 Hz, 1H, *-Ph*), 6.78 (d, J = 1.6 Hz, 1H, C_5HP), 2.45 (d, J = 1.5 Hz, 3H, *4-Me*), 2.33 (s, 6H, *-NMe_2*), 0.48 (d, J = 1.8 Hz, 9H, *-TMS*) ppm.

^{13}C{^{1}H} NMR (151 MHz, C_6D_6) δ 156.5 (d, ^{1}J(C,P) = 87.9 Hz, *C8*), 156.0 (d, ^{1}J(C,P) = 106.3 Hz, *C2*), 155.6 (d, ^{2}J(C,P) = 9.6 Hz, *C6*), 149.4 (d, ^{2}J(C,P) = 12.8 Hz, *C3*), 143.4 (d, ^{2}J(C,P) = 24.3 Hz,

C9), 129.0 (d, ^{3}J(C,P) = 10.5 Hz, *C10*), 128.4 (s, *C11*), 126.3 (s, *C12*), 122.6 (d, ^{3}J(C,P) = 15.7 Hz, *C5*), 42.3 (s, *C7*), 26.0 (d, ^{4}J(C,P) = 2.8 Hz, *C4*), 1.2 (d, ^{3}J(C,P) = 10.9 Hz, *C1*) ppm.

$^{31}P\{^{1}H\}$ NMR (162 MHz, C_6D_6) δ 244 ppm.

HR-ESI MS (*m/z*): 302.1506 g/mol (calculated: 302.1489 g/mol) $[M][H]^{+}$.

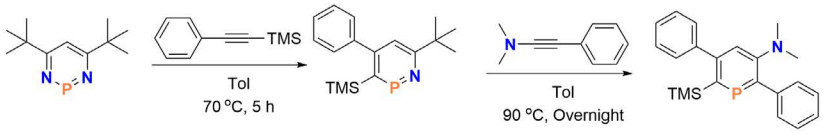

Scheme S3: Synthesis of 7.

(trimethylsilyl)acetylene derivatives: 1-phenyl-2-trimethylsilylacetylene (0.35 g, 2.0 mmol), yield: 589 mg, 0.16 mmol, 81 %.

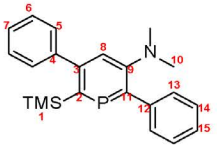

^{1}H NMR (600 MHz, CD_2Cl_2) δ 7.54 (d, *J* = 8.2, 1.2 Hz, 2H, -*Ph*), 7.45 – 7.38 (m, 5H, -*Ph*), 7.34 (dd, *J* = 7.7, 1.7 Hz, 2H, -*Ph*), 7.30 (t, *J* = 7.4, 1.3 Hz, 1H, -*Ph*), 6.95 (d, *J* = 1.5 Hz, 1H, C_5HP), 2.61 (s, 6H, -NMe_2), 0.04 (d, *J* = 1.5 Hz, 9H, -*TMS*) ppm.

$^{13}C\{^{1}H\}$ NMR (151 MHz, CD_2Cl_2) δ 157.5 (s, *C4*), 155.8 (d, ^{1}J(C,P) = 60.6 Hz, *C11*), 155.8 (d, ^{1}J(C,P) = 83.1 Hz, *C2*), 154.7 (d, ^{2}J(C,P) = 9.7 Hz, *C9*), 146.1 (d, ^{2}J(C,P) = 12.8 Hz, *C3*), 143.0 (d, ^{2}J(C,P) = 24.6 Hz, *C12*), 129.0(s, *C5*), 128.8 (d, ^{3}J(C,P) = 10.6 Hz, *C13*), 128.4 (s, *C14*), 127.8 (s, *C6*), 127.3 (s, *C7*), 126.6 (s, *C15*), 122.4 (d, ^{3}J(C,P) = 14.3 Hz, *C8*), 42.6 (s, *C10*), 1.8 (d, ^{3}J(C,P) = 10.1 Hz, *C1*) ppm.

$^{31}P\{^{1}H\}$ NMR (243 MHz, CD_2Cl_2) δ 245 ppm.

The general method for the synthesis of complexes 8-10.

Phosphinine (0.1 mmol) and copper(I) bromide dimethyl sulfide complex (21 mg, 0.1 mmol) were added in Schlenk flask and 4 mL THF solvent followed into flask. All solvent was removed under vacuum after the mixture stirred at room temperature overnight. The single crystal of titled compound was acquired *via* MeCN solution of complex slow evaporation in glovebox.

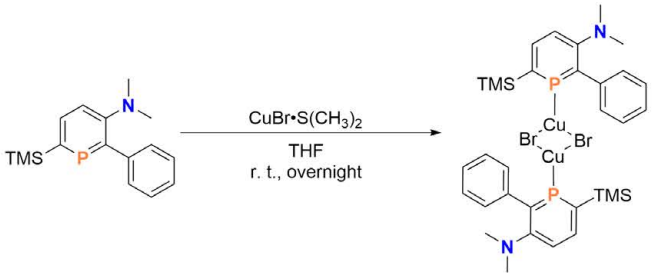

Scheme S4: Synthesis of copper-complex **8**.

Phosphinine **5** (29 mg, 0.1 mmol), yield: 40 mg, 0.047 mmol, 93 %.

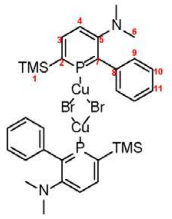

^{1}H NMR (600 MHz, *CD_3CN*) δ 7.98 (dd, ^{3}J(H,P) = 18.9, J = 9.1 Hz, 2H, C_5H_2P), 7.50 (d, J = 7.5 Hz, 4H, *-Ph*), 7.42 (t, J = 7.6 Hz, 4H, *-Ph*), 7.33 (t, J = 7.1 Hz, 2H, *-Ph*), 7.19 (dd, ^{4}J(H,P) = 10.2, 2.6 Hz, 2H, C_5H_2P), 2.58 (s, 12H, *-NMe_2*), 0.38 (s, 18H, *-TMS*) ppm.

^{13}C{^{1}H} NMR (151 MHz, *CD_3CN*) δ 157.5 (d, ^{2}J(C,P) = 8.1 Hz, *C5*), 152.3 (d, ^{1}J(C,P) = 20.1 Hz, *C7*), 150.0 (d, ^{1}J(C,P) = 44.1 Hz, *C2*), 143.0 (d, ^{2}J(C,P) = 18.2 Hz, *C8*), 141.5 (d, ^{2}J(C,P) = 15.2 Hz, *C3*), 130.1 (d, ^{3}J(C,P) = 10.7 Hz, *C9*), 129.5 (s, *C11*), 128.0 (s, *C10*), 120.0 (d, ^{3}J(C,P) = 23.1 Hz, *C4*), 42.9 (s, *C6*), 0.4 (d, ^{3}J(C,P) = 4.9 Hz, *C1*) ppm.

^{31}P{^{1}H} NMR (243 MHz, *CD_3CN*) δ 203 ppm.

HR-ESI MS (*m/z*): 860.1451 g/mol (calculated: 859.9452 g/mol) $[M][H]^{+}$.

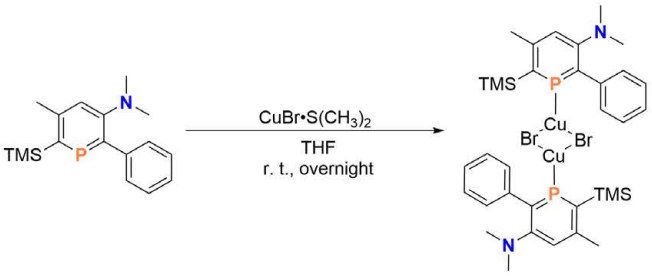

Scheme S5: Synthesis of copper-complex **9**.

Phosphinine **6** (30 mg, 0.1 mmol), yield: 41 mg, 0.047 mmol, 93 %.

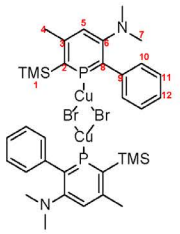

^{1}H NMR (600 MHz, *CD_3CN*) δ 7.49 (d, *J* = 7.6 Hz, 4H, *-Ph*), 7.40 (t, *J* = 7.5 Hz, 4H, *-Ph*), 7.31 (t, *J* = 7.5 Hz, 2H, *-Ph*), 7.02 (s, 2H, C_5HP), 2.59 (d, *J* = 2.0 Hz, 18H, *3-NMe_2 & 5-Me*), 0.42 (s, 18H, *-TMS*) ppm.

^{31}P{^{1}H} NMR (162 MHz, *CD_3CN*) δ 223 ppm.

HR-ESI MS (*m/z*): 888.1794 g/mol (calculated: 887.9765 g/mol) $[M][H]^+$.

A suitable ^{13}C{^{1}H} spectrum could not be obtained due to poor solubility of this compound in organic solvents.

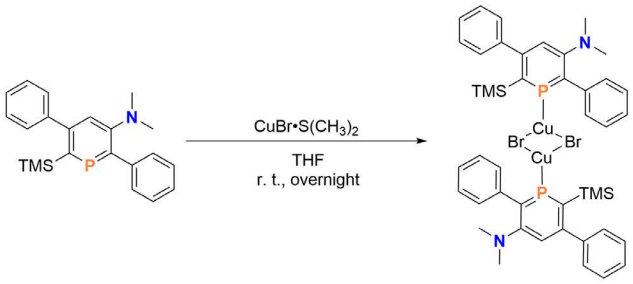

Scheme S6: Synthesis of copper complex **10**.

Phosphinine **7** (36 mg, 0.1 mmol), yield: 45 mg, 0.047 mmol, 88 %.

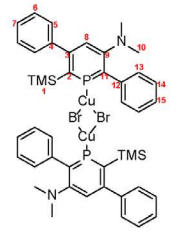

^{1}H NMR (600 MHz, *CD_3CN*) δ 7.55 (dt, *J* = 8.1, 1.3 Hz, 4H, *-Ph*), 7.47 – 7.41 (m, 10H, *-Ph*), 7.37 – 7.32 (m, 6H, *-Ph*), 6.95 (d, ^{4}J(H,P) = 2.3 Hz, 2H, C_5HP), 2.60 (s, 12H, *3-NMe_2*), 0.05 (d, *J* = 1.4 Hz, 18H, *-TMS*) ppm.

$^{13}C\{^{1}H\}$ NMR (151 MHz, *CD_3CN*) δ 155.9 (s, *C4*), 155.7 (d, ^{2}J(C,P) = 13.7 Hz, *C12*), 154.7 (d, ^{2}J(C,P) = 7.5C Hz, *C9*) 149.8 (d, ^{1}J(C,P) = 63.6 Hz, *C2*), 145.7 (s, *C3*), 142.3 (d, ^{1}J(C,P) = 21.8 Hz, *C11*), 130.7 (s, *C5*), 129.0 (s, *C13*), 128.7 (s, *C14*), 128.0 (s, *C6*), 127.6 (s, *C7*), 127.0 (s, *C15*), 122.0 (d, ^{3}J(C,P) = 17.3 Hz, *C8*), 41.9 (s, *C10*), 1.5 (d, ^{3}J(C,P) = 9.2 Hz, *C1*) ppm.

$^{31}P\{^{1}H\}$ NMR (243 MHz, *CD_3CN*) δ 224 ppm.

HR-ESI MS (*m/z*): 1012.2001g/mol (calculated: 1012.0078 g/mol) $[M][H]^{+}$.

The general method for the synthesis of complexes 11-12.

Phosphinine (0.1 mmol) and chloro(dimethylsulfide)gold(I) (30 mg, 0.1 mmol) were added in Schlenk flask and 3 ml THF solvent followed into flask. All solvent was removed under vacuum after the mixture stirred at room temperature overnight. Crystallization was achieved by layering hexanes onto a MeCN solution of complex in a freezer at -30 ºC.

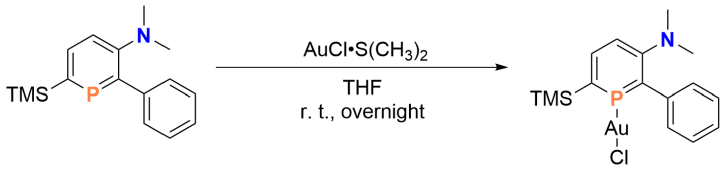

Scheme S7: Synthesis of gold complex **11**.

Phosphinine **5** (29 mg, 0.1 mmol), yield: 47 mg, 0.09 mmol, 90 %.

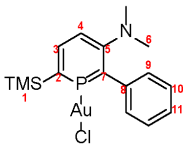

^{1}H NMR (600 MHz, *CD_3CN*) δ 8.11 (ddd, ^{3}J(H,P) = 34.1, 9.3, 1.6 Hz, 1H, C_5H_2P), 7.52 (d, *J* = 9.1 Hz, 2H, *-Ph*), 7.46 (t, *J* = 7.4 Hz, 2H, *1-Ph*), 7.42 (t, *J* = 4.8 Hz, 1H, *-Ph*), 7.23 (dd, ^{4}J(H,P) = 9.8, 6.5 Hz, 1H, C_5H_2P), 2.65 (d, *J* = 1.6 Hz, 6H, *-NMe_2*), 0.45 (d, *J* = 1.7 Hz, 9H, *-TMS*) ppm.

$^{13}C\{^{1}H\}$ NMR (151 MHz, *CD_3CN*) δ 159.3 (s, *C5*), 145.0 (d, ^{1}J(C,P) = 38.6 Hz, *C2*), 143.2 (d, ^{1}J(C,P) = 16.6 Hz, *C7*), 142.4 (s, *C3*), 140.5 (d, ^{2}J(C,P) = 10.2 Hz, *C8*), 130.7 (d, ^{3}J(C,P) = 10.9 Hz, *C9*), 130.0 (s, *C10*), 128.9 (s, *C11*), 120.1 (d, ^{3}J(C,P) = 31.7 Hz, *C4*), 42.8 (s, *C6*), 0.7 (d, ^{3}J(C,P) = 4.3 Hz, *C1*).

$^{31}P\{^{1}H\}$ NMR (243 MHz, *CD_3CN*) δ 193 ppm.

HR-ESI MS (*m/z*): 542.0506 g/mol (calculated: 542.0549 g/mol) $[M]Na^{+}$.

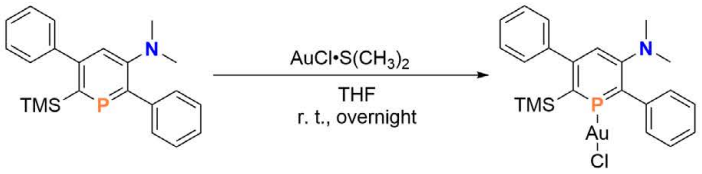

Scheme S8: Synthesis of gold complex **12**.

Phosphinine **7** (36 mg, 0.1 mmol), product yield: 54 mg, 0.09 mmol, 90 %.

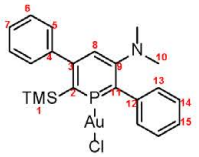

^{1}H NMR (600 MHz, *CD_3CN*) δ 7.57 – 7.53 (m, 2H, *-Ph*), 7.49 – 7.45 (m, 6H, *-Ph*), 7.39 – 7.35 (m, 2H, *-Ph*), 6.96 (d, *J* = 4.0 Hz, 1H, C_5HP), 2.64 (d, *J* = 0.8 Hz, 6H, *-NMe_2*), 0.14 (dd, *J* = 1.6, 0.9 Hz, 9H, *-TMS*) ppm.

^{13}C{^{1}H} NMR (151 MHz, *CD_3CN*) δ 157.4 (d, ^{1}J(C,P) = 53.4 Hz, *C11*), 157.4 (d, ^{1}J(C,P) = 67.7 Hz, *C2*), 157.3 (s, *C4*), 155.9 (s, *C9*), 145.2 (d, ^{2}J(C,P) = 13.6 Hz, *C3*), 130.0 (d, ^{2}J(C,P) = 10.8 Hz, *C12*), 128.8 (s, *C5*), 128.3 (s, *C6*), 128.2 (d, ^{3}J(C,P) = 7.8 Hz, *C13*), 128.0 (s, *C7*), 128.0 (s, *C14*), 127.6 (s, *C15*), 121.6 (d, ^{3}J(C,P) = 26.7 Hz, *C8*), 41.9 (s, *C10*), 2.3 (d, ^{3}J(C,P) = 5.8 Hz, *C1*) ppm.

^{31}P{^{1}H} NMR (243 MHz, *CD_3CN*) δ 205 ppm.

HR-ESI MS (*m/z*): 618.0819 g/mol (calculated: 618.0783 g/mol) $[M]Na^{+}$.

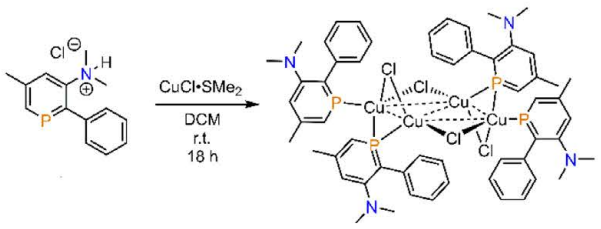

Scheme S9: Synthesis of gold complex **15**.

Protonated phosphinine **14** (30 mg, 0.1 mmol) was dissolved in DCM (3 mL) at room temperature and copper(I) chloride dimethyl sulfide complex (16 mg, 0.1 mmol, 1 eq.) was added to the Schlenk flask. The reaction was stirred at room temperature overnight before

filtering the orange solution through Celite. All volatiles of the filtrate were removed under vacuum yielding **15** as an orange solid. Yield: 92 % (30.2 mg, 0.023 mmol).

Crystals of **15** suitable for single crystal XRD were acquired from a mixture of THF (1 mL) and *n*-hexane (1 mL) in a freezer at -30 °C.

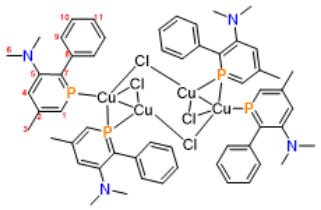

^{1}H NMR (600 MHz, THF-d_8) δ 7.70 (d, $^{2}J_{H,P}$ = 29.9 Hz, 1H, C_5H_2P), 7.51 (d, *J* = 7.5 Hz, 2H, *Ph*), 7.22 (t, *J* = 7.5 Hz, 2H, *Ph*), 7.12 (t, *J* = 7.4 Hz, 1H, *Ph*), 6.96 (d, $^{4}J_{H,P}$ = 3.9 Hz, 1H, C_5H_2P), 2.54 (s, 6H, NMe_2), 2.42 (s, 3H, CH_3) ppm.

^{13}C{^{1}H} NMR (151 MHz, THF-d_8) δ 157.9 (d, ^{2}J(C,P) = 9.0 Hz, *C5*), 147.6 (s, *C9*), 147.3 (d, ^{2}J(C,P) = 15.4 Hz, *C2*), 141.6 (d, ^{1}J(C,P) = 17.2 Hz, *C7*), 137.9 (s, *C4*), 130.5 (d, ^{2}J(C,P) = 10.9 Hz, *C8*), 129.3 (s, *C10*), 127.5 (s, *C11*), 121.8 (d, ^{1}J(C,P) = 19.2 Hz, *C1*), 43.2 (s, *C6*), 26.0 (s, *C3*) ppm.

^{31}P{^{1}H} NMR (162 MHz, THF-d_8) δ 173 ppm.

2. NMR Spectra

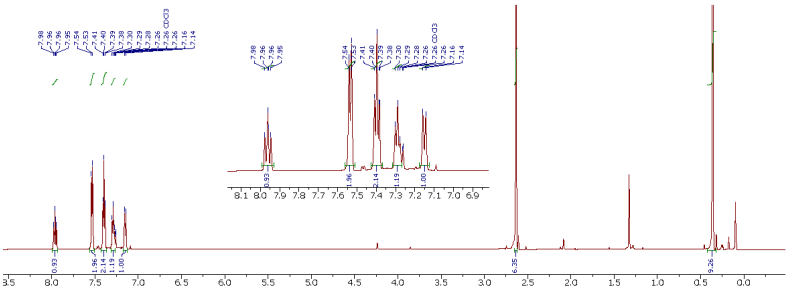

Figure S1. ^{1}H NMR spectrum of compound **5** in $CDCl_3$.

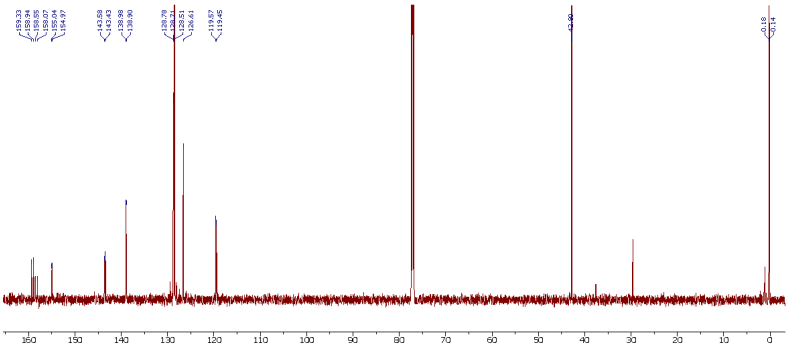

Figure S2. $^{13}C\{^{1}H\}$ NMR spectrum of compound **5** in $CDCl_3$.

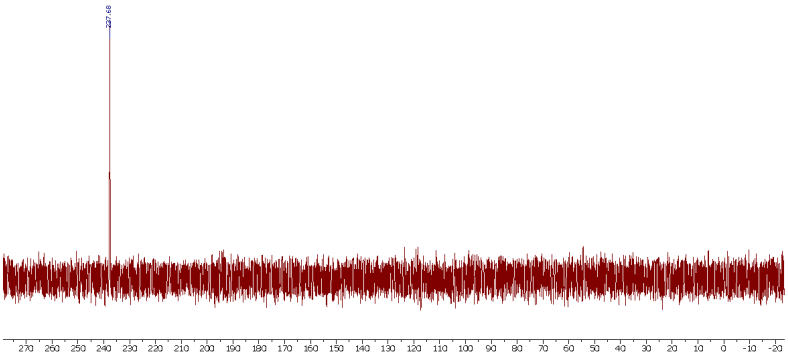

Figure S3. $^{31}P\{^{1}H\}$ NMR spectrum of compound **5** in CD_2Cl_2.

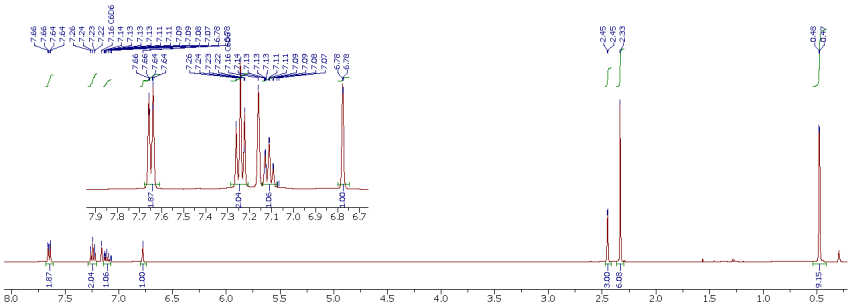

Figure S4. ^{1}H NMR spectrum of compound **6** in C_6D_6.

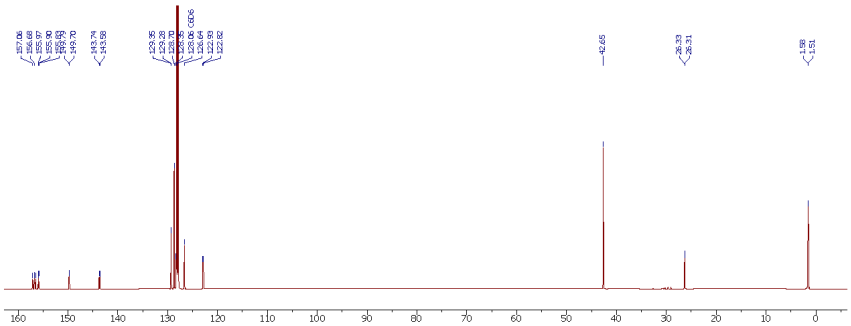

Figure S5. $^{13}C\{^{1}H\}$ NMR spectrum of compound **6** in C_6D_6.

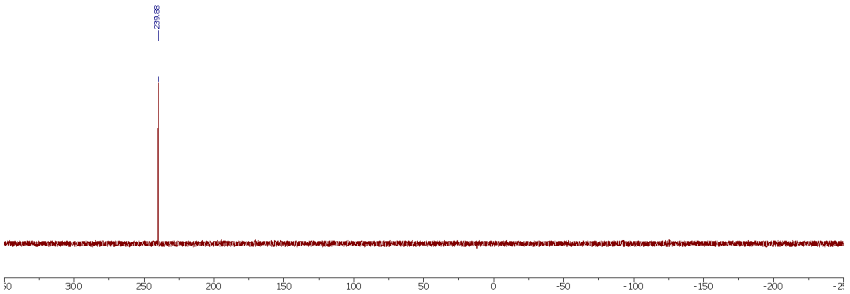

Figure S6. $^{31}P\{^{1}H\}$ NMR spectrum of compound **6** in CD_2Cl_2.

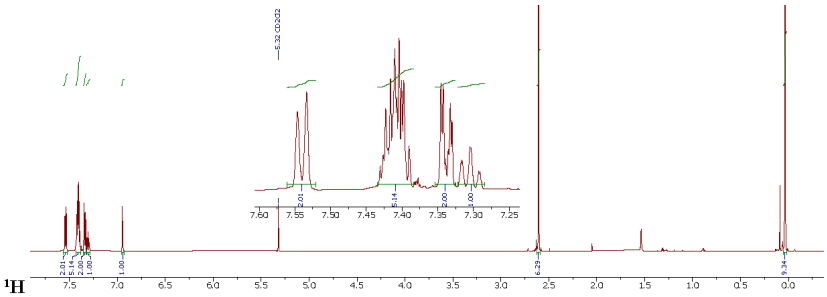

Figure S7. ^{1}H NMR spectrum of compound **7** in CD_2Cl_2.

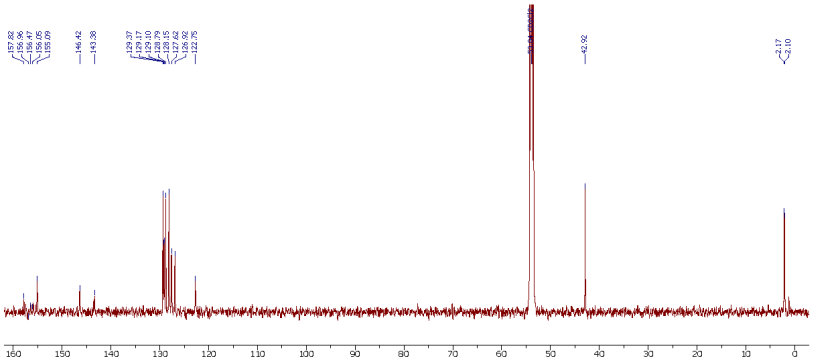

Figure S8. $^{13}C\{^{1}H\}$ NMR spectrum of compound **7** in CD_2Cl_2.

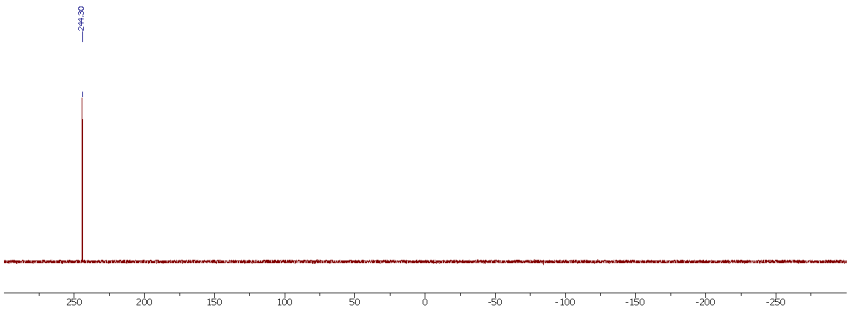

Figure S9. $^{31}P\{^{1}H\}$ NMR spectrum of compound **7** in CD_2Cl_2.

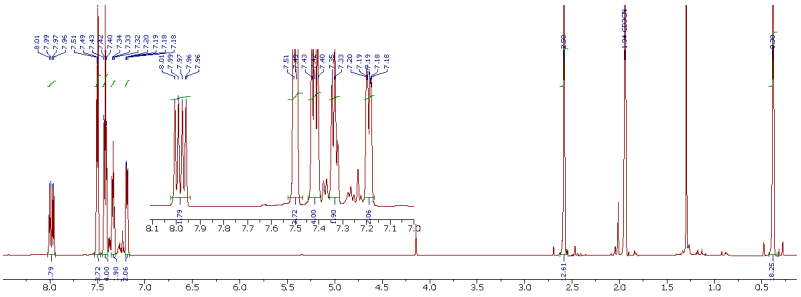

Figure S10. ^{1}H NMR spectrum of complex **8** in CD_3CN.

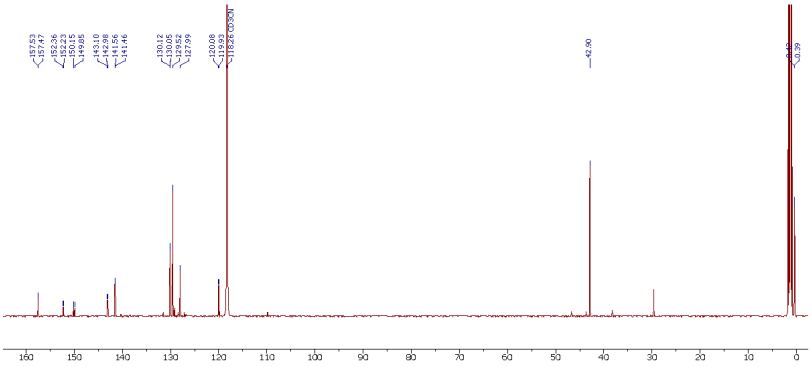

Figure S11. $^{13}C\{^{1}H\}$ NMR spectrum of complex **8** in CD_3CN.

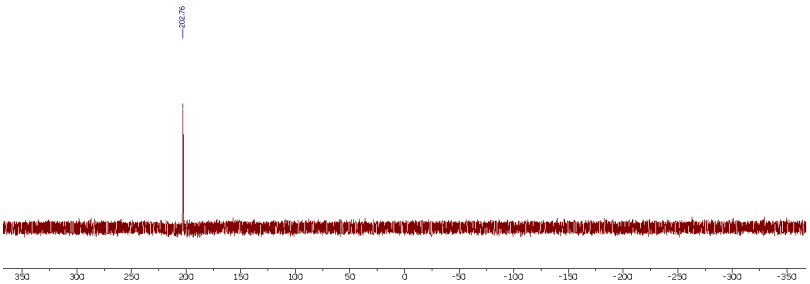

Figure S12. $^{31}P\{^{1}H\}$ NMR spectrum of complex **8** in CD_3CN.

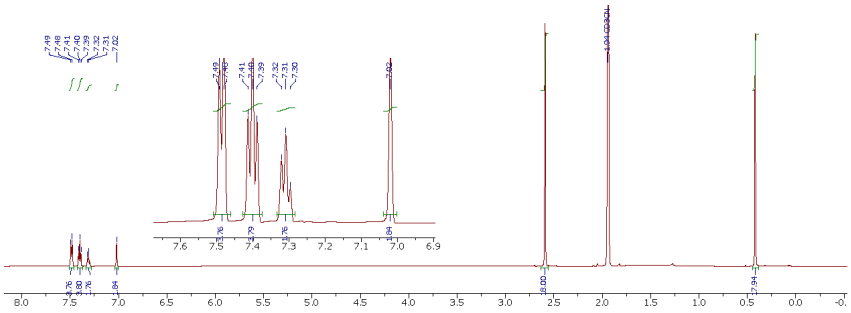

Figure S13. ^{1}H NMR spectrum of complex **9** in CD_3CN.

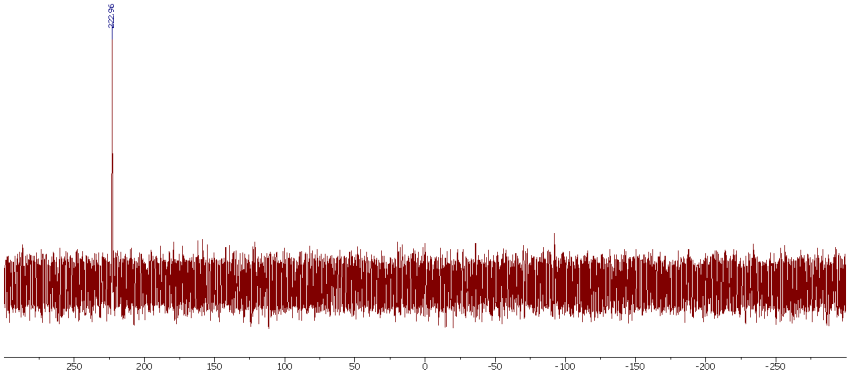

Figure S14. $^{31}P\{^{1}H\}$ NMR spectrum of complex **9** in CD_3CN.

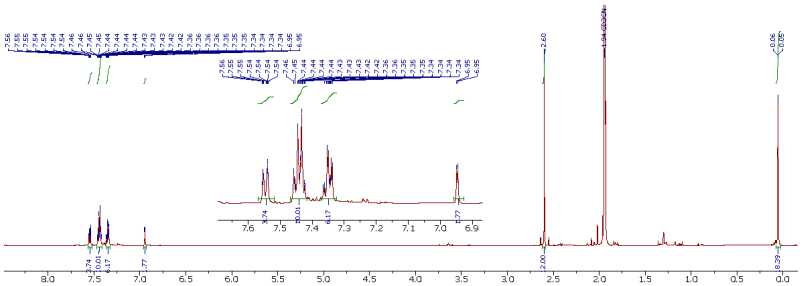

Figure S15. ^{1}H NMR spectrum of complex **10** in CD_3CN.

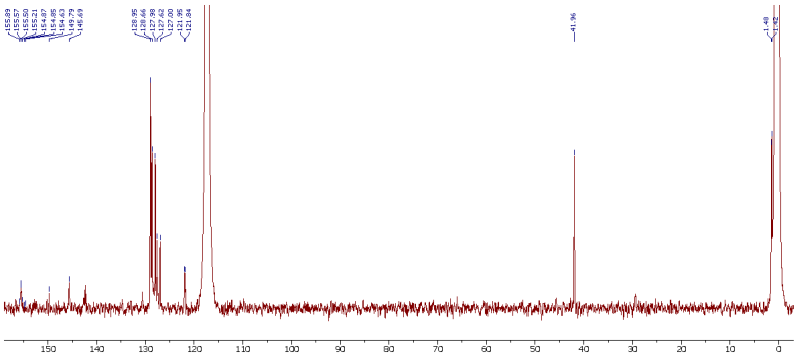

Figure S16. $^{13}C\{^{1}H\}$ NMR spectrum of complex **10** in CD_3CN.

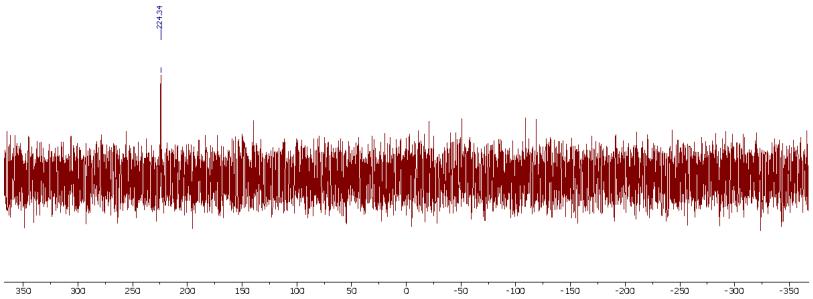

Figure S17. $^{31}P\{^{1}H\}$ NMR spectrum of complex **10** in CD_3CN.

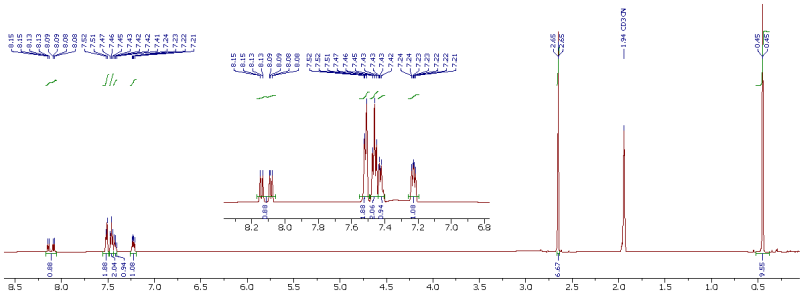

Figure S18. ^{1}H NMR spectrum of complex **11** in CD_3CN.

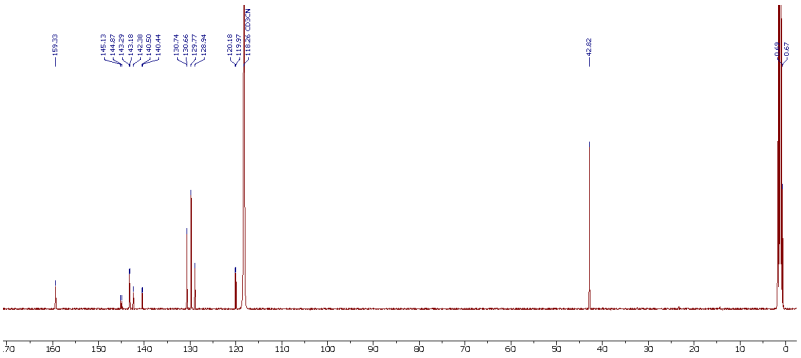

Figure S19. $^{13}C\{^{1}H\}$ NMR spectrum of complex **11** in CD_3CN.

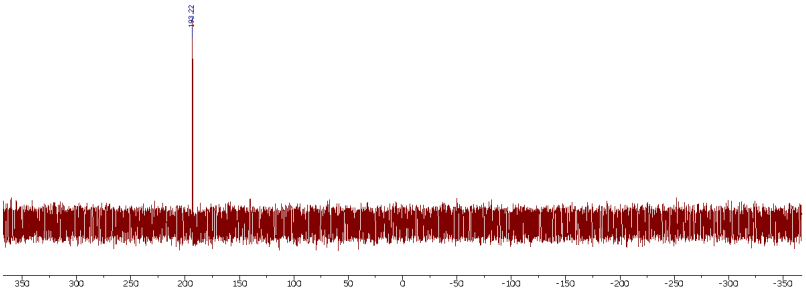

Figure S20. $^{31}P\{^{1}H\}$ NMR spectrum of complex **11** in CD_3CN.

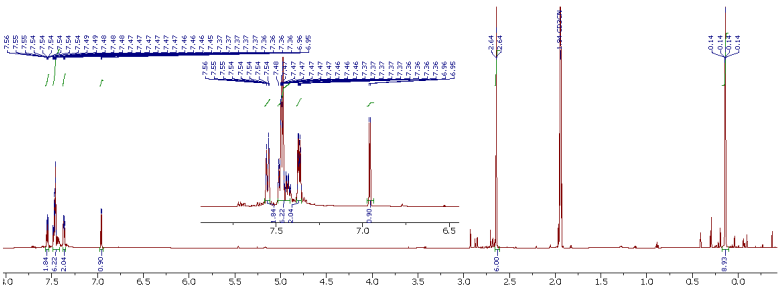

Figure S21. ^{1}H NMR spectrum of complex **12** in CD_3CN.

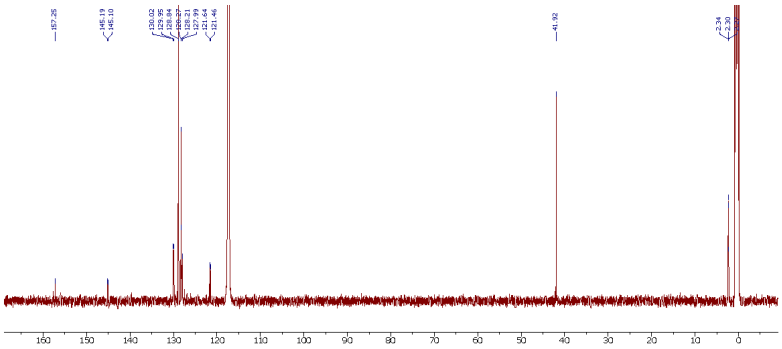

Figure S22. $^{13}C\{^{1}H\}$ NMR spectrum of complex **12** in CD_3CN.

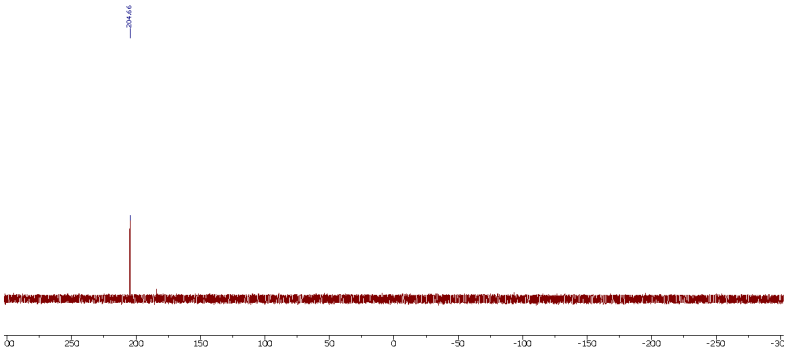

Figure S23. $^{31}P\{^{1}H\}$ NMR spectrum of complex **12** in CD_3CN.

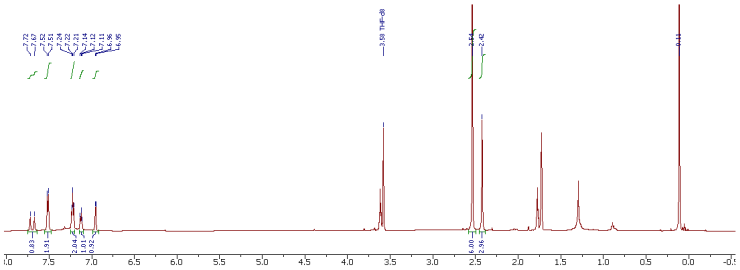

Figure S24. ^{1}H NMR spectrum of complex **15** in THF-d_8.

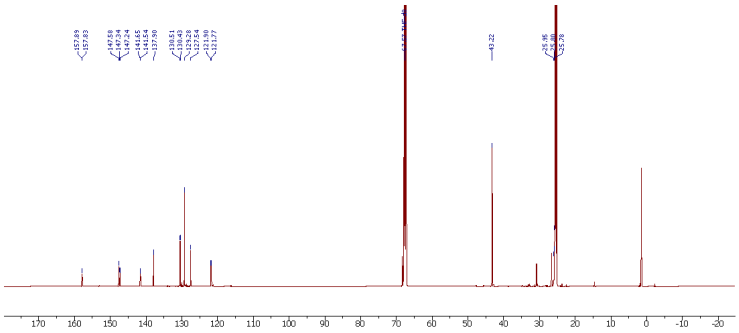

Figure S25. $^{13}C\{^{1}H\}$ NMR spectrum of complex **15** in THF-d_8.

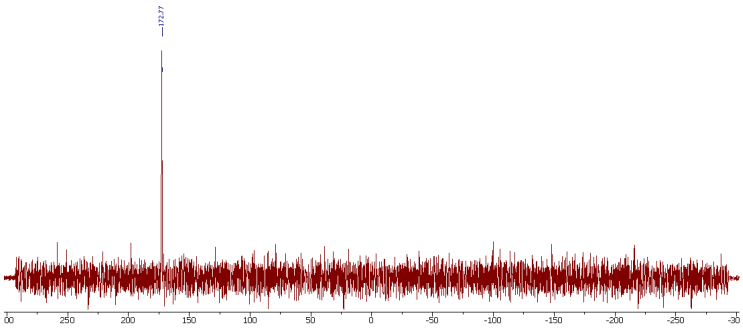

Figure S26. $^{31}P\{^{1}H\}$ NMR spectrum of complex **15** in THF-d_8.

3. Crystallographic Part

Table S1 Selected crystallographic data for **5**, **7**, **8**, **9**, **10**, **11**, **12**, **15**.

	5	**7**	**8**	**9**
Empirical formula	C16H22NPSi	C22H26NPSi	C32H44Br2Cu2N2P2Si2	C34H48Br2Cu2N2P2Si2
CCDC number	2214696	2214697	2214698	2214699
Formula weight	287.40	363.50	861.71	889.76
Temperature / K	100	100	100	100
Crystal system	monoclinic	monoclinic	triclinic	monoclinic
Space group	$P2_1/c$	$P2_1/n$	P-1	$P2_1/c$
a/Å	11.9745(7)	12.1736(2)	10.2016(3)	9.8333(2)
b/Å	10.6819(6)	8.8108(1)	10.3857(3)	18.8139(4)
c/Å	12.7497(6)	18.7609(3)	18.0567(6)	11.3015(2)
α/°	90	90	93.311(1)	90
β/°	97.139(2)	101.061(1)	93.038(1)	96.6519(9)
γ/°	90	90	102.694(1)	90
Volume/Å^3	1618.18(15)	1974.90(5)	1859.00(10)	2076.73(7)
Z	4	4	2	2
Reflections collected	64333	24793	32917	26007
Independent reflections (R_{int})	4909 (0.0306)	5841 (0.0309)	7005 (0.0747)	4252 (0.0292)
R1[I>2σ(I)]	0.0287	0.0336	0.0456	0.0242
wR_2(all data)	0.0747	0.0912	0.1173	0.0562

Continue table **S1**:

	10	**11**	**12**	**15**
Empirical formula	C44H52Br2Cu2N2P2Si2	C20H21AuClPSi	C22H26AuClNPSi	C5H64Cl4Cu4N4P4
CCDC number	2214700	2214701	2214702	2214703
Formula weight	1013.90	552.85	595.91	1312.95
Temperature / K	100	100	100	100
Crystal system	monoclinic	triclinic	triclinic	triclinic
Space group	$P2_1/c$	P-1	P-1	P-1
a/Å	10.0614(3)	9.2859(2)	9.9924(4)	9.8937(2)
b/Å	11.5513(4)	11.4569(2)	11.2338(5)	11.7165(2)
c/Å	19.6138(6)	11.5897(2)	11.3484(4)	12.7199(2)
α/°	90	111.6404(5)	94.376(2)	102.1863(6)
β/°	104.4900(10)	102.0416(6)	107.383(1)	91.8573(6)
γ/°	90	108.1246(6)	108.656(2)	91.6284(6)
Volume/Å^3	2207.05(12)	1014.01(8)	1130.83(8)	1439.56(4)
Z	2	2	2	1
Reflections collected	82274	30279	44140	62388
Independent reflections (R_{int})	7827 (0.0359)	6076 (0.0578)	6741 (0.0608)	8730 (0.0450)
R1[I>2σ(I)]	0.0244	0.0260	0.0278	0.0305
wR_2(all data)	0.0604	0.0555	0.0840	0.0827

Additional refinement details for 9

A solvent mask (SQUEEZE[7]) was implemented. This mask accounted for 0.75 equivalents of pentane per asymmetric unit.

Additional refinement details for 11

Refined as a two component inversion twin (6%).

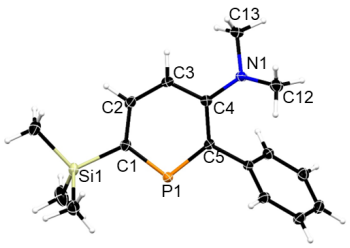

Table S2 List of bond lengths for **5**.

Atom	Atom	Length/Å	Atom	Atom	Length/Å
P1	C5	1.7361(9)	C4	C3	1.4075(13)
P1	C1	1.7311(10)	C5	C6	1.4931(12)
Si1	C1	1.8748(10)	C6	C11	1.3987(13)
Si1	C12	1.8644(11)	C6	C7	1.3985(13)
Si1	C13	1.8661(11)	C2	C1	1.3982(13)
Si1	C14	1.8691(12)	C2	C3	1.3901(13)
N1	C4	1.3932(12)	C11	C10	1.3902(13)
N1	C16	1.4549(12)	C7	C8	1.3958(13)
N1	C15	1.4591(12)	C10	C9	1.3931(15)
C4	C5	1.4191(12)	C8	C9	1.3864(15)

Table S3 List of angles for **5**.

Atom	Atom	Atom	Angle/°	Atom	Atom	Atom	Angle/°
C1	P1	C5	104.72(4)	C6	C5	P1	114.02(6)
C12	Si1	C1	109.73(5)	C11	C6	C5	119.12(8)
C12	Si1	C13	110.72(5)	C7	C6	C5	121.95(8)
C12	Si1	C14	108.64(6)	C7	C6	C11	118.78(9)
C13	Si1	C1	109.02(5)	C3	C2	C1	125.66(9)
C13	Si1	C14	109.72(6)	C10	C11	C6	120.63(9)
C14	Si1	C1	108.99(5)	P1	C1	Si1	118.04(5)
C4	N1	C16	118.64(8)	C2	C1	P1	120.40(7)
C4	N1	C15	119.47(8)	C2	C1	Si1	121.49(7)

C16	N1	C15	111.78(8)	C2	C3	C4	124.90(9)
N1	C4	C5	120.20(8)	C8	C7	C6	120.43(9)
N1	C4	C3	119.55(8)	C11	C10	C9	120.18(9)
C3	C4	C5	120.21(8)	C9	C8	C7	120.28(9)
C4	C5	P1	123.95(7)	C8	C9	C10	119.70(9)
C4	C5	C6	121.67(8)				

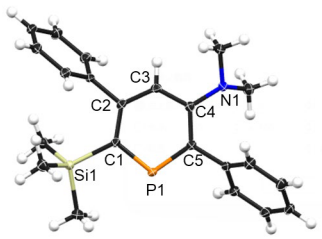

Table S4 List of bond lengths for **7**.

Atom	Atom	Length/Å	Atom	Atom	Length/Å
P1	C1	1.7354(11)	C5	C12	1.4909(15)
P1	C5	1.7370(12)	C6	C7	1.3941(17)
Si1	C1	1.8971(12)	C6	C11	1.3940(17)
Si1	C18	1.8701(13)	C7	C8	1.3948(16)
Si1	C19	1.8683(13)	C8	C9	1.3868(18)
Si1	C20	1.8670(13)	C9	C10	1.3884(19)
N1	C4	1.4151(15)	C10	C11	1.3922(16)
N1	C21	1.4574(15)	C12	C13	1.3986(17)
N1	C22	1.4621(16)	C12	C17	1.3970(17)
C1	C2	1.4081(15)	C13	C14	1.3940(17)
C2	C3	1.3988(16)	C14	C15	1.384(2)
C2	C6	1.5022(15)	C15	C16	1.387(2)
C3	C4	1.4045(15)	C16	C17	1.3920(17)
C4	C5	1.4119(15)			

Table S5 List of angles for **7**.

Atom	Atom	Atom	Angle/°	Atom	Atom	Atom	Angle/°
C1	P1	C5	105.52(5)	C4	C5	P1	123.36(9)
C18	Si1	C1	108.16(6)	C4	C5	C12	123.17(10)
C19	Si1	C1	112.73(6)	C12	C5	P1	113.42(8)
C19	Si1	C18	105.74(6)	C7	C6	C2	121.89(10)
C20	Si1	C1	110.22(5)	C11	C6	C2	119.24(10)

C20	Si1	C18	109.63(6)	C11	C6	C7	118.85(11)
C20	Si1	C19	110.22(6)	C6	C7	C8	120.41(11)
C4	N1	C21	117.22(10)	C9	C8	C7	120.33(12)
C4	N1	C22	115.99(10)	C8	C9	C10	119.55(11)
C21	N1	C22	110.91(10)	C9	C10	C11	120.21(12)
P1	C1	Si1	114.01(6)	C10	C11	C6	120.61(12)
C2	C1	P1	120.50(9)	C13	C12	C5	119.86(11)
C2	C1	Si1	125.36(8)	C17	C12	C5	121.67(11)
C1	C2	C6	120.78(10)	C17	C12	C13	118.39(11)
C3	C2	C1	123.75(10)	C14	C13	C12	120.73(12)
C3	C2	C6	115.42(10)	C15	C14	C13	120.17(13)
C2	C3	C4	126.58(10)	C14	C15	C16	119.75(12)
C3	C4	N1	119.94(10)	C15	C16	C17	120.28(13)
C3	C4	C5	120.25(10)	C16	C17	C12	120.67(12)
C5	C4	N1	119.81(10)				

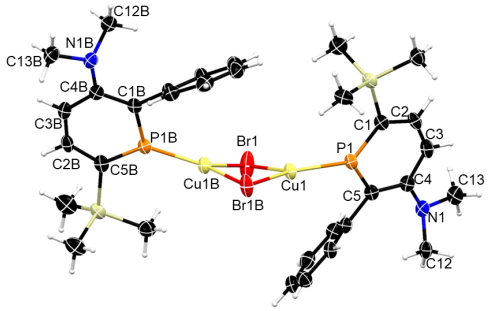

Table S6 List of bond lengths for **8**.

Atom	Atom	Length/Å	Atom	Atom	Length/Å
Br1	Cu2	2.3749(6)	N2	C31	1.463(6)
Br1	Cu1	2.4134(8)	C21	C22	1.481(6)
Cu2	Cu1	2.9527(9)	C21	C20	1.410(6)
Cu2	Br2	2.4152(8)	C1	C2	1.396(6)
Cu2	P2	2.1653(13)	C4	C5	1.399(6)
Cu1	Br2	2.3737(7)	C4	C3	1.398(7)
Cu1	P1	2.1640(13)	C22	C27	1.402(6)
P2	C21	1.735(4)	C22	C23	1.398(6)
P2	C17	1.711(5)	C17	C18	1.399(6)
P1	C1	1.709(5)	C2	C3	1.395(6)
P1	C5	1.727(4)	C5	C6	1.478(6)
Si2	C17	1.882(4)	C18	C19	1.383(6)
Si2	C28	1.873(4)	C6	C7	1.393(6)
Si2	C30	1.870(5)	C6	C11	1.404(6)

Si2	C29	1.855(5)	C27	C26	1.377(7)
Si1	C1	1.885(5)	C20	C19	1.413(7)
Si1	C14	1.857(5)	C7	C8	1.372(7)
Si1	C12	1.859(5)	C23	C24	1.385(7)
Si1	C13	1.861(5)	C26	C25	1.393(7)
N1	C4	1.407(5)	C11	C10	1.377(7)
N1	C16	1.461(6)	C24	C25	1.375(7)
N1	C15	1.462(6)	C8	C9	1.381(8)
N2	C20	1.399(5)	C10	C9	1.383(8)
N2	C32	1.462(5)			

Table S7 List of angles for **8**.

Atom	Atom	Atom	Angle/°	Atom	Atom	Atom	Angle/°
Cu2	Br1	Cu1	76.14(2)	C22	C21	P2	113.0(3)
Br1	Cu2	Cu1	52.52(2)	C20	C21	P2	121.3(3)
Br1	Cu2	Br2	102.42(3)	C20	C21	C22	125.4(4)
Br2	Cu2	Cu1	51.302(19)	P1	C1	Si1	122.0(3)
P2	Cu2	Br1	142.89(4)	C2	C1	P1	118.2(4)
P2	Cu2	Cu1	162.10(4)	C2	C1	Si1	119.5(4)
P2	Cu2	Br2	114.68(4)	C5	C4	N1	118.4(4)
Br1	Cu1	Cu2	51.343(18)	C3	C4	N1	120.4(4)
Br2	Cu1	Br1	102.51(3)	C3	C4	C5	121.1(4)
Br2	Cu1	Cu2	52.57(2)	C27	C22	C21	121.2(4)
P1	Cu1	Br1	128.93(4)	C23	C22	C21	120.8(4)
P1	Cu1	Cu2	166.07(4)	C23	C22	C27	117.8(4)
P1	Cu1	Br2	128.35(4)	P2	C17	Si2	123.2(2)
Cu1	Br2	Cu2	76.13(2)	C18	C17	P2	118.0(3)
C21	P2	Cu2	116.15(16)	C18	C17	Si2	118.7(3)
C17	P2	Cu2	132.85(15)	C3	C2	C1	126.2(4)
C17	P2	C21	108.1(2)	C4	C5	P1	122.0(4)
C1	P1	Cu1	135.08(16)	C4	C5	C6	124.1(4)
C1	P1	C5	107.6(2)	C6	C5	P1	113.3(3)
C5	P1	Cu1	117.19(17)	C19	C18	C17	126.3(4)
C28	Si2	C17	111.57(19)	C7	C6	C5	120.5(4)
C30	Si2	C17	107.4(2)	C7	C6	C11	117.9(5)
C30	Si2	C28	109.7(2)	C11	C6	C5	121.3(4)
C29	Si2	C17	108.1(2)	C2	C3	C4	124.9(4)
C29	Si2	C28	108.9(2)	C26	C27	C22	121.3(4)
C29	Si2	C30	111.1(2)	N2	C20	C21	119.9(4)
C14	Si1	C1	111.1(2)	N2	C20	C19	119.3(4)
C14	Si1	C12	110.7(3)	C21	C20	C19	120.8(4)
C14	Si1	C13	109.3(3)	C8	C7	C6	120.8(4)
C12	Si1	C1	109.3(2)	C24	C23	C22	120.9(4)
C12	Si1	C13	110.1(3)	C27	C26	C25	119.8(4)

C13	Si1	C1	106.2(2)	C18	C19	C20	125.4(4)
C4	N1	C16	116.7(3)	C10	C11	C6	120.7(5)
C4	N1	C15	117.4(4)	C25	C24	C23	120.3(4)
C16	N1	C15	112.2(4)	C24	C25	C26	119.9(5)
C20	N2	C32	118.9(4)	C7	C8	C9	121.1(5)
C20	N2	C31	118.9(3)	C11	C10	C9	120.6(5)
C32	N2	C31	111.5(3)	C8	C9	C10	118.9(5)

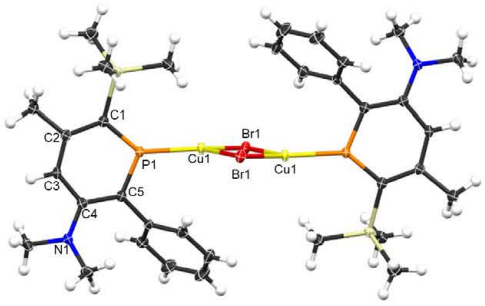

Table S8 List of bond lengths for **9**.

Atom	Atom	Length/Å	Atom	Atom	Length/Å
Br1	Cu1	2.3904(4)	C5	C4	1.415(3)
Br1	Cu1[1]	2.4447(4)	C5	C7	1.489(3)
Cu1	Cu1[1]	2.9913(6)	C1	C2	1.423(3)
Cu1	P1	2.1785(6)	C2	C3	1.391(3)
P1	C5	1.724(2)	C2	C6	1.520(3)
P1	C1	1.717(2)	C4	C3	1.420(3)
Si1	C1	1.890(2)	C7	C12	1.399(3)
Si1	C15	1.879(3)	C7	C8	1.401(3)
Si1	C14	1.872(3)	C12	C11	1.389(4)
Si1	C13	1.868(3)	C8	C9	1.395(4)
N1	C4	1.379(3)	C11	C10	1.388(4)
N1	C16	1.461(3)	C9	C10	1.382(5)
N1	C17	1.463(3)			

Table S9 List of angles for **9**.

Atom	Atom	Atom	Angle/°	Atom	Atom	Atom	Angle/°
Cu1	Br1	Cu1[1]	76.426(13)	C4	C5	C7	123.4(2)
Br1	Cu1	Br1[1]	103.575(13)	C7	C5	P1	114.76(16)
Br1[1]	Cu1	Cu1[1]	50.971(10)	P1	C1	Si1	117.67(13)

Br1	Cu1	Cu1[1]	52.604(11)	C2	C1	P1	118.05(18)
P1	Cu1	Br1[1]	122.99(2)	C2	C1	Si1	124.19(17)
P1	Cu1	Br1	132.70(2)	C1	C2	C6	120.0(2)
P1	Cu1	Cu1[1]	170.72(2)	C3	C2	C1	124.3(2)
C5	P1	Cu1	115.00(8)	C3	C2	C6	115.7(2)
C1	P1	Cu1	135.98(9)	N1	C4	C5	120.7(2)
C1	P1	C5	108.84(11)	N1	C4	C3	119.2(2)
C15	Si1	C1	108.84(11)	C5	C4	C3	120.1(2)
C14	Si1	C1	113.36(12)	C2	C3	C4	126.9(2)
C14	Si1	C15	108.88(13)	C12	C7	C5	119.9(2)
C13	Si1	C1	109.42(11)	C12	C7	C8	118.4(2)
C13	Si1	C15	108.21(13)	C8	C7	C5	121.6(2)
C13	Si1	C14	108.01(13)	C11	C12	C7	120.8(2)
C4	N1	C16	122.2(2)	C9	C8	C7	120.5(3)
C4	N1	C17	120.3(2)	C10	C11	C12	120.1(3)
C16	N1	C17	113.6(2)	C10	C9	C8	120.3(3)
C4	C5	P1	121.46(18)	C9	C10	C11	119.9(3)

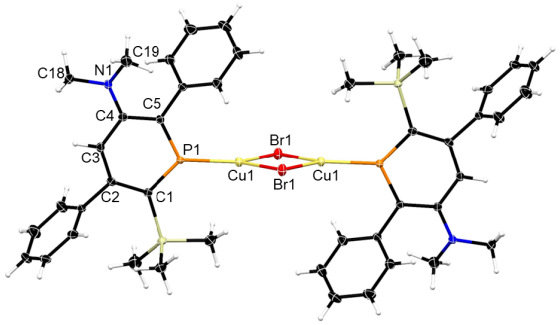

Table S10 List of bond lengths for **10**.

Atom	Atom	Length/Å	Atom	Atom	Length/Å
Br1	Cu1	2.3996(2)	C2	C3	1.3930(16)
Br1	Cu1[1]	2.4362(2)	C2	C6	1.4995(15)
Cu1	Cu1[1]	3.0420(3)	C3	C4	1.4128(16)
Cu1	P1	2.1793(3)	C7	C8	1.3951(17)
P1	C1	1.7238(12)	C7	C6	1.3927(17)
P1	C5	1.7228(12)	C12	C13	1.3947(16)
Si1	C1	1.8913(12)	C12	C17	1.3995(17)
Si1	C18	1.8712(15)	C13	C14	1.3966(18)
Si1	C19	1.8724(16)	C8	C9	1.384(2)

Si1	C20	1.8670(16)	C9	C10	1.386(2)
N1	C4	1.3800(15)	C6	C11	1.3941(18)
N1	C00N	1.4553(17)	C14	C15	1.382(2)
N1	C00O	1.4534(16)	C15	C16	1.391(2)
C1	C2	1.4156(16)	C17	C16	1.3860(18)
C5	C12	1.4909(16)	C10	C11	1.3926(18)
C5	C4	1.4206(16)			

Table S11 List of angles for **10**.

Atom	Atom	Atom	Angle/°	Atom	Atom	Atom	Angle/°
Cu1	Br1	$Cu1^1$	77.956(7)	C4	C5	C12	122.19(10)
Br1	Cu1	$Br1^1$	102.042(7)	C1	C2	C6	120.03(10)
Br1	Cu1	$Cu1^1$	51.558(6)	C3	C2	C1	124.76(10)
$Br1^1$	Cu1	$Cu1^1$	50.485(6)	C3	C2	C6	115.21(10)
P1	Cu1	Br1	131.218(11)	C2	C3	C4	126.34(11)
P1	Cu1	$Br1^1$	126.631(11)	C6	C7	C8	120.51(12)
P1	Cu1	$Cu1^1$	176.044(13)	C13	C12	C5	122.24(11)
C1	P1	Cu1	132.73(4)	C13	C12	C17	118.59(11)
C5	P1	Cu1	118.82(4)	C17	C12	C5	119.07(11)
C5	P1	C1	108.43(6)	C12	C13	C14	120.30(12)
C18	Si1	C1	108.98(6)	N1	C4	C5	120.05(10)
C18	Si1	C19	107.03(8)	N1	C4	C3	119.65(10)
C19	Si1	C1	110.42(7)	C3	C4	C5	120.23(10)
C20	Si1	C1	112.60(7)	C9	C8	C7	119.93(12)
C20	Si1	C18	107.58(8)	C8	C9	C10	119.99(12)
C20	Si1	C19	110.04(8)	C7	C6	C2	121.95(11)
C4	N1	C00N	120.97(11)	C7	C6	C11	119.03(11)
C4	N1	C00O	120.92(10)	C11	C6	C2	119.02(11)
C00O	N1	C00N	113.13(11)	C15	C14	C13	120.49(12)
P1	C1	Si1	117.68(6)	C14	C15	C16	119.65(12)
C2	C1	P1	117.97(9)	C16	C17	C12	120.92(12)
C2	C1	Si1	124.22(8)	C17	C16	C15	120.04(13)
C12	C5	P1	116.04(8)	C9	C10	C11	120.18(14)
C4	C5	P1	121.29(9)	C10	C11	C6	120.31(13)

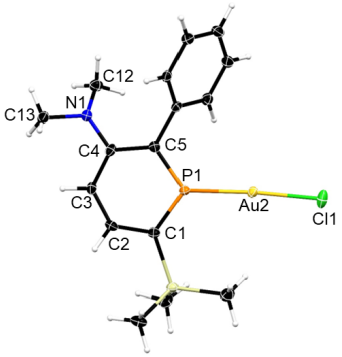

Table S12 List of bond lengths for **11**.

Atom	Atom	Length/Å	Atom	Atom	Length/Å
Au1	Cl1	2.2816(12)	C1	C2	1.397(7)
Au1	P1	2.2130(12)	C2	C3	1.382(7)
P1	C1	1.698(5)	C3	C4	1.406(7)
P1	C5	1.715(5)	C4	C5	1.426(6)
Si1	C1	1.888(5)	C5	C6	1.489(6)
Si1	C12	1.868(5)	C6	C7	1.395(7)
Si1	C13	1.864(5)	C6	C11	1.400(7)
Si1	C14	1.863(5)	C7	C8	1.394(7)
N1	C4	1.386(6)	C8	C9	1.383(8)
N1	C15	1.455(6)	C9	C10	1.391(8)
N1	C16	1.469(6)	C10	C11	1.389(7)

Table S13 List of angles for **11**.

Atom	Atom	Atom	Angle/°	Atom	Atom	Atom	Angle/°
P1	Au1	Cl1	175.98(5)	C3	C2	C1	127.0(5)
C1	P1	Au1	123.89(17)	C2	C3	C4	125.5(4)
C1	P1	C5	110.3(2)	N1	C4	C3	119.3(4)
C5	P1	Au1	125.75(17)	N1	C4	C5	120.2(5)
C12	Si1	C1	104.6(2)	C3	C4	C5	120.5(4)
C13	Si1	C1	108.6(2)	C4	C5	P1	120.0(4)
C13	Si1	C12	110.7(2)	C4	C5	C6	122.9(4)
C14	Si1	C1	113.3(2)	C6	C5	P1	117.1(3)
C14	Si1	C12	110.7(3)	C7	C6	C5	120.9(4)
C14	Si1	C13	108.9(3)	C7	C6	C11	119.1(4)
C4	N1	C15	118.9(4)	C11	C6	C5	120.0(4)
C4	N1	C16	120.7(4)	C8	C7	C6	120.0(5)
C15	N1	C16	113.1(4)	C9	C8	C7	120.6(5)

P1	C1	Si1	125.1(3)	C8	C9	C10	119.9(5)
C2	C1	P1	116.4(4)	C11	C10	C9	119.8(5)
C2	C1	Si1	117.9(3)	C10	C11	C6	120.6(5)

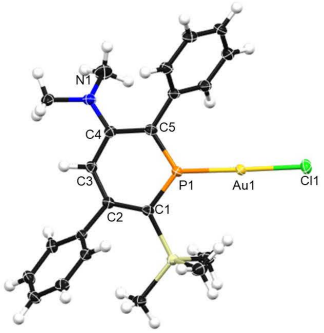

Table S14 List of bond lengths for **12**.

Atom	Atom	Length/Å	Atom	Atom	Length/Å
Au1	P1	2.2092(8)	C6	C11	1.402(4)
Au1	Cl1	2.2722(8)	C6	C7	1.393(4)
P1	C1	1.708(3)	C2	C3	1.393(4)
P1	C5	1.714(3)	C9	C10	1.390(5)
Si1	C1	1.906(3)	C11	C10	1.394(5)
Si1	C20	1.861(4)	C4	C5	1.421(5)
Si1	C18	1.869(4)	C4	C3	1.418(4)
Si1	C19	1.867(4)	C5	C12	1.484(4)
N1	C4	1.373(4)	C12	C17	1.405(5)
N1	C22	1.462(5)	C12	C13	1.397(5)
N1	C21	1.458(5)	C17	C16	1.390(5)
C1	C2	1.418(4)	C15	C16	1.392(5)
C8	C9	1.390(5)	C15	C14	1.377(5)
C8	C7	1.386(5)	C14	C13	1.391(5)
C6	C2	1.494(4)			

Table S15 List of angles for **12**.

Atom	Atom	Atom	Angle/°	Atom	Atom	Atom	Angle/°
P1	Au1	Cl1	178.74(3)	C3	C2	C1	125.2(3)
C1	P1	Au1	128.16(11)	C3	C2	C6	116.2(3)
C1	P1	C5	111.47(15)	C10	C9	C8	120.0(3)
C5	P1	Au1	120.36(12)	C10	C11	C6	120.1(3)
C20	Si1	C1	114.93(15)	N1	C4	C5	120.0(3)
C20	Si1	C18	105.33(19)	N1	C4	C3	120.0(3)
C20	Si1	C19	109.22(19)	C3	C4	C5	120.0(3)

C18	Si1	C1	107.27(15)	C4	C5	P1	119.4(2)
C19	Si1	C1	109.86(16)	C4	C5	C12	125.3(3)
C19	Si1	C18	110.1(2)	C12	C5	P1	115.1(2)
C4	N1	C22	120.2(3)	C17	C12	C5	119.3(3)
C4	N1	C21	120.7(3)	C13	C12	C5	122.2(3)
C21	N1	C22	113.1(3)	C13	C12	C17	118.2(3)
P1	C1	Si1	116.39(17)	C9	C10	C11	120.0(3)
C2	C1	P1	115.7(2)	C16	C17	C12	120.9(3)
C2	C1	Si1	127.8(2)	C8	C7	C6	120.6(3)
C7	C8	C9	120.0(3)	C14	C15	C16	120.5(3)
C11	C6	C2	120.8(3)	C17	C16	C15	119.5(3)
C7	C6	C2	120.0(3)	C15	C14	C13	120.0(3)
C7	C6	C11	119.1(3)	C2	C3	C4	126.8(3)
C1	C2	C6	118.6(3)	C14	C13	C12	120.9(3)

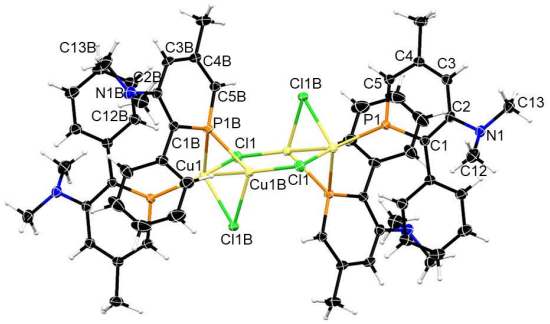

Table S16 List of bond lengths for **15**.

Atom1	Atom2	Length/Å	Atom1	Atom2	Length/Å
Cu1	Cl1	2.3334(4)	C9B	C10B	1.376(3)
Cu1	P1	2.2140(4)	C10B	C11B	1.392(3)
Cu1	Cu1B	2.4586(4)	Cu1	Cl1	2.3334(4)
Cu1	Cl1B	2.4157(4)	Cu1	P1	2.2140(4)
Cu1	P1B	2.3469(5)	Cu1B	Cl1	2.2078(5)
Cu1B	Cl1	2.2078(5)	Cu1B	Cl1B	2.2758(4)
Cu1B	Cl1B	2.2758(4)	Cu1B	P1B	2.2503(4)
Cu1B	P1B	2.2503(4)	P1	C1	1.725(1)
Cu1B	Cu1	2.4586(4)	P1	C5	1.702(2)
Cl1B	Cu1	2.4157(4)	P1B	C1B	1.719(1)
P1	C1	1.725(1)	P1B	C5B	1.709(1)
P1	C5	1.702(2)	N1	C2	1.411(2)
P1B	C1B	1.719(1)	N1	C12	1.467(2)
P1B	C5B	1.709(1)	N1	C13	1.465(2)
P1B	Cu1	2.3469(5)	N1B	C2B	1.413(2)

N1	C2	1.411(2)	N1B	C12B	1.457(3)
N1	C12	1.467(2)	N1B	C13B	1.456(2)
N1	C13	1.465(2)	C1	C2	1.419(2)
N1B	C2B	1.413(2)	C1	C6	1.495(2)
N1B	C12B	1.457(3)	C2	C3	1.405(2)
N1B	C13B	1.456(2)	C1B	C2B	1.416(2)
C1	C2	1.419(2)	C1B	C6B	1.486(2)
C1	C6	1.495(2)	C3	C4	1.395(2)
C2	C3	1.405(2)	C2B	C3B	1.404(2)
C1B	C2B	1.416(2)	C4	C5	1.387(2)
C1B	C6B	1.486(2)	C4	C14	1.510(2)
C3	C4	1.395(2)	C3B	C4B	1.400(2)
C2B	C3B	1.404(2)	C4B	C5B	1.385(2)
C4	C5	1.387(2)	C4B	C14B	1.508(2)
C4	C14	1.510(2)	C6	C7	1.403(2)
C3B	C4B	1.400(2)	C6	C11	1.401(2)
C4B	C5B	1.385(2)	C6B	C7B	1.400(2)
C4B	C14B	1.508(2)	C6B	C11B	1.394(2)
C6	C7	1.403(2)	C8	C9	1.390(2)
C6	C11	1.401(2)	C7B	C8B	1.392(3)
C7	C8	1.392(2)	C9	C10	1.385(2)
C6B	C7B	1.400(2)	C8B	C9B	1.379(3)
C6B	C11B	1.394(2)	C10	C11	1.392(2)
C8	C9	1.390(2)	C9B	C10B	1.376(3)
C7B	C8B	1.392(3)	C10B	C11B	1.392(3)
C9	C10	1.385(2)	C10	C11	1.392(2)
C8B	C9B	1.379(3)			

Table S17 List of angles for **15**.

Atom1	Atom2	Atom3	Angle/°	Atom1	Atom2	Atom3	Angle/°
Cl1	Cu1	P1	117.16(2)	Cu1B	Cu1	Cl1	100.92(1)
Cl1	Cu1	Cu1B	100.92(1)	Cu1B	Cu1	P1	140.28(2)
Cl1	Cu1	Cl1B	107.24(2)	Cl1B	Cu1	P1B	107.18(2)
Cl1	Cu1	P1B	106.56(2)	Cl1B	Cu1	Cl1	107.24(2)
P1	Cu1	Cu1B	140.28(2)	Cl1B	Cu1	P1	99.86(2)
P1	Cu1	Cl1B	99.86(2)	P1B	Cu1	Cl1	106.56(2)
P1	Cu1	P1B	117.78(2)	P1B	Cu1	P1	117.78(2)
Cu1B	Cu1	Cl1B	55.66(1)	Cl1	Cu1	P1	117.16(2)
Cu1B	Cu1	P1B	55.79(1)	Cu1	Cu1B	Cl1	164.22(2)
Cl1B	Cu1	P1B	107.18(2)	Cu1	Cu1B	Cl1B	61.22(1)
Cl1	Cu1B	Cl1B	119.65(2)	Cu1	Cu1B	P1B	59.59(1)
Cl1	Cu1B	P1B	124.20(2)	Cl1	Cu1B	Cl1B	119.65(2)
Cl1	Cu1B	Cu1	164.22(2)	Cl1	Cu1B	P1B	124.20(2)
Cl1B	Cu1B	P1B	115.75(2)	Cl1B	Cu1B	P1B	115.75(2)
Cl1B	Cu1B	Cu1	61.22(1)	Cu1	Cl1	Cu1B	94.78(2)
P1B	Cu1B	Cu1	59.59(1)	Cu1	Cl1B	Cu1B	63.13(1)

Cu1	Cl1	Cu1B	94.78(2)	Cu1	P1	C1	133.91(5)
Cu1B	Cl1B	Cu1	63.13(1)	Cu1	P1	C5	117.60(6)
Cu1	P1	C1	133.91(5)	C1	P1	C5	106.14(7)
Cu1	P1	C5	117.60(6)	Cu1	P1B	Cu1B	64.62(1)
C1	P1	C5	106.14(7)	Cu1	P1B	C1B	116.28(5)
Cu1B	P1B	C1B	120.10(5)	Cu1	P1B	C5B	118.15(5)
Cu1B	P1B	C5B	126.11(5)	Cu1B	P1B	C1B	120.10(5)
Cu1B	P1B	Cu1	64.62(1)	Cu1B	P1B	C5B	126.11(5)
C1B	P1B	C5B	106.32(7)	C1B	P1B	C5B	106.32(7)
C1B	P1B	Cu1	116.28(5)	C2	N1	C12	116.2(1)
C5B	P1B	Cu1	118.15(5)	C2	N1	C13	117.4(1)
C2	N1	C12	116.2(1)	C12	N1	C13	110.4(1)
C2	N1	C13	117.4(1)	C2B	N1B	C12B	114.6(1)
C12	N1	C13	110.4(1)	C2B	N1B	C13B	116.9(1)
C2B	N1B	C12B	114.6(1)	C12B	N1B	C13B	111.8(1)
C2B	N1B	C13B	116.9(1)	P1	C1	C2	120.8(1)
C12B	N1B	C13B	111.8(1)	P1	C1	C6	114.5(1)
P1	C1	C2	120.8(1)	C2	C1	C6	124.4(1)
P1	C1	C6	114.5(1)	N1	C2	C1	118.8(1)
C2	C1	C6	124.4(1)	N1	C2	C3	119.4(1)
N1	C2	C1	118.8(1)	C1	C2	C3	121.8(1)
N1	C2	C3	119.4(1)	P1B	C1B	C2B	121.1(1)
C1	C2	C3	121.8(1)	P1B	C1B	C6B	116.0(1)
P1B	C1B	C2B	121.1(1)	C2B	C1B	C6B	122.9(1)
P1B	C1B	C6B	116.0(1)	C2	C3	C4	126.1(1)
C2B	C1B	C6B	122.9(1)	N1B	C2B	C1B	117.8(1)
C2	C3	C4	126.1(1)	N1B	C2B	C3B	120.4(1)
N1B	C2B	C1B	117.8(1)	C1B	C2B	C3B	121.8(1)
N1B	C2B	C3B	120.4(1)	C3	C4	C5	121.9(1)
C1B	C2B	C3B	121.8(1)	C3	C4	C14	119.3(1)
C3	C4	C5	121.9(1)	C5	C4	C14	118.8(1)
C3	C4	C14	119.3(1)	C2B	C3B	C4B	126.2(1)
C5	C4	C14	118.8(1)	P1	C5	C4	122.9(1)
C2B	C3B	C4B	126.2(1)	C3B	C4B	C5B	122.0(1)
P1	C5	C4	122.9(1)	C3B	C4B	C14B	118.9(1)
C3B	C4B	C5B	122.0(1)	C5B	C4B	C14B	119.1(1)
C3B	C4B	C14B	118.9(1)	C1	C6	C7	120.6(1)
C5B	C4B	C14B	119.1(1)	C1	C6	C11	121.1(1)
C1	C6	C7	120.6(1)	C7	C6	C11	118.1(1)
C1	C6	C11	121.1(1)	P1B	C5B	C4B	122.6(1)
C7	C6	C11	118.1(1)	C6	C7	C8	120.7(1)
P1B	C5B	C4B	122.6(1)	C1B	C6B	C7B	121.1(1)
C6	C7	C8	120.7(1)	C1B	C6B	C11B	120.0(1)
C1B	C6B	C7B	121.1(1)	C7B	C6B	C11B	118.8(2)
C1B	C6B	C11B	120.0(1)	C7	C8	C9	120.4(2)
C7B	C6B	C11B	118.8(2)	C6B	C7B	C8B	119.9(2)
C7	C8	C9	120.4(2)	C8	C9	C10	119.6(2)
C6B	C7B	C8B	119.9(2)	C7B	C8B	C9B	120.4(2)

C8	C9	C10	119.6(2)	C9	C10	C11	120.3(2)
C7B	C8B	C9B	120.4(2)	C8B	C9B	C10B	120.4(2)
C9	C10	C11	120.3(2)	C6	C11	C10	120.9(1)
C8B	C9B	C10B	120.4(2)	C9B	C10B	C11B	119.8(2)
C6	C11	C10	120.9(1)	C6B	C11B	C10B	120.7(2)
C9B	C10B	C11B	119.8(2)	Cu1B	Cu1	Cl1B	55.66(1)
C6B	C11B	C10B	120.7(2)	Cu1B	Cu1	P1B	55.79(1)

4. DFT Calculations

Energy levels of the frontier molecular orbitals

General information

DFT Calculations were carried out with the ORCA 4.2.0 program suite.[8] Initial molecular structures were created in the program Avogadro[9] or were based on crystal structures, if available. Geometry optimizations were then performed with the PBEh-3c method developed by Grimme and co-workers.[10] Numerical Frequency calculations were carried out to confirm the nature of stationary points found by geometry optimizations. The absence of imaginary vibrational frequencies indicated that the optimized structure is a local minimum. Final single point calculations on the optimized structures were conducted with the B3LYP functional.[11] Additionally, for all calculations the empirical Van der Waals Correction (D3) was used.[12]. Standardized convergence criteria were used for the geometry optimization (OPT) and the addition "tight" for SCF-calculations ("TIGHTSCF"). A Triple-ζ-valence-basis set (def2-TZVP) was applied for all atoms (single point calculation).[13] Singe point calculations with the B3LYP-functional were done with the RIJCOSX-approximation[14] and solvent effects were taken into account with the Conductor-like-Polarizable-Continuum-Modell (CPCM)[15] for THF. Molecular orbitals were visualized via the freely available program IBOView v20150427.[16]

Computed Cartesian coordinates (Å) for parent phosphinine (PBEh-3c)

C -6.82758459082452 2.39862006253895 -0.00014009336622

C -6.90473364684224 1.01654590621344 -0.00017063587903

C -4.24938328522251 1.07917228425864 0.00011678914983

C -4.39192325041511 2.45613056244555 0.00003434726274

C -5.62547202848662 3.09346301120752 -0.00004200197887

H	-7.74849355193160	2.97044828678917	-0.00003671247507
H	-5.65107094501903	4.17544798680152	0.00004220584259
H	-3.49913784627841	3.07099034789223	0.00003566487655
P	-5.55092389918300	-0.05802885992600	-0.00025206153820
H	-7.88983786791819	0.56416608379652	0.00036723763951
H	-3.24376908787877	0.67436432798246	0.00004526046617

Computed Cartesian coordinates (Å) for 5 (PBEh-3c)

C	-0.90123311487248	-1.38091952520793	-0.08881300043503
C	-0.60400579138643	-0.36307264720712	0.82205300399243
C	0.44248615734408	0.53808530602156	0.63885374163852
C	1.33670158208173	0.53223835397748	-0.42890453004931
C	1.29870240374404	-0.42247689546010	-1.44961303980066
P	0.07115830068463	-1.64672252592082	-1.50009747283314
H	0.57335923657600	1.30717755395085	1.39191065654068
C	-1.35250670127292	-1.11226856700079	3.08518188764909
C	-2.11656416771874	-0.94649694862281	4.23042940570725
C	-2.94677846991021	0.15712508323794	4.35940054536128
C	-2.99848255154786	1.10083977643253	3.34367334314803
C	-2.23244454735578	0.93513538693601	2.20058974770950
C	2.36838168363664	1.60103688583333	-0.42688449827625
C	3.38071446167780	1.60090299990498	0.52822697153263
C	4.35888055751055	2.58260971136943	0.51704426061231
C	4.32921893085986	3.58433394463199	-0.44233695373714
Si	-2.37989297795135	-2.56933111520590	0.06435030636061

C	-3.93394587823154	-1.70889634980865	0.69369466530523
H	-3.90539603497463	-1.48889715370298	1.75995944154217
H	-4.80043137663118	-2.34861154015064	0.51177499633277
H	-4.10979821059839	-0.76907694393931	0.16861061097133
C	-2.76481979427874	-3.23879305937274	-1.65736703664292
H	-1.95034363387527	-3.82918672671670	-2.07662819835728
H	-2.98687628962014	-2.44105972071324	-2.36745448098356
H	-3.64414440162491	-3.88493561429894	-1.60673191346167
C	-1.93890595072609	-4.04401043795102	1.15801102103547
H	-1.86250555158630	-3.78026062322189	2.21205171862432
H	-0.98893428844203	-4.48575049310888	0.85369078781234
H	-2.70155992805628	-4.82080946537495	1.07345794535853
Si	2.56516433571936	-0.53856282879873	-2.86666506170963
C	2.51153045935463	-2.29917650748438	-3.54385821776127
C	4.32809607125772	-0.20939441743492	-2.28791753878238
C	2.10255569692655	0.62318760207718	-4.28119604286423
H	2.72684926327691	-3.04163643452933	-2.77424678529253
H	3.26608567198191	-2.41129921981721	-4.32574756062425
H	1.54753698792873	-2.55697890541688	-3.98223191025922
H	1.04946463051452	0.51926413709842	-4.54670452074125
H	2.68766358138230	0.38570714368874	-5.17198227013047
H	2.28601663761021	1.67043090839034	-4.04466290027210
H	4.56217547890000	-0.76860426072942	-1.38113211526108
H	4.52748310198826	0.84222148676067	-2.08688386567123

H	5.02798491444860	-0.53626676716812	-3.06020668874093
H	-2.05881581953196	-1.67806384408735	5.02580714342954
H	-3.54658255406475	0.28498737917979	5.25075401259121
H	-3.64110853991552	1.96617317799600	3.43957823112266
H	5.14937153282023	2.56223372639949	1.25569506774184
C	2.33294137325638	2.62127353477453	-1.37162188948459
C	-1.41437433855429	-0.18110066670927	2.05374814337780
H	-2.28147983469275	1.66641430426263	1.40339774425676
C	3.30929813543079	3.60586772654451	-1.38202889701959
H	5.09472216159894	4.34882753325146	-0.45335633024384
H	3.27032969659483	4.39360641601030	-2.12300712268635
H	3.41217492730239	0.81181016103016	1.26921420880062
H	-0.69220355344698	-1.96486021794096	2.99161654955893
H	1.52900632845893	2.64605018334167	-2.09609531599197

Computed Cartesian coordinates (Å) for 6 (PBEh-3c)

C	-1.03366556936605	-1.75827071927463	-1.33044489215600
C	-0.37475883602032	-1.31628865443611	-0.17534766941379
C	0.82959721433194	-0.62412449711150	-0.21590085105993
C	1.56127818786355	-0.28830788242861	-1.36066176415417
C	1.11351501552026	-0.66315467179217	-2.63663994308924
P	-0.37134831874384	-1.51348336079726	-2.90690939481428
H	1.22077077881523	-0.29142921019959	0.73718582574836
N	2.76718104608659	0.40868660053112	-1.22823199657407
Si	-2.66397177172446	-2.71872735002461	-1.31283314936773

C	-3.29779123607231	-2.90383237926623	-3.07798717567788
H	-3.47776313523962	-1.94032699515125	-3.55612597150369
H	-4.24567485852456	-3.44651577864992	-3.06849603450217
H	-2.61007474263940	-3.45838326022623	-3.71643334488330
C	-2.39714080442544	-4.45255718128164	-0.61268946908221
H	-2.06004427632377	-4.45388667039700	0.42423547952381
H	-1.65020004195941	-4.99180084269011	-1.19688512177016
H	-3.32294211885703	-5.03000043520222	-0.65120829380391
C	-4.00230136339473	-1.82463832986686	-0.32290804011091
H	-4.06059752471376	-0.77014761872813	-0.59681321612972
H	-3.85158553047592	-1.87908241855652	0.75480026084580
H	-4.97764800849161	-2.26817544201055	-0.53287394201042
C	1.92606492767073	-0.43145030053882	-3.85392477646349
C	3.24279846195636	-0.88962686602206	-3.93444382065657
C	1.37427081006007	0.19856604551329	-4.96813128810237
C	-0.98297815758412	-1.53156481144222	1.18724754741277
C	3.98183240982615	-0.71352759497038	-5.09122058294107
C	3.42386126322984	-0.07630869791830	-6.19228152494836
C	2.11661298428314	0.37670362466833	-6.12708357542442
H	1.66926297130232	0.87233454348349	-6.97873976617880
H	0.35520809041372	0.56234732423949	-4.92103395002278
H	4.99874600272842	-1.08135879591776	-5.13730275437162
H	4.00497473391172	0.06141587102613	-7.09458181489595
H	3.68356856303383	-1.39119127469479	-3.08398205490320

C	3.45994768663660	0.35920991483327	0.03299937132357
C	2.87430218169564	1.70531195104115	-1.86526806918339
H	2.34840068849505	1.72979910425452	-2.81456191373130
H	3.92178502710599	1.93326559011233	-2.06822519425358
H	2.46680126410595	2.50488909079463	-1.23212607136820
H	3.03349768481969	1.01286073791173	0.80785190327756
H	4.49201727312367	0.67697229222396	-0.12283217349129
H	3.48473566885907	-0.65905782151278	0.41942862206532
H	-1.83644523888313	-0.87006167161722	1.34205216074613
H	-0.26713712905037	-1.33068777532496	1.98345698989671
H	-1.33701227338568	-2.55329338258295	1.32070144020008

Computed Cartesian coordinates (Å) for 7 (PBEh-3c)

C	-1.07415415398905	-1.71784585406149	-1.30191532935311
C	-0.57488091991255	-1.00986496220990	-0.20409184627599
C	0.57671599821058	-0.23131522109397	-0.24209259382956
C	1.39890014632348	-0.03158244023061	-1.35560839637166
C	1.10732497083494	-0.65169455062649	-2.58211742926818
P	-0.26170824334555	-1.68403938889569	-2.83025550546103
H	0.82398403980829	0.29524014839601	0.67062881285993
C	-0.74490585785895	-1.70190883314702	2.19208574259679
C	-1.42146755926158	-1.74415485061174	3.40120963616791
C	-2.64847459393787	-1.11005718686888	3.53517017619888
C	-3.18869720199746	-0.42454216403174	2.45711512334213
C	-2.51195773743813	-0.38611835578582	1.24698835772553

N	2.53194069979917	0.77929501037440	-1.23975762260948
Si	-2.60089497659218	-2.84795371364735	-1.25283386338147
C	-4.19586426884034	-1.86354290455007	-1.48269443908692
H	-4.46441556344049	-1.28505751933211	-0.59949221061346
H	-5.02790385553834	-2.53891199635029	-1.69220420273431
H	-4.11743848968749	-1.17320354826156	-2.32389624531290
C	-2.47580925772158	-4.05347624247062	-2.69988010979592
H	-1.56302000609662	-4.64928315057501	-2.65947762968358
H	-2.49669474212966	-3.55923613525575	-3.67121341408983
H	-3.32011191573378	-4.74590560796580	-2.66876584120624
C	-2.69630604213451	-3.87206601971875	0.32688558997872
H	-2.99946085102171	-3.29328979008761	1.19836455349371
H	-1.73947942681854	-4.34156758074267	0.55877935139177
H	-3.42704281268441	-4.67294396529045	0.19318221098068
C	2.01670030661729	-0.54734298222215	-3.74779712229164
C	3.36552678395715	-0.89139601688571	-3.63830068073281
C	1.53021560547242	-0.15826606004155	-4.99463258211342
H	-0.99286378305692	-2.27805278611308	4.23926569690635
H	-3.17836409834031	-1.14500762052628	4.47789159320309
H	-4.13741505109996	0.08610484551017	2.55923580700124
C	-1.29153340976858	-1.03671452240259	1.09853202886296
H	-2.92673862898519	0.16021894103254	0.40948487987952
H	0.20618941288760	-2.20840790168435	2.08418816065161
C	4.19859966068325	-0.83872232482579	-4.74215414604987

C	3.70453153999910	-0.44054440507423	-5.97787214816104
C	2.36689566045263	-0.10269236055558	-6.10039561474632
H	1.96908423459438	0.20654091836299	-7.05807186923081
H	0.48691094063786	0.11448705365632	-5.09542700182229
H	5.23986570496512	-1.11584230451410	-4.63996765790153
H	4.35910722127522	-0.39848237033455	-6.83841745260763
H	3.75777061508465	-1.20641789698288	-2.68121117335144
C	2.61165785604077	1.95811234161737	-2.07847171922358
C	3.08697130225329	1.00209648228434	0.07058800827526
H	3.14032518508331	0.06891233168374	0.63009796400697
H	2.53403089079004	1.73556437801099	0.67484682318444
H	4.10496789132139	1.37836367638937	-0.04069374995260
H	2.19075297947282	1.77889771281349	-3.06282242651559
H	3.65530619268139	2.24347105820907	-2.21828838896956
H	2.08074760818560	2.81004663563348	-1.63305010396364

5 Reference

[1] a) N. Avarvari, P. Le Floch and F. Mathey, *J. Am. Chem. Soc.*, 1996, **118**, 11978-11979; b) L. Hong, S. Ahles, M. A. Strauss, C. Logemann and H. A. Wegner, *Org. Chem. Front.*, 2017, **4**, 871-875.

[2] J. Lin, N. T. Coles, L. Dettling, L. Steiner, J. F. Witte, B. Paulus, C. Müller, *How to Shrink the Ring: Phospholenes from Phosphabenzenes via Selective Ring Contraction*; (Unpublished manuscript).

[3] G. M. Sheldrick, *Acta Crystallogr. A* **2015**, *71*, 3–8.

[4] G. M. Sheldrick, *Acta Crystallogr, C* **2015**, *71*, 3–8.

[5] P. Müller, *Crystallogr. Rev.* **2009**, *15*, 57–83.

[6] O. V. Dolomanov, L. J. Bourhis, R. J. Gildea, J. A. K. Howard, H. Puschmann, *J. Appl. Crystallogr.* **2009**, *42*, 339–341.

[7] A. L. Spek, *Acta Crystallogr.* C **2015**, 71, 9-18.

[8] a) F. Neese, *Wiley Interdiscip. Rev.-Comput. Mol. Sci.* **2012**, *2*, 73–78; b) F. Neese, *Wiley Interdiscip. Rev.-Comput. Mol. Sci.* **2018**, *8*, e1327.

[9] Avogadro: an open-source molecular builder and visualization tool. Version 1.2.0. modified version with extended ORCA support, http://avogadro.openmolecules.net/ and https://orcaforum.cec.mpg.de.

[10] a) S. Grimme, J. G. Brandenburg, C. Bannwarth, A. Hansen, *J. Chem. Phys.* **2015**, *143*, 54107; b) R. Sure, J. G. Brandenburg, S. Grimme, *ChemistryOpen* **2016**, *5*, 94–109.

[11] a) A. D. Becke, *J. Chem. Phys.* **1993**, *98*, 5648–5652; b) C. Lee, W. Yang, R. G. Parr, *Phys. Rev. B* **1988**, *37*, 785–789.

[12] a) S. Grimme, S. Ehrlich, L. Goerigk, *J. Comput. Chem.* **2011**, *32*, 1456–1465; b) S. Grimme, J. Antony, S. Ehrlich, H. Krieg, *J. Chem. Phys.* **2010**, *132*, 154104; c) S. Grimme, *J. Comput. Chem.* **2006**, *27*, 1787–1799; d) S. Grimme, *J. Comput. Chem.* **2004**, *25*, 1463–1473.

[13] F. Weigend, R. Ahlrichs, *Phys. Chem. Chem. Phys.* **2005**, *7*, 3297–3305.

[14] a) F. Neese, *J. Comput. Chem.* **2003**, *24*, 1740–1747; b) F. Neese, F. Wennmohs, A. Hansen, U. Becker, *Chem. Phys.* **2009**, *356*, 98–109; c) O. Vahtras, J. Almlöf, M. W. Feyereisen, *Chem. Phys. Lett.* **1993**, *213*, 514–518; d) J. L. Whitten, *J. Chem. Phys.* **1973**, *58*, 4496–4501; e) R. Izsák, F. Neese, *J. Chem. Phys.* **2011**, *135*, 144105; f) F. Neese, G. Olbrich, *Chem. Phys. Lett.* **2002**, *362*, 170–178; g) T. Petrenko, S. Kossmann, F. Neese, *J. Chem. Phys.* **2011**, *134*, 54116.

[15] a) A. Klamt, G. Schüürmann, *J. Chem. Soc., Perkin Trans. 2* **1993**, 799–805; b) V. Barone, M. Cossi, *J. Phys. Chem. A.* **1998**, *102*, 1995–2001; c) J. Andzelm, C. Kölmel, A. Klamt, *J. Chem. Phys.* **1995**, *103*, 9312–9320; d) Y. Takano, K. N. Houk, *J. Chem. Theory Comput.* **2005**, *1*, 70–77.

[16] a) G. Knizia, J. E. M. N. Klein, *Angew. Chem.* **2015**, *127*, 5609–5613; b) G. Knizia, J. E. M. N. Klein, *Angew. Chem. Int. Ed.* **2015**, *54*, 5518–5522.

Chapter 5

λ^5-Phosphinines

5.1 Introduction

5.1.1 Properties of λ^5-phosphinines

λ^3- and λ^5-phosphinines have been known for many decades.[4,5] The different electronegativities of the phosphorus (Pauling scale: 2.2) and the carbon atom (Pauling scale: 2.5) leads to a partially positively charged phosphorus atom in $\lambda^3\sigma^2$-phosphinines, while the neighboring carbon atoms are partially negatively charged.[29] Thus, the phosphorus atoms of $\lambda^3\sigma^2$-phosphinines can be attacked by strong nucleophiles for the synthesis of a variety of λ^4-phosphinines and λ^5-phosphinines.[101] The bonding situation in λ^5-phosphinines were studied in detail by Schäfer *et al.* who used photoelectron spectroscopy and CNDO calculations.[85] λ^5-Phosphinines can either be described as aromatic or as phosphonium ylide (Scheme 5.1).

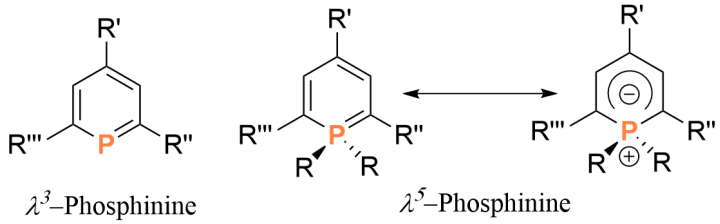

Scheme 5.1: λ^3- and λ^5-phosphinines.

However, recent studies by Schleyer and co-workers have shown that the nature of the substituents at the phosphorus atom plays a predominant role in the extent of cyclic electron delocalization in λ^5-phosphinines. The NICS values calculated at a GIAO-HF/6-31+G*/B3LYP/6-311+G** energy level for λ^5-phosphinines containing electronegative atoms (for example, F: -7.8, Cl: -7.3) at the phosphorus atom are only somewhat smaller than the ones of the parent phosphinine (-10.8) and benzene (-10.6), indicating that these λ^5-phosphinines are aromatic. The compounds with electropositive atoms at the phosphorus atom have, on the other hand, small NICS values (For example, H: -2.6), indicating weak aromatic properties. Thus, the structure of λ^5-phosphinines with electron-withdrawing substituents on the phosphorus atom can be described as

hybrids of internal zwitterions (ylide) and '*Hückel*' aromatic systems, while with electron-donating substituents at the phosphorus atom as a phosphonium ylide.[86]

For example, NR_2- and OR_2- in Figure 5.1 are electron-releasing substituents. The ionization energy of **5-1** and **5-2** recently reported by Müller *et. al.* is low, which is in accordance with an ylide-character. The λ^5-phosphinines **5-1** and **5-2** show two oxidation waves, while no reduction process was observed in the electrochemical windows of the cyclic voltammogram[77].

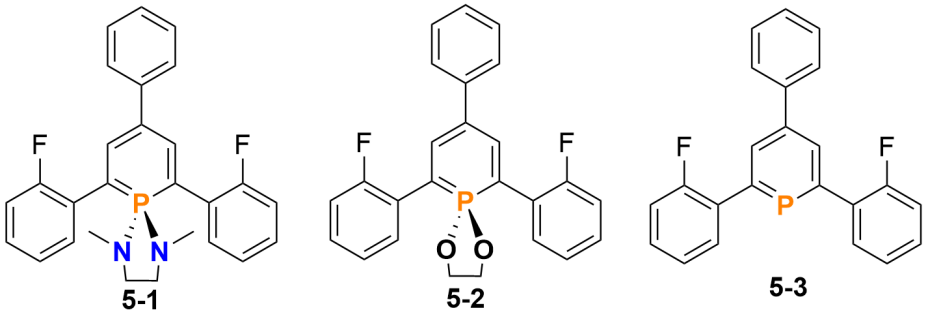

Figure 5.1: 2,4,6-Triaryl-λ^5-phosphinines **5-1** and **5-2**, and -λ^3-phosphinine **5-3**.

The nature of the P-substituents has a significant impact on the HOMO energy. An NR_2-substituent (**5-1**) results in a more destabilized HOMO compared to an OR-substituent (**5-2**) and shows lower E^{ox1} oxidation potentials (Table 5.1).

Table 5.1: Calculated at B3LYP/6-31+G* level HOMO energies [eV], first oxidation potentials (E^{ox1} [V])

Sample name	HOMO [eV][a]	E^{ox1} [V][b]
5-1	-4.91	0.59
5-2	-5.27	0.93

a: All potentials were measured by cyclic voltametric investigations in 0.1 M Bu_4NPF_6 in CH_2Cl_2. Platinum electrode diameter: 1 mm, sweep rate: 200 mV s^{-1}. All reported potentials are referenced to the reversible formal potential of the decamethyl-ferrocene/decamethyl-ferrocenium couple; b: Irreversible process.

In general, λ^3-phosphinines are almost non-fluorescence with quantum yields << 1 %.[6]

In contrast, many λ^5-phosphinines show an intense fluorescence emission in solution.[87-95] The most effective fluorescent materials are based on conjugated C=C double bonds, while phosphinines contain a conjugated system with a P=C double bond. Theoretical and experimental results show that the P=C double bond in λ^3-phosphinines is not responsible for their non-luminescent behavior.[96-98] TD-DFT calculations showed that the red-edge absorption band for λ^3-phosphinine **5-3**, assigned to $\pi \rightarrow \pi^*$ transition, is partially forbidden due to the small change in the dipole moment (both HOMO and LUMO have the same b_1 symmetry), resulting in a low luminescent intensity (quantum yields << 1%). For the λ^5-phosphinines **5-1** and **5-2**, the band maxima of absorption are essentially the HOMO-LUMO transitions that are strongly allowed, due to a change of parity, causing rather large oscillator strength (more than 0.2) and high fluorescence in solution (Figure 5.2).[6]

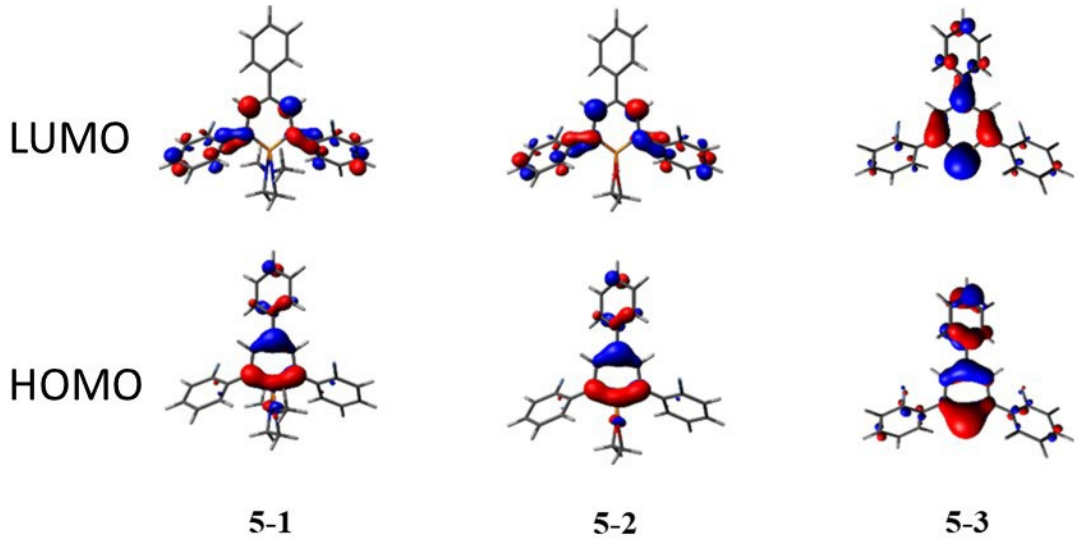

Figure 5.2: HOMO and LUMO orbitals of **5-1**, **5-2** and **5-3** at the B3LYP/6-31+G level of theory.

5.1.2 Synthesis of λ^5-phosphinines

λ^3-phosphinines are still the main starting materials for the synthesis of λ^5-phosphinines.[52,99,100] Dimroth and co-workers succeeded in synthesizing λ^5-phosphinines in 1968. For example, starting from triphenylphosphinine, they were able to obtain the corresponding 1,1'-dimethoxy-λ^5-phosphinines. Most likely, the oxidation

reaction with $Hg(OAc)_2$ involves the formation of radicals. In the presence of alcohol or phenols, the formation of λ^5-phosphinines is observed. (Scheme 5.2).

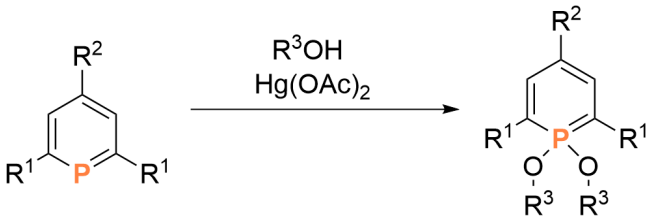

Scheme 5.2: Synthesis of λ^5-phosphinines by the oxidation of $Hg(OAc)_2$ in the presence of alcohols.

The group of Müller has adopted this method for the synthesis of a series of λ^5-phosphinines.[6,77] The λ^5-phosphinine **5-1** has a rather large oscillator strength and exhibits intensive blue-emission in solution.

Dimroth and co-workers reported the access to the first 1,1'-dihalo-λ^5-phosphinines by a light-induced addition of halogens, for example by reaction with PCl_5 or elemental bromine, to the phosphorus atom of λ^3-phosphinines in 1972. These 1,1'-dihalo-λ^5-phosphinines are especially useful intermediates for the preparation of λ^5-phosphinines containing alkyl- or aryl- substituents (Scheme 5.3).[101]

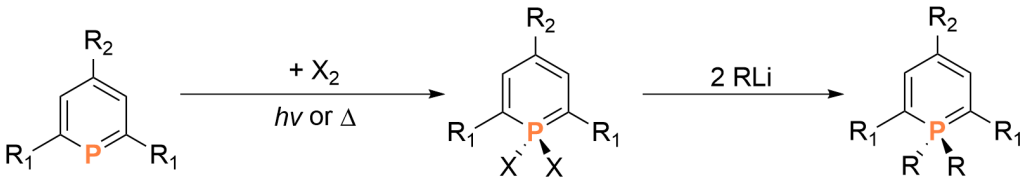

Scheme 5.3: Synthesis of λ^5-phosphinine from 1,1-dihalogen-λ^5-phosphinines.

Another efficient way to obtain λ^5-phosphinines is to react λ^3-phosphinines with strong nucleophilic reagents, such as organolithium compounds, to form λ^4-phosphinine anions. These can further react with organoiodines to produce the desired products (Scheme 5.4).[102-105] The benefit of this method is that most products can be synthesized at room temperature. However, the disadvantage of this method is the possible formation of by-products which cannot be separated from the products.

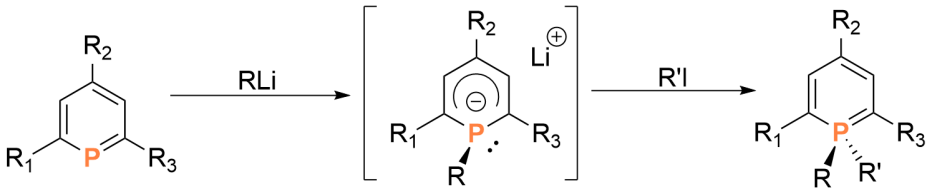

Scheme 5.4: Synthesis of λ^5-phosphinines from λ^4-phosphinines and organoiodines.

Another interesting route for the synthesis of λ^5-phosphinines is the reaction of bis(cyanomethyl)-phosphonium salts with aldimine. Hashimoto *et. al.* have reported a variety of 2,6-dicyano-λ^5-phosphinines by using this procedure (Scheme 5.5).[95] The photophysical properties of the 2,6-dicyano-λ^5-phosphinines were modified by introducing different substituents at the 4-position of the aromatic heterocycle, which resulted in a fluorescence, ranging from blue to yellow with a maximum quantum yield of 92 % in solution. The disadvantage of this method is that it is impossible to modify the substituents at the phosphorus atom and at the 2,6-positions of the phosphorus heterocycles. Also, the maximum emission wavelength of these λ^5-phosphinines only reaches the yellow region in solution.

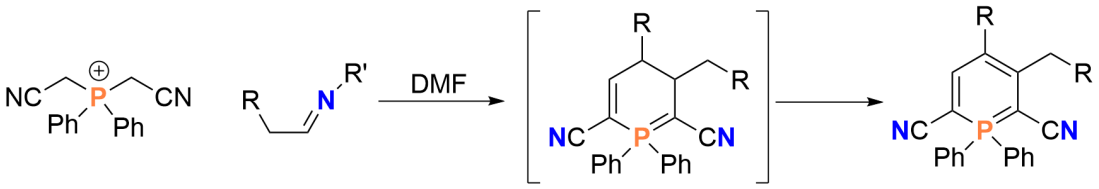

Scheme 5.5: Synthesis of λ^5-phosphinines *via* bis(cyanomethyl)-phosphonium salts and aldimine.

In 1969, Märkl reported the first synthesis of spiro-λ^5-phosphinine compound by heating 2,4,6-triphenylphosphinine and [1,1′-biphenyl]-2,2′-diylmercury to 300 °C (Scheme 5.6). This reaction produced highly toxic mercury vapors, which severely limited the use of this synthetic method.[123] Even though this reaction was mentioned more than 50 years ago, no further reports on the synthesis and characterization of spiro-λ^5-phosphinine compounds have been published since.

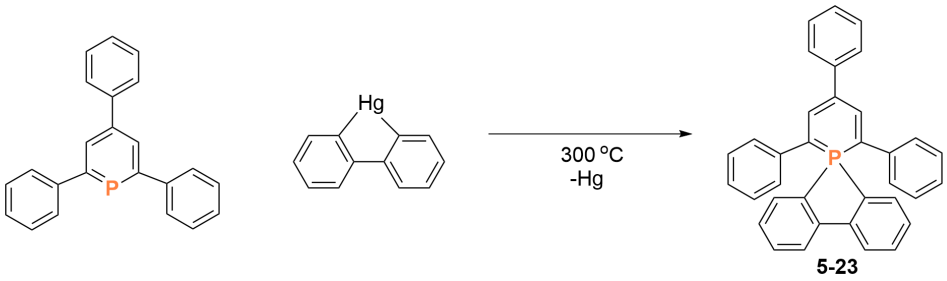

Scheme 5.6: Synthesis of spiro-λ^5-phosphinine **5-23**.

Recently, Kostyuk *et al.* prepared a variety of λ^5-phosphinines by electrocyclization of phosphahexatrienes generated in *situ*. Starting from commercially available hexatrienes, they were able to synthesize λ^5-phosphinines in high yield in four steps (Scheme 5.7).[106] By this method one can, however, only introduce a limited number of functional groups to the phosphorus atom of the parent phosphinine.

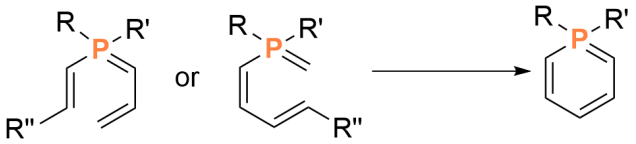

Scheme 5.7: Synthesis of λ^5-phosphinines by electrocyclization of hexatrienes.

Overall, although several methods have been developed for the synthesis of λ^5-phosphinines, they all have their own advantages and drawbacks (*vide supra*).

5.2 Result and discussion

By combining different synthetic methods, a variety of λ^5-phosphinines have been obtained. These λ^5-phosphinines involve not only the modification of the substituents at the 2-, 4-, 6-positions of the phosphorus heterocycle, but also the introduction of different substituents at the phosphorus atom. This gives an insight into the correlation between optical properties of λ^5-phosphinines and substitution patterns. Furthermore, these λ^5-phosphinines show intense fluorescence emission in solution, with a quantum yield up to 72 %. Moreover, the emission of λ^5-phosphinine **5-22** reaches the red region for the first time, with a maximum emission wavelength close to λ = 650 nm. It should be noted that λ^5-phosphinines **5-23**–**5-26** show no luminescence in the visible and near-

infrared regions, either at room temperature or at low temperatures, in the solid state or in solution. A more detailed theoretical insight and additional experiments are required to reveal the luminescence properties of compounds **5-23**–**5-26** completely.

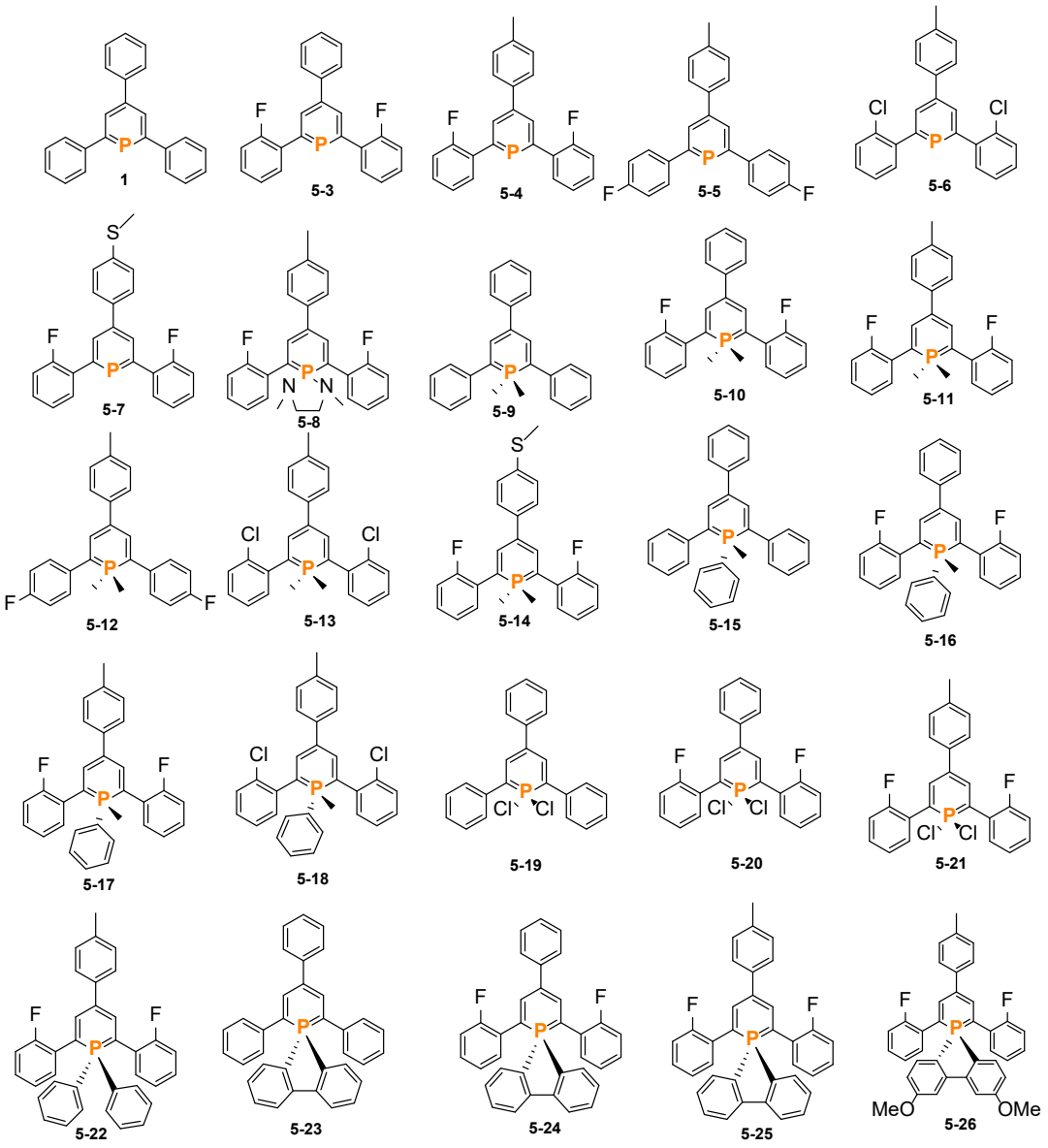

Scheme 5.8: Overview of synthesized λ^5-phosphinines and λ^3-phosphinines.

For all λ^5-phosphinines included in this chapter (Scheme 5.8), their fluorescence properties, particular the absorption and emission features are essentially not affected by the different substituents in the 4-position of the phosphorus heterocycle, in contrast to the observations reported by Hayashi and co-workers.[95] The different substituents at the 2,6-positions of the phosphorus heterocycle have an obvious effect on the

absorption, emission and quantum yields of λ^5-phosphinines. However, the substituents connected to the phosphorus atom play a predominant role in the photophysical properties of λ^5-phosphinines (*vide infra*). More detailed investigations on the photophysical and photochemical properties of these λ^5-phosphinines are currently performed.

5.3 Synthesis of λ^3-phosphinines

A library of λ^5-phosphinines was synthesized by oxidation of λ^3-phosphinines.[4] Therefore, the corresponding pyrylium salts were first synthesized. It is known that aldehydes react with ketones in a Claisen-Schmidt condensation to give chalcones, which subsequently react with another ketone in the presence of $HBF_4 \cdot Et_2O$ to pyrylium salts. Pyrylium salts can be converted to the corresponding phosphinines by an O^+/P exchange with a suitable phosphorus source, such as $P(SiMe_3)_3$ (Scheme 5.9). The analytical data for λ^3-phosphinines **1** and **5-3**–**5-7** are not described in here, as they have already been reported in literature by Müller *et. al.*.[8]

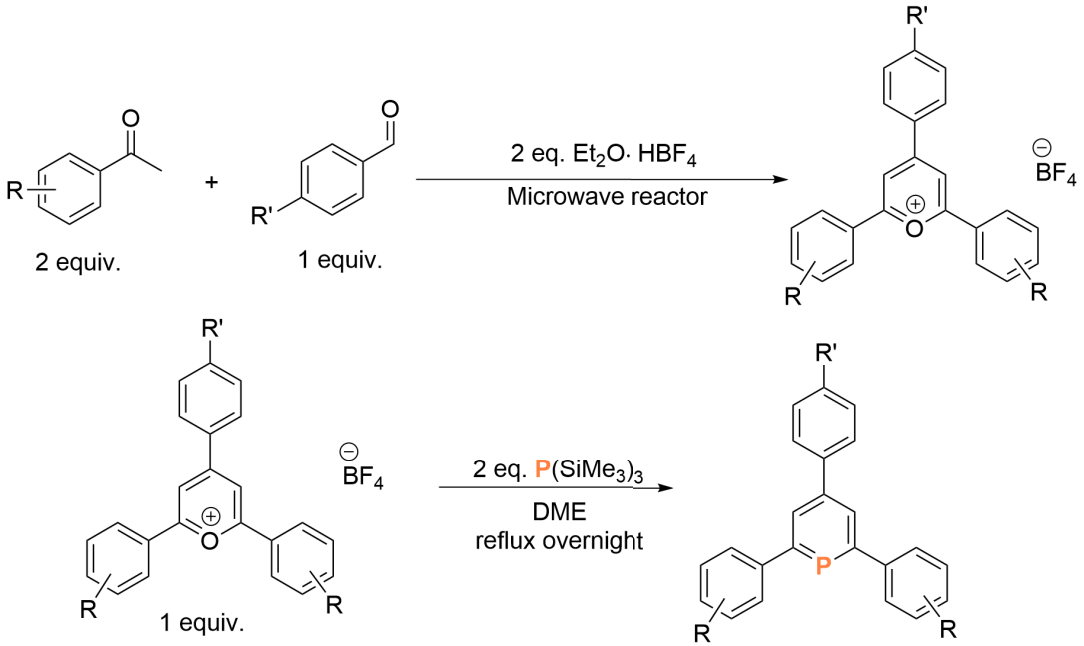

Scheme 5.9: Synthesis of λ^3-phosphinines *via* the pyrylium salt route.

5.4 Synthesis and characterization of λ^5-phosphinines

The λ^3-phosphinine **5-4** was further converted quantitatively to λ^5-phosphinine **5-8** by reaction with mercury(II) acetate as oxidation reagent in the presence of N,N'-dimethyl-ethylenediamine, according to a modified procedure described by Dimroth and co-workers (Scheme 5.10).[100] After stirring for overnight, the solution was filtered over silica (3 cm) to remove the mercury residues. The solvent of the neon yellow filtrate was then removed under vacuum and the residue was washed with pentane. After drying under a high vacuum, the product was obtained as a neon yellow solid.

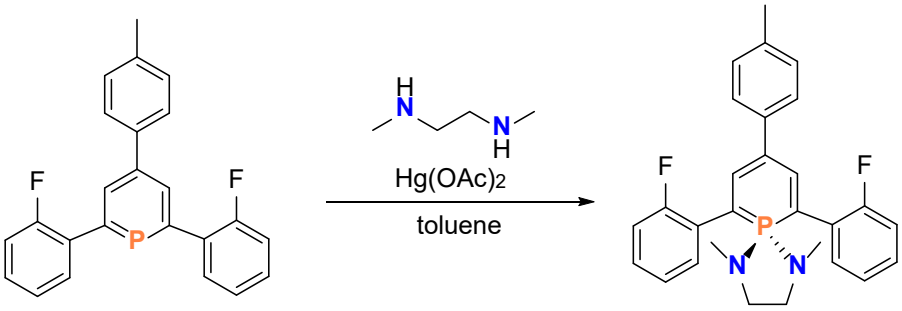

Scheme 5.10: Synthesis of **5-8**.

Due to the oxidation of the λ^3- to the λ^5-phosphinine, a substantial upfield shift from δ(ppm) = 193.0 to 34.7 was observed in the $^{31}P\{^1H\}$ NMR spectrum. The proton resonances of the phosphorus heterocycle were found in the ^1H NMR spectrum as doublet of doublets with a coupling constant of $^3J_{H,P}$ = 33.8 Hz at δ(ppm) = 7.60 (Figure 5.3).

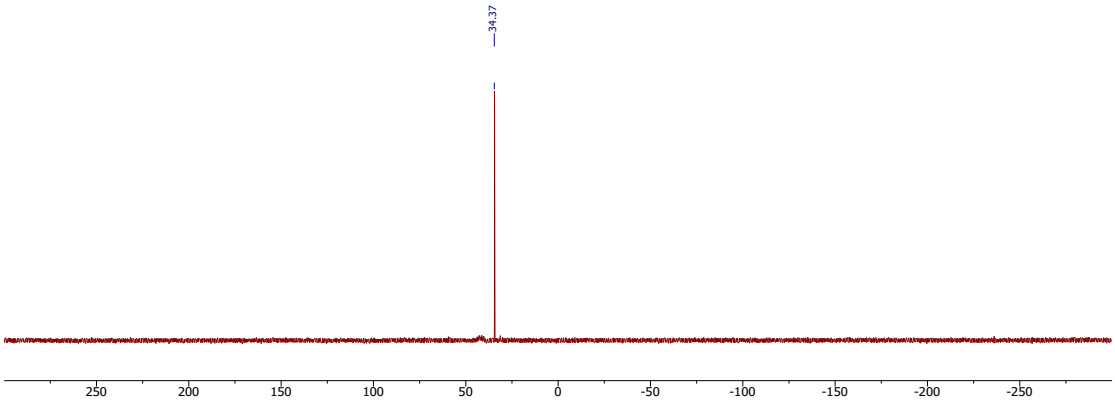

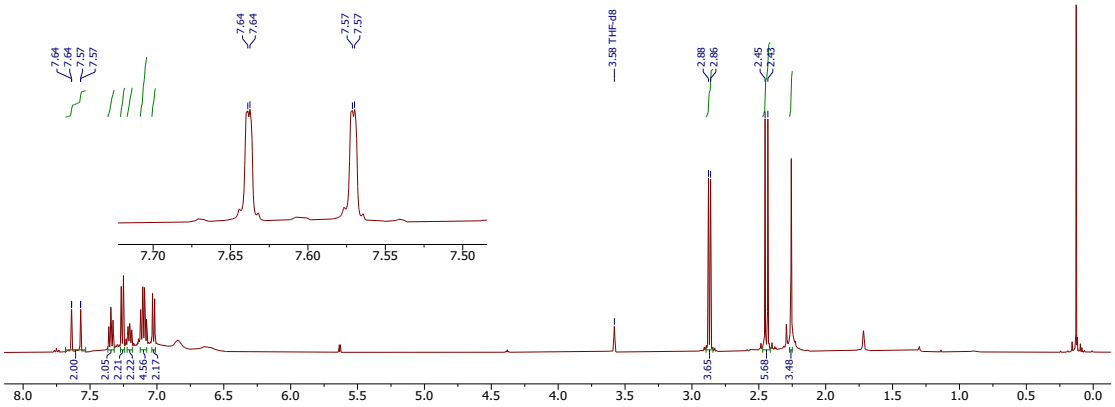

Figure 5.3: $^{31}P\{^{1}H\}$ (top) and ^{1}H NMR (bottom) spectra of **5-8**.

Although **5-8** is relatively straightforward to synthesize and to purify, it is, however, problematic to crystalize. After using different recrystallisation methods, crystals, suitable for single crystal X-ray diffraction, were finally obtained. The first step was dissolving the crude **5-8** in methanol followed by several repeated hot recrystallizations. The purified product was dissolved in ethanol, heated to reflux and allowed to cool to room temperature very slowly. Finally, the solution was placed in a freezer at T = -20 °C for recrystallization. The molecular structure of **5-8** in the crystal is depicted in Figure 5.4, along with selected bond lengths and angles.

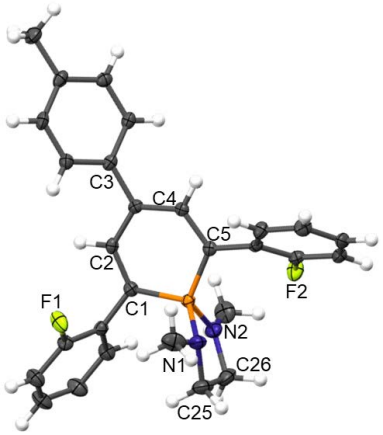

Figure 5.4: Molecular structure of **5-8** in the crystal. Displacement ellipsoids are shown at the 50% probability level. Selected bond lengths (Å) and angles (°): P1-N1: 1.644(2); P1-N2: 1.668(2); P1-C1: 1.732(3); P1-C5: 1.742(1); F1-C7: 1.356(3); F2-C20: 1.366(3); N1-C25: 1.465(4); N2-C26: 1.462(4); C1-P1-C5: 103.9(1); N1-P1-N2: 91.9(1); P1-N1-N2-C26: 155.8(2).

In **5-8**, the P1-C1 and P1-C5 bond lengths of 1.732(3) Å and 1.742(2) Å are significantly shorter compared to those in λ^3-phosphinine **5-3** (1.756(6) and 1.753(6) Å). The C1-P1-C5 angle of 103.9(1)° is considerably larger in **5-8** than the one in λ^3-phosphinine **5-3** (99.4(3)°). This can be explained by the formal sp^3-hybridization of the phosphorus atom in **5-8**. The N1-P1-N2 angle in **5-8** is 91.9(1)°, which is significantly smaller than the C1-P1-C5 angle. Overall, the phosphorus atom shows a distorted tetrahedral environment. The C-C distances in the phosphorus heterocycle are averaged between a C-C single bond and a C=C double bond. The ring formed by the P1-N1-C25-C26-N2 atoms is not planar and has a significant distortion (155.8(2)°).

The λ^3-phosphinines **1**, **5-3**–**5-7** were reacted first with methyllithium in diethyl ether to form the corresponding λ^4-phosphinine anions, which were subsequently reacted with methyl iodide, resulting in **5-9**–**5-14** (Scheme 5.11).

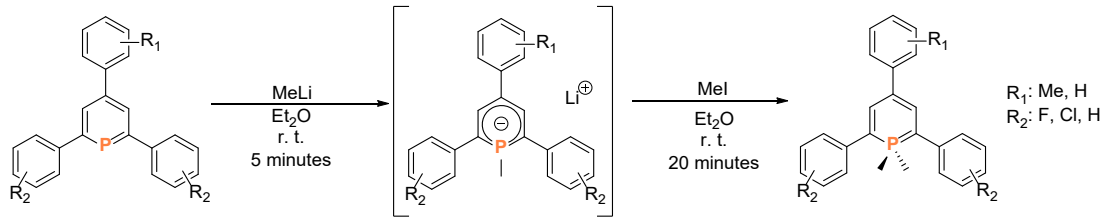

Scheme 5.11: Synthesis of λ^5-phosphinines **5-9**–**5-14**.

The solvent was removed under vacuum after the end of the reaction. The purification of these λ^5-phosphinines is rather challenging, as λ^5-phosphinines are usually soluble in common organic solvents. Moreover, some λ^5-phosphinines are very sensitive towards air and moisture, which makes them difficult to purify by column chromatography. More importantly, if by-products are produced during the reaction, they may not be purified at all using regular purification methods. Fortunately, the reactions of **1**, **5-3**–**5-7** with organolithium compounds and methyl iodide were remarkably selective to produce **5-9**–**5-14**, respectively. **5-9**–**5-12** can be dissolved in ethanol and recrystallized in a freezer at T = -20°C. For compounds **5-13** and **5-14**, crystals suitable for single crystal X-ray diffraction were not obtained up to date.

The molecular structures of **5-9**–**5-12** in the crystal are depicted in Figures 5.5–5.8,

along with selected bond lengths and angles.

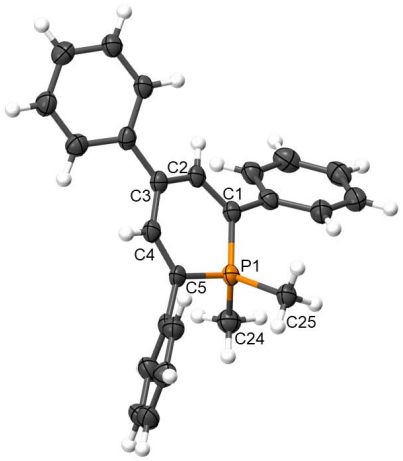

Figure 5.5: Molecular structure of **5-9** in the crystal. Displacement ellipsoids are shown at the 50% probability level. Selected bond lengths (Å) and angles (°): P1-C1: 1.756(3); P1-C5: 1.748(4); P1-C25: 1.801(6); P1-C24:1.812(4); C1-P1-C5: 104.6(2); C25-P1-C24: 102.0(2); C5-C1-P1-C3: 4.9(2).

Compound **5-9** crystallized in the triclinic crystal system in the space group *P*-1. Based on the bond lengths and angles in the molecule, a comparison can be made to λ^5-phosphinine **5-8**. The P1-C1 and P1-C5 bond lengths of 1.756(3) Å and 1.763(1) Å in **5-9** are significantly longer compared to those in **5-8** (1.732(3) and 1.748(4) Å). This observation is consistent with the fact that more electronegative atoms are connected to the phosphorus atom of the λ^5-phosphinines, resulting in shorter P-C bond lengths. The C1-P1-C5 angle of 103.90(7)° in **5-9** is similar to that in **5-8** (103.9(1)°), as the phosphorus atom shows a distorted tetrahedral environment by its four bonding partners. **5-10** crystallized with four independent molecules in the asymmetric unit (Figure 5.6).

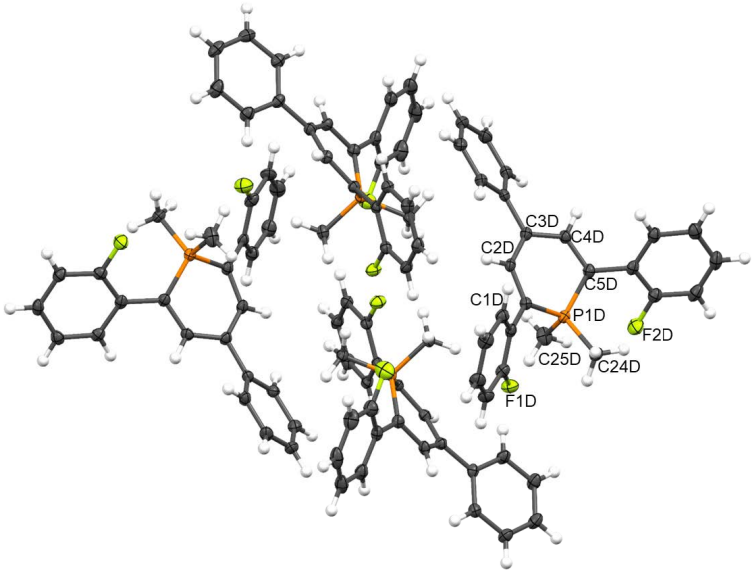

Figure 5.6: Molecular structure of **5-10** in the crystal. Displacement ellipsoids are shown at the 50% probability level. Selected bond lengths (Å) and angles (°): P1D-C1D: 1.762(3); P1D-C5D: 1.768(3); P1D-C25D: 1.813(4); P1D-C24D:1.798(3); C1D-P1D-C5D: 104.1(2); C25D-P1D-C24D: 109.0(2); C5D-C1D-P1D-C3D: 27.19(7).

The P1D-C1D and P1D-C5D bond lengths of 1.765(2) Å and 1.763(1) Å in **5-10** are similar to those in **5-9**. The C5D-C1D-P1D-C3D torsion angle of 27.19(7)° in the phosphorus heterocycle of **5-10** is much larger than the corresponding angle of 4.9(2)° in **5-9**, which shows that the 2,6-substituents have an impact on the torsion angle of the phosphorus heterocycle.

5-11 crystallized with two independent molecules in the asymmetric unit. Its structural information is similar to that of **5-10**, so it will not be repeated here.

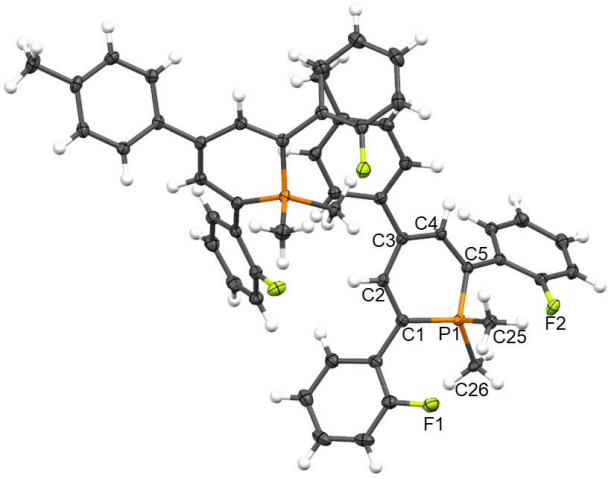

Figure 5.7: Molecular structure of **5-11** in the crystal. Displacement ellipsoids are shown at the 50% probability level. Selected bond lengths (Å) and angles (°): P1-C1: 1.765(2); P1-C5: 1.763(1); P1-C25: 1.808(1); P1-C26:1.803(1); C1-P1-C5: 103.90(7); C25-P1-C26: 108.93(7); C5-C1-P1-C3: 25.8(2).

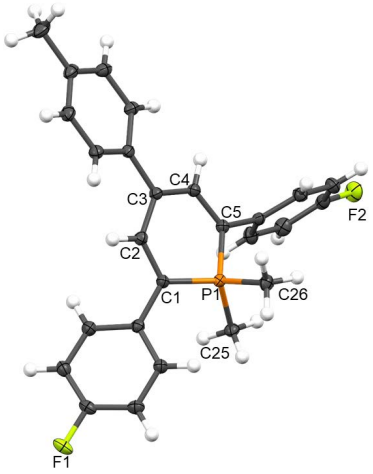

Figure 5.8: Molecular structure of **5-12** in the crystal. Displacement ellipsoids are shown at the 50% probability level. Selected bond lengths (Å) and angles (º): P1-C1: 1.749(1); P1-C5: 1.749(1); P1-C25: 1.810(1); P1-C26:1.803(1); C1-P1-C5: 103.95(6); C25-P1-C26: 103.44(6); C5-C1-P1-C3: 20.42(7).

For compound **5-12**, the fluorine atoms are at the *para*-position of the 2,6-substituents of the heterocyclic ring. **5-12** crystallized in the monoclinic crystal system in the space group $P2_1/n$. The P1-C1 and P1-C5 bond distances in **5-12** are equal (1.749(1) Å) and

significantly smaller than the P1-C1 and P1-C5 bond lengths in **5-11** (P1-C1: 1.765(2) Å; P1-C5: 1.763(1) Å). This suggests that the P-C bond lengths in λ^5-phosphinines may be influenced not only by the substituents on the phosphorus atom, but also by the 2,6-substituents of the phosphorus heterocycle.

5-13 is an air, moisture and temperature sensitive compound. In the $^{31}P\{^1H\}$ NMR spectrum, a resonance is found at δ(ppm) = -7.03. In the ^1H NMR spectrum, the chemical shift of the methyl groups at the phosphorus atom appears at δ(ppm) = 1.55, with a $^2J_{H,P}$ coupling constant of 12.5 Hz (Figure 5.9). Unfortunately, no suitable crystals for single crystal X-ray diffraction measurement were obtained.

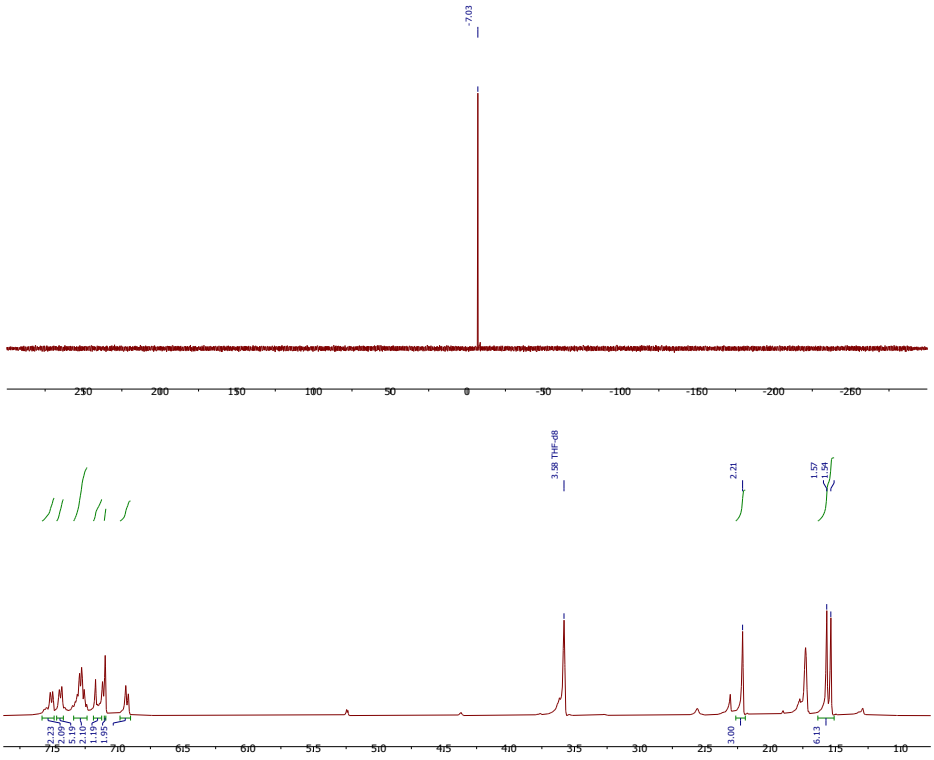

Figure 5.9: $^{31}P\{^1H\}$(top) and ^1H NMR (bottom) spectra of **5-13**.

Crystals of **5-14** are not available up to date. **5-14** has a very good solubility in common organic solvents.

Next, it was investigated whether it is possible to introduce two different substituents at the phosphorus atom. This has not been achieved before. Thus the reaction of λ^3-phosphinines first with phenyl lithium and subsequently with methyl iodide was investigated. Indeed, λ^3-phosphinines **1**, **5-3**–**5-6** react with phenyl lithium in diether

ethyl to form the corresponding λ^4-phosphinine anions, which further react with methyl iodide to give compounds **5-15**–**5-18** (Scheme 5.12).

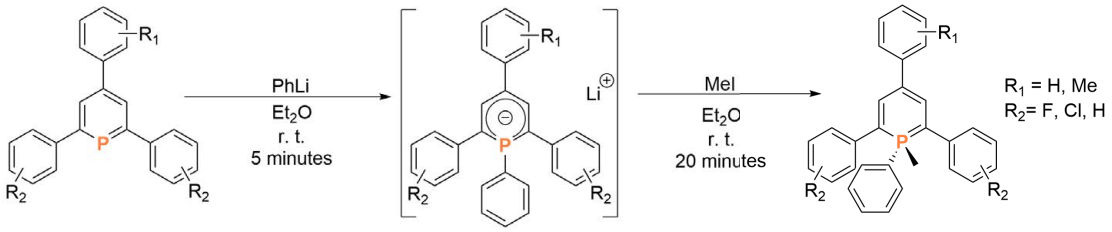

Scheme 5.12: Synthesis of **5-15**, **5-16**, **5-17** and **5-18**.

The resonances of these compounds were found in the range of δ(ppm) = -5.9-2.4 in the $^{31}P\{^1H\}$ NMR spectra. In the ^1H NMR spectra, the chemical shift of the methyl groups connected directly to the phosphorus atoms was observed as doublet resonances at δ(ppm) ≈ 2.1 with coupling constants of $^2J_{H,P}$ ≈ 13 Hz. The molecular structures of **5-15**–**5-18** are depicted in Figures 5.10–5.13, along with selected bond lengths and angles.

Compounds **5-15**, **5-17** and **5-18** crystallized in the monoclinic crystal system, while **5-16** crystallized in the orthorhombic crystal system. The C1-P1-C5 angles in these λ^5-phosphinines are around 104°, which is similar to that in 1,1'-dimethyl-λ^5-phosphinines.

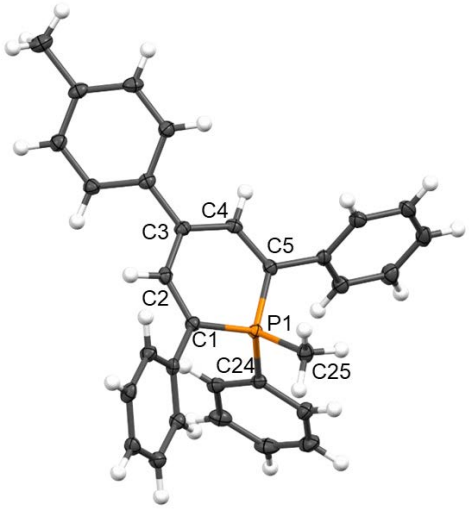

Figure 5.10: Molecular structure of **5-15** in the crystal. Displacement ellipsoids are shown at the 50% probability level. Selected bond lengths (Å) and angles (°): P1-C1: 1.753(2); P1-C5: 1.753 (2); P1-C25: 1.821(2); P1-C24:1.801(2); C1-P1-C5: 104.79(9); C25-P1-C24: 104.81(9); C5-C1-P1-C3: 8.2 (1).

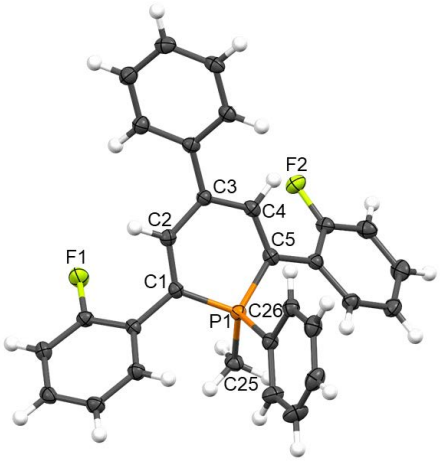

Figure 5.11: Molecular structure of **5-16** in the crystal (H atoms were omitted for clarify). Displacement ellipsoids are shown at the 50% probability level. Selected bond lengths (Å) and angles (°): P1-C1: 1.763(2); P1-C5: 1.763 (2); P1-C25: 1.822(2); P1-C24:1.807(2); C1-P1-C5: 104.6(2); C25-P1-C24: 103.8(1); C5-C1-P1-C3: 16.0 (1).

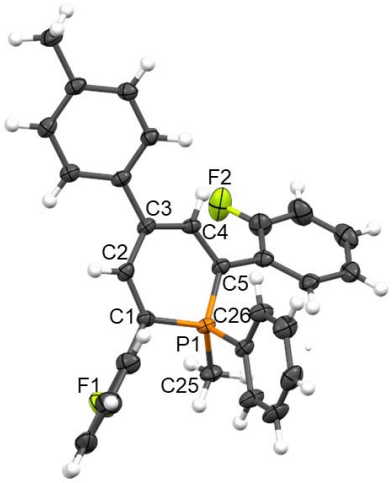

Figure 5.12: Molecular structure of **5-17** in the crystal. Displacement ellipsoids are shown at the 50% probability level. Selected bond lengths (Å) and angles (°): P1-C1: 1.750(3); P1-C5: 1.764(3); P1-C25: 1.809(3); P1-C26:1.818(3); C1-P1-C5: 104.6(2); C25-P1-C26: 105.3(1); C5-C1-P1-C3: 9.3 (2).

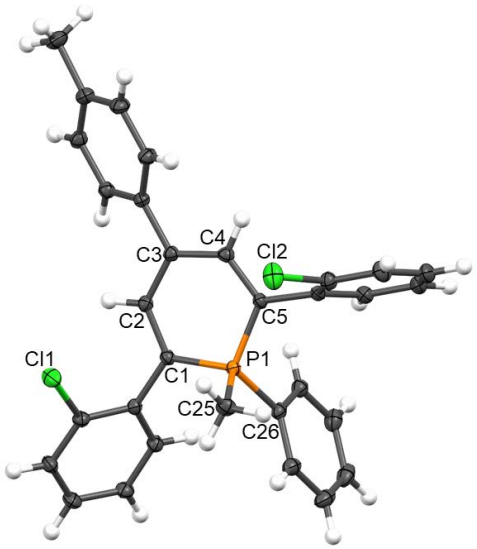

Figure 5.13: Molecular structure of **5-18** in the crystal. Displacement ellipsoids are shown at the 50% probability level. Selected bond lengths (Å) and angles (°): P1-C1: 1.749(2); P1-C5: 1.752 (2); P1-C25: 1.808(1); P1-C26:1.817(1); Cl1-C7: 1.743(2); Cl2-C20: 1.742(1); C1-P1-C5: 104.83(7); C25-P1-C26: 104.33(7); C5-C1-P1-C3: 7.03(3).

The attempt to synthesize λ^5-phosphinines **5-22**–**5-26** by reaction between λ^3-phosphinines with the corresponding organolithium compounds resulted in a mixture of unidentified compounds that could not be separated. Thus, 1,1'-dichloro-λ^5-phosphinines were synthesized first, as the reaction of 1,1'-dichloro-λ^5-phosphinine with organolithium compounds selectively produces λ^5-phosphinines with alkyl- and aryl- substituents. **5-19**–**5-21** were synthesized in accordance to the literature.[101] λ^3-phosphinines **1**, **5-3** and **5-4** react with PCl_5 in toluene under irradiation with UV light, resulting in the corresponding 1,1'-dichloro-λ^5-phosphinines (Scheme 5.13).

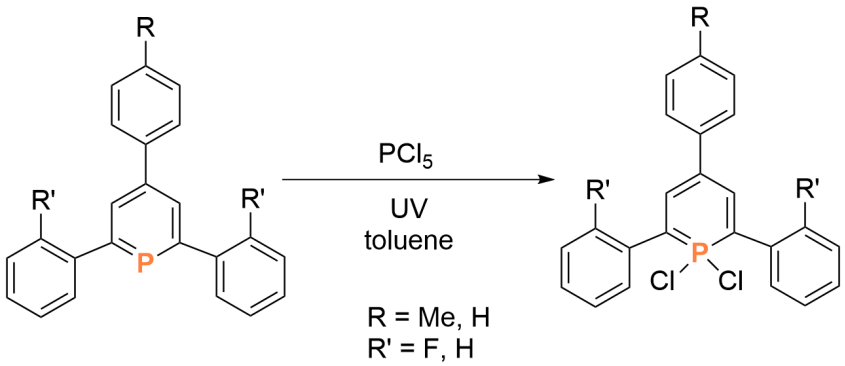

Scheme 5.13: Synthesis of **5-19**, **5-20** and **5-21**.

After the reaction was complete, the volatiles were removed under vacuum and the residual solid was dissolved in refluxing acetonitrile for recrystallization. The 1,1'-dichloro-λ^5-phosphinines are sensitive to air and moisture. **5-21** crystallized with two independent molecules in the asymmetric unit (Figure 5.14).

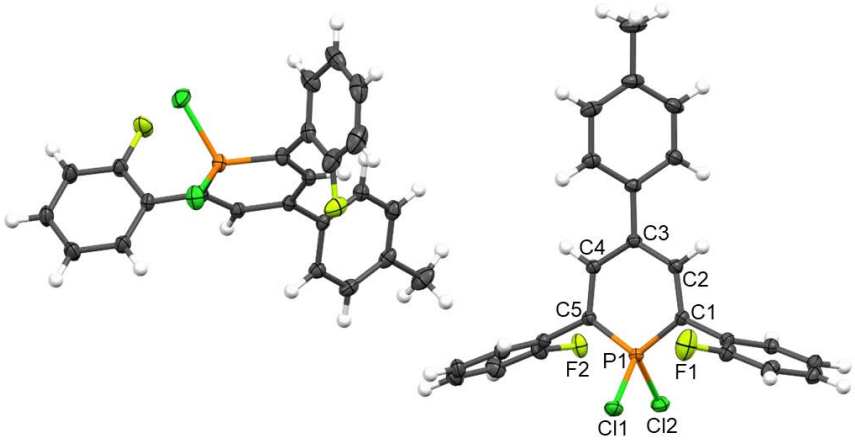

Figure 5.14: Molecular structure of **5-21** in the crystal. Displacement ellipsoids are shown at the 50% probability level. Selected bond lengths (Å) and angles (°): P1-C1: 1.708(1); P1-C5: 1.705 (1); P1-C25: 1.808(1); C5-C1-P1-C3: 0.78(6).

The P1-C5 and P1-C1 bond lengths in **5-21** are 1.708(1) Å and 1.705(1) Å, respectively, which are much shorter than those in **5-11**(1.765(2) and 1.763(1) Å) and λ^3-phosphinine **5-3**(1.756(6) and 1.753(6) Å). This is due to the high electronegativity of the Cl atoms (*vide supra*).

λ^5-phosphinine **5-22** was obtained by reaction of 1,1'-dichloro-λ^5-phosphinine **5-21** with PhMgBr in a mixture of toluene and diethyl ether (Scheme 5.14). After the reaction was complete, the volatiles were removed under vacuum and the residual solid was purified by recrystallization. Crystals were obtained by evaporating the MeCN solution of **5-22** in the glovebox. Using PhMgBr in this reaction is necessary as the reaction between phenyl lithium and **5-21** mainly produces the λ^3-phosphinine **5-4**.

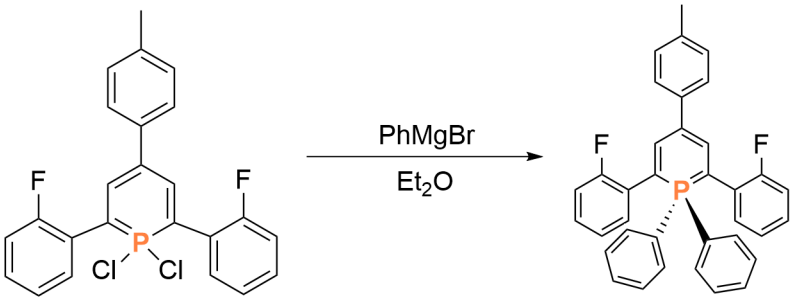

Scheme 5.14: Synthesis of **5-22**.

λ^5-phosphinine **5-22** shows a single resonance at δ(ppm) = 5.2 in the $^{31}P\{^1H\}$ NMR spectrum. The ^1H NMR spectrum displays the proton resonances of the phosphorus heterocycle at δ(ppm) = 7.94 with a coupling constant of $^3J_{H,P}$ = 30.2 Hz.

The molecular structure of **5-22** is depicted in Figure 5.15, along with selected bond lengths and angles. The P1-C1 and P1-C5 bond lengths in **5-22** are 1.753(1) Å and 1.752(1) Å, respectively, which are similar to those to **5-18**.

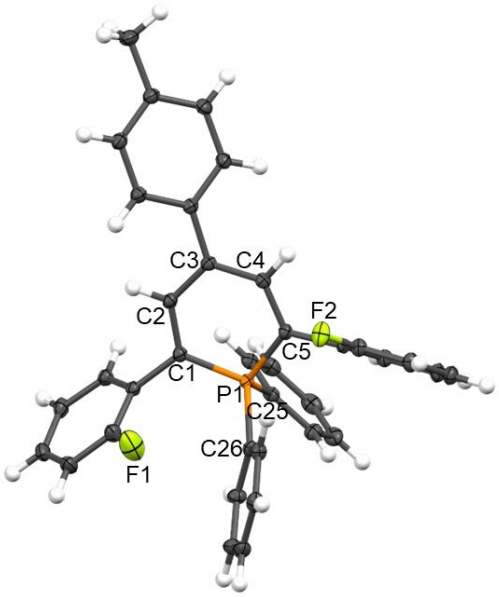

Figure 5.15: Molecular structure of **5-22** in the crystal. Displacement ellipsoids are shown at the 50% probability level. Selected bond lengths (Å) and angles (°): P1-C1: 1.753(1); P1-C5: 1.752 (1); P1-C25: 1.823(1); P1-C31:1.812(1); C1-P1-C5: 103.91(5); C25-P1-C31: 103.79(5); C5-C1-P1-C3: 7.94(5).

Next, an attempt was made to synthesize spiro-λ^5-phosphinines, which have already been described in literature. Only one procedure has been reported in literature, which

involves the use of toxic [1,1′-biphenyl]-2,2′-diylmercury. It can be considered that 1,1'-dichloro-λ^5-phosphinines might react with 2,2'-dilithiobiphenyl derivatives to form spiro-λ^5-phosphinines. Indeed, reaction of 1,1'-dichloro-λ^5-phosphinines with 2,2'-dilithiobiphenyl derivatives leads selectively to 1,1'-bipheyl-λ^5-phosphinines **5-23**–**5-26** (Scheme 5.15). It is important that the syntheses were carried out by very slow dropwise addition of a toluene solution of 1,1'-dichloro-λ^5-phosphinines to an ether solution of 2,2'-dilithiobiphenyl derivatives at T = -78 ºC. The reaction mixtures were allowed to warm up to room temperature slowly and continued to stir for overnight. At the end of the reaction, the mixtures were filtered to remove the lithium chloride and the solvent was removed under vacuum to obtain a clean compound. **5-23**–**5-26** are air- and moisture-sensitive orange and dark red solids. The purified **5-25** was dissolved in hot acetonitrile for recrystallization. Crystals suitable for single crystal X-ray diffraction, were obtained upon cooling the solution down to T = -20 ºC.

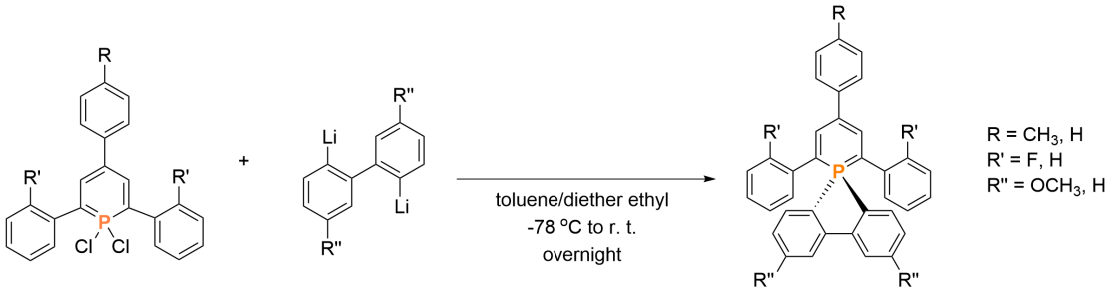

Scheme 5.15: Synthesis of **5.20**, **5.21**, **5.22** and **5.24**.

5-25 shows a resonance at δ(ppm) = 0.9 in the $^{31}P\{^1H\}$ NMR spectrum. The proton signals of the phosphorus heterocycle appear at δ(ppm) = 7.65 ($^3J_{H,P}$= 30.9, $J_{H,H}$ = 1.2 Hz) in the ^1H NMR spectrum (Figure 5.16 and 5.17).

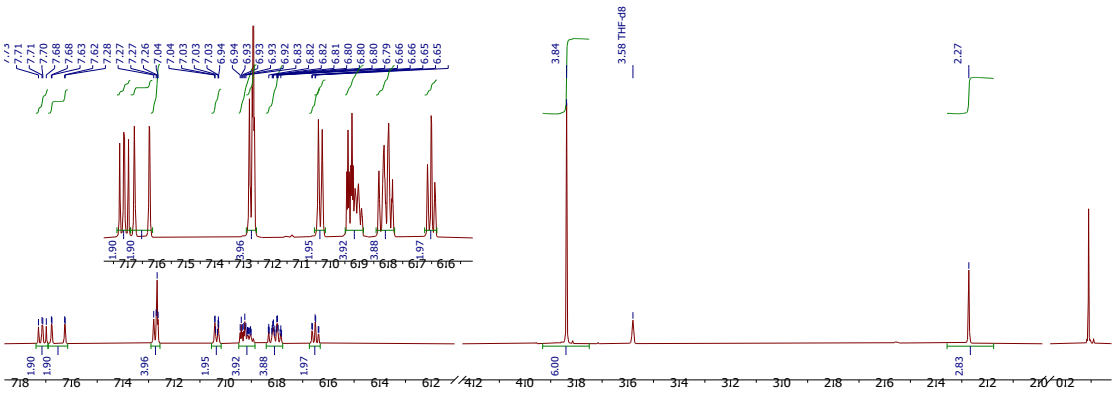

Figure 5.16: ^{1}H NMR spectrum of **5-24**.

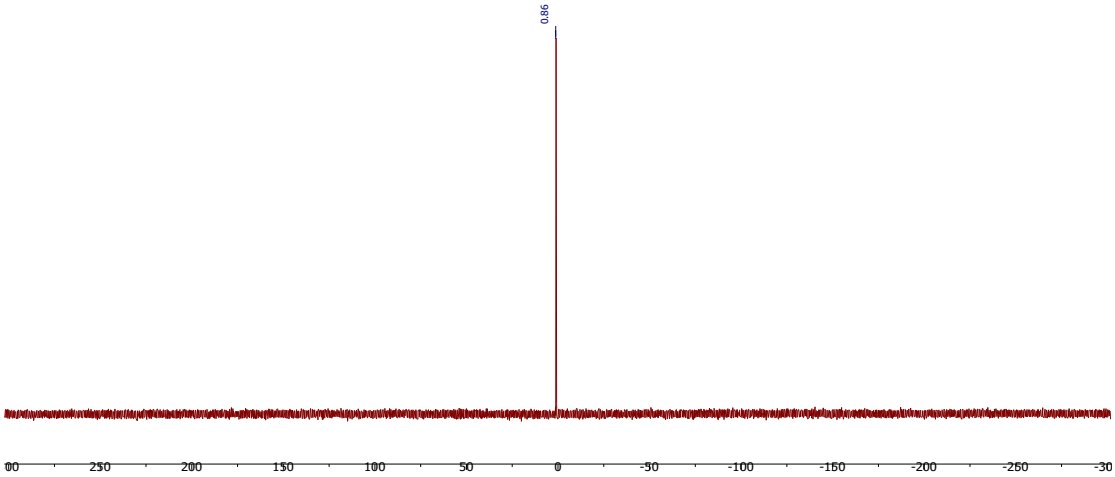

Figure 5.17: ^{31}P{^{1}H} NMR spectrum of **5-24**.

The molecular structure of **5-25** in the crystal is depicted in Figure 5.18, along with selected bond lengths and angles. **5-25** crystallized in the triclinic crystal system in the space group *P*-1. The crystallographic characterization of **5-25** shows a tetrahedral environment around the phosphorus atom, while the biphenyl unit is almost perpendicular to the plane of the phosphorus heterocycle. The C25-P1-C36 angle of 90.5(1)° in **5-25** is even slightly smaller than that in **5-8** [91.9(1)°]. This can be explained by the biphenyl substituent at the phosphorus atom that forms a closed 5-membered ring with the P1-C25-C30-C31-C36 atoms.

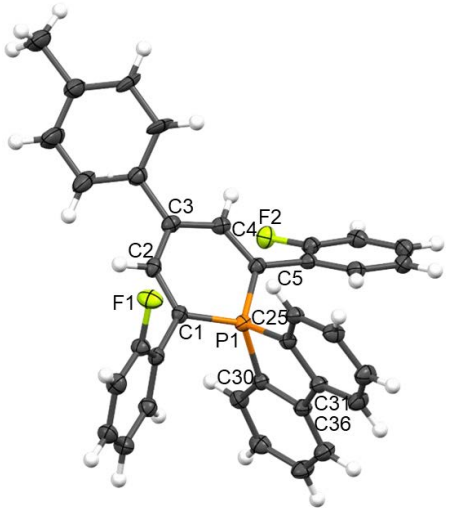

Figure 5.18: Molecular structure of **5-25** in the crystal. Displacement ellipsoids are shown at the 50% probability level. Selected bond lengths (Å) and angles (°): P1-C1: 1.738(2); P1-C5: 1.751 (2); P1-C25: 1.808(2); P1-C36:1.819(2); C1-P1-C5: 105.1(1); C25-P1-C36: 90.5(1); C5-C1-P1-C3: 2.1(1).

5-23, **5-24** and **5-26** are similar to **5-25** in terms of NMR spectroscopic data. Crystals, suitable for single crystal X-ray diffraction, were not available up to date, therefore these compounds are not discussed in detail.

5.5 Photophysical properties of λ^5-phosphinines

In cooperation with the group of Prof. Muriel Hissler (Université de Rennes, France), the photophysical properties of selected λ^5-phosphinines were investigated.

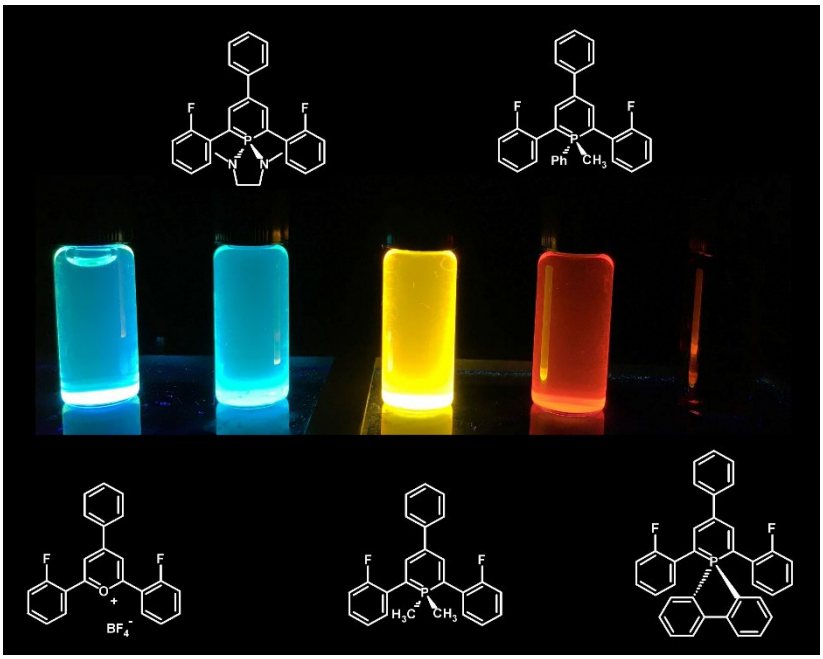

Figure 5.19: Fluorescence emission of λ^5- phosphinines and pyrylium salt under UV light.

The analysis of the absorption and emission spectra of **5-10**, **5-11** and **5-14** reveals that the different substituents at the 4-position of phosphorus heterocycle have almost no effect on the optical properties of the λ^5-phosphinines (Figures 5.20 and 5.21). These results contrast with the previously reports by Hayashi and co-workers as their derivatives of 2,6-dicyano-λ^5-phosphinines show differences in the luminescence properties when different substituents at the 4-position of phosphorus heterocycle are introduced.[91]

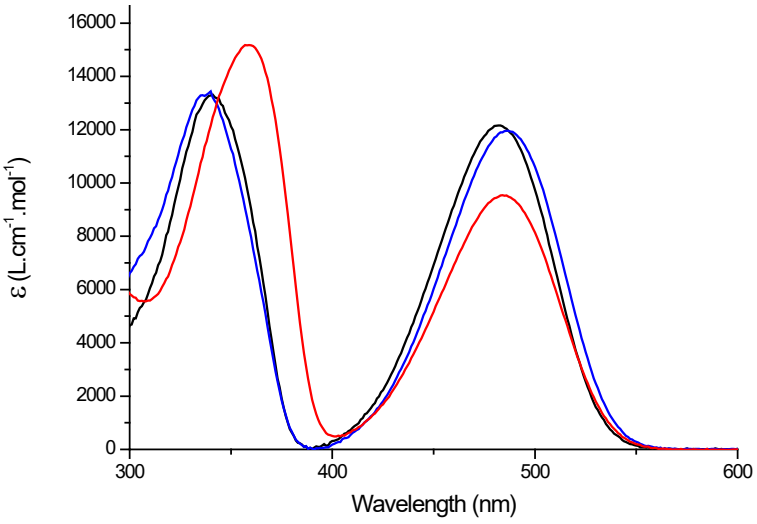

Figure 5.20: UV absorption spectra of **5-10**(black), **5-11**(blue) and **5-14**(red) in toluene.

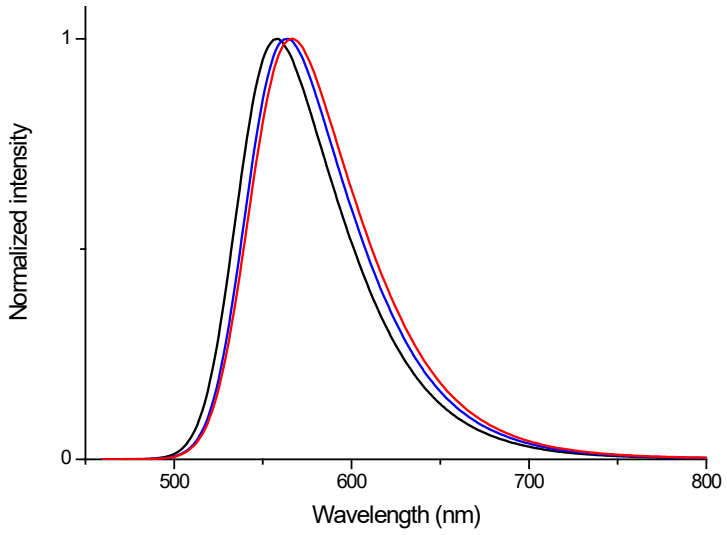

Figure 5.21: Emission spectra of **5-10**(black), **5-11**(blue) and **5-14**(red) in toluene.

The absorption spectra of **5-10**, **5-11** and **5-14** show the maximum lowest energy (red-edge) absorption band at around $\lambda_{abs,max} \approx 483$ nm with an extinction coefficient of $\varepsilon \approx 11500$ L/(mol·cm). The fluorescence emission of **5-10**, **5-11** and **5-14** is intense in solution with quantum yields of $\Phi_f \approx 72$ % and slightly red-shifted compared to the maximum of the red-edge absorption band (Stoke shift: $\Delta\lambda \approx 80$ nm) to $\lambda_{em,max} \approx 563$ nm.

Furthermore, studies were carried out on how different substituents at the 2,6-positions of the aromatic ring can impact the photophysical properties of λ^5-phosphinines. The absorption spectra shown in Figure 5.22 exhibit that different 2,6-substituents at the phosphinine ring have a significant effect on the absorption properties of the corresponding λ^5-phosphinines. A comparison of **5-9**, **5-11**, **5-12** and **5-13** revealed that the maximum of the red-edge absorption band ($\lambda = 486$ nm) of λ^5-phosphinine **5-11** (*ortho*-F-substituted) has the highest ε-value and a slight red-shift, while the maximum of the lowest energy absorption band of **5-13** (*ortho*-Cl-substituted) is obviously blue-shifted ($\lambda_{abs,max} = 450$ nm) and has the lowest ε-value, which is only 20 % of that of **5-11**. The wavelength differences in the fluorescence emission of λ^5-phosphinines **5-9**, **5-10**, **5-11** and **5-12** are within 20 nm (Figure 5.23). However, the photoluminescence quantum yield (PLQY) of **5-13** ($\Phi_f = 36$ %) is only 50 % of that of **5-11**, which can be

explained by the fact that **5-13** has a significantly lower extinction coefficient. Overall, different 2,6-substituents at the phosphorus heterocycle have major effects on the absorption and the PLQY properties of the corresponding λ^5-phosphinines.

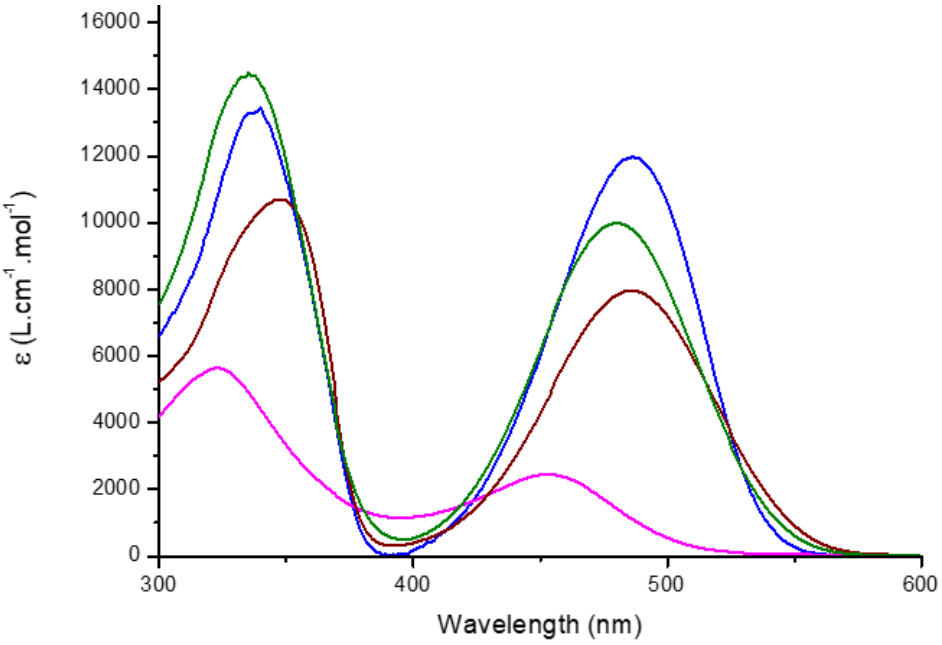

Figure 5.22: UV absorption spectra of **5-9**(brown), **5-11**(blue), **5-12**(green) and **5-13**(violet) in toluene.

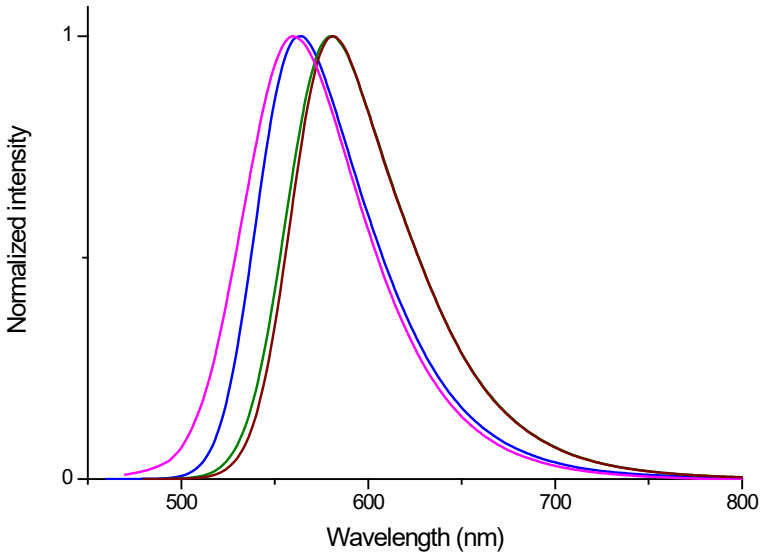

Figure 5.23: Emission spectra of **5-9**(brown), **5-11**(blue), **5-12**(green) and **5-13**(violet) in toluene.

Finally, the photophysical properties of λ^5-phosphinines containing different substituents at the phosphorus atom were investigated in detail. Figure 5.24 shows the

absorption spectra of **5-8**, **5-10**, **5-17**, **5-22** and **5-23**. It can be observed that the different substituents at the phosphorus atoms result in a significant effect on the absorption spectra of the corresponding λ^5-phosphinines, with the maxima of lowest energy absorption bands ranging from λ = 398 nm for **5-7** to λ = 498 nm for **5-22**. **5-10** has the highest extinction coefficient of ε = 12000 L/(mol·cm) and **5-22** has an intensity of less than 3000 L/(mol·cm). Also **5-25** presents an intense band centered at λ = 454 nm along with a red-shifted shoulder tailing down to λ = 600 nm.

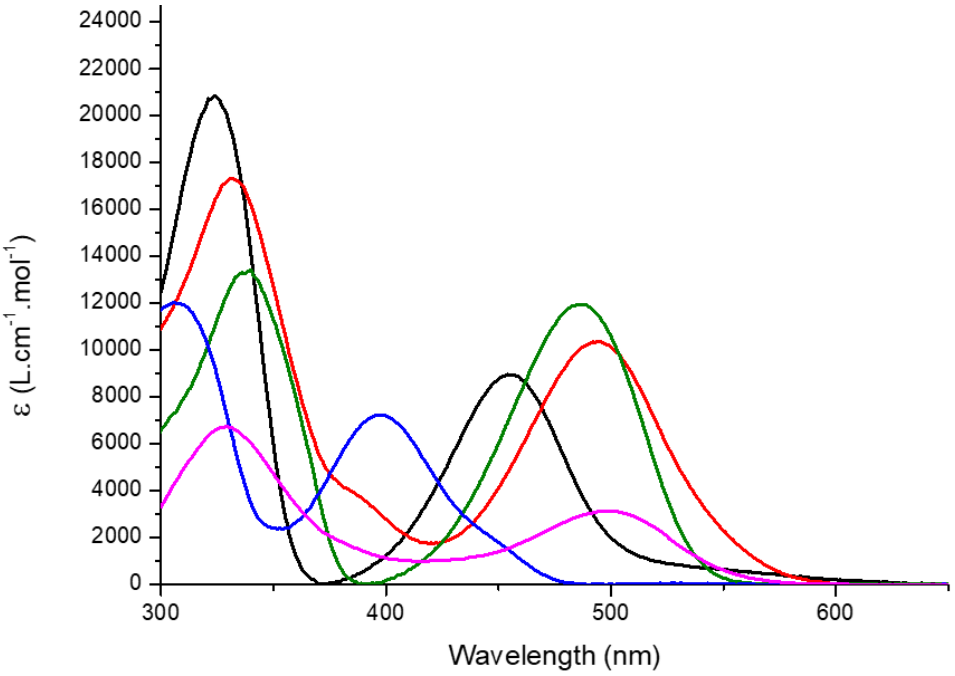

Figure 5.24: UV absorption spectra of **5-8**(blue), **5-10**(green), **5-17**(red), **5-22** (violet) and **5-25**(black) in toluene.

From the analysis of the absorption spectra, it can be anticipated that the fluorescence emissions of λ^5-phosphinines are also significantly affected by the substituents at the phosphorus atoms. Figure 5.25 shows the emission spectra of **5-8**, **5-10**, **5-17** and **5-22**. The fluorescence emissions of **5-17** and **5-22** can reach $\lambda_{em,max}$ > 620 nm. The λ^5-phosphinine **5-17** is the first case in which fluorescence emission in solution can reach to the region of red light. Under UV light, **5-8** and **5-10** exhibit blue and green fluorescence in the solution, respectively. The quantum yields of **5-8**, **5-10**, **5-17** and **5-22** were 17%, 74%, 15% and 3%, respectively. This suggests a remarkable relationship

between the decrease in the quantum yields of λ^5-phosphinines and the increase in the number of phenyl substituents to the phosphorus atom.

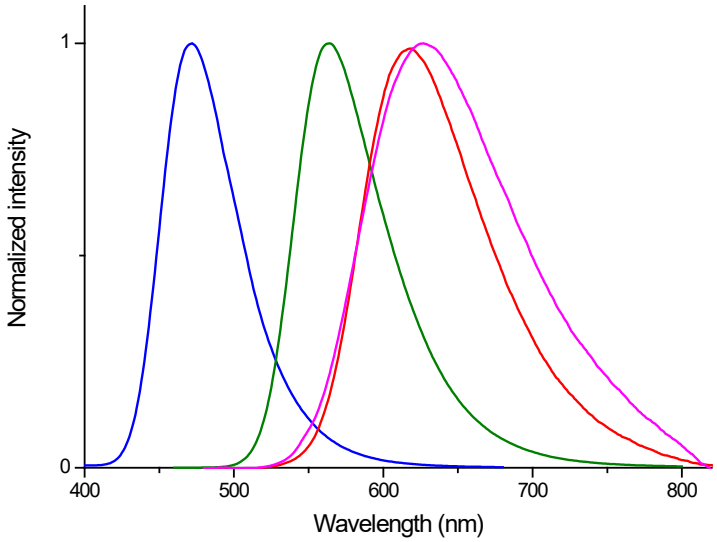

Figure 5.25: Emission spectra of **5-8**(blue), **5-10**(green), **5-17**(red), and **5-22** (violet) in toluene.

At room and low temperatures, no fluorescence emission was detected in the visible and NIR regions for **5-23**, **5-24**, **5-25** and **5-26** both in solution and in the solid state. **5-23** shows an intense band centered at λ = 480 nm along with a red-shifted shoulder tailing down to about λ = 660 nm, which indicates a small spiro-conjugation (Figure 5.26).[122]

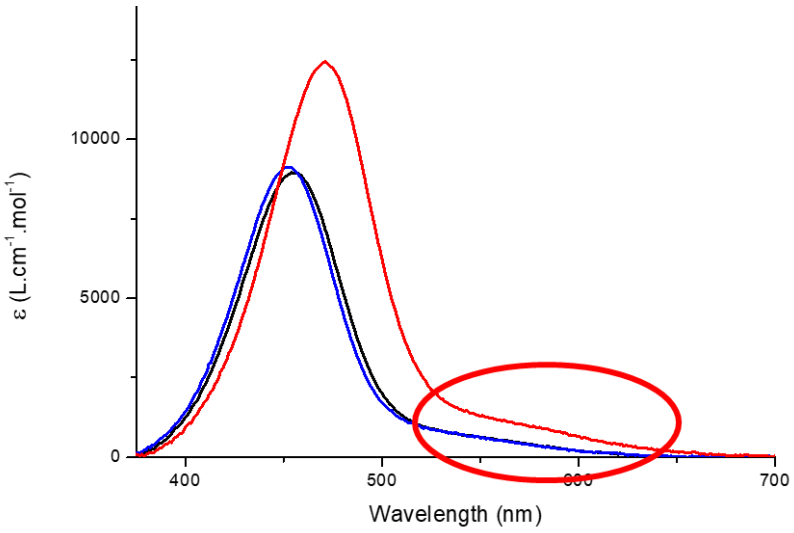

Figure 5.26 UV absorption spectra of **5-20**(black), **5-21**(blue), **5-22**(red) and **5-24**(orange) in toluene.

Overall, the substituents at the phosphorus atom have the most significant effect on the optical properties of the λ^5-phosphinines compared to the substituents at the other positions of the phosphorus heterocycle.

Table 5.2 summarizes the data from the optical measurements of selected λ^5-phosphinines.

Table 5.2: Optical data of selected λ^5-phosphinines in solution

Sample name	$\lambda_{max,abs}$ [nm][a]	ε [L/mol·cm]	$\lambda_{max,em}$ [nm][a]	Φ_f [%]
5-7	483	9700	567	70 [c]
5-8	398	7150	472	17 [b]
5-10	480	10050	580	65 [d]
5-11	486	12000	564	74 [c]
5-13	453	2400	560	36 [c]
5-15	519	5850	628	16 [d]
5-16	494	10250	619	15 [d]
5-18	484	4500	616	9 [d]
5-22	498	3020	627	3 [d]
5-25	454	9000	-	-
5-26	453	8500	-	-

[a] Measured in toluene. [b] Fluorescence quantum yields determined using quinine sulfate as standard, ±15%. [c] Fluorescence quantum yields determined using fluorescein λ_{exc} = 450 nm as standard, ±15%. [d] Fluorescence quantum yields determined using Rhodamine 6G as standard, ±15%.

5.6 Experimental details

5.6.1 General remarks

Unless otherwise stated, all syntheses were performed under an inert argon atmosphere using modified Schlenk techniques or in a MBraun glovebox. All commercially available chemicals were used as received. Dry, deoxygenated solvents were prepared using standard techniques or collected from a MBraun solvent purification system. The NMR spectra were recorded on a JEOL ECX400 (400 MHz), Bruker 500 MHz and 600

MHz spectrometers and chemical shifts are reported relative to the residual resonance in the deuterated solvents. λ^3-Phosphinines, **5-15, 5-19**, **5-20**, 2,2'-dilithiobiphenyl and 2,2'-dilithio-4,4'-dimethoxy-biphenyl were prepared according to the literature.[101,107,108] UV/Vis spectra were recorded at room temperature with a VARIAN Cary 5000 spectrophotometer. UV/Vis/NIR emission and excitation spectra measurements were recorded with an FL 920 Edinburgh Instrument equipped with a Hamamatsu R5509-73 photomultiplier for the NIR domain (300-1700 nm) and corrected for the response of the photomultiplier. Quantum yields were calculated relative to quinine sulfate (H_2SO_4, 0.1 M, $\Phi_{ref} = 0.55$), fluorescein λ_{exc} = 450 nm and Rhodamine 6G.

5.6.2 Synthesis of 5-8

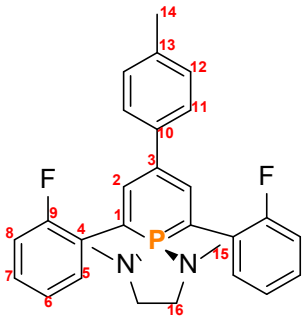

Phosphinine (**5-4**, 520 mg, 1.39 mmol) and mercury acetate (486 mg, 1.53 mmol) were dissolved in toluene (15 mL) and subsequently mixed with N,N'-dimethylethylenediamine (0.16 ml, 1.53 mmol) at room temperature. After stirring overnight, the solution was filtered over silica (3 cm) to remove the mercury residues. The solvent of the neon yellow filtrate was then removed under vacuum and the residue was washed with pentane. After drying under vacuum, the product was obtained as a neon yellow solid. Yield: 352 mg (0.84 mmol, 55%).

^{1}H NMR (500 MHz, THF-d_8) δ 7.60 (d, $^3J_{H,P}$ = 33.8 Hz, C_5H_2P), 7.34 (tt, J = 7.8, 1.6 Hz, 2H, *2,6-Ar*), 7.26 (d, J = 8.1 Hz, 2H, *4-Tol*), 7.21 (m, 2H, *2,6-Ar*), 7.14 – 7.07 (m, 4H, *2,6-Ar*), 7.03 (d, J = 8.1 Hz, 2H, *4- Tol*), 2.87 (d, J = 7.8 Hz, 4H, -CH_2-CH_2), 2.44 (d, $^3J_{H,P}$ = 10.4 Hz, 6H, -NCH_3), 2.26 (s, 3H, *4-Tol*).

$^{13}C\{^1H\}$ NMR (126 MHz, THF-d_8) δ 161.1 (dd, $^1J_{C,F}$ = 244.4 Hz, $^3J_{C,P}$ = 5.8 Hz, *C9*), 140.7 (d, *J* = 2.1 Hz, *C10*), 139.9 (d, $^3J_{C,P}$ = 9.1 Hz, *C3*), 132.6 (s, *C13*), 132.3 (t, $^3J_{C,F}$ = 7.5 Hz, *C5*), 128.7 (s, *C12*), 127.9 – 127.6 (m, *C4*), 127.5 (d, $^3J_{C,F}$ = 7.6 Hz, *C7*), 124.8 (s, *C11*), 123.5 (d, $^4J_{C,F}$ = 4.3 Hz, *C6*), 115.5 (d, $^2J_{C,F}$ = 23.5 Hz, *C8*), 112.6 (d, $^2J_{C,P}$ = 15.0 Hz, *C2*), 88.8 (d, $^1J_{C,P}$ = 129.2 Hz, *C1*), 47.1 (d, *J* = 8.7 Hz, *C16*), 30.4 (s, *C15*), 20.1 (s, *C14*) ppm.

$^{31}P\{^1H\}$ NMR (162 MHz, C_6D_6) δ 34 ppm.

^{19}F NMR (376 MHz, C_6D_6) δ -114 ppm.

HR-ESI MS (*m/z*): 460.1870 g/mol (calculated: 460.1874 g/mol) $[M]^+$.

General method for synthesis of 5-9, 5-10, 5-11, 5-12, 5-13 and 5-14

λ^3-Phosphinine (0.56 mmol) was dissolved in Et_2O (10 ml) and MeLi (1.6 M, 0.39 ml, 1.1 equiv., 0.62 mmol) was added slowly at room temperature. After stirring for 5 minutes, MeI (0.042 ml, 1.2 equiv., 0.67 mmol) was added to solution. The reaction was stirred for another 20 minutes at room temperature and after this time the solvent was removed under vacuum. Finally, the crude solid was dissolved in hot ethanol and crystals were acquired upon cooling the solution down.

5.6.3 Synthesis of 5-9

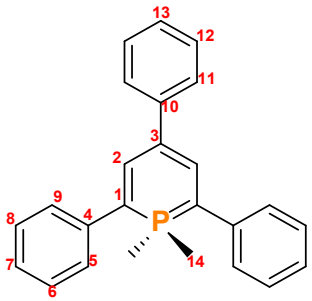

Starting materials: Phosphinine (**1**, 181.6 mg, 0.56 mmol). Yield: 48 mg (0.13 mmol, 24 %).

^1H NMR (400 MHz, *MeCN-d_3*) δ 7.50 – 7.40 (m, 5H, *2,6-Ar*), 7.40 – 7.30 (m, 7H, C_5H_2P/*2,6-Ar/4-Ph*), 7.22 (dtd, *J* = 9.6, 7.4, 1.5 Hz, 4H, *2,6-Ar*), 7.04 – 6.96 (m, 1H, *4-Ph*), 1.88 (d, $^2J_{H,P}$ = 12.5 Hz, 6H, 1,1'-CH_3) ppm.

$^{13}C\{^1H\}$ NMR (101 MHz, *MeCN-d_3*) δ 144.3 (s, *C10*), 141.4 (s, *C9*), 141.3 (s, *C5*), 138.2 (d,

$^{2}J_{C,P}$ = 6.7 Hz, *C4*), 129.6 (s, *C12*), 129.4 (s, *C7*), 128.8 (d, $^{3}J_{C,P}$ = 5.3 Hz, *C3*), 126.0 (s, *C6*), 124.3 (s, *C11*), 123.9 (s, *C13*), 113.6 (s, *C8*), 111.9 (d, $^{2}J_{C,P}$ = 12.6 Hz, *C2*), 84.8 (d, $^{1}J_{C,P}$ = 94.1 Hz, *C1*), 19.3 (d, $^{1}J_{C,P}$ = 56.9 Hz, *C14*) ppm.

^{31}P{^{1}H} NMR (162 MHz, *MeCN-d*$_3$) δ -6 ppm.

5.6.4 Synthesis of 5-10

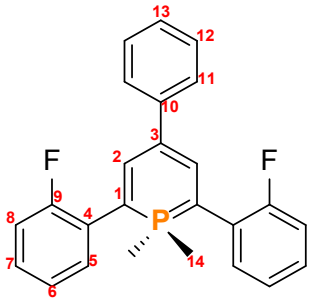

Starting materials: Phosphinine (**5-3**, 201.8 mg, 0.56 mmol). Yield: 142 mg (0.36 mmol, 65 %).

^{1}H NMR (600 MHz, THF-*d*$_8$) δ 7.35 (d, $^{3}J_{H,P}$ = 27.4 Hz, 2H, C_5H_2P), 7.34 (m, 4H, *2,6-Ar*) 7.23 – 7.07 (m, 8H, *4-Ph/2,6-Ar*), 6.93 (ddd, *J* = 8.4, 6.8, 1.1 Hz, 1H, *4-Ph*), 1.68 (d, $^{2}J_{H,P}$ = 13.0 Hz, 6H, 1,1'-CH_3) ppm.

^{13}C{^{1}H} NMR (151 MHz, THF-*d*$_8$) δ 161.5 (dd, $^{1}J_{C,F}$ = 240.8 Hz, $^{3}J_{C,P}$ = 3.2 Hz, *C9*), 144.4 (s, *C10*), 139.4 (d, $^{3}J_{C,P}$ = 6.0 Hz, *C3*), 133.6 (t, $^{3}J_{C,F}$ = 9.2 Hz, *C5*), 129.1 (s, *C12*), 129.1 – 128.9 (m, *C4*) 128.2 (d, $^{3}J_{C,F}$ = 8.3 Hz, *C7*), 125.6 (d, $^{4}J_{C,F}$ = 3.3 Hz, *C6*), 124.4 (s, *C11*), 123.9 (s, *C13*), 116.2 (d, $^{2}J_{C,F}$ = 23.6 Hz, *C8*), 114.3 (d, $^{2}J_{C,P}$ = 12.2 Hz, *C2*), 76.6 (d, $^{1}J_{C,P}$ = 98.4 Hz, *C1*), 16.9 (d, $^{1}J_{C,P}$ = 58.4 Hz, *C14*) ppm.

^{31}P{^{1}H} NMR (202 MHz, THF-*d*$_8$) δ -3 ppm.

^{19}F NMR (565 MHz, THF-*d*$_8$) δ -112 ppm.

5.6.5 Synthesis of 5-11

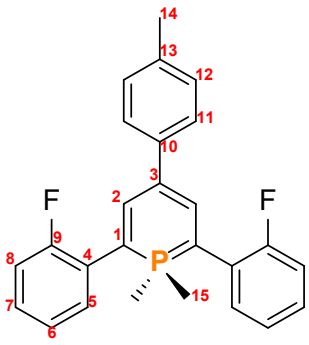

Starting materials: Phosphinine (**5-4**, 209.6 mg, 0.56 mmol). Yield: 118 mg (0.29 mmol, 52 %).

^{1}H NMR (400 MHz, THF-*d*$_8$) δ 7.33 (d, $^{3}J_{H,P}$ = 27.2 Hz, 2H, C_5H_2P), 7.34 – 7.29 (m, 2H, *2,6-Ar*), 7.25 (d, *J* = 8.3 Hz, 2H, *4-Tol*), 7.21 – 7.06 (m, 6H, *2,6-Ar*), δ 7.01 (d, *J* = 8.3 Hz, 2H, *4-Tol*), 2.25 (s, 3H, *4-Tol*), 1.67 (dt, $^{2}J_{H,P}$ = 13.0, 2.4 Hz, 6H, *1,1'-CH*$_3$) ppm.

^{13}C{^{1}H} NMR (101 MHz, THF-*d*$_8$) δ 161.4 (dd, $^{1}J_{C,F}$ = 240.8 Hz, $^{3}J_{C,P}$ = 3.2 Hz, *C9*), 141.6 (s, *C10*), 139.2 (d, $^{3}J_{C,P}$ = 5.8 Hz, *C3*), 133.5 (t, $^{3}J_{C,F}$ = 12.34 Hz, *C5*), 133.0 (s, *C13*), 129.8 (s, *C12*), 129.1 (m, *C4*), 128.0 (d, $^{3}J_{C,F}$ = 8.2 Hz, *C7*), 125.6 (d, $^{4}J_{C,F}$ = 3.3 Hz, *C6*), 124.5 (s, *C11*), 116.2 (d, $^{2}J_{C,F}$ = 23.6 Hz, *C8*), 114.5 (d, $^{2}J_{C,P}$ = 12.2 Hz, *C2*), 76.2 (d, $^{1}J_{C,P}$ = 98.7 Hz, *C1*), 21.6 (s, C*14*), 16.9 (d, $^{1}J_{C,P}$ = 58.2 Hz, *C15*) ppm.

^{19}F NMR (471 MHz, C_6D_6) δ -111 ppm.

^{31}P{^{1}H} NMR (202 MHz, C_6D_6) δ -4 ppm.

HR-ESI MS (*m/z*): 404.1493 g/mol (calculated: 404.1500 g/mol) $[M]^+$.

5.6.6 Synthesis of 5-12

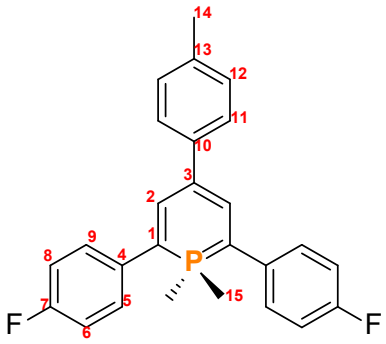

Starting materials: Phosphinine (**5-5**, 209.6 mg, 0.56 mmol). The crude solid was dissolved in acetonitrile and crystals were acquired upon evaporating the solution under the glovebox. Yield: 102 mg (0.25 mmol, 45 %).

^{1}H NMR (400 MHz, THF-*d*$_8$) δ 7.39 – 7.32 (m, 4H, *2,6-Ar*), 7.27 (d, $^{3}J_{H,P}$ = 29.1 Hz, 2H, C_5H_2P), 7.15 (d, *J* = 8.2 Hz, 2H, *4-Tol*), 7.06 – 6.99 (m, 4H, *2,6-Ar*), 6.95 (d, *J* = 7.8 Hz, 2H, *4-Tol*), 2.21 (s, 3H, *4-Tol*), 1.79 (d, $^{2}J_{H,P}$ = 12.4 Hz, 6H, 1,1'-CH_3) ppm.

^{13}C{^{1}H} NMR (101 MHz, THF-*d*$_8$) δ 162.2 (d, $^{1}J_{C,F}$ = 243.6 Hz, *C8*), 141.9(s, *C10*), 139.1 (d, $^{3}J_{C,F}$ = 6.9 Hz, *C4*), 138.4 (d, $^{3}J_{C,P}$ = 3.1 Hz, *C3*), 138.3 (d, $^{3}J_{C,F}$ = 3.3 Hz, *C6*), 132.8 (s, *C13*), 130.9 (d, $^{4}J_{C,F}$ = 2.7 Hz, *C5*), 130.9 (d, $^{2}J_{C,F}$ = 12.7 Hz, *C7*), 129.8 (s, *C12*), 124.4 (s, *C11*), 116.2 (d, $^{2}J_{C,F}$ = 21.3 Hz, C9), 112.1 (d, $^{2}J_{C,P}$ = 12.0 Hz, *C2*), 83.1 (d, $^{1}J_{C,P}$ = 95.3 Hz, *C1*), 21.1 (s, *C14*), 19.5 (d, $^{1}J_{C,P}$ = 56.4 Hz, *C15*) ppm.

^{31}P NMR (162 MHz, THF-*d*$_8$) δ -7 (m) ppm.

^{19}F NMR (377 MHz, THF-*d*$_8$) δ -119 (d, *J* = 1.8 Hz) ppm.

5.6.7 Synthesis of 5-13

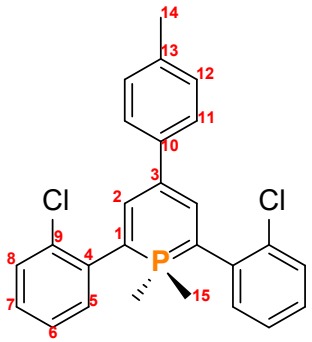

Starting materials: Phosphinine (**5-6**, 221.3 mg, 0.56 mmol). Yield: 151 mg (0.35 mmol, 62 %).

^{1}H NMR (400 MHz, *THF-d*$_8$) δ 7.50 (d, *J* = 7.6 Hz, 2H, *2,6-Ar*), 7.44 (d, *J* = 7.2 Hz, 2H, *2,6-Ar*), 7.34 – 7.23 (m, 5H, *4-Tol/2,6-Ar*), 7.14 (d, ^{3}J(H,P) = 21.3 Hz, 2H, C_5H_2P), 7.10 (s, 1H, *2,6-Ar*), 6.93 (d, *J* = 8.0 Hz, 2H, *4-Tol*), 2.21 (s, 3H, CH_3), 1.55 (d, ^{2}J(H,P) = 12.5 Hz, 6H, 1,1'-CH_3) ppm.

^{13}C{^{1}H} NMR (151 MHz, THF-*d*$_8$) δ 141.9 (s, *C10*), 141.6 (d, $^{2}J_{C,P}$ = 6.5 Hz, *C2*), 139.9 (d, $^{2}J_{C,P}$ = 9.0 Hz, *C4*), 134.9 (d, ^{2}J(C,Cl) = 3.0 Hz, *C8*), 132.5 (s, *C13*), 131.0 (s, *C12*), 129.7 (s,

C11), 129.2 (d, ^{3}J(C,Cl) = 1.2 Hz, *C7*), 127.6 (d, ^{3}J(C,Cl) = 1.4 Hz, *C5*), 124.3 (s, *C6*), 109.7 (d, ^{1}J(C,Cl) = 11.9 Hz, *C9*), 106.7 (s, *C3*), 81.9 (d, $^{1}J_{C,P}$ = 97.0 Hz, *C1*), 21.1 (s, *C14*), 19.9 (d, $^{1}J_{C,P}$ = 57.3 Hz, *C15*) ppm.

^{31}P{^{1}H} NMR (162 MHz, THF-*d*$_8$) δ -7 ppm.

5.6.8 Synthesis of 5-14

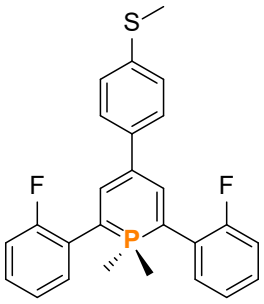

Starting materials: Phosphinine (**5-7**, 213.2 mg, 0.56 mmol). Yield: 153 mg (0.35 mmol, 62 %).

^{1}H NMR (600 MHz, THF-*d*$_8$) δ 7.37 – 7.27 (m, 7H, *Ar*), 7.24 – 7.07 (m, 7H, *Ar*), 2.40 (s, 3H, O*Me*), 1.68 (dt, $^{2}J_{H,P}$ = 13.0, $J_{H,H}$ = 2.3 Hz, 6H, 1,1'-C*H*$_3$).

^{31}P{^{1}H} NMR (162 MHz, THF-*d*$_8$) δ -5 ppm.

^{19}F NMR (377 MHz, THF-*d*$_8$) δ -112 ppm.

General method for synthesis of 5-16, 5-17 and 5-18

λ^3-Phosphinine (0.56 mmol) was dissolved in Et_2O (10 ml) and PhLi (1.9 M, 0.35 ml, 1.2 equiv., 0.67 mmol) was added slowly at room temperature. After stirring for 5 minutes, MeI (0.042 ml, 1.2 equiv., 0.67 mmol) was added to the solution. The reaction was stirred for another 20 minutes at room temperature and after this time the solvent was removed under vacuum. Finally, the crude solid was dissolved in hot ethanol and crystals were acquired upon cooling the solution down.

5.6.9 Synthesis of 5-16

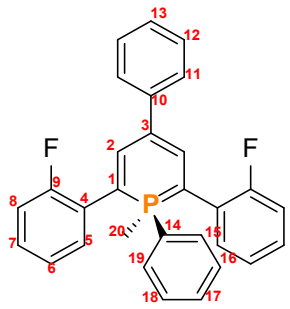

Starting materials: Phosphinine (**5-3**, 201.8 mg, 0.56 mmol). Yield: 192 mg (0.43 mmol, 76 %)

^{1}H NMR (600 MHz, THF-*d*$_8$) δ 7.57 – 7.53 (m, 2H, *1-Ar*), 7.49 (d, $^{3}J_{H,P}$ = 28.8 Hz, 2H, C_5H_2P), 7.37 (dd, *J* = 12.2, 4.9 Hz, 5H, *4-Ph*/*1-Ar*), 7.18 (t, *J* = 7.7 Hz, 2H, *2,6-Ar*), 7.09 (t, *J* = 7.4 Hz, 4H, *4-Ph*/*2,6-Ar*), 6.99 – 6.92 (m, 5H, *4-Ph*/*2,6-Ar*), 2.11 (d, $^{2}J_{H,P}$ = 12.0 Hz, 3H, -CH_3) ppm.

^{13}C{^{1}H} NMR (151 MHz, THF-*d*$_8$) δ 161.7 (d, $^{1}J_{C,F}$ = 244.4 Hz, *C9*), 144.5 (s, *C10*), 140.1 (s, *C17*), 136.8 (d, $^{2}J_{C,P}$ = 12 Hz, *C19*), 135.9 (d, $^{1}J_{C,P}$ = 82.2 Hz, *C14*), 134.0 (m, *C4*), 133.1 (d, $^{3}J_{C,P}$ = 5.2 Hz, *C16*), 133.0 (s, *C13*), 132.1 (d, $^{3}J_{C,F}$ = 8.5 Hz, *C5*), 129.5 (d, $^{3}J_{C,P}$ = 7.1 Hz, *C18*), 129.1 (s, *C12*), 128.6 (d, $^{2}J_{C,P}$ = 12 Hz, *C15*), 128.1 (d, *J* = 8.1 Hz, *C7*), 125.0 (s, *C6*), 124.6 (s, *C11*), 124.0 (s, *C3*), 116.3 (d, $^{2}J_{C,F}$ = 23.3 Hz, *C8*), 112. (d, $^{2}J_{C,P}$ = 12.9 Hz, *C2*), 78.1 (d, $^{1}J_{C,P}$ = 98.1 Hz, *C1*), 13.3 (d, $^{1}J_{C,P}$ = 64.0 Hz, *C20*) ppm.

^{31}P NMR (243 MHz, THF-*d*$_8$) δ 2 ppm.

^{19}F NMR (565 MHz, THF-*d*$_8$) δ -114 ppm.

HR-ESI MS (*m/z*): 452.1498 g/mol (calculated: 452.1500 g/mol) $[M]^+$.

5.6.10 Synthesis of 5-17

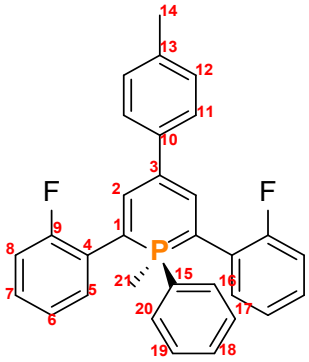

Starting materials: Phosphinine (**5-4**, 209.6 mg, 0.56 mmol). Yield: 209 mg (0.45 mmol, 80 %).

^{1}H NMR (400 MHz, THF-*d*$_8$) δ 7.60 – 7.51 (m, 2H, *1-Ar*), 7.45 (d, $^{3}J_{H,P}$ = 28.9 Hz, 2H, C_5H_2P), 7.40 – 7.35 (m, 3H, *1-Ar*), 7.26 (d, *J* = 7.9 Hz, 2H, *4-Tol*), 7.15 – 6.87 (m, 10 H, *4-Tol*/*2,6-Ar*), 2.26 (s, 3H, *4-Tol*), 2.12 (d, $^{2}J_{H,P}$ = 13.3 Hz, 3H, -CH_3).

^{13}C{^{1}H} NMR (151 MHz, THF-*d*$_8$) δ 161.7 (dd, $^{1}J_{C,F}$ = 243.3 Hz, $^{3}J_{C,P}$ = 4.4 Hz, *C9*), 141.7 (s, *C10*), 140.0 (d, $^{2}J_{C,P}$ = 19.7 Hz, *C20*), 136.0 (d, $^{1}J_{C,P}$ = 81.1 Hz, *C15*), 133.1 (s, *C13*), 133.0 (d, $^{3}J_{C,P}$ = 8.4 Hz, *C17*), 132.1 (d, $^{3}J_{C,F}$ = 10.1 Hz, *C5*), 132.0 (d, $^{4}J_{C,P}$ = 3.2 Hz, *C18*), 129.7 (m, *C4*), 129.8 (s, *C3*), 129.3 (d, $^{2}J_{C,P}$ = 11.7 Hz, *C16*), 129.1 (s, *C12*), 128.4 (d, $^{3}J_{C,P}$ = 6.2 Hz, *C19*), 128.0 (d, $^{3}J_{C,F}$ = 7.9 Hz, *C7*), 125.0 (d, $^{4}J_{C,F}$ = 3.5 Hz, *C6*), 124.6 (s, *C11*), 116.3 (d, $^{2}J_{C,F}$ = 23.3 Hz, *C8*), 112.8 (d, $^{2}J_{C,P}$ = 12.2 Hz, *C2*), 77.7 (d, $^{1}J_{C,P}$ = 98.9 Hz, *C1*), 21.1 (s, *C14*), 13.5 (d, $^{1}J_{C,P}$ = 64.0 Hz, *C21*) ppm.

^{31}P{^{1}H} NMR (162 MHz, THF-*d*$_8$) δ -5 ppm.

^{19}F NMR (565 MHz, THF-*d*$_8$) δ -112 ppm.

HR-ESI MS (*m/z*): 466.1655 g/mol (calculated: 466.1656 g/mol) $[M]^+$.

5.6.11 Synthesis of 5-18

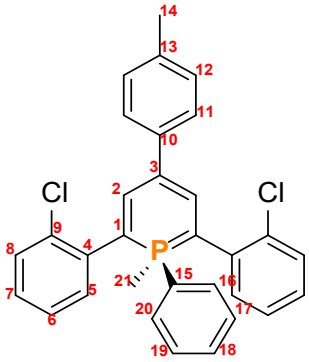

Starting materials: Phosphinine (**5-6**, 221.3 mg, 0.56 mmol). Yield: 120 mg (0.24 mmol, 43 %).

^{1}H NMR (600 MHz, *THF-d$_8$*) δ 7.59 (ddd, *J* = 12.6, 7.6, 1.8 Hz, 2H, *1-Ar*), 7.46 – 7.40 (m, 4H, *4-Tol/1-Ar*), 7.39 (s, 1H, *1-Ar*), 7.34 (d, $^{3}J_{H,P}$ = 30.3 Hz, 2H, C_5H_2P), 7.20 (d, *J* = 8.2 Hz, 2H, *2,6-Ar*), 7.11 (ddd, *J* = 7.7, 6.8, 1.5 Hz, 2H, *2,6-Ar*), 7.02 (td, *J* = 7.5, 1.4 Hz, 2H, *4-Tol*), 7.00 – 6.94 (m, 4H, *2,6-Ar*), 2.24 (s, 3H, *4-Tol*), 2.05 (d, $^{2}J_{H,P}$ = 13.0 Hz, 3H, 1,1'-CH_3) ppm.

^{13}C{^{1}H} NMR (151 MHz, *THF-d$_8$*) δ 141.8 (s, *C10*), 141.7 (d, $^{2}J_{C,P}$ = 6.2 Hz, *C2*), 139.8 (d, $^{2}J_{C,P}$ = 9.4 Hz, *C4*), 136.9 (d, $^{3}J_{C,P}$ = 5.5 Hz, *C17*), 136.8 (d, $^{1}J_{C,P}$ = 78.9 Hz, *C15*), 133.9 (d, ^{2}J(C,Cl) = 3.1 Hz, *C8*), 132.8 (s, *C13*), 132.6 (d, $^{2}J_{C,P}$ = 10.4 Hz, *C16*), 132.2 (d, $^{4}J_{C,P}$ = 3.0 Hz, *C18*), 131.1 (s, *C12*), 129.7 (s, *C11*), 129.4 (d, $^{2}J_{C,P}$ = 11.8 Hz, *C20*), 128.7 (s, *C7*), 127.3 (s, *C5*), 126.7 (d, $^{3}J_{C,P}$ = 5.1 Hz, *C19*), 124.5 (s, *C6*), 110.0 (d, ^{1}J(C,Cl) = 11.8 Hz, *C9*), 106.7 (s, *C3*), 82.0 (d, $^{1}J_{C,P}$ = 98.4 Hz, *C1*), 21.1 (s, *C14*), 14.9 (d, $^{1}J_{C,P}$ = 63.7 Hz, *C21*) ppm.

^{31}P{^{1}H} NMR (162 MHz, *THF-d$_8$*) δ -3 ppm.

5.6.12 Synthesis of 5-21

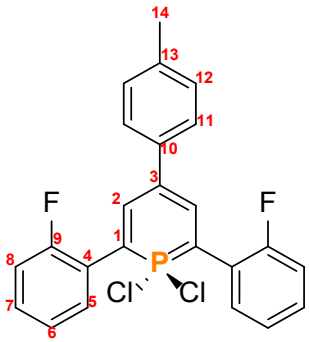

Phosphinine (**5-4**, 209.6 mg, 0.56 mmol) was dissolved in toluene (15 mL) and then PCl_5 (152 mg, 1.3 eq, 0.73 mmol) was added to the solution at room temperature. After stirring for 2 hours under UV irradiation (~ 365 nm), the solution was filtered to remove excess PCl_5. The solvent of the filtrate was then removed under vacuum and the residue was dissolved into hot acetonitrile. Finally, crystals were acquired upon cooling the solution. Yield: 150 mg (0.34 mmol, 60 %).

^{1}H NMR (400 MHz, MeCN-*d*$_3$) δ 7.74 (d, $^{3}J_{H,P}$ = 50.6 Hz, 2H; C_5H_2P), 7.75 – 7.69 (m, 2H, *2,6-Ar*), 7.59 – 7.46 (m, 2H, *4-Tol*), 7.38 – 7.26 (m, 6H, *2,6-Ar*), 7.16 (d, *J* = 8.1 Hz, 2H, *4-Tol*), 2.31 (s, 3H) ppm.

^{13}C NMR (101 MHz, MeCN-*d*$_3$) δ 161.9 (dd, $^{1}J_{C,F}$ = 245.8, $^{3}J_{C,P}$ = 8.3 Hz, C9), 142.0 (d, $^{3}J_{C,F}$ = 8.6 Hz, C7), 138.5 (C10), 136.9 (s, C13), 134.0 (d, $^{3}J_{C,F}$ = 6.3 Hz, C5), 131.8 (d, $^{3}J_{C,P}$ = 8.3, C3), 130.3 (s, C12), 126.8 (s, C11), 125.4 (d, $^{4}J_{C,F}$ = 3.3 Hz, C6), 123.5 (d, $^{2}J_{C,F}$ = 20.3 Hz), 121.4 (d, $^{2}J_{C,F}$ = 23.5 Hz, C8), 117.0 (d, $^{2}J_{C,P}$ = 22.7 Hz, C2), 97.4 (d, $^{1}J_{C,P}$ = 111.9 Hz, C1), 20.9 (s, C14) ppm.

^{31}P{^{1}H} NMR (162 MHz, MeCN-*d*$_3$) δ 21 ppm.

^{19}F NMR (376 MHz, MeCN-*d*$_3$) δ -115 ppm.

5.6.13 Synthesis of 5-22

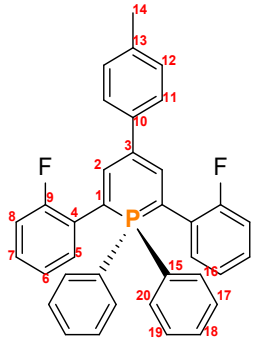

Phosphinine (**5-21**, 44.5 mg, 0.1 mmol) was dissolved in toluene (4 ml) and this solution was added slowly to PhMgBr (3 M, 0.07 mL, 2.2 eq, 0.22 mmol) in Et_2O (4 ml) at 0 °C. The reaction was allowed to warm to room temperature and stirred overnight. After this time the solvent was removed under vacuum yielding the crude product which was

dissolved in acetonitrile and crystals were acquired upon evaporating the solution under the glovebox. Yield: 14.7 mg (0.028 mmol, 30 %).

^{1}H NMR (400 MHz, C_6D_6) δ 7.94 (d, $^{3}J_{H,P}$ = 30.2 Hz, 2H, C_5H_2P), 7.77 – 7.63 (m, 4H, *1,1'-Ar*), 7.50 (d, *J* = 8.2 Hz, 2H, *4-Tol*), 7.08 (d, *J* = 7.9 Hz, 2H, *4-Tol*), 6.99 – 6.88 (m, 8H, *1,1'-Ar/2,6-Ar*), 6.77 – 6.65 (m, 4H, *2,6-Ar*), 6.60 – 6.55 (m, 2H, *2,6-Ar*), 2.21 (s, 3H, CH_3) ppm.

^{13}C{^{1}H} NMR (101 MHz, *THF-d$_8$*) δ 162.1 (d, $^{1}J_{C,F}$ = 244.4 Hz, *C9*), 141.5 (s, *C10*), 141.1 (d, $^{3}J_{C,P}$ = 5.2 Hz, *C3*), 134.3 (d, $^{2}J_{C,P}$ = 10.4 Hz, *C20*), 133.2 (s, *C13*) 133.1 (t, $^{3}J_{C,F}$ = 6.2 Hz, *C5*), 132.3 (d, $^{3}J_{C,P}$ = 3.1 Hz, *C17*), 131.3 (d, $^{1}J_{C,P}$ = 86.1 Hz, *C15*), 129.8 (d, $^{3}J_{C,P}$ = 3.4 Hz, *C19*), 129.6 (s, *C18*), 129.3 (m, *C4*), 129.2 (d, $^{2}J_{C,P}$ = 12.3 Hz, *C16*), 129.1 (s, *C12*), 128.4 (d, $^{3}J_{C,F}$ = 8.1 Hz, *C7*), 124.8 (s, *C11*), 124.4 (d, $^{2}J_{C,P}$ = 3.7 Hz, *C6*), 116.6 (d, $^{2}J_{C,F}$ = 23.6 Hz, *C8*), 112.1 (d, $^{2}J_{C,P}$ = 12.3 Hz, *C2*), 77.4 (d, $^{1}J_{C,P}$ = 99.5 Hz, *C1*), 21.1 (s, *C14*) ppm.

^{31}P{^{1}H} NMR (162 MHz, C_6D_6) δ 5 ppm.

^{19}F NMR (376 MHz, C_6D_6) δ -111 (d, *J* = 5.6 Hz) ppm.

General method for synthesis of 5-23, 5-24, 5-25 and 5-26

Phosphinine (0.5 mmol) was dissolved in toluene (20 ml) and added slowly to organolithium compounds (1 equiv., 0.5 mmol) in Et_2O (20 ml) at -78 ºC. The reaction was allowed to warm to room temperature slowly and stirred overnight. After this time the solvent was removed under vacuum yielding the crude product. Finally, the crude solid was dissolved in hot acetonitrile and crystals were acquired upon cooling the solution down.

5.6.14 Synthesis of 5-23

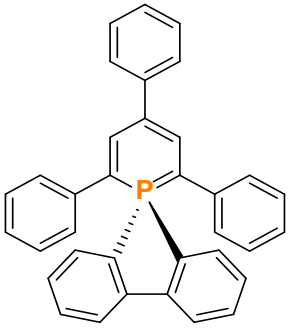

Starting materials: Phosphinine (**5-19**, 197.6 mg, 0.5 mmol), 2,2'-dilithiobiphenyl (83 mg, 1 equiv., 0.5 mmol). Yield: 102 mg (0.22 mmol, 43 %).

^{1}H NMR (400 MHz, THF-*d*$_8$) δ 7.94 (m, 2H, *1,1'-Ar*), 7.90 (d, $^{3}J_{H,P}$ = 31.0 Hz, 2H, C_5H_2P), 7.72 (dd, *J* = 10.6, 7.3 Hz, 2H, *1,1'-Ar*), 7.61 – 7.47 (m, 4H, *4-Ph/1,1'-Ar*), 7.38 (qd, *J* = 8.0, 7.4, 3.7 Hz, 2H, *1,1'-Ar*), 7.27 (t, *J* = 7.8 Hz, 2H, *4-Ph*), 7.04 (t, *J* = 7.4 Hz, 1H, *4-Ph*), 6.89 (ddd, *J* = 25.5, 17.9, 7.5 Hz, 8H, *2,6-Ar*) ppm.

^{31}P{^{1}H} NMR (162 MHz, THF-*d*$_8$) δ -1 ppm.

HR-ESI MS (*m/z*): 476.1686 g/mol (calculated: 476.1688 g/mol) $[M]^+$.

A suitable ^{13}C{^{1}H} spectrum could not obtain due to the poor solubility of this compound in organic solvents.

5.6.15 Synthesis of 5-24

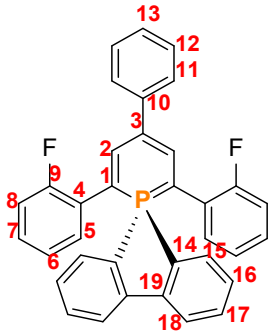

Starting materials: Phosphinine (**5-20**, 215.6 mg, 0.5 mmol), 2,2'-dilithiobiphenyl (83.0 mg, 1 equiv., 0.5 mmol). Yield: 97 mg (0.19 mmol, 38 %).

^{1}H NMR (600 MHz, THF-*d*$_8$) δ 7.91 – 7.81 (m, 2H, *1,1'-Ar*), 7.75 (d, $^{3}J_{H,P}$ = 20.6 Hz, 2H, C_5H_2P), 7.72 (s, 2H, *1,1'-Ar*), 7.48 (t, *J* = 7.8 Hz, 2H, *4-Ph*), 7.44 – 7.35 (m, 4H, *1,1'-Ar*), 7.22 (t, *J* = 7.8 Hz, 2H, *4-Ph*), 7.01 (d, *J* = 8.0 Hz, 1H, *4-Ph*), 6.91 (q, *J* = 6.8, 6.1 Hz, 2H, *2,6-Ar*), 6.80 (t, *J* = 9.1 Hz, 4H, *2,6-Ar*), 6.65 (t, *J* = 7.7 Hz, 2H, *2,6-Ar*) ppm.

^{13}C{^{1}H} NMR (151 MHz, THF-*d*$_8$) δ 161.4 (dd, $^{1}J_{C,F}$ = 245.5 Hz, $^{3}J_{C,P}$ = 5.7 Hz, *C9*), 144.3 (s, *C10*), 142.5 (dd, $^{3}J_{C,P}$ = 6.9, 2.8 Hz, *C3*), 141.7 (d, $^{2}J_{C,P}$ = 20.0 Hz, *C19*), 135.6 (d, $^{1}J_{C,P}$ = 89.9 Hz, *C14*), 134.1 (s, *C13*), 132.8 (d, $^{3}J_{C,F}$ = 11.0 Hz, *C5*), 132.2 (t, $^{3}J_{C,P}$ = 3.7 Hz, *C16*), 130.4 (d, $^{2}J_{C,P}$ = 11.8 Hz, *C18*), 129.2 (s, *C12*), 129.0 – 128.7 (m, *C4*), 128. 4 (d, $^{3}J_{C,F}$ = 8.0 Hz, *C7*), 125.1 (s, *C11*), 124.4 (s, *C17*), 124.3 (d, $^{4}J_{C,F}$ = 3.9 Hz, *C6*), 122.2 (d, $^{2}J_{C,P}$ = 9.5 Hz, *C15*),

116.3 (d, $^{2}J_{C,F}$ = 23.3 Hz, *C8*), 112.7 (d, $^{2}J_{C,P}$ = 12.7 Hz, *C2*), 78.6 (d, $^{1}J_{C,P}$ = 96.2 Hz,*C1*).

^{31}P{^{1}H} NMR (243 MHz, THF-*d*$_8$) δ 5 ppm.

^{19}F NMR (565 MHz, THF-*d*$_8$) δ -114 ppm.

HR-ESI MS (*m/z*) 512.1490 g/mol (calculated: 512.1500 g/mol) $[M]^{+}$.

5.6.16 Synthesis of 5-25

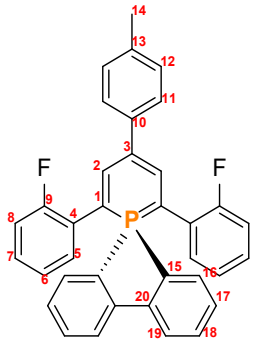

Starting materials: Phosphinine (**5-21**, 22.3 mg, 0.05 mmol), 2,2'-dilithiobiphenyl (8.3 mg, 1 equiv., 0.05 mmol). Yield: 14.7 mg (0.028 mmol, 56 %).

^{1}H NMR (500 MHz, THF-*d*$_8$) δ 7.86 – 7.80 (m, 2H, *1,1'-Ar*), 7.72 (d, $^{3}J_{H,P}$ = 31 Hz, 2H, C_5H_2P), 7.72 – 7.67 (m, 2H, *1,1'-Ar*), 7.45 (tt, *J* = 7.5, 1.4 Hz, 2H, *1,1'-Ar*), 7.39 – 7.33 (m, 2H, *1,1'-Ar*), 7.30 (d, *J* = 8.2 Hz, 2H, *4-Tol*), 7.06 (d, *J* = 8.2 Hz, 2H, *4-Tol*), 6.93 – 6.85 (m, 2H, *2,6-Ar*), 6.83 – 6.74 (m, 4H, *2,6-Ar*), 6.69 – 6.59 (m, 2H, *2,6-Ar*), 2.28 (s, 3H, -CH_3) ppm.

^{13}C{^{1}H} NMR (126 MHz, THF-*d*$_8$) δ 161.6 (dd, $^{1}J_{C,F}$ = 245.2 Hz, $^{3}J_{C,P}$ = 5.9 Hz, *C9*), 142.3 (d, $^{3}J_{C,P}$ = 6.5 Hz, *C3*), 141.6 (d, $^{2}J_{C,P}$ = 20.3 Hz, *C20*), 141.5 (s, *C10*), 135.7 (d, $^{1}J_{C,P}$ = 89.9 Hz, *C15*), 134.1 (d, $^{3}J_{C,P}$ = 2.5 Hz, *C17*), 133.6 (s, *C13*), 132.8 (t, $^{3}J_{C,F}$ = 11 Hz, *C5*), 132.2 (d, $^{4}J_{C,P}$ = 2.7 Hz, *C18*), 130.3 (d, $^{3}J_{C,P}$ = 11.7 Hz, *C19*), 129.9 (s, *C12*), 129. 1 – 128.8 (m, *C4*), 128.4 (d, $^{3}J_{C,F}$ = 7.8 Hz, *C7*), 125. 1 (s, *C11*), 124.3 (d, $^{4}J_{C,F}$ = 3.6 Hz, *C6*), 122.2 (d, $^{2}J_{C,P}$ = 9.5 Hz, *C16*), 116.3 (d, $^{2}J_{C,F}$ = 23.3 Hz, *C8*), 112.7 (d, $^{2}J_{C,P}$ = 12.9 Hz, *C2*), 78.3 (d, $^{1}J_{C,P}$ = 96.4 Hz, *C1*), 21.2 (s, *C14*).

^{31}P{^{1}H} NMR (162 MHz, C_6D_6) δ 5 ppm.

^{19}F NMR (376 MHz, C_6D_6) δ -113 ppm.

HR-ESI MS (*m/z*): 526.1696 g/mol (calculated: 526.1656 g/mol) $[M]^{+}$.

5.6.17 Synthesis of 5-26

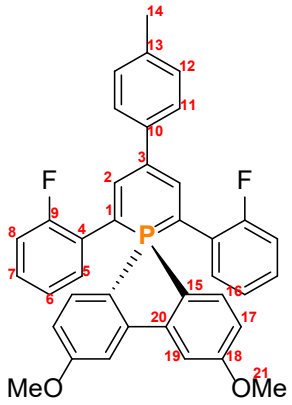

Starting materials: Phosphinine (**5-21**, 201.1 mg, 0.45 mmol), 2,2'-dilithio-5,5'-dimethoxy-biphenyl (176.6 mg, 1.05 equiv., 0.475 mmol). Yield: 166 mg (0.28 mmol, 63 %).

^{1}H NMR (600 MHz, THF-*d*$_8$) δ 7.71 (dd, *J* = 10.1, 8.2 Hz, 2H, *1,1'-Ar*), 7.65 (dd, $^{3}J_{H,P}$ = 30.9, 1.2 Hz, 2H, C_5H_2P), 7.35 – 7.22 (m, 4H, *1,1'-Ar*), 7.07 – 7.00 (m, 2H, *4-Tol*), 6.97 – 6.88 (m, 4H, *1,1'-Ar & 2,6-Ar*), 6.85 – 6.76 (m, 4H, *2,6-Ar*), 6.65 (td, *J* = 7.5, 1.3 Hz, 2H, *2,6-Ar*), 3.84 (s, 6H, -O*Me*), 2.27 (s, 3H, -CH_3).

^{13}C{^{1}H} NMR (151 MHz, THF-*d*$_8$) δ 165.3 (d, $^{4}J_{C,P}$ = 2.6 Hz, *C18*), 161.7 (dd, $^{1}J_{C,F}$ = 245.2, $^{3}J_{C,P}$ = 6.0 Hz, *C9*), 143.7 (d, $^{2}J_{C,P}$ = 21.0 Hz, *C20*), 142.0 (dd, $^{3}J_{C,P}$ = 6.9, 3.0 Hz, *C3*), 141.7 (s, *C10*), 134.0 (d, $^{3}J_{C,F}$ = 12.3 Hz, *C5*), 133.3 (s, *C13*), 132.2 (t, $^{3}J_{C,P}$ = 3.7 Hz, *C19*), 129.8 (s, *C12*), 129.4 (dd, $^{2}J_{C,F}$ = 14.8, $^{2}J_{C,P}$ = 9.8 Hz, *C4*), 128.2 (d, $^{1}J_{C,P}$ = 96.0 Hz, *C15*), 128.1 (d, $^{3}J_{C,F}$ = 7.9 Hz, *C7*), 125.0 (s, *C11*), 124.2 (d, $^{4}J_{C,F}$ = 3.6 Hz, *C6*), 116.3 (d, $^{2}J_{C,F}$ = 23.4 Hz, *C8*), 115.9 (d, $^{2}J_{C,P}$ = 12.5 Hz, *C2*), 112.0 (d, $^{2}J_{C,P}$ = 12.4 Hz, *C16*), 108.2 (d, $^{3}J_{C,P}$ = 10.3 Hz, *C17*), 79.2 (d, $^{1}J_{C,P}$ = 98.0 Hz, *C1*), 56.0 (s, *C21*), 21.14 (s, *C14*) ppm.

^{31}P{^{1}H} NMR (162 MHz, THF-*d*$_8$) δ 0.9 ppm.

^{19}F NMR (377 MHz, THF-*d*$_8$) δ -115 (q, *J* = 3.9 Hz) ppm.

5.7 Crystallographic details

The structures were solved by dual-space methods using SHELXT[109] and refined against F^2 on all data by full-matrix least squares with SHELXL-2017[110] following

established refinement strategies[111]. The program Olex2[112] was also used to aid in the refinement. All non-hydrogen atoms were refined anisotropically. All hydrogen atoms were included into the model at geometrically calculated positions and refined using a riding model. The isotropic displacement parameters of all hydrogen atoms were fixed to 1.2 times the *U*-value of the atoms they are linked to (1.5 times for methyl groups). Details of the data quality and a summary of the residual values of the refinements are listed in **Table S1** below. Tables **S2**, **S4**, **S6**, **S8**, **S10**, **S12**, **S14**, **S16**, **S18**, **S20**, **S22** and **S24** give all bond lengths for the structures, and **S3**, **S5**, **S7**, **S9**, **S11**, **S13**, **S15**, **S17**, **S19**, **S21**, **S23** and **S25** give all bond angles for the structures.

Details of the data quality and a summary of the residual values of the refinements are listed in **Table S1** below.

Table S1 – Selected crystallographic data for λ^5-phosphinines.

Sample name	**5-8**	**5-11**	**5-10**	**5-12**	**5-17**	**5-16**
Empirical formula	$C_{28}H_{27}F_2N_2P$	$C_{26}H_{23}F_2P$	$C_{25}H_{21}F_2P$	$C_{26}H_{23}F_2P$	$C_{31}H_{25}F_2P$	$C_{30}H_{23}F_2P$
Formula Weight	460.48	404.41	390.13	404.41	466.48	452.45
Temperature / K	100.0	100.0	100.0	100.0	100.0	101.0
Crystal system	Monoclinic	Triclinic	Monoclinic	Monoclinic	Monoclinic	Orthorhombic
Space group	$P2_1/c$	P-1	$P2_1$	$P2_1/n$	$P2_1$	$P2_12_12_1$
a/Å	8.1653(6)	10.1293(2)	10.27267(7)	9.4907(7)	10.6308(7)	10.7601(3)
b/Å	20.8817(14)	12.9688(2)	24.35141(17)	20.3747(15)	9.5488(6)	11.4595(3)
c/Å	14.0144(9)	16.8564(3)	15.78910(11)	11.3339(8)	12.1149(8)	18.4725(5)
α/°	90	68.9190(10)	90	90	90	90
β/°	99.573(4)	85.9210(10)	91.2737(3)	110.947(3)	103.732(2)	90
γ/°	90	86.6020(10)	90	90	90	90
Volume/Å^3	2356.3(3)	2059.56(6)	3948.73(5)	2046.8(3)	1194.65(13)	2277.76(11)
Z	4	4	8	4	2	4
Reflections collected	36924	39209	131300	63306	23827	44741
Independent reflections (R_{int})	4150 (0.0660)	8082 (0.0404)	13915 (0.0376)	6800 (0.0461)	4349 (0.0351)	6931 (0.0628)
R_1 [I>2σ (I)]	0.0466	0.0342	0.0345	0.0407	0.0351	0.0407
wR_2 (all data)	0.1136	0.0887	0.0916	0.1008	0.0939	0.1099

continue **Table1**:

Sample name	**5-15**	**5-18**	**5-21**	**5-22**	**5-25**	**5-9**
Empirical formula	$C_{30.5}ClH_{26}P$	$C_{31}H_{25}Cl_2P$	$C_{24}H_{17}Cl_2F_2P$	$C_{36}H_{27}F_2P$	$C_{40}H_{31}F_2N_2P$	$C_{25}H_{23}P$
Formula Weight	416.47	499.38	445.24	528.54	608.64	351.40
Temperature / K	100.0	99.9	100.0	100.0	100.0	100.0
Crystal system	Monoclinic	Monoclinic	Monoclinic	Monoclinic	Triclinic	Triclinic
Space group	$P2_1/n$	$P2_1/n$	$P2_1/c$	$P2_1/n$	P-1	P-1
a/Å	9.5876(7)	11.7692(12)	13.5294(5)	12.9361(5)	10.0816(5)	9.34495(8)
b/Å	12.0991(9)	13.7101(15)	17.3996(6)	10.2256(4)	12.7201(5)	9.94785(8)
c/Å	20.7220(15)	16.3551(17)	17.8896(7)	20.1593(8)	12.9298(7)	12.45875(11)
α/°	90	90	90	90	94.798(2)	111.4151(5)
β/°	98.013(3)	109.340(4)	99.4210(10)	90.0780(10)	92.671(2)	95.1736(5)
γ/°	90	90	90	90	107.413(2)	112.1885(4)

Volume/Å^3	2380.3(3)	2059.56(6)	4154.5(3)	2666.66(18)	1572.09(13)	962.807(12)
Z	4	4	8	4	2	2
Reflections collected	90080	40862	110589	43476	55377	17955
Independent reflections (R_{int})	6177 (0.0710)	7570 (0.0539)	11662 (0.0237)	8061 (0.0325)	7833 (0.0632)	3429 (0.1124)
R_1 [I>2σ (I)]	0.0527	0.0433	0.0306	0.0388	0.0601	0.0748
wR_2 (all data)	0.1262	0.1117	0.0849	0.1026	0.1836	0.1844

Table S2: Bond lengths for **5-8**.

Atom	Atom	Length/Å	Atom	Atom	Length/Å
P1	N1	1.644(2)	C4	C5	1.380(3)
P1	N2	1.668(2)	C12	C17	1.400(3)
P1	C1	1.732(2)	C19	C5	1.497(3)
P1	C5	1.742(2)	C19	C20	1.387(3)
F1	C7	1.356(3)	C19	C24	1.389(3)
F2	C20	1.366(3)	C14	C15	1.395(3)
N1	C27	1.434(3)	C7	C8	1.384(3)
N1	C25	1.465(3)	C20	C21	1.382(3)
N2	C26	1.462(3)	C9	C8	1.377(4)
N2	C28	1.455(4)	C9	C10	1.387(4)
C2	C1	1.402(3)	C16	C15	1.388(4)
C2	C3	1.391(3)	C16	C17	1.387(3)
C6	C1	1.494(3)	C15	C18	1.510(3)
C6	C7	1.385(3)	C11	C10	1.386(3)
C6	C11	1.403(3)	C24	C23	1.393(3)
C3	C4	1.404(3)	C23	C22	1.382(4)
C3	C12	1.489(3)	C21	C22	1.382(4)
C13	C12	1.397(3)	C25	C26	1.507(4)
C13	C14	1.393(3)			

Table 3: Bond angles for **5-8**.

Atom	Atom	Atom	Angle/°	Atom	Atom	Atom	Angle/°
N1	P1	N2	91.92(11)	C20	C19	C24	116.1(2)
N1	P1	C1	121.43(11)	C24	C19	C5	123.5(2)
N1	P1	C5	112.58(11)	C13	C14	C15	121.3(2)
N2	P1	C1	111.70(11)	F1	C7	C6	118.8(2)
N2	P1	C5	115.74(11)	F1	C7	C8	117.0(2)
C1	P1	C5	103.91(11)	C8	C7	C6	124.2(2)
C27	N1	P1	125.00(19)	C4	C5	P1	122.18(17)
C27	N1	C25	119.6(2)	C4	C5	C19	120.0(2)
C25	N1	P1	115.33(18)	C19	C5	P1	117.66(16)
C26	N2	P1	111.61(17)	F2	C20	C19	118.2(2)
C28	N2	P1	119.98(18)	F2	C20	C21	117.8(2)
C28	N2	C26	116.8(2)	C21	C20	C19	124.0(2)
C3	C2	C1	127.2(2)	C8	C9	C10	119.9(2)
C7	C6	C1	124.4(2)	C17	C16	C15	121.6(2)

Table S4: Bond lengths for **5-11**.

Atom	Atom	Length/Å	Atom	Atom	Length/Å
P1	C1	1.7646(13)	P2	C27	1.7633(14)
P1	C5	1.7628(13)	P2	C31	1.7644(13)
P1	C25	1.8077(14)	P2	C51	1.8122(14)
P1	C26	1.8034(13)	P2	C52	1.8006(13)
F1	C7	1.3649(17)	F3	C33	1.3643(17)
F2	C20	1.3683(16)	F4	C46	1.3640(17)
C1	C2	1.3889(18)	C27	C28	1.3935(18)
C1	C6	1.4767(18)	C27	C32	1.4772(18)
C2	C3	1.4069(19)	C28	C29	1.4077(18)
C3	C4	1.4061(19)	C29	C30	1.4043(19)
C3	C12	1.4822(18)	C29	C38	1.4841(18)
C4	C5	1.3922(18)	C30	C31	1.3898(19)
C5	C19	1.4737(18)	C31	C45	1.4716(19)
C6	C7	1.393(2)	C32	C33	1.3918(19)
C6	C11	1.407(2)	C32	C37	1.406(2)
C7	C8	1.383(2)	C33	C34	1.380(2)
C8	C9	1.385(2)	C34	C35	1.387(2)
C9	C10	1.389(2)	C35	C36	1.390(2)
C10	C11	1.389(2)	C36	C37	1.390(2)
C12	C13	1.4022(19)	C38	C39	1.3980(19)
C12	C17	1.4022(19)	C38	C43	1.4030(19)
C13	C14	1.3887(19)	C39	C40	1.3951(19)
C14	C15	1.396(2)	C40	C41	1.391(2)
C15	C16	1.389(2)	C41	C42	1.398(2)
C15	C18	1.5064(18)	C41	C44	1.5082(19)
C16	C17	1.3911(19)	C42	C43	1.3882(19)
C19	C20	1.3939(19)	C45	C46	1.394(2)
C19	C24	1.4044(19)	C45	C50	1.405(2)
C20	C21	1.379(2)	C46	C47	1.378(2)
C21	C22	1.389(2)	C47	C48	1.384(2)
C22	C23	1.390(2)	C48	C49	1.391(2)
C23	C24	1.389(2)	C49	C50	1.386(2)

Table S5: Bond angles for **5-11**.

Atom	Atom	Atom	Angle/°	Atom	Atom	Atom	Angle/°
C1	P1	C25	110.04(6)	C27	P2	C31	103.66(6)
C1	P1	C26	111.53(6)	C27	P2	C51	109.93(7)
C5	P1	C1	103.90(6)	C27	P2	C52	112.92(6)
C5	P1	C25	109.14(6)	C31	P2	C51	110.69(7)
C5	P1	C26	113.19(6)	C31	P2	C52	112.11(6)
C26	P1	C25	108.93(6)	C52	P2	C51	107.56(7)
C2	C1	P1	116.14(10)	C28	C27	P2	115.39(10)
C2	C1	C6	120.38(12)	C28	C27	C32	121.29(12)
C6	C1	P1	123.48(10)	C32	C27	P2	123.27(10)
C1	C2	C3	126.35(12)	C27	C28	C29	126.61(12)
C2	C3	C12	121.03(12)	C28	C29	C38	119.80(12)
C4	C3	C2	119.63(12)	C30	C29	C28	119.65(12)
C4	C3	C12	119.03(12)	C30	C29	C38	120.02(12)
C5	C4	C3	127.12(12)	C31	C30	C29	126.59(12)
C4	C5	P1	115.19(10)	C30	C31	P2	115.77(10)
C4	C5	C19	120.58(12)	C30	C31	C45	120.46(12)
C19	C5	P1	124.23(10)	C45	C31	P2	123.77(10)
C7	C6	C1	124.35(13)	C33	C32	C27	123.97(13)
C7	C6	C11	115.11(13)	C33	C32	C37	114.94(12)
C11	C6	C1	120.52(12)	C37	C32	C27	121.09(12)
F1	C7	C6	118.55(12)	F3	C33	C32	118.33(12)
F1	C7	C8	117.06(13)	F3	C33	C34	117.12(12)
C8	C7	C6	124.39(14)	C34	C33	C32	124.55(14)
C7	C8	C9	118.69(14)	C33	C34	C35	118.71(13)

Atom	Atom	Atom	Angle/°	Atom	Atom	Atom	Angle/°
C8	C9	C10	119.52(14)	C34	C35	C36	119.44(13)
C11	C10	C9	120.37(15)	C35	C36	C37	120.22(14)
C10	C11	C6	121.92(14)	C36	C37	C32	122.09(13)
C13	C12	C3	122.74(12)	C39	C38	C29	120.56(12)
C17	C12	C3	120.10(12)	C39	C38	C43	117.50(12)
C17	C12	C13	117.15(12)	C43	C38	C29	121.93(12)
C14	C13	C12	121.19(13)	C40	C39	C38	121.30(13)
C13	C14	C15	121.21(13)	C41	C40	C39	121.02(13)
C14	C15	C18	121.36(13)	C40	C41	C42	117.78(12)
C16	C15	C14	117.92(12)	C40	C41	C44	121.16(14)
C16	C15	C18	120.71(13)	C42	C41	C44	121.05(13)
C15	C16	C17	121.14(13)	C43	C42	C41	121.48(13)
C16	C17	C12	121.33(13)	C42	C43	C38	120.89(13)
C20	C19	C5	124.03(12)	C46	C45	C31	124.16(13)
C20	C19	C24	114.74(12)	C46	C45	C50	114.96(13)
C24	C19	C5	121.20(12)	C50	C45	C31	120.85(13)
F2	C20	C19	117.99(12)	F4	C46	C45	117.72(12)
F2	C20	C21	117.25(12)	F4	C46	C47	117.60(13)
C21	C20	C19	124.74(13)	C47	C46	C45	124.64(14)
C20	C21	C22	118.60(13)	C46	C47	C48	118.60(14)
C21	C22	C23	119.41(13)	C47	C48	C49	119.43(14)
C24	C23	C22	120.20(13)	C50	C49	C48	120.46(15)
C23	C24	C19	122.27(13)	C49	C50	C45	121.88(14)

Table S6: Bond lengths for **5-10**.

Atom	Atom	Length/Å	Atom	Atom	Length/Å
P1	C1	1.762(3)	P1C	C1C	1.765(3)
P1	C5	1.768(3)	P1C	C5C	1.762(3)
P1	C24	1.799(3)	P1C	C24C	1.797(3)
P1	C25	1.812(4)	P1C	C25C	1.803(3)
F1	C7	1.356(4)	F1C	C7C	1.365(4)
F2	C13	1.365(4)	F2C	C13C	1.363(4)
C1	C2	1.387(5)	C1C	C2C	1.394(5)
C1	C6	1.477(4)	C1C	C6C	1.471(4)
C2	C3	1.417(4)	C2C	C3C	1.412(5)
C3	C4	1.405(4)	C3C	C4C	1.396(5)
C3	C18	1.483(5)	C3C	C18C	1.481(5)
C4	C5	1.390(4)	C4C	C5C	1.392(5)
C5	C12	1.474(4)	C5C	C12C	1.479(4)
C6	C7	1.389(5)	C6C	C7C	1.394(5)
C6	C11	1.403(5)	C6C	C11C	1.406(5)
C7	C8	1.382(5)	C7C	C8C	1.376(5)
C8	C9	1.382(6)	C8C	C9C	1.387(5)
C9	C10	1.376(7)	C9C	C10C	1.381(5)
C10	C11	1.394(5)	C10C	C11C	1.388(5)
C12	C13	1.397(5)	C12C	C13C	1.390(5)
C12	C17	1.403(5)	C12C	C17C	1.408(5)
C13	C14	1.377(5)	C13C	C14C	1.384(5)
C14	C15	1.376(5)	C14C	C15C	1.384(6)
C15	C16	1.389(5)	C15C	C16C	1.373(7)
C16	C17	1.388(5)	C16C	C17C	1.387(5)
C18	C19	1.399(5)	C18C	C19C	1.404(5)
C18	C23	1.402(5)	C18C	C23C	1.410(5)
C19	C20	1.392(5)	C19C	C20C	1.384(5)
C20	C21	1.389(5)	C20C	C21C	1.391(6)
C21	C22	1.384(5)	C21C	C22C	1.383(5)
C22	C23	1.389(5)	C22C	C23C	1.390(5)

Table S7: Bond angles for **5-10**.

Atom	Atom	Atom	Angle/°	Atom	Atom	Atom	Angle/°
C1	P1	C5	104.10(16)	C1C	P1C	C24C	113.95(16)

Atom	Atom	Atom	Angle/°	Atom	Atom	Atom	Angle/°
C1	P1	C24	110.18(15)	C1C	P1C	C25C	108.86(15)
C1	P1	C25	110.73(16)	C5C	P1C	C1C	104.11(16)
C5	P1	C24	113.83(16)	C5C	P1C	C24C	110.25(16)
C5	P1	C25	108.95(15)	C5C	P1C	C25C	110.76(16)
C24	P1	C25	108.99(16)	C24C	P1C	C25C	108.86(16)
C2	C1	P1	117.0(2)	C2C	C1C	P1C	115.2(2)
C2	C1	C6	120.3(3)	C2C	C1C	C6C	120.7(3)
C6	C1	P1	122.7(2)	C6C	C1C	P1C	124.0(2)
C1	C2	C3	125.9(3)	C1C	C2C	C3C	126.6(3)
C2	C3	C18	120.2(3)	C2C	C3C	C18C	119.7(3)
C4	C3	C2	119.7(3)	C4C	C3C	C2C	120.1(3)
C4	C3	C18	119.8(3)	C4C	C3C	C18C	119.8(3)
C5	C4	C3	127.5(3)	C5C	C4C	C3C	126.5(3)
C4	C5	P1	115.4(2)	C4C	C5C	P1C	116.2(2)
C4	C5	C12	120.8(3)	C4C	C5C	C12C	120.4(3)
C12	C5	P1	123.9(2)	C12C	C5C	P1C	123.4(2)
C7	C6	C1	124.8(3)	C7C	C6C	C1C	123.8(3)
C7	C6	C11	114.6(3)	C7C	C6C	C11C	114.7(3)
C11	C6	C1	120.7(3)	C11C	C6C	C1C	121.5(3)
F1	C7	C6	118.2(3)	F1C	C7C	C6C	117.7(3)
F1	C7	C8	117.2(3)	F1C	C7C	C8C	117.2(3)
C8	C7	C6	124.6(4)	C8C	C7C	C6C	125.0(3)
C9	C8	C7	118.5(4)	C7C	C8C	C9C	118.2(3)
C10	C9	C8	120.1(3)	C10C	C9C	C8C	119.6(3)
C9	C10	C11	119.8(4)	C9C	C10C	C11C	120.7(3)
C10	C11	C6	122.5(4)	C10C	C11C	C6C	121.8(3)
C13	C12	C5	123.9(3)	C13C	C12C	C5C	124.1(3)
C13	C12	C17	114.4(3)	C13C	C12C	C17C	115.5(3)
C17	C12	C5	121.6(3)	C17C	C12C	C5C	120.4(3)
F2	C13	C12	117.7(3)	F2C	C13C	C12C	118.4(3)
F2	C13	C14	117.1(3)	F2C	C13C	C14C	117.7(4)
C14	C13	C12	125.1(3)	C14C	C13C	C12C	123.8(4)
C15	C14	C13	118.3(3)	C15C	C14C	C13C	118.8(4)
C14	C15	C16	119.7(3)	C16C	C15C	C14C	119.6(3)
C17	C16	C15	120.4(3)	C15C	C16C	C17C	120.8(4)
C16	C17	C12	122.0(3)	C16C	C17C	C12C	121.4(4)
C19	C18	C3	121.9(3)	C19C	C18C	C3C	121.1(3)
C19	C18	C23	117.6(3)	C19C	C18C	C23C	117.1(3)
C23	C18	C3	120.4(3)	C23C	C18C	C3C	121.8(3)
C20	C19	C18	120.9(3)	C20C	C19C	C18C	121.8(3)
C21	C20	C19	120.4(3)	C19C	C20C	C21C	120.3(3)
C22	C21	C20	119.6(3)	C22C	C21C	C20C	119.0(3)
C21	C22	C23	120.1(3)	C21C	C22C	C23C	121.2(3)
C22	C23	C18	121.4(3)	C22C	C23C	C18C	120.6(3)
C1B	P1B	C24B	113.40(16)	C1D	P1D	C5D	103.77(16)
C1B	P1B	C25B	109.50(17)	C1D	P1D	C24D	110.98(16)
C5B	P1B	C1B	103.75(16)	C1D	P1D	C25D	111.58(17)
C5B	P1B	C24B	111.00(16)	C5D	P1D	C24D	112.97(16)
C5B	P1B	C25B	111.06(17)	C5D	P1D	C25D	109.76(17)
C24B	P1B	C25B	108.12(19)	C24D	P1D	C25D	107.81(18)
C2B	C1B	P1B	115.5(2)	C2D	C1D	P1D	116.7(2)
C2B	C1B	C6B	121.2(3)	C2D	C1D	C6D	120.3(3)
C6B	C1B	P1B	123.3(2)	C6D	C1D	P1D	123.0(2)
C1B	C2B	C3B	127.7(3)	C1D	C2D	C3D	126.4(3)
C2B	C3B	C4B	119.4(3)	C2D	C3D	C4D	120.0(3)
C2B	C3B	C18B	120.4(3)	C2D	C3D	C18D	120.4(3)
C4B	C3B	C18B	120.0(3)	C4D	C3D	C18D	119.1(3)
C5B	C4B	C3B	125.9(3)	C5D	C4D	C3D	126.5(3)
C4B	C5B	P1B	116.9(2)	C4D	C5D	P1D	115.8(2)
C4B	C5B	C12B	119.9(3)	C4D	C5D	C12D	120.5(3)
C12B	C5B	P1B	123.2(2)	C12D	C5D	P1D	123.7(2)
C7B	C6B	C1B	124.3(3)	C7D	C6D	C1D	123.9(3)
C7B	C6B	C11B	114.7(3)	C7D	C6D	C11D	115.3(3)

Atom	Atom	Atom	Angle/°	Atom	Atom	Atom	Angle/°
C11B	C6B	C1B	120.9(3)	C11D	C6D	C1D	120.8(3)
F1B	C7B	C6B	118.4(3)	F1D	C7D	C6D	117.8(3)
F1B	C7B	C8B	116.7(3)	F1D	C7D	C8D	117.4(3)
C8B	C7B	C6B	124.9(3)	C8D	C7D	C6D	124.7(3)
C7B	C8B	C9B	118.4(3)	C9D	C8D	C7D	118.4(4)
C8B	C9B	C10B	119.3(3)	C8D	C9D	C10D	119.5(3)
C11B	C10B	C9B	120.5(3)	C9D	C10D	C11D	120.7(4)
C10B	C11B	C6B	122.0(3)	C10D	C11D	C6D	121.4(3)
C13B	C12B	C5B	123.5(3)	C13D	C12D	C5D	123.7(3)
C13B	C12B	C17B	115.2(3)	C13D	C12D	C17D	115.4(3)
C17B	C12B	C5B	121.3(3)	C17D	C12D	C5D	120.9(3)
F2B	C13B	C12B	118.3(3)	F2D	C13D	C12D	118.5(3)
F2B	C13B	C14B	117.4(3)	F2D	C13D	C14D	117.6(3)
C14B	C13B	C12B	124.3(3)	C14D	C13D	C12D	123.9(4)
C13B	C14B	C15B	118.7(4)	C15D	C14D	C13D	118.9(3)
C14B	C15B	C16B	119.6(3)	C14D	C15D	C16D	120.1(3)
C15B	C16B	C17B	120.5(3)	C15D	C16D	C17D	119.7(4)
C16B	C17B	C12B	121.7(3)	C16D	C17D	C12D	122.0(3)
C19B	C18B	C3B	120.2(3)	C19D	C18D	C3D	121.3(3)
C23B	C18B	C3B	122.5(3)	C23D	C18D	C3D	121.3(3)
C23B	C18B	C19B	117.3(3)	C23D	C18D	C19D	117.5(3)
C20B	C19B	C18B	121.0(3)	C20D	C19D	C18D	120.6(3)
C21B	C20B	C19B	120.4(3)	C21D	C20D	C19D	121.2(3)
C22B	C21B	C20B	119.2(3)	C20D	C21D	C22D	119.0(3)
C21B	C22B	C23B	120.8(3)	C23D	C22D	C21D	120.3(3)
C22B	C23B	C18B	121.2(3)	C22D	C23D	C18D	121.5(3)

Table S8: Bond lengths for **5-12**.

Atom	Atom	Length/Å	Atom	Atom	Length/Å
P1	C1	1.7494(12)	C8	C9	1.3788(18)
P1	C5	1.7487(12)	C9	C10	1.3757(18)
P1	C25	1.8100(13)	C10	C11	1.3884(17)
P1	C26	1.8030(12)	C12	C13	1.4065(17)
F1	C9	1.3619(14)	C12	C17	1.4038(17)
F2	C22	1.3633(14)	C13	C14	1.3917(17)
C1	C2	1.3934(16)	C14	C15	1.3930(19)
C1	C6	1.4734(16)	C15	C16	1.3901(19)
C2	C3	1.4020(16)	C15	C18	1.5070(18)
C3	C4	1.4170(16)	C16	C17	1.3913(17)
C3	C12	1.4828(16)	C19	C20	1.3945(17)
C4	C5	1.3796(16)	C19	C24	1.3962(17)
C5	C19	1.4907(16)	C20	C21	1.3950(17)
C6	C7	1.3987(17)	C21	C22	1.377(2)
C6	C11	1.4014(17)	C22	C23	1.375(2)
C7	C8	1.3905(17)	C23	C24	1.3927(18)

Table S9: Bond angles for **5-12**.

Atom	Atom	Atom	Angle/°	Atom	Atom	Atom	Angle/°
C1	P1	C25	114.85(6)	C10	C9	C8	122.82(11)
C1	P1	C26	113.31(6)	C9	C10	C11	117.91(12)
C5	P1	C1	103.95(6)	C10	C11	C6	121.90(12)
C5	P1	C25	108.65(6)	C13	C12	C3	121.58(11)
C5	P1	C26	112.84(6)	C17	C12	C3	122.24(11)
C26	P1	C25	103.43(6)	C17	C12	C13	116.16(11)
C2	C1	P1	117.50(9)	C14	C13	C12	121.77(12)
C2	C1	C6	120.54(10)	C13	C14	C15	121.42(12)
C6	C1	P1	121.92(8)	C14	C15	C18	121.27(13)
C1	C2	C3	127.94(11)	C16	C15	C14	117.23(11)
C2	C3	C4	118.65(10)	C16	C15	C18	121.47(13)
C2	C3	C12	119.98(10)	C15	C16	C17	121.73(12)
C4	C3	C12	120.89(10)	C16	C17	C12	121.63(12)

Atom	Atom	Atom	Angle/°	Atom	Atom	Atom	Angle/°
C5	C4	C3	126.50(11)	C20	C19	C5	120.87(11)
C4	C5	P1	118.93(9)	C20	C19	C24	118.66(11)
C4	C5	C19	121.01(10)	C24	C19	C5	120.45(11)
C19	C5	P1	119.83(8)	C19	C20	C21	120.84(12)
C7	C6	C1	122.75(11)	C22	C21	C20	118.19(12)
C7	C6	C11	117.61(11)	F2	C22	C21	118.65(12)
C11	C6	C1	119.64(11)	F2	C22	C23	118.22(12)
C8	C7	C6	121.42(12)	C23	C22	C21	123.13(12)
C9	C8	C7	118.28(12)	C22	C23	C24	117.83(12)
F1	C9	C8	118.62(11)	C23	C24	C19	121.32(12)
F1	C9	C10	118.56(12)				

Table S10: Bond lengths for **5-17**.

Atom	Atom	Length/Å	Atom	Atom	Length/Å
P1	C1	1.750(3)	C12	C13	1.409(4)
P1	C5	1.764(3)	C12	C17	1.389(4)
P1	C25	1.810(3)	C13	C14	1.388(4)
P1	C26	1.818(3)	C14	C15	1.397(5)
F2	C20	1.329(4)	C15	C16	1.388(5)
C1	C2	1.396(4)	C15	C18	1.507(4)
C1	C6	1.480(4)	C16	C17	1.396(4)
C2	C3	1.395(4)	C19	C20	1.385(5)
C3	C4	1.404(4)	C19	C24	1.395(5)
C3	C12	1.485(3)	C20	C21	1.386(5)
C4	C5	1.376(4)	C21	C22	1.373(6)
C5	C19	1.491(4)	C22	C23	1.383(6)
C6	C7	1.380(4)	C23	C24	1.394(5)
C6	C11	1.396(4)	C26	C27	1.387(5)
C7	C8	1.383(4)	C26	C31	1.392(4)
C7	F1	1.323(4)	C27	C28	1.381(5)
C8	C9	1.372(5)	C28	C29	1.389(5)
C9	C10	1.388(6)	C29	C30	1.362(6)
C10	C11	1.372(5)	C30	C31	1.392(5)
C11	F1A	1.279(6)			

Table S11: Bond angles for **5-17**.

Atom	Atom	Atom	Angle/°	Atom	Atom	Atom	Angle/°
C1	P1	C5	104.61(13)	C13	C12	C3	120.3(3)
C1	P1	C25	111.47(14)	C17	C12	C3	122.4(3)
C1	P1	C26	115.86(14)	C17	C12	C13	117.3(2)
C5	P1	C25	114.95(15)	C14	C13	C12	121.4(3)
C5	P1	C26	104.80(14)	C13	C14	C15	120.6(3)
C25	P1	C26	105.29(14)	C14	C15	C18	120.3(3)
C2	C1	P1	118.9(2)	C16	C15	C14	118.3(3)
C2	C1	C6	119.1(2)	C16	C15	C18	121.4(3)
C6	C1	P1	122.0(2)	C15	C16	C17	121.1(3)
C3	C2	C1	128.0(3)	C12	C17	C16	121.3(3)
C2	C3	C4	119.9(2)	C20	C19	C5	123.7(3)
C2	C3	C12	119.8(2)	C20	C19	C24	116.7(3)
C4	C3	C12	120.3(2)	C24	C19	C5	119.6(3)
C5	C4	C3	126.8(3)	F2	C20	C19	118.1(3)
C4	C5	P1	120.3(2)	F2	C20	C21	118.7(3)
C4	C5	C19	120.6(3)	C19	C20	C21	123.2(3)
C19	C5	P1	116.4(2)	C22	C21	C20	118.7(4)
C7	C6	C1	124.5(3)	C21	C22	C23	120.4(3)
C7	C6	C11	114.6(3)	C22	C23	C24	119.8(4)
C11	C6	C1	120.8(3)	C23	C24	C19	121.1(4)
C6	C7	C8	124.1(3)	C27	C26	P1	117.4(2)
F1	C7	C6	119.1(3)	C27	C26	C31	119.3(3)
F1	C7	C8	116.8(3)	C31	C26	P1	122.7(2)
C9	C8	C7	119.1(3)	C28	C27	C26	120.5(3)

Atom	Atom	Atom	Angle/°	Atom	Atom	Atom	Angle/°
C8	C9	C10	119.0(3)	C27	C28	C29	119.6(3)
C11	C10	C9	120.0(3)	C30	C29	C28	120.5(3)
C10	C11	C6	122.8(3)	C29	C30	C31	120.3(3)
F1A	C11	C6	124.8(5)	C30	C31	C26	119.8(3)
F1A	C11	C10	112.3(5)				

Table S12: Bond lengths for **5-16**.

Atom	Atom	Length/Å	Atom	Atom	Length/Å
P1	C1	1.763(3)	C12	C13	1.398(3)
P1	C5	1.763(2)	C12	C17	1.407(3)
P1	C24	1.808(3)	C13	C14	1.379(3)
P1	C25	1.822(3)	C13	F2	1.351(3)
C1	C2	1.389(3)	C14	C15	1.391(4)
C1	C6	1.474(3)	C15	C16	1.388(4)
C2	C3	1.401(3)	C16	C17	1.385(4)
C3	C4	1.409(3)	C18	C19	1.405(4)
C3	C18	1.481(3)	C18	C23	1.405(4)
C4	C5	1.382(3)	C19	C20	1.389(4)
C5	C12	1.478(3)	C20	C21	1.394(4)
C6	C7	1.396(4)	C21	C22	1.384(4)
C6	C11	1.397(3)	C22	C23	1.391(4)
C7	C8	1.375(4)	C25	C26	1.398(4)
C7	F1	1.345(3)	C25	C30	1.400(4)
C8	C9	1.391(4)	C26	C27	1.385(4)
C9	C10	1.380(4)	C27	C28	1.390(4)
C10	C11	1.384(4)	C28	C29	1.385(4)
C11	F1A	1.342(3)	C29	C30	1.393(4)

Table S13: Bond angles for **5-16**.

Atom	Atom	Atom	Angle/°	Atom	Atom	Atom	Angle/°
C1	P1	C5	103.78(12)	F1A	C11	C10	114.7(3)
C1	P1	C24	113.54(12)	C13	C12	C5	121.0(2)
C1	P1	C25	111.72(12)	C13	C12	C17	115.4(2)
C5	P1	C24	109.79(12)	C17	C12	C5	123.6(2)
C5	P1	C25	112.10(11)	C14	C13	C12	123.7(2)
C24	P1	C25	106.04(13)	F2	C13	C12	119.3(2)
C2	C1	P1	118.66(19)	F2	C13	C14	117.1(2)
C2	C1	C6	121.4(2)	C13	C14	C15	119.2(2)
C6	C1	P1	119.85(18)	C16	C15	C14	119.3(2)
C1	C2	C3	127.4(2)	C17	C16	C15	120.4(2)
C2	C3	C4	119.5(2)	C16	C17	C12	122.0(2)
C2	C3	C18	121.2(2)	C19	C18	C3	121.2(2)
C4	C3	C18	119.3(2)	C19	C18	C23	117.6(2)
C5	C4	C3	127.1(2)	C23	C18	C3	121.1(2)
C4	C5	P1	119.40(19)	C20	C19	C18	121.1(3)
C4	C5	C12	120.6(2)	C19	C20	C21	120.3(3)
C12	C5	P1	119.95(18)	C22	C21	C20	119.3(2)
C7	C6	C1	124.3(2)	C21	C22	C23	120.7(3)
C7	C6	C11	113.9(2)	C22	C23	C18	121.0(3)
C11	C6	C1	121.8(2)	C26	C25	P1	116.8(2)
C8	C7	C6	125.0(3)	C26	C25	C30	119.2(2)
F1	C7	C6	120.8(2)	C30	C25	P1	124.0(2)
F1	C7	C8	114.2(2)	C27	C26	C25	120.6(3)
C7	C8	C9	118.5(3)	C26	C27	C28	120.0(3)
C10	C9	C8	119.3(3)	C29	C28	C27	120.1(3)
C9	C10	C11	120.1(3)	C28	C29	C30	120.4(3)
C10	C11	C6	123.1(2)	C29	C30	C25	119.8(3)
F1A	C11	C6	122.1(3)				

Table S14: Bond lengths for **5-15**.

Atom	Atom	Length/Å	Atom	Atom	Length/Å
P1	C25	1.8206(19)	C4	C5	1.397(2)
P1	C1	1.7528(19)	C18	C19	1.402(3)
P1	C5	1.753(2)	C18	C5	1.483(3)
P1	C24	1.8012(19)	C18	C23	1.406(3)
C30	C25	1.389(3)	C1	C6	1.485(3)
C30	C29	1.389(3)	C6	C11	1.402(2)
C2	C3	1.409(3)	C19	C20	1.383(3)
C2	C1	1.381(2)	C13	C14	1.389(2)
C3	C12	1.482(2)	C20	C21	1.385(3)
C3	C4	1.389(3)	C23	C22	1.385(3)
C7	C6	1.396(3)	C8	C9	1.390(3)
C7	C8	1.388(3)	C21	C22	1.380(3)
C16	C15	1.383(3)	C28	C29	1.375(3)
C16	C17	1.390(3)	C28	C27	1.368(3)
C25	C26	1.387(3)	C10	C9	1.376(3)
C15	C14	1.383(3)	C10	C11	1.387(3)
C12	C17	1.400(3)	C27	C26	1.384(3)

Table S15: Bond angles for **5-15**.

Atom	Atom	Atom	Angle/°	Atom	Atom	Atom	Angle/°
C1	P1	C25	109.42(8)	C2	C1	P1	120.54(16)
C1	P1	C24	110.83(10)	C2	C1	C6	120.48(17)
C5	P1	C25	114.83(10)	C6	C1	P1	118.96(13)
C5	P1	C1	104.79(9)	C7	C6	C1	119.78(16)
C5	P1	C24	112.25(9)	C7	C6	C11	117.93(19)
C24	P1	C25	104.81(9)	C11	C6	C1	122.27(18)
C29	C30	C25	119.98(18)	C20	C19	C18	121.63(18)
C1	C2	C3	126.73(18)	C4	C5	P1	118.90(15)
C2	C3	C12	119.65(17)	C4	C5	C18	120.94(18)
C4	C3	C2	119.73(16)	C18	C5	P1	120.15(14)
C4	C3	C12	120.62(17)	C14	C13	C12	121.15(19)
C8	C7	C6	121.41(18)	C19	C20	C21	120.47(19)
C15	C16	C17	120.21(18)	C15	C14	C13	120.51(18)
C30	C25	P1	124.22(14)	C22	C23	C18	121.12(19)
C26	C25	P1	116.90(14)	C7	C8	C9	119.5(2)
C26	C25	C30	118.84(17)	C22	C21	C20	118.99(19)
C14	C15	C16	119.36(17)	C27	C28	C29	119.76(18)
C17	C12	C3	121.18(17)	C28	C29	C30	120.51(18)
C13	C12	C3	121.34(17)	C9	C10	C11	120.67(18)
C13	C12	C17	117.47(16)	C10	C9	C8	119.9(2)
C16	C17	C12	121.29(18)	C10	C11	C6	120.5(2)
C3	C4	C5	128.12(19)	C21	C22	C23	120.92(19)
C19	C18	C5	120.76(17)	C28	C27	C26	120.44(19)
C19	C18	C23	116.85(18)	C27	C26	C25	120.47(19)
C23	C18	C5	122.39(18)				

Table S16: Bond lengths for **5-18**.

Atom	Atom	Length/Å	Atom	Atom	Length/Å
Cl1	C7	1.7429(16)	C12	C13	1.401(2)
Cl2	C20	1.7418(15)	C12	C17	1.398(2)
P1	C1	1.7491(14)	C13	C14	1.390(2)
P1	C5	1.7516(14)	C14	C15	1.394(2)
P1	C25	1.8082(15)	C15	C16	1.391(2)
P1	C26	1.8174(15)	C15	C18	1.509(2)
C1	C2	1.3857(19)	C16	C17	1.389(2)
C1	C6	1.4910(19)	C19	C20	1.404(2)
C2	C3	1.4004(19)	C19	C24	1.4018(19)
C3	C4	1.4007(19)	C20	C21	1.390(2)
C3	C12	1.4796(19)	C21	C22	1.384(2)
C4	C5	1.3838(19)	C22	C23	1.385(2)
C5	C19	1.4855(19)	C23	C24	1.389(2)

Atom	Atom	Length/Å	Atom	Atom	Length/Å
C6	C7	1.400(2)	C26	C27	1.400(2)
C6	C11	1.403(2)	C26	C31	1.397(2)
C7	C8	1.388(2)	C27	C28	1.390(2)
C8	C9	1.386(2)	C28	C29	1.389(2)
C9	C10	1.389(2)	C29	C30	1.386(3)
C10	C11	1.389(2)	C30	C31	1.393(2)

Table S17: Bond angles for **5-18**.

Atom	Atom	Atom	Angle/°	Atom	Atom	Atom	Angle/°
C1	P1	C5	104.83(7)	C17	C12	C3	121.55(12)
C1	P1	C25	112.53(7)	C17	C12	C13	117.15(13)
C1	P1	C26	112.21(7)	C14	C13	C12	121.15(14)
C5	P1	C25	110.12(7)	C13	C14	C15	121.52(14)
C5	P1	C26	113.00(7)	C14	C15	C18	121.70(14)
C25	P1	C26	104.33(7)	C16	C15	C14	117.30(13)
C2	C1	P1	119.78(10)	C16	C15	C18	120.97(15)
C2	C1	C6	119.64(12)	C17	C16	C15	121.61(14)
C6	C1	P1	120.35(10)	C16	C17	C12	121.24(13)
C1	C2	C3	127.49(13)	C20	C19	C5	122.99(12)
C2	C3	C4	119.73(12)	C24	C19	C5	120.91(13)
C2	C3	C12	120.09(12)	C24	C19	C20	116.09(13)
C4	C3	C12	120.10(12)	C19	C20	Cl2	120.67(11)
C5	C4	C3	127.35(13)	C21	C20	Cl2	116.80(11)
C4	C5	P1	119.99(10)	C21	C20	C19	122.53(13)
C4	C5	C19	120.99(12)	C22	C21	C20	119.36(14)
C19	C5	P1	118.85(10)	C21	C22	C23	120.02(14)
C7	C6	C1	122.12(13)	C22	C23	C24	119.87(14)
C7	C6	C11	116.31(13)	C23	C24	C19	122.12(14)
C11	C6	C1	121.46(13)	C27	C26	P1	118.18(11)
C6	C7	Cl1	119.85(11)	C31	C26	P1	122.34(12)
C8	C7	Cl1	117.49(12)	C31	C26	C27	119.37(14)
C8	C7	C6	122.66(15)	C28	C27	C26	120.23(15)
C9	C8	C7	119.36(15)	C29	C28	C27	119.92(16)
C8	C9	C10	119.83(14)	C30	C29	C28	120.31(15)
C11	C10	C9	119.97(15)	C29	C30	C31	120.07(15)
C10	C11	C6	121.87(15)	C30	C31	C26	120.08(16)
C13	C12	C3	121.29(13)				

Table S18: Bond lengths for **5-21**.

Atom	Atom	Length/Å	Atom	Atom	Length/Å
Cl1	P1	2.0548(4)	Cl3	P2	2.0521(4)
Cl2	P1	2.0429(4)	Cl4	P2	2.0409(4)
P1	C1	1.7077(11)	P2	C25	1.7079(12)
P1	C5	1.7055(11)	P2	C29	1.7082(11)
C1	C2	1.3946(15)	F3	C31	1.3435(13)
C1	C6	1.4929(15)	C015	C30	1.3972(16)
C2	C3	1.3996(15)	C015	C34	1.3934(17)
C3	C4	1.3979(15)	C25	C26	1.3928(15)
C3	C18	1.4836(14)	C25	C30	1.4894(15)
C4	C5	1.3935(14)	C26	C27	1.4014(14)
C5	C12	1.4914(15)	C27	C28	1.3987(15)
C6	C7	1.3904(16)	C27	C41	1.4841(15)
C6	C11	1.3974(16)	C28	C29	1.3951(15)
C7	C8	1.3835(16)	C29	C35	1.4917(15)
C7	F1	1.3420(14)	C30	C31	1.3889(16)
C8	C9	1.3888(19)	C31	C32	1.3830(16)
C9	C10	1.3877(19)	C32	C33	1.3862(18)
C10	C11	1.3923(16)	C33	C34	1.3894(18)
C11	F1A	1.315(5)	C35	C36	1.3857(18)
C12	C13	1.3876(16)	C35	C40	1.3856(19)
C12	C17	1.3934(16)	C36	C37	1.3908(18)

Atom	Atom	Length/Å	Atom	Atom	Length/Å
C13	C14	1.3837(16)	C36	F4	1.2878(18)
C13	F2	1.3354(14)	C37	C38	1.383(2)
C14	C15	1.3865(19)	C38	C39	1.379(3)
C15	C16	1.382(2)	C39	C40	1.3866(19)
C16	C17	1.3946(17)	C40	F4A	1.260(2)
C17	F2A	1.295(4)	C41	C42	1.3983(15)
C18	C19	1.3973(16)	C41	C46	1.4000(15)
C18	C23	1.3972(16)	C42	C43	1.3914(16)
C19	C20	1.3913(16)	C43	C44	1.3943(18)
C20	C21	1.388(2)	C44	C45	1.3930(18)
C21	C22	1.387(2)	C44	C47	1.5105(17)
C21	C24	1.5082(17)	C45	C46	1.3913(16)
C22	C23	1.3930(17)			

Table S19: Bond angles for **5-21**.

Atom	Atom	Atom	Angle/°	Atom	Atom	Atom	Angle/°
Cl2	P1	Cl1	95.504(16)	C22	C23	C18	120.55(12)
C1	P1	Cl1	112.23(4)	Cl4	P2	Cl3	96.042(19)
C1	P1	Cl2	114.05(4)	C25	P2	Cl3	112.71(4)
C5	P1	Cl1	113.37(4)	C25	P2	Cl4	112.98(4)
C5	P1	Cl2	112.46(4)	C25	P2	C29	108.70(5)
C5	P1	C1	108.84(5)	C29	P2	Cl3	111.70(4)
C2	C1	P1	118.36(8)	C29	P2	Cl4	114.37(4)
C2	C1	C6	120.46(10)	C34	C015	C30	120.92(11)
C6	C1	P1	121.13(8)	C26	C25	P2	118.65(8)
C1	C2	C3	126.74(10)	C26	C25	C30	121.95(10)
C2	C3	C18	119.07(10)	C30	C25	P2	119.40(8)
C4	C3	C2	120.79(10)	C25	C26	C27	126.54(10)
C4	C3	C18	120.09(9)	C26	C27	C41	119.48(10)
C5	C4	C3	126.61(10)	C28	C27	C26	120.89(10)
C4	C5	P1	118.61(8)	C28	C27	C41	119.61(9)
C4	C5	C12	120.48(9)	C29	C28	C27	126.58(10)
C12	C5	P1	120.91(8)	C28	C29	P2	118.58(8)
C7	C6	C1	121.66(10)	C28	C29	C35	121.18(10)
C7	C6	C11	116.68(10)	C35	C29	P2	120.08(8)
C11	C6	C1	121.56(10)	C015	C30	C25	122.05(10)
C8	C7	C6	123.15(11)	C31	C30	C015	117.37(10)
F1	C7	C6	118.88(10)	C31	C30	C25	120.58(10)
F1	C7	C8	117.96(11)	F3	C31	C30	118.50(10)
C7	C8	C9	118.82(11)	F3	C31	C32	118.58(11)
C10	C9	C8	119.96(11)	C32	C31	C30	122.91(11)
C9	C10	C11	119.93(12)	C31	C32	C33	118.58(11)
C10	C11	C6	121.45(11)	C32	C33	C34	120.44(11)
F1A	C11	C6	116.8(4)	C33	C34	C015	119.78(12)
F1A	C11	C10	121.7(4)	C36	C35	C29	122.70(11)
C13	C12	C5	120.66(10)	C40	C35	C29	121.09(12)
C13	C12	C17	116.88(10)	C40	C35	C36	116.20(12)
C17	C12	C5	122.38(10)	C35	C36	C37	122.95(13)
C14	C13	C12	123.17(11)	F4	C36	C35	119.23(13)
F2	C13	C12	118.70(10)	F4	C36	C37	117.69(14)
F2	C13	C14	118.14(11)	C38	C37	C36	118.51(14)
C13	C14	C15	118.68(12)	C39	C38	C37	120.56(13)
C16	C15	C14	119.99(11)	C38	C39	C40	119.04(15)
C15	C16	C17	120.16(12)	C35	C40	C39	122.74(15)
C12	C17	C16	121.11(12)	F4A	C40	C35	120.26(14)
F2A	C17	C12	117.6(3)	F4A	C40	C39	116.62(16)
F2A	C17	C16	120.9(4)	C42	C41	C27	120.64(10)
C19	C18	C3	121.17(10)	C42	C41	C46	118.27(10)
C23	C18	C3	120.81(10)	C46	C41	C27	121.08(10)
C23	C18	C19	118.00(10)	C43	C42	C41	120.60(11)
C20	C19	C18	120.85(12)	C42	C43	C44	121.22(11)
C21	C20	C19	121.06(12)	C43	C44	C47	121.20(12)

Atom	Atom	Atom	Angle/°	Atom	Atom	Atom	Angle/°
C20	C21	C24	120.58(14)	C45	C44	C43	118.10(11)
C22	C21	C20	118.19(11)	C45	C44	C47	120.68(12)
C22	C21	C24	121.22(13)	C46	C45	C44	121.15(11)
C21	C22	C23	121.29(12)	C45	C46	C41	120.66(11)

Table S20: Bond lengths for **5-22**.

Atom	Atom	Length/Å	Atom	Atom	Length/Å
P1	C1	1.7527(10)	C15	C18	1.5112(15)
P1	C5	1.7517(10)	C16	C17	1.3926(14)
P1	C25	1.8227(10)	C19	C20	1.3938(14)
P1	C31	1.8117(10)	C19	C24	1.3980(14)
F1	C7	1.3583(12)	C20	C21	1.3859(14)
C1	C2	1.3920(13)	C20	F2	1.3528(13)
C1	C6	1.4865(13)	C21	C22	1.3836(17)
C2	C3	1.4023(13)	C22	C23	1.3838(17)
C3	C4	1.4062(13)	C23	C24	1.3909(15)
C3	C12	1.4811(13)	C24	F2A	1.324(3)
C4	C5	1.3848(13)	C25	C26	1.3964(14)
C5	C19	1.4907(13)	C25	C30	1.4018(14)
C6	C7	1.3939(13)	C26	C27	1.3950(15)
C6	C11	1.4005(13)	C27	C28	1.3844(17)
C7	C8	1.3793(14)	C28	C29	1.3896(17)
C8	C9	1.3912(16)	C29	C30	1.3921(15)
C9	C10	1.3891(16)	C31	C32	1.3993(14)
C10	C11	1.3947(14)	C31	C36	1.3978(14)
C12	C13	1.4040(14)	C32	C33	1.3916(15)
C12	C17	1.4031(14)	C33	C34	1.3902(17)
C13	C14	1.3939(14)	C34	C35	1.3866(17)
C14	C15	1.3953(15)	C35	C36	1.3922(15)
C15	C16	1.3944(15)			

Table S21: Bond angles for **5-22**.

Atom	Atom	Atom	Angle/°	Atom	Atom	Atom	Angle/°
C1	P1	C25	113.78(5)	C16	C15	C14	117.39(10)
C1	P1	C31	112.23(5)	C16	C15	C18	121.02(10)
C5	P1	C1	103.90(5)	C17	C16	C15	121.51(10)
C5	P1	C25	111.40(5)	C16	C17	C12	121.41(10)
C5	P1	C31	111.98(5)	C20	C19	C5	121.97(9)
C31	P1	C25	103.80(5)	C20	C19	C24	115.99(9)
C2	C1	P1	120.62(7)	C24	C19	C5	121.99(9)
C2	C1	C6	120.91(8)	C21	C20	C19	123.35(10)
C6	C1	P1	118.47(7)	F2	C20	C19	119.13(9)
C1	C2	C3	127.06(9)	F2	C20	C21	117.50(9)
C2	C3	C4	119.39(9)	C22	C21	C20	118.85(10)
C2	C3	C12	121.68(9)	C21	C22	C23	119.96(10)
C4	C3	C12	118.91(9)	C22	C23	C24	120.00(11)
C5	C4	C3	127.32(9)	C23	C24	C19	121.82(10)
C4	C5	P1	120.70(7)	F2A	C24	C19	122.6(2)
C4	C5	C19	119.71(9)	F2A	C24	C23	115.5(2)
C19	C5	P1	119.59(7)	C26	C25	P1	117.83(8)
C7	C6	C1	120.94(9)	C26	C25	C30	119.22(9)
C7	C6	C11	115.80(9)	C30	C25	P1	122.71(8)
C11	C6	C1	123.25(9)	C27	C26	C25	120.33(10)
F1	C7	C6	118.40(9)	C28	C27	C26	120.07(10)
F1	C7	C8	117.58(9)	C27	C28	C29	120.08(10)
C8	C7	C6	124.03(9)	C28	C29	C30	120.28(10)
C7	C8	C9	118.68(10)	C29	C30	C25	120.01(10)
C10	C9	C8	119.63(10)	C32	C31	P1	120.96(8)
C9	C10	C11	120.19(10)	C36	C31	P1	119.00(8)
C10	C11	C6	121.64(9)	C36	C31	C32	119.57(9)
C13	C12	C3	121.48(9)	C33	C32	C31	120.30(10)

Atom	Atom	Atom	Angle/°	Atom	Atom	Atom	Angle/°
C17	C12	C3	121.53(9)	C34	C33	C32	119.66(10)
C17	C12	C13	116.81(9)	C35	C34	C33	120.40(10)
C14	C13	C12	121.41(10)	C34	C35	C36	120.24(10)
C13	C14	C15	121.39(10)	C35	C36	C31	119.81(10)
C14	C15	C18	121.59(10)				

Table S22: Bond lengths for **5-25**.

Atom	Atom	Length/Å	Atom	Atom	Length/Å
P1	C1	1.738(2)	C18	C23	1.413(3)
P1	C5	1.751(2)	C19A	C20A	1.3900
P1	C25	1.808(2)	C20A	C21	1.3900
P1	C36	1.819(2)	C21	C22A	1.3900
F1	C7	1.357(3)	C21	C24	1.549(3)
F2	C13	1.362(2)	C21	C20	1.337(4)
C1	C2	1.395(3)	C21	C22	1.402(4)
C1	C6	1.485(3)	C22A	C23A	1.3900
C2	C3	1.402(3)	C25	C26	1.390(3)
C3	C4	1.408(3)	C25	C30	1.404(3)
C3	C18	1.506(3)	C26	C27	1.394(3)
C4	C5	1.386(3)	C27	C28	1.389(3)
C5	C12	1.480(3)	C28	C29	1.392(3)
C6	C7	1.392(3)	C29	C30	1.392(3)
C6	C11	1.399(3)	C30	C31	1.481(3)
C7	C8	1.380(3)	C31	C32	1.393(3)
C8	C9	1.388(3)	C31	C36	1.405(3)
C9	C10	1.388(4)	C32	C33	1.398(3)
C10	C11	1.391(3)	C33	C34	1.387(3)
C12	C13	1.398(3)	C34	C35	1.397(3)
C12	C17	1.404(3)	C35	C36	1.390(3)
C13	C14	1.380(3)	C19	C20	1.397(4)
C14	C15	1.386(3)	C22	C23	1.393(4)
C15	C16	1.390(3)	N1	C37	1.148(4)
C16	C17	1.387(3)	C37	C38	1.452(4)
C18	C19A	1.3900	N2	C39	1.135(5)
C18	C23A	1.3900	C39	C40	1.471(5)
C18	C19	1.366(3)			

Table S23: Bond angles for **5-25**.

Atom	Atom	Atom	Angle/°	Atom	Atom	Atom	Angle/°
C1	P1	C5	105.09(10)	C19	C18	C3	121.8(2)
C1	P1	C25	112.33(10)	C19	C18	C23	119.0(2)
C1	P1	C36	120.93(10)	C23	C18	C3	119.2(2)
C5	P1	C25	116.77(10)	C20A	C19A	C18	120.0
C5	P1	C36	111.44(10)	C19A	C20A	C21	120.0
C25	P1	C36	90.55(10)	C20A	C21	C22A	120.0
C2	C1	P1	120.43(16)	C20A	C21	C24	118.6(2)
C2	C1	C6	121.23(19)	C22A	C21	C24	121.3(2)
C6	C1	P1	118.22(15)	C20	C21	C24	121.1(3)
C1	C2	C3	127.4(2)	C20	C21	C22	120.3(2)
C2	C3	C4	119.24(19)	C22	C21	C24	118.5(3)
C2	C3	C18	121.4(2)	C23A	C22A	C21	120.0
C4	C3	C18	119.3(2)	C22A	C23A	C18	120.0
C5	C4	C3	127.6(2)	C26	C25	P1	126.55(16)
C4	C5	P1	120.15(17)	C26	C25	C30	121.6(2)
C4	C5	C12	120.33(19)	C30	C25	P1	111.84(16)
C12	C5	P1	119.52(15)	C25	C26	C27	118.5(2)
C7	C6	C1	121.15(19)	C28	C27	C26	120.0(2)
C7	C6	C11	116.0(2)	C27	C28	C29	121.5(2)
C11	C6	C1	122.9(2)	C30	C29	C28	118.9(2)
F1	C7	C6	118.3(2)	C25	C30	C31	112.58(19)
F1	C7	C8	118.0(2)	C29	C30	C25	119.4(2)

Atom	Atom	Atom	Angle/°	Atom	Atom	Atom	Angle/°
C8	C7	C6	123.7(2)	C29	C30	C31	128.0(2)
C7	C8	C9	118.9(2)	C32	C31	C30	126.8(2)
C8	C9	C10	119.6(2)	C32	C31	C36	119.8(2)
C9	C10	C11	120.2(2)	C36	C31	C30	113.37(19)
C10	C11	C6	121.6(2)	C31	C32	C33	119.0(2)
C13	C12	C5	121.3(2)	C34	C33	C32	121.3(2)
C13	C12	C17	115.9(2)	C33	C34	C35	119.9(2)
C17	C12	C5	122.8(2)	C36	C35	C34	119.2(2)
F2	C13	C12	118.85(19)	C31	C36	P1	111.01(16)
F2	C13	C14	117.5(2)	C35	C36	P1	128.11(17)
C14	C13	C12	123.7(2)	C35	C36	C31	120.8(2)
C13	C14	C15	118.8(2)	C18	C19	C20	120.8(3)
C14	C15	C16	119.7(2)	C21	C20	C19	120.7(3)
C17	C16	C15	120.4(2)	C23	C22	C21	119.7(3)
C16	C17	C12	121.5(2)	C22	C23	C18	119.3(3)
C19A	C18	C3	119.14(17)	N1	C37	C38	178.9(4)
C19A	C18	C23A	120.0	N2	C39	C40	178.2(5)
C23A	C18	C3	120.85(17)				

Table S24: Bond lengths for **5-9**.

Atom	Atom	Length/Å	Atom	Atom	Length/Å
P1	C1	1.756(4)	C9	C10	1.394(6)
P1	C5	1.748(4)	C10	C11	1.377(6)
P1	C24	1.813(4)	C12	C13	1.406(6)
P1	C25	1.801(4)	C12	C17	1.382(6)
C1	C2	1.381(5)	C13	C14	1.387(6)
C1	C6	1.481(5)	C14	C15	1.378(7)
C2	C3	1.405(5)	C15	C16	1.374(7)
C3	C4	1.408(5)	C16	C17	1.385(5)
C3	C18	1.471(5)	C18	C19	1.407(5)
C4	C5	1.381(5)	C18	C23	1.411(5)
C5	C12	1.497(5)	C19	C20	1.381(6)
C6	C7	1.400(5)	C20	C21	1.379(5)
C6	C11	1.409(5)	C21	C22	1.393(6)
C7	C8	1.372(6)	C22	C23	1.385(6)
C8	C9	1.384(6)			

Table S25: Bond angles for **5-9**.

Atom	Atom	Atom	Angle/°	Atom	Atom	Atom	Angle/°
C1	P1	C24	116.77(17)	C7	C8	C9	120.9(4)
C1	P1	C25	110.75(19)	C8	C9	C10	118.5(4)
C5	P1	C1	104.64(18)	C11	C10	C9	121.0(4)
C5	P1	C24	108.02(18)	C10	C11	C6	120.7(4)
C5	P1	C25	115.04(19)	C13	C12	C5	121.1(4)
C25	P1	C24	102.02(19)	C17	C12	C5	120.9(4)
C2	C1	P1	119.8(3)	C17	C12	C13	118.0(4)
C2	C1	C6	121.2(3)	C14	C13	C12	120.8(4)
C6	C1	P1	118.9(3)	C15	C14	C13	120.0(4)
C1	C2	C3	128.3(3)	C16	C15	C14	119.6(4)
C2	C3	C4	118.7(3)	C15	C16	C17	120.8(4)
C2	C3	C18	120.4(3)	C12	C17	C16	120.8(4)
C4	C3	C18	120.9(3)	C19	C18	C3	122.7(3)
C5	C4	C3	127.5(4)	C19	C18	C23	115.8(4)
C4	C5	P1	120.4(3)	C23	C18	C3	121.5(3)
C4	C5	C12	121.2(3)	C20	C19	C18	122.2(3)
C12	C5	P1	117.7(3)	C21	C20	C19	121.0(4)
C7	C6	C1	122.1(3)	C20	C21	C22	118.3(4)
C7	C6	C11	117.3(4)	C23	C22	C21	121.0(4)
C11	C6	C1	120.6(3)	C22	C23	C18	121.6(4)
C8	C7	C6	121.6(4)				

Chapter 6

Summary

Additional donor-substituents on the aromatic phosphorus heterocycle significantly modify their stereo-electronic properties and their coordination abilities. This class of phosphinines shows a significantly enhanced basicity and nucleophilicity compared to the parent phosphinine C_5H_5P. Moreover, the electrophilic nature of the phosphorus atom in phosphinines allows a nucleophilic attack by organolithium compounds to form λ^5-phosphinines. This leads to the possibility of introducing different substituents at the phosphorus atom of λ^3-phosphinines.

This dissertation describes the details exploration of the reactivity of functionalized phosphinines and first attempts to use phosphinines in more applied research fields.

1. Phosphinine borane adduct

Upon reaction of 3,5-bis($SiMe_3$)phosphinine with $B(C_6F_5)_3$, the first phosphinine borane adduct **6-1** was isolated and characterized (Figure 6.1).

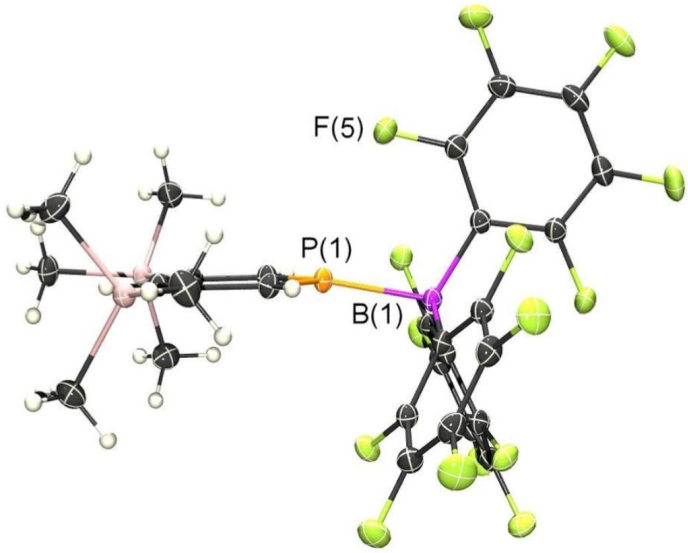

Figure 6.1: Molecular structure of **6-1** in the solid-state.

Interestingly, **6-1** turned out to be very reactive towards C-C multiple bonds. A zwitterionic alkenyl-phosphininium borate salt forms by insertion of phenylacetylene into the dative P-B bond of **6-1** and reacts further with a second equivalent of phenylacetylene to form **6-2**. The first example of a dihydro-1-phosphabarrelene derivative **6-3** was formed by reacting **6-1** with styrene. The reaction of **6-1** with an

ester proceeds instantaneously and forms a 1-*R*-phosphininium salt that further reacts with styrene or phenylacetylene to form a dihydro-1-*R*-phosphabarrelenium (**6-4)** and a 1-*R*-phosphabarrelenium salt **6-5**, respectively (Figure 6.2). These results provide fascinating new perspectives for the future, particularly with respect to the activation of small molecules and the synthesis of adducts of phosphinines with other main group elements and main-group-based compounds.

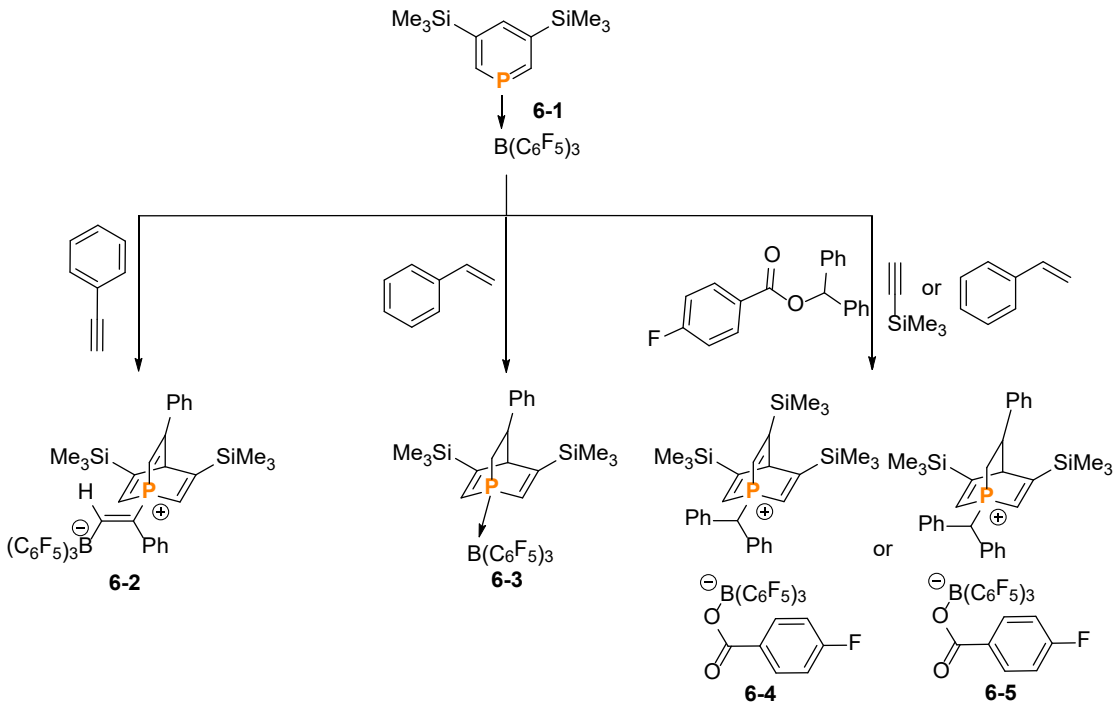

Figure 6.2: Reactivity of **6-1** towards C-C multiple bonds.

2. Phosphinine selenides

The phosphinine selenide (**6-6**) in the form of the cocrystalline adduct **6-7** with the organoiodine 1,4-TFDIB was structurally characterized by X-ray diffraction for the first time. The molecular structure of **6-7** in the solid state is mainly stabilized by several non-bonding interactions including π-π stacking, hydrogen bonding, F-F- and Se-I interactions. It demonstrates that phosphinine selenides can be used as a multifunctional molecules for crystal design. Furthermore, **6-6** can react with diiodine to form the adduct **6-8**. The labile P=Se bond in **6-6** allows the formation of KSeCN **6-9** in the presence of KCN, which shows that **6-6** can act as an efficient selenium transfer reagent (Figure 6.3).

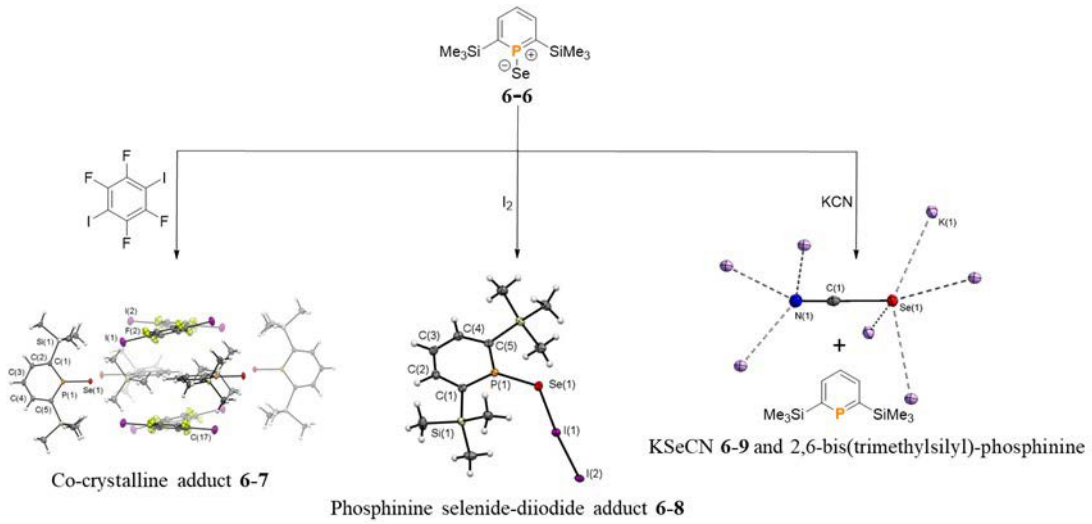

Figure 6.3: Co-crystalline adduct **6-7** and reactivity of phosphinine selenide **6-6**.

3. 3-N,N-dimethylaminophosphinine derivatives

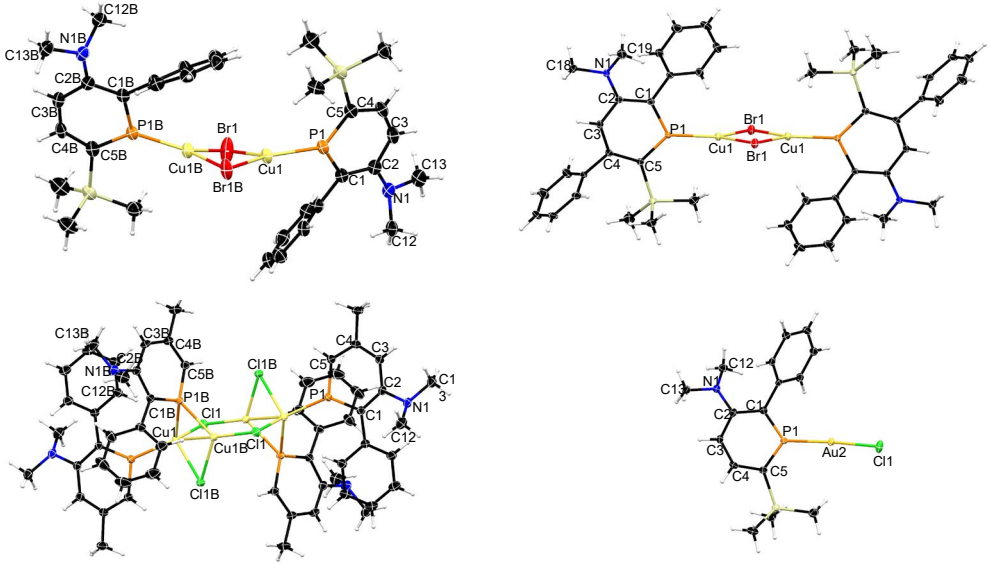

Figure 6.4: Molecular structures of phosphinine-coinage metal complexes.

Novel 3-aminofunctionalized phosphinines were synthesized and characterized. The neutral 3-aminofunctionalized phosphinines show a classical σ-2e terminal coordination mode with $CuBr{\cdot}S(CH_3)_2$. The pronated 3-aminofunctionalized phosphinine shows both the classical terminal 2e donation *via* the lone pair of the phosphorus atom and the uncommon μ_2-bridging 2e-lone-pair donation to the Cu^I center when reacted with $CuCl{\cdot}S(CH_3)_2$. Upon reaction with $AuCl{\cdot}S(CH_3)_2$, the 3-

aminofunctionalized phosphinines show an expected σ-2e terminal coordination mode (Figure 6.4).

Moreover, in the presence of water and HCl, the phosphinine **6-10** undergoes a hitherto unknown, selective ring contraction to form a hydroxylphospholene oxide. DFT calculations and labelling experiments were performed to get insight into the reaction mechanism (Figure 6.5).

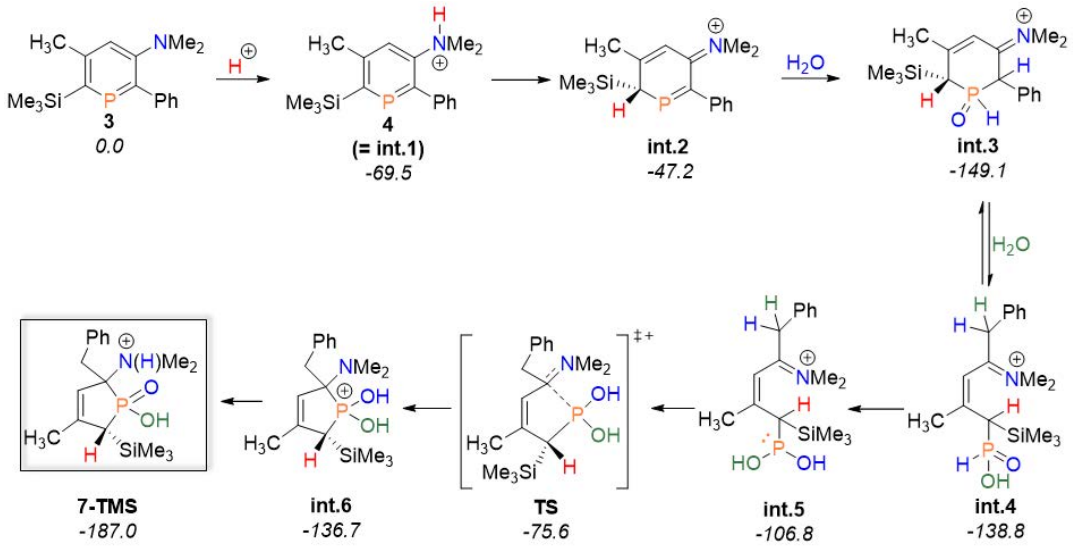

Figure 6.5: Proposed reaction mechanism for the reaction of **6-10** with HCl in the presence of water. **6-11** is the main product under vigorous stirring; Relative Gibbs free Energies (in kJ/mol) are given below the compound name; Int.: intermediate.

4. λ^5-phosphinines

A series of functionalized λ^5-phosphinines were synthesized by combining four different synthetic methods to introduce different substituents at the 2-, 4- and 6-positions as well as the phosphorus atom of the phosphorus heterocycle. **5-22** is the first λ^5-phosphinine with fluorescence emission that reaches the red region in solution. Furthermore, these λ^5-phosphinines exhibit a colorful fluorescence emission (ranging from blue to deep red) when they were irradiated with UV light (Figure 6.6). By investigating the effects of the substituents at different positions of the phosphorus heterocycle, the luminescent properties of λ^5-phosphinines were further clarified. These investigations provided a foundation for the design and synthesis of functionalized λ^5-

phosphinines for applications in optoelectronic devices in the future.

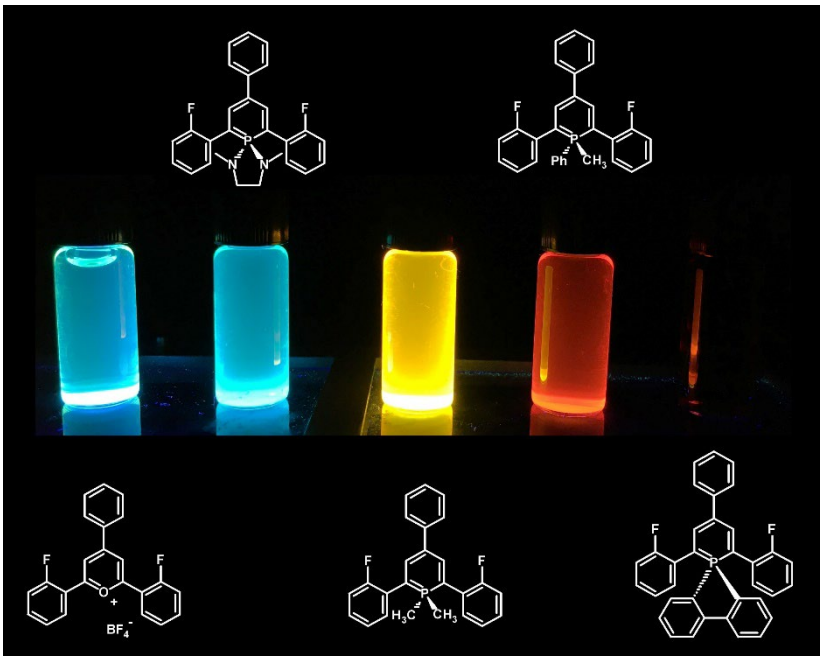

Figure 6.6: The fluorescent emission of λ^5- phosphinines and pyrylium salt under UV light.

Donor-Substituenten an Phosphininen verändern deren stereoelektronische Eigenschaften und Koordinationsfähigkeiten erheblich. Diese Klasse von Phosphininen besitzen eine deutlich höhere Basizität und Nukleophilie als die Stammverbindung C_5H_5P. Darüber hinaus ermöglicht der elektrophile Charakter des Phosphoratoms in Phosphininen den nukleophilen Angriff von Organolithiumverbindungen, um λ^5-Phosphinine zu bilden. Dieses eröffnet die Möglichkeit, verschiedene Substituenten am Phosphoratom der λ^3-Phosphinine einzuführen.

Diese Dissertation beschreibt die detaillierte Untersuchung der Reaktivität von Phosphininen und ihre Anwendung in weiteren Forschungsbereichen.

1. Phosphinin-Boran-Addukt

Nach der Reaktion von 3,5-Bis(trimethylsilyl)phosphinin mit $B(C_6F_5)_3$ wurde das erste Phosphinin-Boran-Addukt **6-1** isoliert und charakterisiert. Die Festkörperstruktur von **6-1** weist einen P(1)-B(1)-Bindungsabstand von 2.0415(12) Å (Abbildung 6.1).

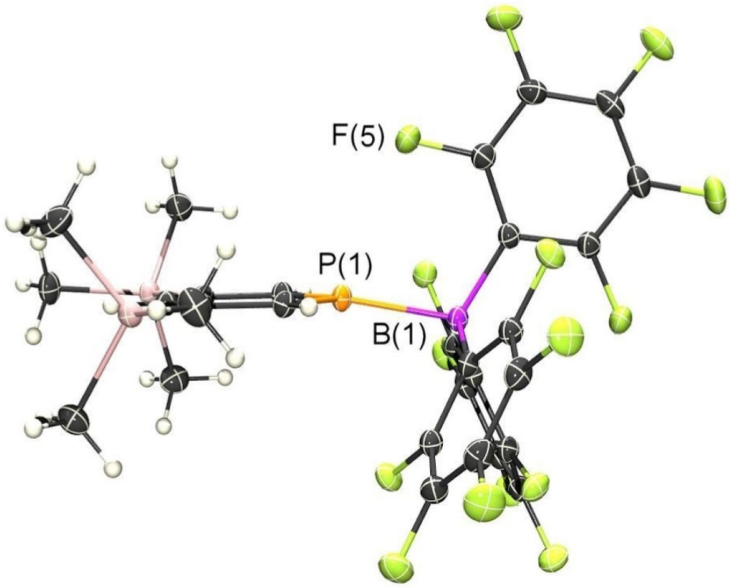

Abbildung 6.1: Molekularstruktur von **6-1** im Festkörper.

Interessanterweise erwies sich **6-1** als sehr reaktiv gegenüber C-C-Mehrfachbindungen. Durch Insertion von Phenylacetylen in die dative P-B-Bindung von **6-1** bildet sich ein zwitterionisches Alkenyl-Phosphininium-Borat-Salz, das mit einem zweite Äquivalent Phenylacetylen weiter zum Endprodukt **6-2** reagiert. Das erste Beispiel für ein Dihydro-

1-phosphabarrelenderivat **6-3** wurde durch die Reaktion von **6-1** mit Styrol gebildet. Mit einem Ester reagiert **6-1** unmittelbar unter Bildung eines 1-*R*-Phosphininiumsalzes, das mit Styrol oder Phenylacetylen unter Bildung eines Dihydro-1-*R*-phosphabarrelenium-(**6-4**) bzw. 1-*R*-Phosphabarreleniumsalzes **6-5** weiterreagiert (Abbildung 6.2). Diese Ergebnisse eröffnen faszinierende neue Perspektiven für die Zukunft, insbesondere im Hinblick auf die Aktivierung kleiner Moleküle und die Synthese von Addukten von Phosphininen mit anderen Elementen und Hauptgruppenelementverbindungen.

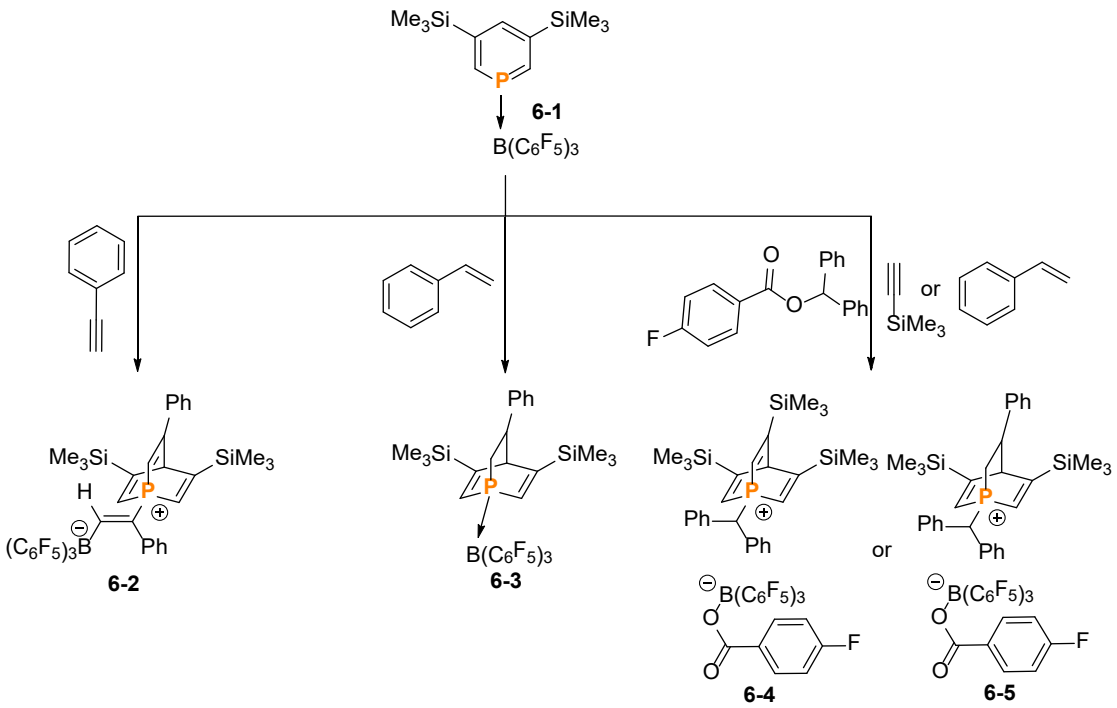

Abbildung 6.2: Reaktivität von **6-1** gegenüber C-C-Mehrfachbindungen.

2. Phosphinin-Selenid

Es wurde erstmals das Phosphinin-Selenid (**6-6**) in Form eines cokristallinen Addukts mit der Iod-organischen Verbindung 1,4-TFDIB (**6-7**) strukturell charakterisiert. Die Molekülstruktur von **6-7** im Kristall wird hauptsächlich durch mehrere nicht bindende Wechselwirkungen stabilisiert, darunter π-π-Stapelung, Wasserstoffbrückenbindungen, F-F- und Se-I-Wechselwirkungen. Es zeigt sich, dass das Phosphinin-Selenid als multifunktionales Molekül für das Kristalldesign genutzt werden kann. Darüber hinaus

kann **6-6** mit Iod reagieren und das Addukt **6-8** bilden. Die labile P=Se-Bindung in **6-6** ermöglicht die Bildung von KSeCN **6-9** in Gegenwart von KCN, was zeigt, dass **6-6** als effizientes Selentransferreagenz fungieren kann (Abbildung 6.3).

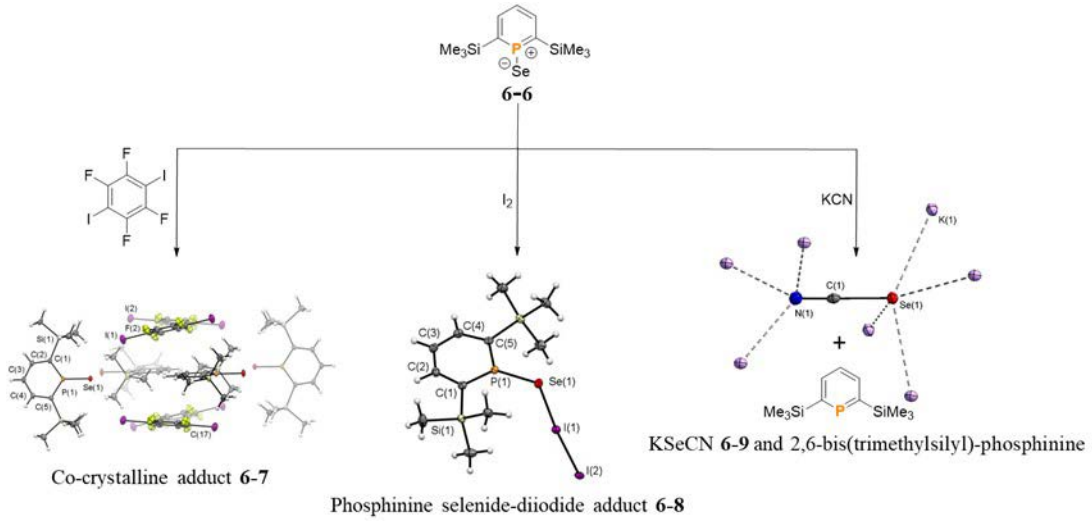

Abbildung 6.3: Cokristallines Addukt **6-7** und Reaktivität von Phosphinselenid **6-6**.

3. 3-N,N-Dimethylaminophosphinin-Derivate

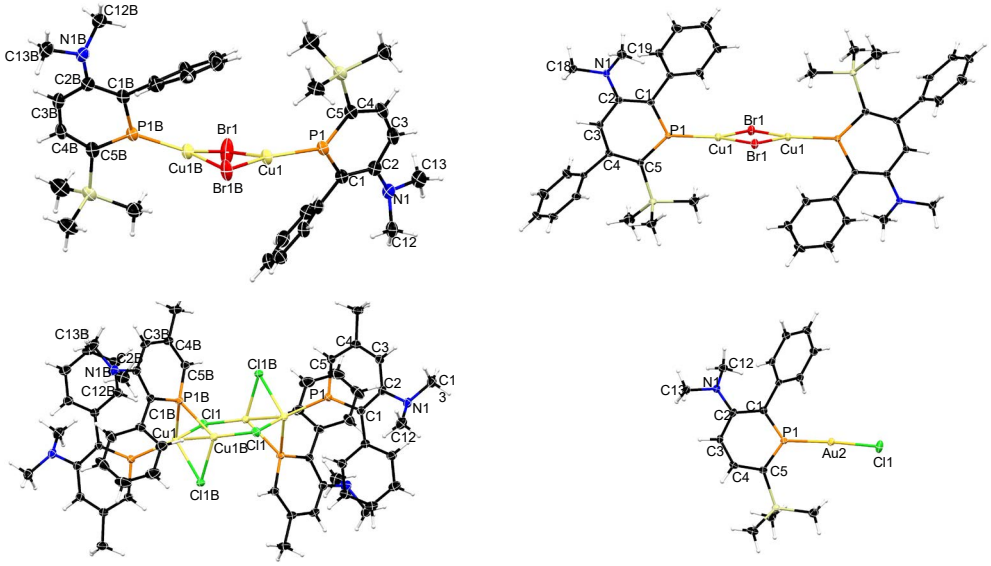

Abbildung 6.4: Molekülstruktur von Phosphinin-Münzmetall-Komplexen.

Neue 3-aminofunktionalisierte Phosphinine wurden synthetisiert und charakterisiert. Die neutralen 3-aminofunktionalisierten Phosphinine zeigen eine klassische σ-2e-terminale Koordination mit $CuBr{\cdot}S(CH_3)_2$. Das pronierte 3-aminofunktionalisierte

Phosphinin zeigt bei der Reaktion mit $CuCl{\cdot}S(CH_3)_2$ sowohl die klassische terminale 2e-Bindung über das freie Elektronenpaar, als auch die ungewöhnliche μ^2-verbrückende Koordination über das freie Elektronenpaar der Phosphoratom an das Cu^I-Zentrum. Die Bildung des Goldkomplexes durch Reaktion von $AuCl{\cdot}S(CH_3)_2$ und der 3-aminofunktionalisierten Phosphinine zeigt die Standardkoordination für fast alle Goldchloridkomplexe (Abbildung 6.4).

In Anwesenheit von Wasser und Salzsäure kommt es außerdem zu einer bisher unbekannten, selektiven Ringkontraktion des Phosphinins **6-10** unter Bildung eines Hydroxylphospholenoxids (**6-11**). Um einen Einblick in den Reaktionsmechanismus zu erhalten, wurden DFT-Berechnungen und Markierungsexperimente durchgeführt (Abbildung 6.5).

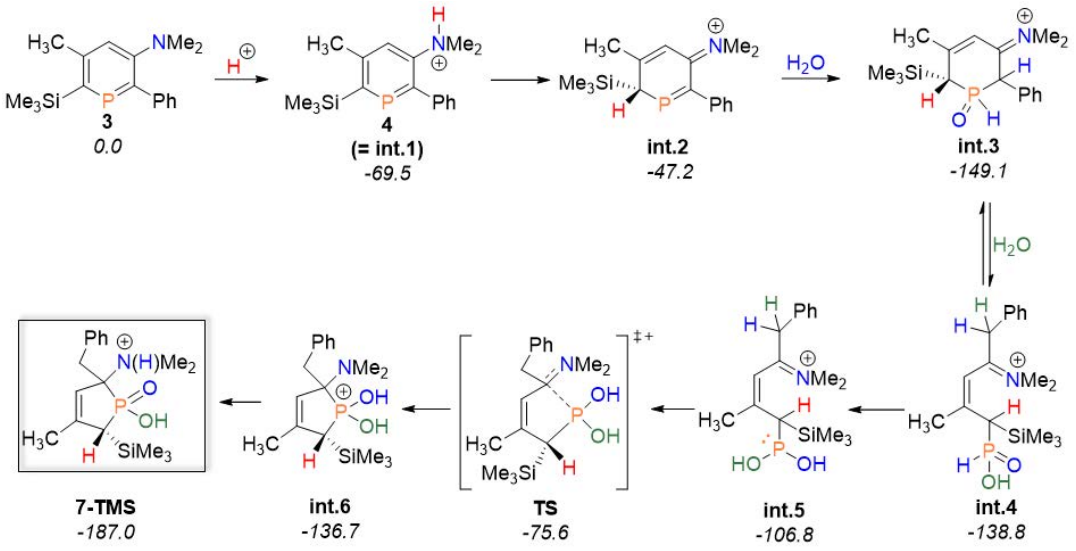

Abbildung 6.5: Vorgeschlagener Reaktionsmechanismus für die Reaktion von **6-10** mit HCl in Gegenwart von Wasser. **6-11** ist das Hauptprodukt unter kräftigem Rühren; die relativen freien Gibbs-Energien (in kJ/mol) sind unter dem Verbindungsnamen angegeben; Int.: Zwischenprodukt.

4. λ^5-Phosphinine

Eine Reihe von funktionalisierten λ^5-Phosphininen wurden durch die Kombination von vier verschiedenen Synthesemethoden synthetisiert, um verschiedene Substituenten an den 2-, 4- und 6-Positionen und am Phosphoratom des Phosphorheterozyklus einzuführen. **5-22** ist das erste λ^5-Phosphinin, das in Lösung den roten Bereich der

Fluoreszenzemission erreicht. Darüber hinaus zeigen diese λ^5-Phosphinine bei Bestrahlung mit UV-Licht eine farbige Fluoreszenzemission (von blau bis tiefrot) (Abbildung 6.6). Durch die Untersuchung der Veränderungen der Lumineszenzeigenschaften, die durch unterschiedliche Substituenten an verschiedenen Positionen des Phosphorheterozyklus verursacht werden, wurde die Lumineszenzfähigkeit von λ^5-Phosphininen in Verbindung mit ihren Substitutionsmustern und Substituenten weiter geklärt, was eine Grundlage für das Design und die Synthese von funktionalisierten λ^5-Phosphininen und ihren Einsatz in optoelektronischen Komponenten in der Zukunft darstellt.

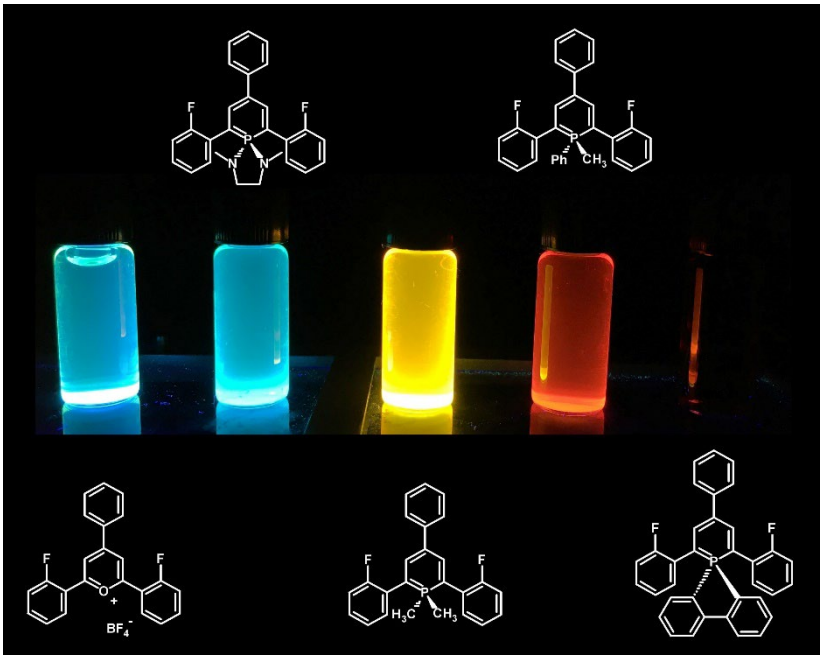

Abbildung 6.6: Die Fluoreszenzemission von λ^5-Phosphininen und Pyryliumsalz unter UV-Licht.

Chapter 7

Reference

Reference

[1] E. Musina, A. Balueva, A. Karasik, *Organophosphorus Chem*. **2019**, *48*, 1-63.

[2] A. Kraszewski, J. Stawinski, *Pure Appl. Chem.* **2007**, *79*, 2217-2227.

[3] G. Märkl, *Angew. Chem.* **1966**, *78*, 907-908.

[4] A. J. Ashe III, *J. Am. Chem. Soc.* **1971**, *93*, 3293-3295.

[5] P. L. E. Floch, in *Phosphorus-Carbon Heterocyc. Chem. Rise a New Domain* (Ed: F. Mathyl), Elsevier Science, **2001**, pp. 485-533.

[6] C. Müller, D. Wasserberg, J. J. Weemers, E. A. Pidko, S. Hoffmann, M. Lutz, A. L. Spek, S. C. Meskers, R. A. Janssen, R. A. van Santen, *Chem. Eur. J.* **2007**, *13*, 4548-4559.

[7] M. Bruce, G. Meissner, M. Weber, J. Wiecko, C. Müller, *Eur. J. Inorg. Chem.* **2014**, *2014*, 1719-1726.

[8] L. E. Broeckx, S. Güven, F. J. Heutz, M. Lutz, D. Vogt, C. Müller, *Chem. Eur. J.* **2013**, *19*, 13087-13098.

[9] G. Pfeifer, P. Ribagnac, X. F. Le Goff, J. Wiecko, N. Mézailles, C. Müller, *Eur. J. Inorg. Chem.* **2015**, *2015*, 240-249.

[10] A. Loibl, I. de Krom, E. A. Pidko, M. Weber, J. Wiecko, C. Müller, *Chem. Commun.* **2014**, *50*, 8842-8844.

[11] J. A. Joule, K. Mills, *Heterocyclic Chemistry*, 5. Ed., Wiley: Chichester, **2010**.

[12] M. Rigo, J. Sklorz, N. Hatje, F. Noack, M. Weber, J. Wiecko, C. Müller, *Dalton Trans.* **2016**, *45*, 2218-2226.

[13] M. Rigo, *Phosphinines as platforms for the design of new phosphorus based ligands*, Dissertation, Freie Universität Berlin, Berlin, **2017**.

[14] F. Mathey, *Tetrahedron Lett.* **1979**, *20*, 1753-1756.

[15] W. Rösch, M. Regitz, *Z. Naturforsch. B* **1986**, *41*, 931-934.

[16] N. Avarvari, P. Le Floch, F. Mathey, *J. Am. Chem. Soc.* **1996**, *118*, 11978-11979.

[17] K. M. Doxsee, J. B. Farahi, *J. Am. Chem. Soc.* **1988**, *110*, 7239-7240.

[18] K. M. Doxsee, J. B. Farahi, *J. Chem. Soc., Chem. Commun.* **1990**, 1452-1454.

[19] K. M. Doxsee, J. B. Farahi, H. Hope, *J. Am. Chem. Soc.* **1991**, *113*, 8889-8898.

[20] K. M. Doxsee, J. J. Juliette, J. K. Mouser, K. Zientara, *Organometallics* **1993**, *12*, 4682-4686.

[21] N. A. Petasis, D. K. Fu, *Organometallics* **1993**, *12*, 3776-3780.

[22] K. Nakajima, S. Takata, K. Sakata, Y. Nishibayashi, *Angew. Chem.* **2015**, *127*, 7707-7711.

[23] A. Modelli, B. Hajgató, J. F. Nixon, L. Nyulászi, *J. Phys. Chem. A* **2004**, *108*, 7440-7447.

[24] L. Nyulászi, T. Veszprémi, *J. Phys. Chem.* **1996**, *100*, 6456-6462.

[25] L. Nyulászi, *Chem. Rev.* **2001**, *101*, 1229-1246.

[26] P. Burrow, A. Ashe III, D. Bellville, K. Jordan, *J. Am. Chem. Soc.* **1982**, *104*, 425-429.

[27] L. Nyulaszi, T. Veszpremi, J. Reffy, B. Burkhardt, M. Regitz, *J. Am. Chem. Soc.* **1992**, *114*, 9080-9084.

[28] K. K. Baldridge, M. S. Gordon, *J. Am. Chem. Soc.* **1988**, *110*, 4204-4208.

[29] P. Jutzi, *Angew. Chem. Int. Ed.* **1975**, *14*, 232-245.

[30] G. Frison, A. Sevin, N. Avarvari, F. Mathey, P. Le Floch, *J. Org. Chem.* **1999**, *64*, 5524-5529.

[31] D. Lide, *CHC Handbook of Chemistry and Physics*, 87. Ed., CRC Press/Taylor and Francis Group: Boca Ralton, **2007**.

[32] N.-N. Pham-Tran, G. Bouchoux, D. Delaere, M. T. Nguyen, *J. Phys. Chem. A* **2005**, *109*, 2957-2963.

[33] C. Batich, E. Heilbronner, V. Hornung, A. Ashe, D. Clark, U. Cobley, D. Kilcast, I. Scanlan, *J. Am. Chem. Soc.* **1973**, *95*, 928-930.

[34] M. H. Habicht, F. Wossidlo, T. Bens, E. A. Pidko, C. Müller, *Chem. Eur. J.* **2018**, *24*, 944-952.

[35] F. Wossidlo, D. S. Frost, J. Lin, N. T. Coles, K. Klimov, M. Weber, T. Böttcher, C. Müller, *Chem. Eur. J.* **2021**, *27*, 12788-12795.

[36] A. J. Ashe III, *Acc. Chem. Res.* **1978**, *11*, 153-157.

[37] A. J. Ashe III, T. W. Smith, *Tetrahedron Lett.* **1977**, *18*, 407-410.

[38] C. Müller, M. Lutz, A. L. Spek, D. Vogt, *J. Chem. Crystallogr.* **2006**, *36*, 869-874.

[39] J. Daly, *J. Chem. Soc.* **1964**, 3799-3810.

[40] J. Bart, *Angew. Chem. Int. Ed.* **1968**, *7*, 730-730.

[41] N. Fey, A. G. Orpen, J. N. Harvey, *Coord. Chem. Rev.* **2009**, *253*, 704-722.

[42] N. Fey, *Dalton Trans.* **2010**, *39*, 296-310.

[43] J. A. Bilbrey, W. D. Allen, in *Annual Reports in Computational Chemistry, Vol. 9* (Ed.: R. A. Wheeler), Elsevier Science, **2013**, pp. 3-23.

[44] D. J. Durand, N. Fey, *Chem. Rev.* **2019**, *119*, 6561-6594.

[45] C. A. Tolman, *Chem. Rev.* **1977**, *77*, 313-348.

[46] C. Müller, L. E. Broeckx, I. de Krom, J. J. Weemers, *Eur. J. Inorg. Chem.* **2013**, *2013*, 187-202.

[47] E. F. DiMauro, M. C. Kozlowski, *J. Chem. Soc., Perkin Trans. 1* **2002**, 439-444.

[48] N. Mézailles, F. Mathey, P. Le Floch, in *Progress in Inorganic Chemistry*, *Vol. 49* (Ed.: K. D. Karlin), Wiley, **2001**, pp. 455-550.

[49] P. Le Floch, F. Mathey, *Coord. Chem. Rev.* **1998**, *178*, 771-791.

[50] P. Le Floch, *Coord. Chem. Rev.* **2006**, *250*, 627-681.

[51] N. Mézailles, P. Le Floch, K. Waschbüsch, L. Ricard, F. Mathey, C. P. Kubiak, *J. Organomet. Chem.* **1997**, *541*, 277-283.

[52] P. L. Floch, in *Phosphorous Heterocycles I, Vol. 20* (Ed.: R. Bansal), Springer: Berlin Heidelberg, **2008**, pp. 147-184.

[53] F. Mathey, P. Le Floch, *Chem. Inform.* **2005**, *36*, 49-245.

[54] J. Deberitz, H. Nöth, *J. Organomet. Chem.* **1973**, *49*, 453-468.

[55] H. Vahrenkamp, H. Nöth, *Chem. Ber.* **1973**, *106*, 2227-2235.

[56] J. Deberitz, H. Nöth, *Chem. Ber.* **1970**, *103*, 2541-2547.

[57] H. Vahrenkamp, H. Nöth, *Chem. Ber.* **1972**, *105*, 1148-1157.

[58] M. Doux, L. Ricard, F. Mathey, P. L. Floch, N. Mézailles, *E. J. Inorg. Chem.* **2003**, *2003*, 687-698.

[59] C. Elschenbroich, F. Baer, E. Bilger, D. Mahrwald, M. Nowotny, B. Metz, *Organometallics* **1993**, *12*, 3373-3378.

[60] K. Nainan, C. T. Sears, *J. Organomet. Chem.* **1978**, *148*, C31-C34.

[61] Y. Mao, K. M. H. Lim, Y. Li, R. Ganguly, F. Mathey, *Organometallics* **2013**, *32*, 3562-3565.

[62] M. T. Reetz, E. Bohres, R. Goddard, M. C. Holthausen, W. Thiel, *Chem. Eur. J.* **1999**, *5*, 2101-2108.

[63] B. Schmid, L. M. Venanzi, A. Albinati, F. Mathey, *Inorg. Chem.* **1991**, *30*, 4693-4699.

[64] R. Newland, M. F. Wyatt, R. Wingad, S. M. Mansell, *Dalton Trans.* **2017**, *46*, 6172-6176.

[65] A. J. Arce, A. J. Deeming, Y. De Sanctis, J. Manzur, *J. Chem. Soc., Chem. Commun.* **1993**, 325-326.

[66] P. Rosa, P. Le Floch, L. Ricard, F. Mathey, *J. Am. Chem. Soc.* **1997**, *119*, 9417-9423.

[67] Y. Hou, Z. Li, Y. Li, P. Liu, C.-Y. Su, F. Puschmann, H. Grützmacher, *Chem. Sci.* **2019**, *10*, 3168-3180.

[68] S. Giese, K. Klimov, A. Mikeházi, Z. Kelemen, D. S. Frost, S. Steinhauer, P. Müller, L. Nyulászi, C. Müller, *Angew. Chem. Int. Ed.* **2021**, *60*, 3581-3586.

[69] Y. Zhang, F. S. Tham, J. F. Nixon, C. Taylor, J. C. Green, C. A. Reed, *Angew. Chem.* **2008**, *120*, 3861-3864.

[70] K. Dimroth, in *Phosphorus-Carbon Double Bonds*, *Vol. 38*, Springer: Berlin Heidelberg New York, **1973**, pp. 1-147.

[71] A. Moores, L. Ricard, P. Le Floch, *Angew. Chem.* **2003**, *115*, 5090-5094.

[72] L. Fischer, F. Wossidlo, D. Frost, N. T. Coles, S. Steinhauer, S. Riedel, C. Müller, *Chem. Commun*. **2021**, *57*, 9522–9525.

[73] A. Moores, T. Cantat, L. Ricard, N. Mézailles, P. Le Floch, *New J. Chem.* **2007**, *31*, 1493-1498.

[74] R. K. Bansal, N. Gupta, S. K. Kumawat, *Z. Naturforsch. B* **2008**, *63*, 321-330.

[75] D. G. Holah, A. N. Hughes, K. L. Knudsen, *J. Chem. Soc., Chem. Commun.* **1988**, 493-495.

[76] K. Dimroth, W. Städe, *Angew. Chem.* **1968**, *80*, 966-967.

[77] G. Pfeifer, F. Chahdoura, M. Papke, M. Weber, R. Szűcs, B. Geffroy, D. Tondelier, L. Nyulászi, M. Hissler, C. Müller, *Chem. Eur. J.* **2020**, *26*, 10534-10543.

[78] H. Kanter, K. Dimroth, *Angew. Chem. Int. Ed.* **1972**, *11*, 1090-1091.

[79] T. N. Dave, H. Kaletsh, K. Dimroth, *Angew. Chem.* **1984**, *96*, 984-985.

[80] M. Bruce, M. Papke, A. W. Ehlers, M. Weber, D. Lentz, N. Mézallies, J. C. Slootweg, C. Müller, *Chem. Eur. J.* **2019**, *25*, 14332-14340.

[81] G. Märkl, F. Lieb, *Angew. Chem. Int. Ed.* **1968**, *7*, 733-733.

[82] G. Märkl, F. Lieb, C. Martin, *Tetrahedron Lett.* **1971**, *12*, 1249-1252.

[83] C. Wallis, P. G. Edwards, M. Hanton, P. D. Newman, A. Stasch, C. Jones, R. P. Tooze, *Dalton Trans.* **2009**, 2170-2177.

[84] B. Breit, E. Fuchs, *Chem. Commun.* **2004**, 694-695.

[85] W. Schaefer, A. Schweig, K. Dimroth, H. Kanter, *J. Am. Chem. Soc.* **1976**, *98*, 4410-4418.

[86] Z. X. Wang, P. v. R. Schleyer, *Helv. Chim. Acta* **2001**, *84*, 1578-1600.

[87] P. Roesch, J. R. Nitsch, M. Lutz, J. Wiecko, A. Steffen, C. Müller, *Inorg. Chem.* **2014**, *53*, 9855-9859.

[88] J. Moussa, T. Cheminel, G. R. Freeman, L.-M. Chamoreau, J. G. Williams, H. Amouri, *Dalton Trans.* **2014**, *43*, 8162-8165.

[89] X. Chen, Z. Li, F. Yanan, H. Grützmacher, *Eur. J. Inorg. Chem.* **2016**, *2016*, 633-638.

[90] Y. Li, Z. Li, Y. Hou, Y.-N. Fan, C.-Y. Su, *Inorg. Chem.* **2018**, *57*, 13235-13245.

[91] A. Yoshimura, H. Kimura, A. Handa, N. Hashimoto, M. Yano, S. Mori, T. Shirahata, M. Hayashi, Y. Misaki, *Tetrahedron Lett.* **2020**, *61*, 151724.

[92] M. Soleilhavoup, A. Baceiredo, F. Dahan, G. Bertrand, *Inorg. Chem.* **1992**, *31*, 1500-1504.

[93] X. Tang, U. Balijapalli, D. Okada, B. S. Karunathilaka, C. A. Senevirathne, Y. T. Lee, Z. Feng, A. S. Sandanayaka, T. Matsushima, C. Adachi, *Adv. Funct. Mater.* **2021**, *31*, 2104529.

[94] U. Balijapalli, X. Tang, D. Okada, Y. T. Lee, B. S. Karunathilaka, M. Auffray, G. Tumen‐Ulzii, Y. Tsuchiya, A. S. Sandanayaka, T. Matsushima, *Adv. Opt. Mater.* **2021**, *9*, 2101122.

[95] N. Hashimoto, R. Umano, Y. Ochi, K. Shimahara, J. Nakamura, S. Mori, H. Ohta, Y. Watanabe, M. Hayashi, *J. Am. Chem. Soc.* **2018**, *140*, 2046-2049.

[96] L. Nyulaszi, T. Veszpremi, J. Reffy, *J. Phys. Chem.* **1993**, *97*, 4011-4015.

[97] J. A. Sklorz, S. Hoof, N. Rades, N. De Rycke, L. Koenczoel, D. Szieberth, M. Weber, J. Wiecko, L. Nyulaszi, M. Hissler, *Chem. Eur. J.* **2015**, *21*, 11096-11109.

[98] S. Sarkar, J. D. Protasiewicz, B. D. Dunietz, *J. Phys. Chem. Lett.* **2018**, *9*, 3567-3572.

[99] J. Huang, J. Tarábek, R. Kulkarni, C. Wang, M. Dračínský, G. J. Smales, Y. Tian, S. Ren, B. R. Pauw, U. Resch‐Genger, *Chem. Eur. J.* **2019**, *25*, 12342-12348.

[100] A. N. Kostyuk, Y. V. Svyashchenko, D. M. Volochnyuk, D. A. Sibgatulin, A. M. Pinchuk, *Phosphorus Sulfur Silicon Relat. Elem.* **2008**, *183*, 558-560.

[101] H. Kanter, W. Mach, K. Dimroth, *Chem. Ber.* **1977**, *110*, 395-422.

[102] G. Märkl, F. Lieb, A. Merz, *Angew. Chem. Int. Ed.* **1967**, *6*, 87-88.

[103] G. Märkl, A. Merz, *Tetrahedron Lett.* **1968**, *9*, 3611-3614.

[104] G. Märkl, A. Merz, *Tetrahedron Lett.* **1971**, *12*, 1215-1218.

[105] G. Märkl, C. Martin, *Angew. Chem. Int. Ed.* **1974**, *13*, 408-409.

[106] A. Savateev, Y. Vlasenko, N. Shtil, A. Kostyuk, *Eur. J. Inorg. Chem.* **2016**, *2016*, 628-632.

[107] C. A. Mike, R. Ferede, N. T. Allison, *Organometallics* **1988**, *7*, 1457-1459.

[108] M. Ito, H. Kubo, I. Itani, K. Morimoto, T. Dohi, Y. Kita, *J. Am. Chem. Soc.* **2013**, *135*, 14078-14081.

[109] G. M. Sheldrick, *Acta Crystallogr. A* **2015**, *71*, 3–8.

[110] G. M. Sheldrick, *Acta Crystallogr. C* **2015**, *71*, 3–8.

[111] P. Müller, *Crystallogr. Rev.* **2009**, *15*, 57–83.

[112] O. v. Dolomanov, L. J. Bourhis, R. J. Gildea, J. A. K. Howard, H. Puschmann, *J. Appl. Crystallogr.* **2009**, *42*, 339–341.

[113] L. Cavallo, A. Correa, C. Costabile, H. Jacobsen, *J. Organomet. Chem.* **2005**, *690*, 5407–5413.

[114] A. Poater, F. Ragone, S. Giudice, C. Costabile, R. Dorta, S. P. Nolan, L. Cavallo, *Organometallics* **2008**, *27*, 2679–2681.

[115] H. Clavier, S. P. Nolan, *Chem. Commun.* **2010**, *46*, 841–861.

[116] M. Rigo, E. R. M. Habraken, K. Bhattacharyya, M. Weber, A. W. Ehlers, N. Mézailles, J. C. Slootweg, C. Müller, *Chem. Eur. J.* **2019**, *25*, 8769–8779.L.

[117] M. Taylor, L. Grant, C. Sands, *J. Am. Chem. Soc.* ***1955****, 77,* 1506–1507.

[118] S. Erhardt, G. Frenking, *Chem. Eur. J.* **2006**, *12*, 4620–4629.

[119] J. Schröder, D. Himmel, T. Böttcher, *Chem. Eur. J.* **2017**, *23*, 10763–10767.

[120] F. Wossidlo, D. S. Frost, J. Lin, N. T. Coles, K. Klimov, M. Weber, T. Böttcher, C. Müller, *Chem. Eur. J.* **2021**, *27*, 12788–12795.

[121] M. H. Habicht, F. Wossidlo, M. Weber, C. Müller, *Chem.Eur. J*. **2016**, *22*, 12877–12883.

[122] K. Rakstys, M. Saliba, P. Gao, P. Gratia, E. Kamarauskas, S. Paek, V. Jankauskas, M. K. Nazeeruddin, *Angew. Chem. Int. Ed*. **2016**, *55*, 7464–7468.

[123] G. Märkl, A. Merz, *Tetrahedron Lett*. **1969**, *16*, 1231–1234.